

TOPICS IN CURRENT CHEMISTRY

277

Volume Editor T. Schrader

Creative Chemical Sensor Systems

 Springer

277

Topics in Current Chemistry

Editorial Board:

**V. Balzani · A. de Meijere · K. N. Houk · H. Kessler · J.-M. Lehn
S. V. Ley · S. L. Schreiber · J. Thiem · B. M. Trost · F. Vögtle
H. Yamamoto**

Topics in Current Chemistry

Recently Published and Forthcoming Volumes

Creative Chemical Sensor Systems

Volume Editor: Schrader, T.

Vol. 277, 2007

In situ NMR Methods in Catalysis

Volume Editors: Bargon, J., Kuhn, L. T.

Vol. 276, 2007

Sulfur-Mediated Rearrangements II

Volume Editor: Schaumann, E.

Vol. 275, 2007

Sulfur-Mediated Rearrangements I

Volume Editor: Schaumann, E.

Vol. 274, 2007

Bioactive Conformation II

Volume Editor: Peters, T.

Vol. 273, 2007

Bioactive Conformation I

Volume Editor: Peters, T.

Vol. 272, 2007

Biominerization II

Mineralization Using Synthetic Polymers and Templates

Volume Editor: Naka, K.

Vol. 271, 2007

Biominerization I

Crystallization and Self-Organization Process

Volume Editor: Naka, K.

Vol. 270, 2007

Novel Optical Resolution Technologies

Volume Editors:

Sakai, K., Hirayama, N., Tamura, R.

Vol. 269, 2007

Atomistic Approaches in Modern Biology

From Quantum Chemistry to Molecular Simulations

Volume Editor: Reiher, M.

Vol. 268, 2006

Glycopeptides and Glycoproteins

Synthesis, Structure, and Application

Volume Editor: Wittmann, V.

Vol. 267, 2006

Microwave Methods in Organic Synthesis

Volume Editors: Larhed, M., Olofsson, K.

Vol. 266, 2006

Supramolecular Chirality

Volume Editors: Crego-Calama, M.,

Reinhoudt, D. N.

Vol. 265, 2006

Radicals in Synthesis II

Complex Molecules

Volume Editor: Gansäuer, A.

Vol. 264, 2006

Radicals in Synthesis I

Methods and Mechanisms

Volume Editor: Gansäuer, A.

Vol. 263, 2006

Molecular Machines

Volume Editor: Kelly, T. R.

Vol. 262, 2006

Immobilisation of DNA on Chips II

Volume Editor: Wittmann, C.

Vol. 261, 2005

Immobilisation of DNA on Chips I

Volume Editor: Wittmann, C.

Vol. 260, 2005

Creative Chemical Sensor Systems

Volume Editor: Thomas Schrader

With contributions by

E. V. Anslyn · L. Baltzer · A. W. Coleman · B. E. Collins
M. Dupin · Y. Guo · T. D. James · R. Jelinek · S. Kolusheva
S. Litvinchuk · S. Matile · A. Moussa · S. Otto · F. Perret
H. Perron · J. D. Revell · C. Schmuck · K. Severin · H. Tanaka
H. Wennemers · P. Wich · A. T. Wright

The series *Topics in Current Chemistry* presents critical reviews of the present and future trends in modern chemical research. The scope of coverage includes all areas of chemical science including the interfaces with related disciplines such as biology, medicine and materials science. The goal of each thematic volume is to give the nonspecialist reader, whether at the university or in industry, a comprehensive overview of an area where new insights are emerging that are of interest to a larger scientific audience.

As a rule, contributions are specially commissioned. The editors and publishers will, however, always be pleased to receive suggestions and supplementary information. Papers are accepted for *Topics in Current Chemistry* in English.

In references *Topics in Current Chemistry* is abbreviated Top Curr Chem and is cited as a journal.

Visit the TCC content at springerlink.com

ISSN 0340-1022

ISBN 978-3-540-71546-7 Springer Berlin Heidelberg New York

DOI 10.1007/978-3-540-71547-4

This work is subject to copyright. All rights are reserved, whether the whole or part of the material is concerned, specifically the rights of translation, reprinting, reuse of illustrations, recitation, broadcasting, reproduction on microfilm or in any other way, and storage in data banks. Duplication of this publication or parts thereof is permitted only under the provisions of the German Copyright Law of September 9, 1965, in its current version, and permission for use must always be obtained from Springer. Violations are liable for prosecution under the German Copyright Law.

Springer is a part of Springer Science+Business Media

springer.com

© Springer-Verlag Berlin Heidelberg 2007

The use of registered names, trademarks, etc. in this publication does not imply, even in the absence of a specific statement, that such names are exempt from the relevant protective laws and regulations and therefore free for general use.

Cover design: WMXDesign GmbH, Heidelberg

Typesetting and Production: LE-TeX Jelonek, Schmidt & Vöckler GbR, Leipzig

Printed on acid-free paper 02/3180 YL - 5 4 3 2 1 0

Volume Editor

Prof. Dr. Thomas Schrader

Institute of Organic Chemistry
Department of Chemistry
University Duisburg-Essen
Univeritätsstraße 5
45117 Essen
Germany
Thomas.Schrader@uni-due.de

Editorial Board

Prof. Vincenzo Balzani

Dipartimento di Chimica „G. Ciamician“
University of Bologna
via Selmi 2
40126 Bologna, Italy
vincenzo.balzani@unibo.it

Prof. Dr. Armin de Meijere

Institut für Organische Chemie
der Georg-August-Universität
Tammanstr. 2
37077 Göttingen, Germany
ameijer1@uni-goettingen.de

Prof. Dr. Kendall N. Houk

University of California
Department of Chemistry and
Biochemistry
405 Hilgard Avenue
Los Angeles, CA 90024-1589
USA
houk@chem.ucla.edu

Prof. Dr. Horst Kessler

Institut für Organische Chemie
TU München
Lichtenbergstraße 4
86747 Garching, Germany
kessler@ch.tum.de

Prof. Jean-Marie Lehn

ISIS
8, allée Gaspard Monge
BP 70028
67083 Strasbourg Cedex, France
lehn@isis.u-strasbg.fr

Prof. Steven V. Ley

University Chemical Laboratory
Lensfield Road
Cambridge CB2 1EW
Great Britain
Svl1000@cus.cam.ac.uk

Prof. Stuart L. Schreiber

Chemical Laboratories
Harvard University
12 Oxford Street
Cambridge, MA 02138-2902
USA
sls@slsiris.harvard.edu

Prof. Dr. Joachim Thiem

Institut für Organische Chemie
Universität Hamburg
Martin-Luther-King-Platz 6
20146 Hamburg, Germany
thiem@chemie.uni-hamburg.de

Prof. Barry M. Trost

Department of Chemistry
Stanford University
Stanford, CA 94305-5080
USA
bmtrost@leland.stanford.edu

Prof. Dr. Hisashi Yamamoto

Department of Chemistry
The University of Chicago
5735 South Ellis Avenue
Chicago, IL 60637
USA
yamamoto@uchicago.edu

Prof. Dr. F. Vögtle

Kekulé-Institut für Organische Chemie
und Biochemie
der Universität Bonn
Gerhard-Domagk-Str. 1
53121 Bonn, Germany
voegtle@uni-bonn.de

Topics in Current Chemistry Also Available Electronically

For all customers who have a standing order to Topics in Current Chemistry, we offer the electronic version via SpringerLink free of charge. Please contact your librarian who can receive a password or free access to the full articles by registering at:

springerlink.com

If you do not have a subscription, you can still view the tables of contents of the volumes and the abstract of each article by going to the SpringerLink Homepage, clicking on “Browse by Online Libraries”, then “Chemical Sciences”, and finally choose Topics in Current Chemistry.

You will find information about the

- Editorial Board
- Aims and Scope
- Instructions for Authors
- Sample Contribution

at springer.com using the search function.

Preface

Since several excellent books have appeared on the issue of chemical and biochemical sensing, this compendium concentrates on recent creative new approaches using *chemical means* for the detection and quantification of important analytes. These are presented either from a technical viewpoint or from the perspective of selective molecular recognition with artificial receptor molecules. Consequently, the entire book is subdivided into two categories, i.e., natural targets and detection techniques.

In the first part, the challenging task of sensing peptides and proteins as well as saccharides is addressed from several perspectives: Small libraries with maximum diversity are efficiently used to reach high affinity and selectivity of artificial hosts for short peptide sequences. Preorganized aromatic vessels are tailored for certain protein epitopes and shown to selectively address the prion protein, and a new conjugation technique operating at physiological conditions on helix-loop-helix motifs, leads to protein binders of exquisite affinity. Finally, elegant sensor systems for multifunctional carbohydrates in their natural form, which use the principle of photo-induced electron transfer for fluorescence detection, are presented.

The second part of this book is devoted to creative detection techniques employing chemical processes: Liposomes with integral self-assembled diacetylene lipid areas show an intense blue color, which gradually changes to red if biological analytes of various sizes specifically interact with embedded hosts. Principal component analysis and artificial neuronal networks are novel methods to quantitatively analyze complex mixtures. An alternative approach uses artificial peptidic pores, which are able to release self-quenched fluorophores that are substituted by tighter binding analytes. The last two chapters of this book highlight new promising areas of combinatorial chemistry: A fluorescence signal indicates that among thousands of candidates a certain organocatalyst has performed a successful asymmetric aldol reaction. Adding equilibrating conditions to combinatorial screening paves the way to generating self-optimized receptors and sensors, with a minimum need for design.

All chapters are written by leading experts in their fields and demonstrate that the fascinating topic of sensing, although often inspired by nature, goes far beyond biological principles and even today opens new doors to interdisciplinary research. Some of these areas are so new that technical applications have

not yet evolved. However, according to the editor, it can only be a question of time before chemical noses and dynamic combinatorial libraries are integrated into commercial sensor systems, to pick just two prominent examples.

I am indebted to the authors of this timely compilation, who presented their very latest research in an easy-to-read fashion. Their cutting edge contributions are intended to stimulate further research in other groups and to provide the advanced reader with latest sensing concepts and techniques originating from the realm of chemistry. Many thanks are also due to Dr. Marion Hertel and Birgit Kollmar-Thoni for their encouragement and professional support throughout the entire process of putting the book together.

Essen, March 2007

Thomas Schrader

Contents

Part I

Creative Sensing of Natural Targets

The Development of Artificial Receptors for Small Peptides Using Combinatorial Approaches

C. Schmuck · P. Wich 3

Calix[n]arenes as Protein Sensors

A. W. Coleman · F. Perret · A. Moussa · M. Dupin · Y. Guo · H. Perron . . . 31

Polypeptide Conjugate Binders for Protein Recognition

L. Baltzer 89

Saccharide-Selective Boronic Acid Based Photoinduced Electron Transfer (PET) Fluorescent Sensors

T. D. James 107

Part II

Creative Detection Techniques

Biomolecular Sensing with Colorimetric Vesicles

R. Jelinek · S. Kolusheva 155

Combining Molecular Recognition, Optical Detection, and Chemometric Analysis

B. E. Collins · A. T. Wright · E. V. Anslyn 181

Analyte Sensing Across Membranes with Artificial Pores

S. Matile · H. Tanaka · S. Litvinchuk 219

Identification of Catalysts in Combinatorial Libraries

J. D. Revell · H. Wennemers 251

Dynamic Combinatorial Libraries for the Development of Synthetic Receptors and Sensors	
S. Otto · K. Severin	267
Author Index Volumes 251–277	289
Subject Index	301

Contents of Volume 269

Novel Optical Resolution Technologies

Volume Editors: Sakai, K., Hirayama, N., Tamura, R.

ISBN: 978-3-540-46317-7

Preferential Crystallization

G. Coquerel

Mechanism and Scope of Preferential Enrichment, a Symmetry-Breaking Enantiomeric Resolution Phenomenon

R. Tamura · H. Takahashi · D. Fujimoto · T. Ushio

Racemization, Optical Resolution and Crystallization-Induced Asymmetric Transformation of Amino Acids and Pharmaceutical Intermediates

R. Yoshioka

Advantages of Structural Similarities of the Reactants in Optical Resolution Processes

F. Faigl · J. Schindler · E. Fogassy

Dutch Resolution of Racemates and the Roles of Solid Solution Formation and Nucleation Inhibition

R. M. Kellogg · B. Kaptein · T. R. Vries

New Resolution Technologies Controlled by Chiral Discrimination Mechanisms

K. Sakai · R. Sakurai · H. Nohira

Molecular Mechanisms of Dielectrically Controlled Resolution (DCR)

K. Sakai · R. Sakurai · N. Hirayama

From Racemates to Single Enantiomers – Chiral Synthetic Drugs over the last 20 Years

H. Murakami

Part I
Creative Sensing of Natural Targets

The Development of Artificial Receptors for Small Peptides Using Combinatorial Approaches

Carsten Schmuck (✉) · Peter Wich

Institut für Organische Chemie, Universität Würzburg, Am Hubland, 97074 Würzburg, Germany
schmuck@chemie.uni-wuerzburg.de

1	Introduction	4
1.1	Combinatorial Methods	4
1.2	Supramolecular Chemistry	4
2	Artificial Peptide Receptors	5
2.1	Rational Design and Synthesis	5
2.2	Combinatorial Receptor Finding	8
2.2.1	Split and Mix Approach	9
2.2.2	Large and Random Libraries	10
2.2.3	Small but Focused Libraries	16
2.2.4	Spatially Separated Libraries	18
2.2.5	QSAR Analysis	23
2.2.6	Insights into Structure and Reactivity	24
2.3	Dynamic Combinatorial Chemistry	26
3	Conclusion and Perspectives	28
	References	28

Abstract In this article we describe some examples how combinatorial libraries are applied in supramolecular chemistry e.g. to identify artificial receptors for peptide binding in aqueous solvent. Whereas in the classical combinatorial approach mainly large but completely random libraries are used, nowadays also the use of small but focused libraries is coming into focus. We discuss the pros and cons of these two different approaches, using examples from literature work and our own studies in this field.

Keywords Combinatorial libraries · Peptides · Receptors · Supramolecular chemistry

Abbreviations

Ac	Acetyl
Bn	Benzyl
Boc	<i>tert</i> -Butoxycarbonyl
CBS	Carboxylate binding site
dansyl	(Dimethylamino)naphthalene-1-sulfonyl
Fmoc	9-Fluorenylmethoxycarbonyl
Ph	Phenyl
Suc	Succinic acid

1 Introduction

1.1 Combinatorial Methods

The use of combinatorial chemistry has fundamentally changed the pace and scope of scientific research in some areas. The introduction of synthetic peptide libraries has proven that combinatorial chemistry is a powerful tool for the generation of libraries with immense molecular diversity. But the hype as a new tool mainly in the pharmaceutical industry at the beginning of the 1990s has slowed down in recent years. The original hope that the screening of large libraries that contain millions of compounds would produce many new drug candidates has not been fulfilled with complete satisfaction. Nevertheless, combinatorial chemistry has established itself as a powerful tool—among others—in chemistry, even though it is not the magic bullet initially anticipated by some. However, combinatorial chemistry is currently changing once more and is coming again into the focus of scientists. Besides the large but random libraries initially employed, small but focused libraries are also increasingly used to address specific problems in various fields of research. The progress in the development of dynamic combinatorial libraries is also a promising development. This article will describe first some general aspects of combinatorial chemistry and then give a summary of different approaches in artificial receptor finding for biologically relevant small peptides over the years, with a focus on the advantages of small and focused libraries as used in our own research.

1.2 Supramolecular Chemistry

Combinatorial chemistry was initially mainly considered as a versatile tool for drug discovery, but has evolved in recent years into broad fields of applications as diverse as materials science [1–3], catalyst development [4–7], and biochemistry to identify the substrates of novel enzymes [8–10]. It also opens the way in the widespread area of supramolecular chemistry. We use combinatorial methods in this context to find new receptors that are capable of binding to a given target peptide, even in aqueous solvents. This can help us to increase our knowledge of molecular recognition in general and to design biosensors for the targeting of cellular processes or for the discovery of new therapeutics. But what should a peptide receptor look like? In principle there are two distinct paths one can follow [11]. One can try to rationally design a complete receptor *de novo* with the help of theoretical calculations [12]. However, the larger the substrate, the more difficult this gets as theoretical methods such as force field calculations are not yet

reliable enough to completely design a tailor-made artificial host for a large substrate. Another possibility is to use a random trial and error approach and to identify suitable receptors with the help of combinatorial chemistry using large and random libraries [13–15]. The best way, of course, will be to combine both approaches and to use small libraries with tailor-made building blocks specifically designed to bind a peptide target. Combinatorial studies in supramolecular chemistry at the beginning most often involved the synthesis of a large peptide library that was then screened against a given receptor in order to get at a better understanding of host–guest interactions. The alternative strategy, the preparation of combinatorial libraries of hostlike molecules followed by identification of those receptors that bind a given substrate selectively, has only come into focus in recent years. In the next paragraphs, we will discuss some examples of both the rational and the combinatorial approaches to developing artificial peptide receptors.

2

Artificial Peptide Receptors

2.1

Rational Design and Synthesis

A characteristic property of biological macromolecules is that most bind their preferred substrates with extraordinarily high selectivity. Almost all biological systems rely not only on selective binding events but also on the sequence-selective binding of oligopeptides or peptidic substructures of proteins. In recent years, chemists have worked to create synthetic small molecules, receptors for amino acids and small peptides, with similar binding properties to get a deeper understanding of these recognition events [16–19].

However, one of the biggest problems is the high flexibility of the peptidic substrates. The binding affinity of the noncovalent interactions in polar solvents like water is often not high enough to obtain a stable receptor–substrate complex. Only very few artificial receptors exist that allow the complexation of an oligopeptide in aqueous solvents (e.g., under physiological conditions) [20–28].

The design of a specific receptor for a given peptide sequence is hence a still open and challenging task. We recently designed a receptor **1** (Fig. 1) that was able to bind dipeptides in aqueous solvents with association constants up to $K_{\text{ass}} = 50\,000\text{ M}^{-1}$ [29].

To ensure strong complexation in polar solvents, a carboxylate binding site in the form of a cationic guanidiniocarbonyl pyrrole group was introduced. As we could show, these are among the most efficient binding motifs for carboxylates, even in aqueous solutions, known so far [30–34]. But this re-

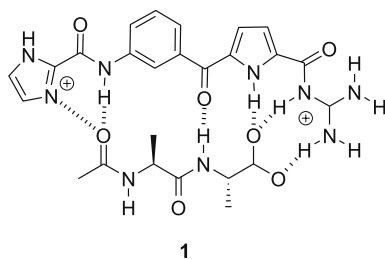


Fig. 1 An artificial dipeptide receptor 1 which was developed based on theoretical predictions

ceptor could not distinguish between different dipeptides, as the interactions between receptor and substrate were mainly limited to the amide backbone of the dipeptide. Hence, the receptor did prefer dipeptides over amino acids but the selectivity between dipeptides of different sequences was only modest, as complexation did not invoke any direct interactions with the amino acid side chains [35, 36]. The receptor had a modest preference for large and bulky amino acids over smaller ones, e.g., Val-Val was bound better than Ala-Ala which was bound better than Gly-Gly. However, this trend in affinities most likely just reflects the overall hydrophobic character of the corresponding dipeptides.

In continuation of this rational design approach we synthesized an artificial receptor that was specifically designed to bind alanine-containing anionic dipeptides, which are of considerable biological relevance. For example, the natural antibiotic vancomycin recognizes the bacterial dipeptide sequence D-Ala-D-Ala very efficiently ($K_{\text{ass}} \sim 10^6 \text{ M}^{-1}$) [28, 37]. This dipeptide sequence is part of the peptidoglycan and plays an important role in bacterial cell wall maturation. The mode of action of vancomycin has been the subject of many studies and the noncovalent interactions involved in complex formation have been analyzed in detail [39, 40]. Unfortunately, vancomycin-resistant bacterial strains have emerged in the last 10 years caused by a substitution of the C-terminal D-alanine by D-lactate, resulting in a 1000-fold decrease in affinity and therefore ineffective antibiotic activity of vancomycin. For the identification of an artificial receptor able to recognize these peptide/depsipeptide sequences, various combinatorial libraries as well as otherwise developed receptors have been employed with more or less success [41, 42]. Some examples will be discussed later on.

In our approach to a selective receptor for this dipeptide we used molecular modeling calculations and assembled different building blocks *in silico*. The resulting receptors were then checked for their complementarity to the dipeptide D-Ala-D-Ala. The most promising candidate was receptor 2 (Fig. 2), which consists of two major building blocks: a carboxylate binding site attached to an aromatic cavity. As the binding site for the dipeptide's carboxylate we used again the cationic guanidiniocarbonyl pyrrole moiety

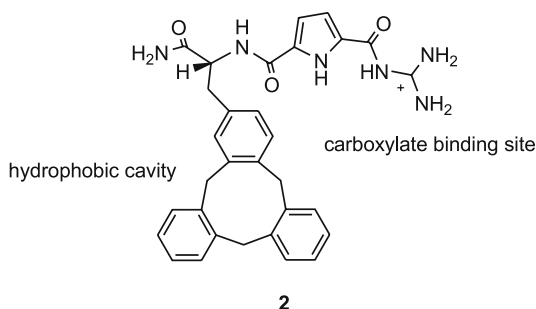


Fig. 2 An artificial receptor **2** with preference for alanine-containing anionic dipeptides

mentioned before. To mimic at least a part of the aromatic cavity formed by vancomycin's several aromatic rings we chose a cyclotriphenylene unit. This moiety consists of a hydrophobic bowl which is just large enough to accommodate a methyl but not any other alkyl group [43, 44], hopefully providing the selectivity for alanine. Molecular mechanics calculations (vide infra) predicted that receptor **2** should be able to preferentially bind dipeptides with an N-terminal alanine. The binding studies confirmed that receptor **2** is indeed able to strongly bind the dipeptide D-Ala-D-Ala in buffered water with an association constant of $K_{\text{ass}} = 33\,100\text{ M}^{-1}$, and even more important selectively over other dipeptides such as D-Val-D-Val ($K_{\text{ass}} < 1000\text{ M}^{-1}$).

Molecular modeling studies are consistent with the idea of this rational approach and can explain the results of the experiments. The obtained complex structure is shown in Fig. 3. The dipeptide is bound in a conformation which allows for ion pairing with the guanidinium cation of receptor **2** and H-bond formation between the backbone amides. Furthermore,

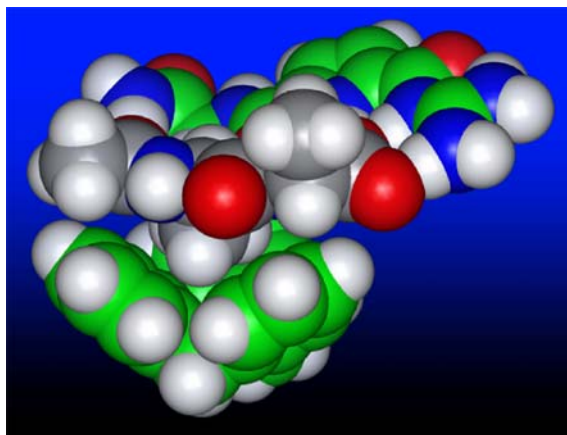


Fig. 3 Energy-minimized structure for the complex between receptor **2** (green) and the dipeptide D-Ala-D-Ala (gray)

the N-terminal methyl group is directly situated above the cyclotribenzylene bowl. This should allow for favorable hydrophobic interactions between those two groups in water.

However, the rational, structure-based design methods that have proven so useful in making receptors for small substrates are not yet up to the task of designing more challenging host molecules. So how are we to approach the next step of making synthetic molecules that behave like real biological receptors? One of the main differences between host molecules synthesized by chemists and biological receptors (e.g., antibodies) is often the size and complexity of the substrates these molecules bind. However, the larger the substrate or host, the more difficult the design gets, as theoretical calculations are not yet reliable enough to completely create a tailor-made artificial host for a large substrate. Also, the syntheses of such large molecules can become challenging. Another possibility is to use a random trial and error approach based on rather small molecules and to identify suitable receptors with the help of combinatorial chemistry. This will be described in the following section.

2.2

Combinatorial Receptor Finding

The general concept of combinatorial libraries, as first developed for peptides [45, 46], involves the generation of all possible sequence permutations for a peptide of a given length in connection with a subsequent screening and selection process that enables the identification of unique, highly active peptides in the presence of inactive peptides, i.e., in terms of binding activity to a certain target. For this identification of active ligands for syn-

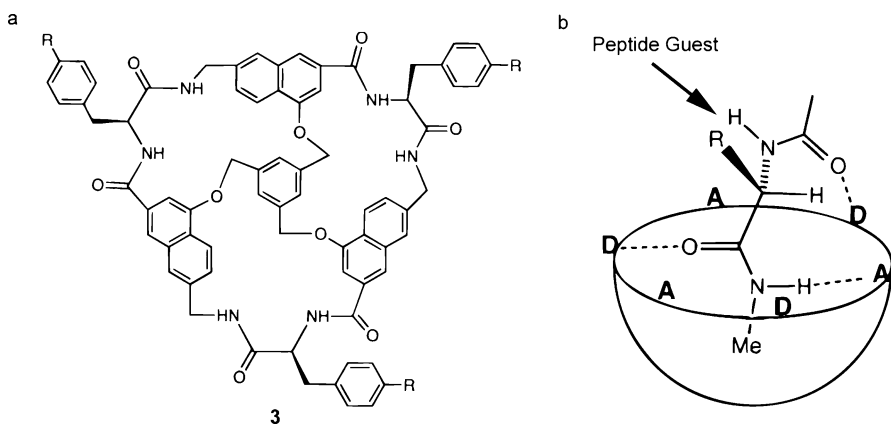


Fig. 4 Peptide receptor 3 by Still, providing a binding pocket with several hydrogen-bond donors (D) and acceptors (A)

thetic receptors, Still and coworkers originally introduced small molecules covalently attached to lipophilic dyes to screen encoded combinatorial libraries in organic media, and identified beads carrying molecules interacting with these conjugates by their color change [47, 48]. The synthetic receptors (Fig. 4) had little conformational flexibility according to molecular mechanics. The most stable conformations were characterized by deep binding cavities with peripheral arrays of hydrogen-bond donors and acceptors ideally situated for the interaction with H-donor/acceptor sites in substrates such as small peptides.

The applications of combinatorial methods in supramolecular chemistry have expanded since the pioneering work by Still and coworkers to include proteins [49, 50], synthetic oligomers [51], small molecules [52, 53], or oligosaccharides [54], as well as host and guest libraries. However, we will focus in the following on combinatorial approaches to find artificial receptors for peptides.

2.2.1

Split and Mix Approach

The majority of immobilized libraries reported use a resin as solid support and the split and mix method [55, 56], generating one-bead-one-compound libraries [57]. Combinatorial libraries prepared via this approach contain only one single library member, which in the case of a peptide library corresponds to one sequence of amino acids on a single 100- μm -diameter bead. The result of such a split synthesis is a collection of beads, each containing one specific peptide sequence consisting of every possible combination of every amino acid used in the synthesis. Figure 5 illustrates the fast and easy synthesis of a combinatorial library with 27 different products from three different building blocks, in only three steps requiring only nine individual reactions. One problem of this approach is, however, that it is only applicable to the synthesis of sequenceable oligomers.

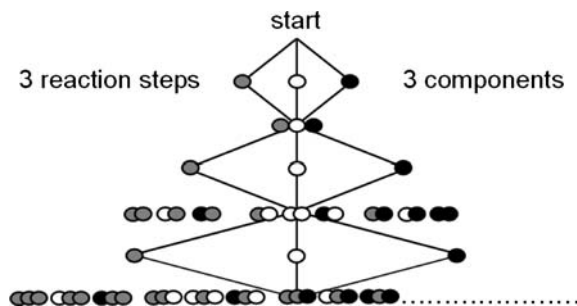


Fig. 5 Schematic representation of the split and mix approach: three components react in three consecutive steps to give $3 \times 3 \times 3 = 27$ different products

These libraries are then typically screened in a solid-phase assay, which is based on the selection of positively reacting resin beads, followed by analysis of the compounds attached to those “active” beads. In this way active library members can be qualitatively identified, for example by some color change as shown by Still and coworkers. However, the main problem of such one-bead-one-compound libraries is the low loading of the resin. One bead carries only approximately 100 pmol ($\sim 10^{13}$ molecules) of each library member. While that quantity is adequate for modern Edman sequencing of small peptides, it is generally too little for any other spectroscopic technique or analytical method. Hence, the identity of the active library members as seen in those screening assays is difficult to establish, especially when it comes to libraries of non-peptides, which cannot be analyzed by Edman degradation. Therefore, unique chemical tags to encode the structure of the library compound on each resin bead were developed [58], which can then be decoded by sequencing or some other analysis, for example, gas chromatography or high-performance liquid chromatography (HPLC). In principle, almost any type of molecule can be used as a tag. However, there are practical limitations because tags need to be chemically inert and reliably analyzed on femtomolar scales from a single bead. But even then, the problem remains that the screening of the library and the subsequent decoding is tedious and challenging, and in most cases provides only indirect answers to the identity of the library member under study.

2.2.2

Large and Random Libraries

One of the first attempts to prepare synthetic receptors for peptide ligands was based on tweezer receptors which, despite their inherent flexibility, have proven to be highly selective for certain peptide sequences in both nonpolar [59–62] and aqueous solvent systems [63–65] (Fig. 6).

Kelly was the first to synthesize successfully such a tweezer receptor in solution, even though not using a combinatorial approach. The design was

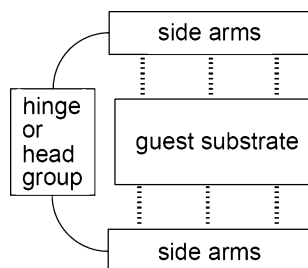


Fig. 6 Schematic representation of a tweezer receptor with head group and side arms providing a “binding pocket” for suitable guest substrates

based on a dibenzofuran scaffold with two side arms with alternating hydrophobic and basic amino acids. The aim was to get strong noncovalent interactions by hydrogen bonding between the substrate and the peptidic backbone of the receptor (Fig. 7). In tests for binding activity the receptor was able to bind the tetrapeptide Suc-Glu-Leu-Glu-Leu-NH-Bn in water with a binding constant of $4.9 \times 10^2 \text{ M}^{-1}$ [66, 67].

For the specific recognition of the C-terminus of a peptide, Kilburn et al. improved the binding activity of tweezer receptors by incorporation of a guanidinium head group (carboxylate binding site, CBS). They synthesized combinatorial libraries of such two-armed tweezer receptors, based on a bis(aminoalkyl)guanidinium scaffold. However, these libraries had limited diversity; this is because both arms of the receptor are synthesized simultaneously on the solid support, which leads to a library of 2200 symmetrical tweezer receptors each containing two arms with an identical amino acid sequence [68].

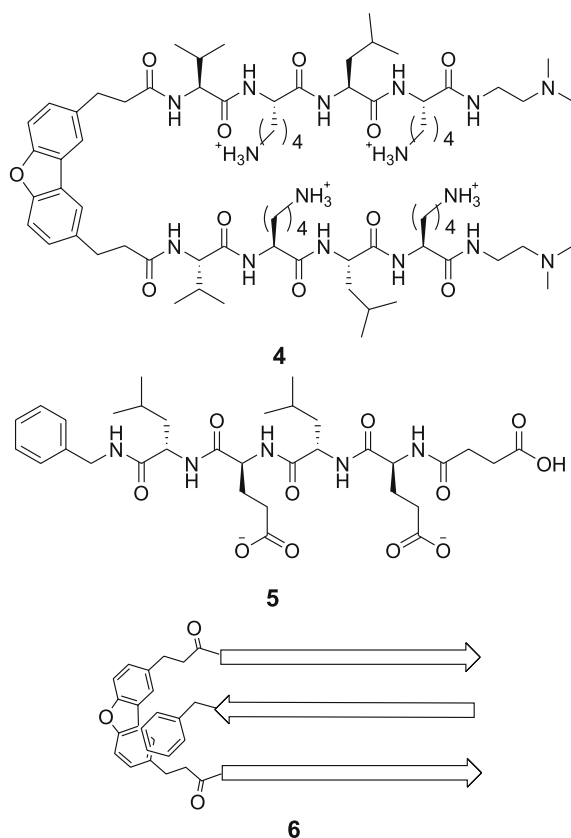


Fig. 7 Tweezer peptide receptor (4) and substrate (5) used by Kelly and a schematic representation of complex formation (6)

This library was then screened, in aqueous solvent, to identify a selective receptor for the dye-labeled tripeptide Glu(OtBu)-Ser(OtBu)-Val (Fig. 8). The receptor with the best binding affinity (AA¹-AA²-AA³: L-Pro-L-Leu-L-Met) was then resynthesized in solution. Subsequent screening experiments were carried out using an aqueous buffer solution (pH 9.2 with 15% DMSO) and showed a high binding activity of $K_{\text{ass}} = 8 \times 10^4 \text{ M}^{-1}$ for the protected substrate **8** [69]. However, the less hydrophobic substrate, the side-chain deprotected analogue **9**, showed no binding, which under these conditions is in good agreement with the importance of hydrophobic effects in polar solvents. Furthermore, no binding was observed for the screening of the library against the dye-labeled dipeptide sequence D-Ala-D-Ala.

Extending this work, Kilburn and coworkers just recently reported on the screening of a large combinatorial library of tweezer receptors (> 15 000 members) for the binding of the tripeptide *N*-Ac-L-Lys-D-Ala-D-Ala [70]. For the synthesis of this large library, they developed two routes to unsymmetrical tweezer receptors (**10**) using two different strategies with a careful use of orthogonal protecting groups. The first strategy was the successive preparation of each peptide arm by split and mix synthesis of Boc- and Fmoc-protected

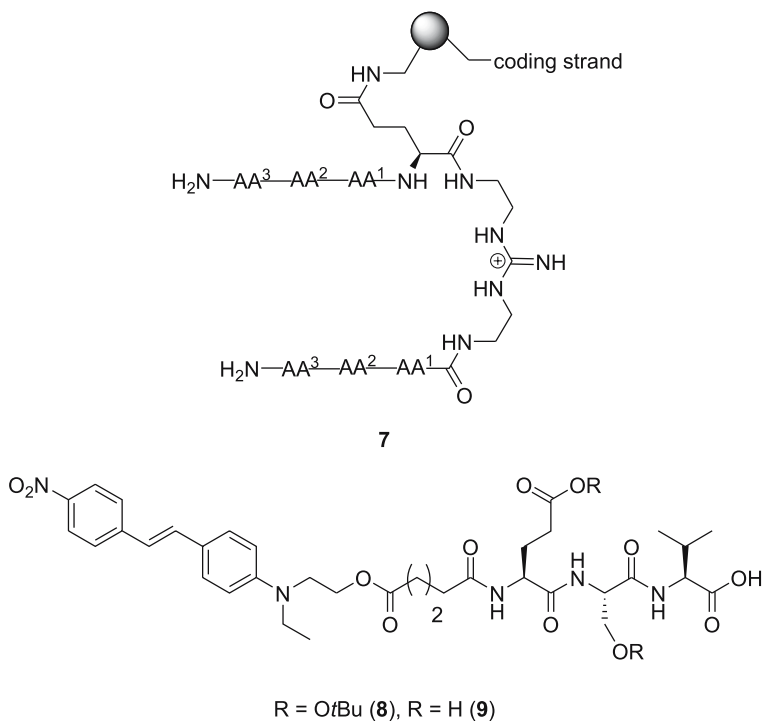


Fig. 8 Combinatorial library **7** of tweezer receptors derived from a guanidinium scaffold to identify a selective receptor for dye-labeled Glu(OtBu)-Ser(OtBu)-Val (**8**).

amino acids, respectively (Fig. 9). They restricted the choice of amino acids in each arm to avoid any ambiguity as to which arm the respective amino acid originates from. That is necessary because during the identification process of the final Edman sequencing two amino acids, one of each arm, are cleaved at the same time. Hence, the choice of amino acids used in the first position (AA^1) of the first arm must differ from the first position (AA^4) of the second arm. The same holds for the second and third positions (Fig. 9).

An alternative approach was the attachment of a separate coding strand on the beads composed of the same amino acids as used for both arms (Fig. 10). In addition, phenylalanine was introduced in the coding strand as a useful check that the library synthesis and the sequencing chemistry have worked efficiently. Its only function is the confirmation of the accurate peptide synthesis and the subsequent analysis of the peptide composition. For every bead the last amino acid during the Edman degradation must then be phenylalanine. If not, this indicates a problem in the synthesis of one of the two peptide arms.

These large libraries were screened in aqueous buffer (pH 8.5, borate) with the dye-labeled tripeptide *N*-Ac-Lys-D-Ala-D-Ala, using a qualitative binding assay by the observation of stained beads, visualized under a microscope. Some receptors with high binding affinity were identified and the most promising one was then resynthesized and studied in more detail. Binding with low-millimolar affinities was found for two diastereomeric tripeptides

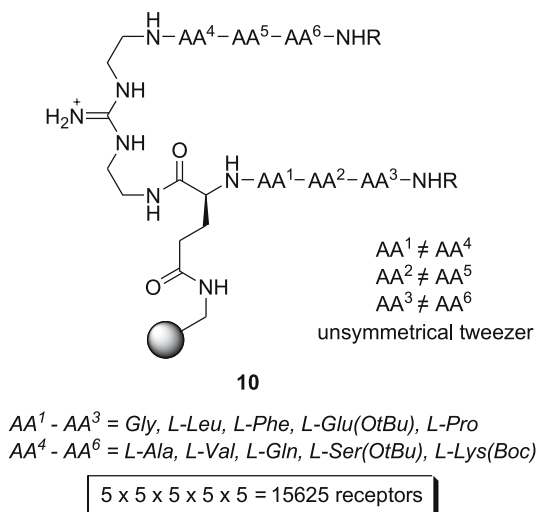


Fig. 9 Two-armed tweezer receptor library 10 with a guanidinium head group as a carboxylate binding site for the binding of D-Ala-D-Ala-OH in aqueous solution. The arms are synthesized sequentially to give a structurally more diverse library of unsymmetrical receptors

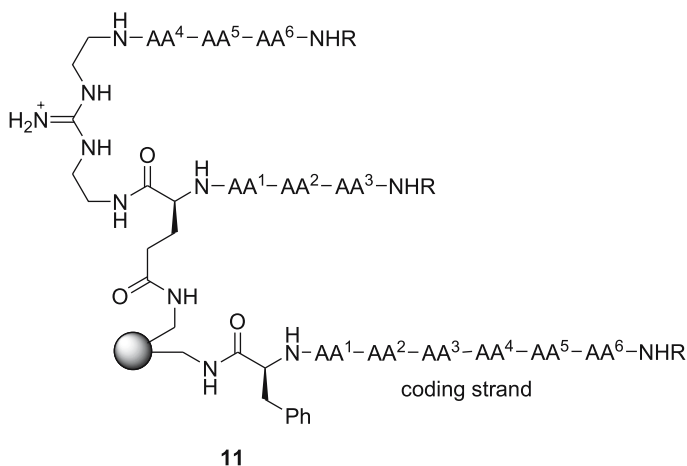
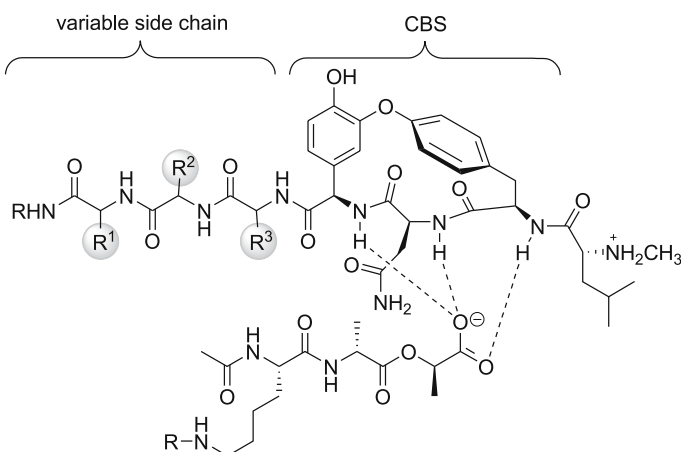


Fig. 10 An additional heptapeptide coding strand allows the synthesis of tweezer receptors 11 with unsymmetrical arms, the sequence of which can be determined via Edman degradation of that coding strand

with the resin-bound receptor, but no binding data in free solution could be obtained [70]. This shows the limits of large libraries. Positive hits can only be selected qualitatively and have to be resynthesized on a bigger scale for further analysis.

The group of Ellman pursued an even more tailor-made approach in the synthesis of a receptor library specially designed for the recognition of a certain peptide substrate [71]. The aim was the identification of synthetic receptors that bind with high affinity to *L*-Lys-*D*-Ala-*D*-Lac to provide a future strategy for overcoming vancomycin resistance. Therefore, the design of the library was based on the biological role model mimicking its binding site. Ellman tried to preserve the carboxylate binding pocket of vancomycin in order to retain a significant element of the hydrogen-bonding network and hydrophobic interactions that are common to the *D*-Ala-*D*-Ala and *D*-Ala-*D*-Lac complexes. The other part of vancomycin was replaced with a variable tripeptide unit (Fig. 11). The amino acid side chains and the stereochemistry in the tripeptide unit were then combinatorially varied and the resulting receptors selected according to their ability to bind the two model substrates.

A large library of 39 000 members was prepared by split synthesis with 34 amino acids used to introduce diversity at the R^1 , R^2 , and R^3 positions. The amino acids were selected mainly on the basis of proteinogenic amino acids; however, they also included a number of artificial amino acids to enhance the rigidity of the receptors. The best receptor had a binding activity of $100\,000\text{ M}^{-1}$ for the substrate *N*-Ac₂-Lys-*D*-Ala-*D*-Ala-OH, as determined by microcalorimetry, which is still a power of ten less than that of vancomycin. This receptor also showed reduced binding by a factor of 3 to the substrate



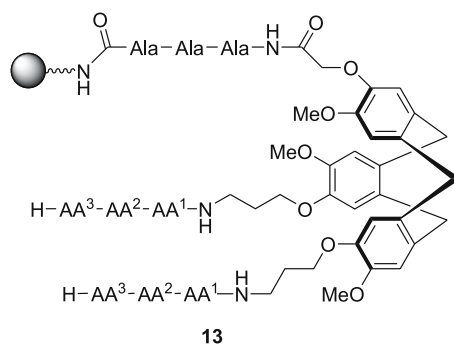
12

Fig. 11 Peptide receptor by Ellman; combinatorial library for the complexation of small peptides with a free carboxylate. The carboxylate binding site of the receptor is based on the antibiotic vancomycin

containing D-lactate, compared to the one with D-alanine. This small difference indicates a complexation event which is mainly based on ion-pair formation with the carboxylate and hence shows only sequence selectivity. The influence of the combinatorially varied side chain is obviously too small to induce a pronounced substrate selectivity.

For the same target type Liskamp reported the screening of a large combinatorial receptor library derived from a cyclotrimeratrylene (CTV) with three attached peptide arms for the binding of D-Ala-D-Ala and D-Ala-D-Lac, respectively [72]. Using a color-coded substrate a 2197-member library (13) of CTV-based synthetic tripodal receptors was screened in water with phosphate buffer (0.1 N, pH = 7.0) (Fig. 12). Efficient receptors could be identified qualitatively by picking active beads and subjecting them to Edman degradation. The best receptors could bind the dipeptide more efficiently than the related depsipeptide D-Ala-D-Lac. But no quantitative information on binding affinities or substrate selectivity was provided, due to the lack of macroscopic amounts of material as a result of the one-bead-one-compound strategy.

Wennemers went the opposite way to find good binding peptide receptors. She synthesized different receptors (14) based on a diketopiperazine scaffold with two peptide arms (Fig. 13). Combinatorial screening against a library of 25 000 tripeptides (15) revealed that these tweezer receptors bind short peptides with remarkable selectivities and binding affinities in the range of $k = 4800\text{--}24\,000\text{ M}^{-1}$ [73, 74]. However, the good binding is limited to organic solvents. The binding affinity of the diketopiperazine receptors in aqueous solutions is too low to allow good complexation for most substrates [75].



$AA^1 - AA^{13} = \text{Gly, Val, Ala, Pro, Leu, Ser, Phe, Tyr, His, Asp, Glu, Gln, Lys}$

$13 \times 13 \times 13 = 2197$ receptors

Fig. 12 Combinatorial library of 2197 different artificial tripodal receptors **13** based on a cyclotrimeratrylene (CTV) scaffold. Screening and Edman sequencing revealed peptide sequences which are either able to bind dye-labeled D-Ala-D-Ala or D-Ala-D-Lac-containing ligands

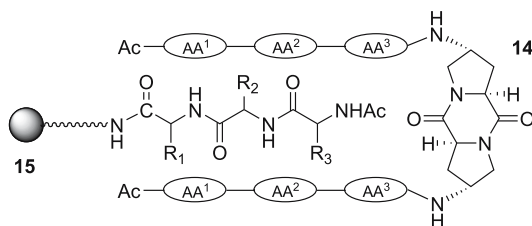


Fig. 13 Screening of several dye-marked diketopiperazine receptors (**14**) (AA^1 carries dye in the amino acid side chain) against an encoded side-chain-protected tripeptide library with 25 000 members (**15**)

However, all these approaches show the high potential of combinatorial libraries in supramolecular chemistry. Nevertheless, often the synthetic effort is far too high compared to the results obtained. This led to an increased interest in focused libraries, which will be discussed in more detail in the following section.

2.2.3

Small but Focused Libraries

Contrary to the expectations scientists had some years ago, that large libraries would cause the discovery of many hit and lead structures, the results of several studies pointed out that the biological relevance, design, and diversity of the library are more important than pure size. In recent years, the concept

of target-oriented synthesis (TOS) has been of increasing interest [76–78]. It is used in solid-phase syntheses aimed, for example, at drug discovery, in particular in syntheses of focused libraries, where collections of compounds with common structural features that facilitate binding to a preselected target are synthesized. For example, Waldmann recently suggested that the use of a biologically validated starting point for combinatorial libraries would significantly improve the hit rate. Natural products often embody privileged structures that can also evolve into binding to other proteins which are not their initial targets as well, and therefore may result in new lead compounds with enhanced quality [79].

The validity of this approach was demonstrated by Waldmann and Gianis et al. [80, 81], for example. Nakijiquinones are the only known naturally occurring inhibitors of the Her-2/Neu receptor tyrosine kinase, which is over-expressed in breast, ovary, and gastric carcinomas. In light of the concept described above, a library of 56 analogues of this lead structure was synthesized and the compounds were screened for their inhibitory activity against other receptor tyrosine kinases involved in cell signaling and proliferation. Whereas none of the already existing natural products (**16a–d**) exhibited significant inhibitory activity against the new set of receptor kinases, six members of the library of artificial analogues were identified as kinase inhibitors in the low micromolar range (**17–22**) (Fig. 14). This result stresses the importance of combinatorial libraries based on natural products, in contrast to using only the natural substances by themselves. If only natural substances had been screened, these inhibitors would have been missed.

However, it remains questionable whether the regions of chemical space defined by natural products and known drugs are really the best or most fertile regions to use as starting points for combinatorial chemistry. This question led to the concept of diversity-oriented synthesis (DOS) that included the development of pathways leading to the efficient (three- to five-step) synthesis of collections of small molecules having rich skeletal and stereochemical diversity with defined coordinates in chemical space, also mainly derived from known natural products. The systematic screening of this collection of compounds should advance the fundamental understanding of the roles these diversity elements play, for example in small molecule–protein interactions.

In such a focused combinatorial library the chances of finding a hit are much higher than in a completely random library, as the structural diversity is already positively biased for a given problem, e.g., binding to a specific target protein. Hence, it is sufficient to use much smaller libraries with only a couple of hundred of different members. This concept of small but focused libraries has already been applied successfully in pharmaceutical and medicinal chemistry [79]. We were interested to use the same approach of small but focused libraries also in the field of supramolecular chemistry for the discovery of artificial peptide receptors.

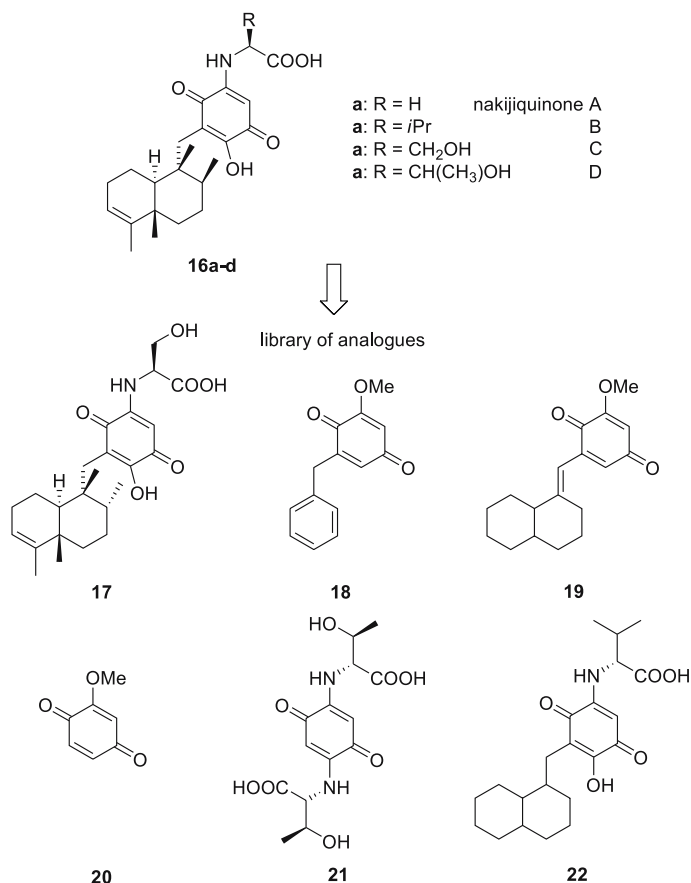


Fig. 14 Some members (17–22) of a 56-membered library of nakijiquinone analogues showed a significant inhibitory activity against a new set of receptor kinases

2.2.4

Spatially Separated Libraries

As already described above, the best way to find an artificial peptide receptor is most likely to combine a rational design approach with the power of combinatorial chemistry. Using such a combined approach, we recently described the screening of a medium-sized combinatorial library of fully flexible one-armed cationic peptide receptors (**23**) for the binding of tetrapeptides in water. The receptors of the library are composed of a carboxylate binding site attached to a variable tripeptide unit (Fig. 15). To ensure strong complexation in polar solvents, even for such a short β -sheet, the carboxylate binding site in the form of a cationic guanidiniocarbonyl pyrrole group was introduced. A combinatorial variation of the three amino acids in the receptor side chain

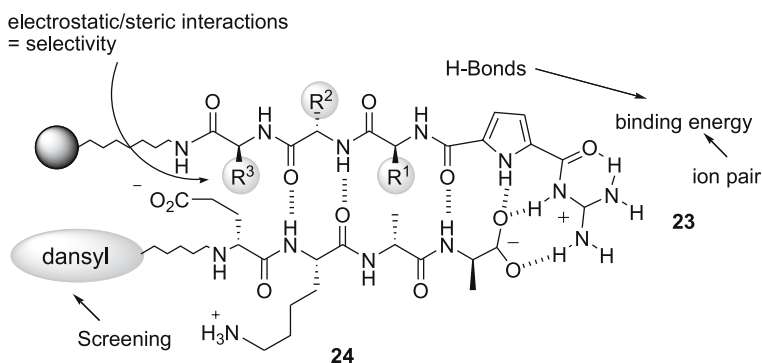


Fig. 15 Schematic representation of complex formation between the receptor library 23 and the dansylated tetrapeptide substrate 24

can then be used to identify receptors in which additional electrostatic and steric interactions between these side chains and the substrates further enhance the binding within the complex, and also render the recognition event selective for a specific tetrapeptide. As one of the first target peptides we chose the two tetrapeptides EKAA (24) and AAKE (25) [20]. As mentioned above, the EKAA tetrapeptide sequence (= D-Glu-L-Lys-D-Ala-D-Ala-OH) is interesting in terms of its relevance to bacterial cell wall maturation upon treatment with vancomycin, leading to bacteria death.

The receptor library was synthesized on Amino-TentaGel® as the solid support according to a standard Fmoc protocol using the split and mix approach (vide supra) in combination with the IRORI™ radio-frequency tagging technology [82–84]. The IRORI microreactors are miniaturized devices that contain both a functionalized solid support and a unique tag identifier (Fig. 16).

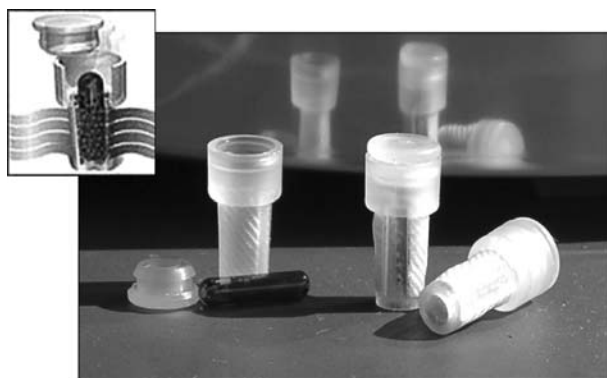


Fig. 16 The IRORI MikroKan® system with a loading of up to 30 mg resin per reactor. A radio-frequency chip inside allows the identification of the resin-bound peptide sequence.

The radio-frequency tagging technology operates with a radio-frequency chip fused in a glass mantle. A unique binary code on every chip allows read-out with a scanning station. Thus, each reactor is “tagged” with a unique ID which makes it possible to determine the synthesized product in every step of the preparation.

The cans are designed to be loaded with up to 30 mg of resin beads. That allows the spatially separated synthesis of some micromoles of each library member (compared to only some picomoles using the classical one-bead-one-compound approach). This is enough material of each library member for advanced qualitative and quantitative experiments on binding activity. The synthesis takes place as reagents flow through the outer mesh walls of the microreactors using normal laboratory glassware. A further advantage of this system is that the number of necessary synthesis steps can be kept at a minimum, compared to bigger libraries requiring an additional chemical tagging in every step [85]. (The “teabag” method is an alternative approach for spatially separated libraries [86, 87].) Only the actual building blocks of the receptor have to be attached to the resin. No further tagging reaction is required. There is no need for any coding strands or chemical markers. However, the maximal number of library members is limited in a normal chemistry laboratory to approximately 1000, compared to libraries with several tens of thousands of members or more using chemical tagging, due to higher demands on time and costs. During the synthesis of the receptor library **23** the following eight different amino acids were used in each of the three coupling steps: Lys, Tyr, Ser, Glu, Phe, Val, Leu, and Trp giving rise to a library with 512 different members. These specific amino acids were carefully chosen among the proteinogenic amino acids to provide a representative range of varying polar, charged, and hydrophobic residues within the final receptor library.

The advantage of such a small and focused solid-phase bound combinatorial receptor library is, besides the fast and time saving synthesis, that the whole library can be tested for a specific feature, in this case its binding properties toward the tetrapeptide substrate, in a single experiment (Fig. 17). For this purpose a fluorescent label in form of a dansyl group was attached via a water-soluble spacer to the N-terminus of the tetrapeptide substrate. To probe the entire receptor library qualitatively for its binding properties, aliquots of the 512 resin-bound deprotected receptors **23** were pooled and the combined mixture incubated with a 5 μM solution of the tetrapeptide substrate in 20 μM Bis-Tris buffer of pH 6.0 in water. After the supernatant solution was washed off, the beads were screened under UV light using a fluorescence microscope. Selective binding of the tetrapeptide substrate by some—but not all—of the 512 receptors **23** can be observed, as indicated by the strong fluorescence activity of individual beads. Only those beads on which the attached receptor is able to bind the peptide can show the characteristic fluorescence of the dansyl group. All the other receptors which do

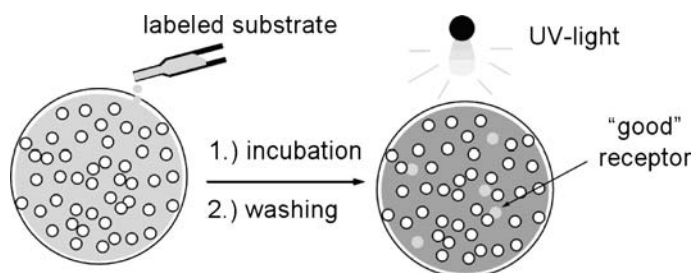


Fig. 17 Qualitative on-bead assay for the identification of “active” receptors within the library

not bind the peptide under the specific experimental conditions remain dark (Fig. 18).

Based on this qualitative screening it is also possible to determine the binding constants of all library members in an on-bead assay quantitatively using a high-throughput microtiter plate reader [88–90] (Fig. 19). From the fluorescence intensity of the substrate in solution before and after incubation and the loading of the resin the association constants for each receptor can be calculated. Of course, the resin does influence the binding constants compared to the situation in free solution. There might also be some remaining uncertainties due to irregularities in the quality of the resin and problems with the exact determination of resin loading. But in general *relative* binding data for each library member can be obtained quite reliably as these effects are similar for all library members. Using this technique the binding affinities within the library for tetrapeptide 24 (EKAA) were found to vary from

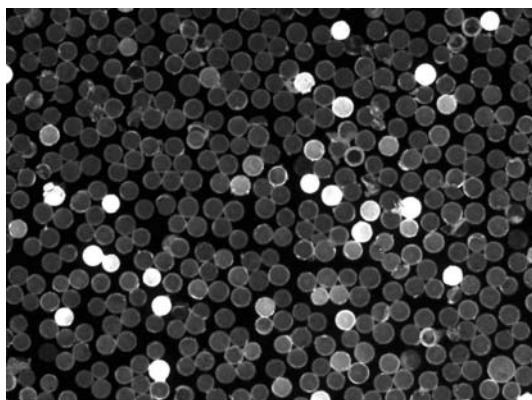


Fig. 18 Incubation of the solid-phase bound receptor library with a fluorescence-labeled substrate reveals a selective interaction with only some substrates within the library, as indicated by the high fluorescence intensity of individual beads

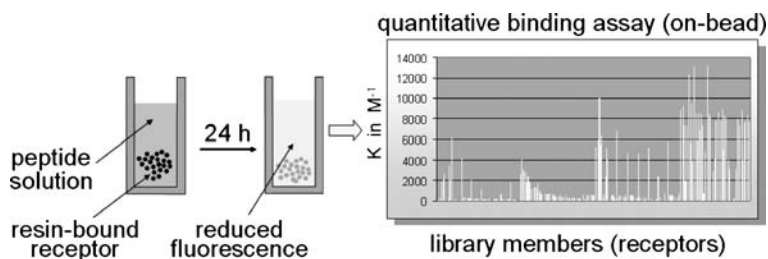


Fig. 19 Determination of binding constants on-bead from a quantitative screening of all library members

$K_{\text{ass}} = 17\,000\text{ M}^{-1}$ for the best (CBS-KKF) to $< 20\text{ M}^{-1}$ in buffered water for the worst receptors. Hence, a difference in activity of more than two orders of magnitude! For such a structurally closely related library of necessarily limited diversity this represents a remarkable selectivity. The binding of 25 (AAKE) is somewhat less efficient ($K_{\text{ass}} = 6000\text{ M}^{-1}$ for the most efficient receptors). In all experiments the binding data obtained from the solid-phase screening could be validated by complexation studies of resynthesized receptors in free solution with NMR and UV titration experiments. Hence, much more information is obtained for each library member compared to the traditional approach. Not only is a qualitative yes/no answer provided, but also real quantitative data that can be further analyzed and interpreted in detail.

Even though such binding constants determined on a solid support are not the same and in general are less accurate than data obtained in solution, a comparison of relative data within a series of related receptors can at least help rationalize aspects such as complex structure, stability, and selectivity on a molecular basis. One can identify structural features that are associated with strong or weak binding. Which parts of our modular receptors are most important for binding or selectivity? What kind of binding sites, electrostatic or hydrophobic, in the various positions of the receptor are needed? In other words a supramolecular structure–binding relationship can be derived from binding data obtained on a solid support. This is not possible from the pure qualitative screening of large random libraries, as discussed above.

A good example is the formation of a β -sheet-like complex between the tetrapeptide Ac-Val-Val-Ile-Ala-OH and the receptor Gua-Lys(Boc)-Ser(*O**t*Bu)-Phe, as recently reported by us [22]. This tetrapeptide represents the C-terminal part of the amyloid- β -peptide ($A\beta$) responsible for plaque formation in Alzheimer's disease. Especially, hydrophobic interactions to this tetrapeptide sequence are thought to promote the self-aggregation of the 42 amino acid long $A\beta$. Our quantitative screening of a combinatorial receptor library did indeed show a high preference for a hydrophobic Lys(Boc) in a certain position enabling hydrophobic interactions with the first (Val) and third (Ile) amino acids of the tetrapeptide according to modeling studies. The *t*Boc

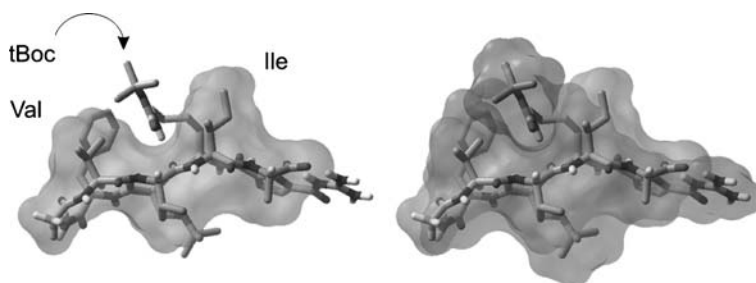


Fig. 20 The *t*Boc group of the lysine side chain of the receptor fits nicely into the hydrophobic gap between the first (Val) and third (Ile) side chain of the substrate, leading to high binding affinity due to hydrophobic interactions

group is placed between these two side chains of the substrate, thereby closing the hydrophobic gap in between. This minimizes the solvent-accessible surface (Fig. 20) and therefore stabilizes the complex. A similar hydrophobic interaction has been predicted, based on molecular mechanics calculations, to play a significant role in the native system [91].

This work shows the high potential of small and focused libraries in combinatorial chemistry, i.e., for identifying structural features responsible for high binding activity. Without also the quantitative binding data of the bad receptors this analysis would have not been possible. This kind of structure–activity correlation is not obtainable with the use of large one-bead-one-compound libraries where you get only a binary yes or no answer.

2.2.5

QSAR Analysis

However, when using such small libraries of only a couple of hundred members the question remains of whether the size of the initial library is sufficient to provide significant results. In other words, does a small library really provide the best possible receptor, or are the results suboptimal due to the fact that the library simply did not contain the correct diversity for the given problem? We could answer this question by corroborating the results obtained for the binding affinities of our flexible receptors for the tetrapeptide EKAA by an additional statistical analysis [21]. Quantitative structure–activity relationships (QSAR) correlate properties of the chemical structures under scrutiny to their activity with a mathematical model. The latter can be used to detect patterns and trends in the data. Moreover, it can be used to make predictions for compounds not yet synthesized. We fitted a model based on 49 diverse physical–chemical descriptors for each amino acid in each of the three variable positions in the receptor to the quantitative binding data obtained from the library screening. A plot of the experimental $\log(K_{\text{ass}})$ values versus the cross-validated predictions of $\log(K_{\text{ass}})$ is shown in Fig. 21, underlining the

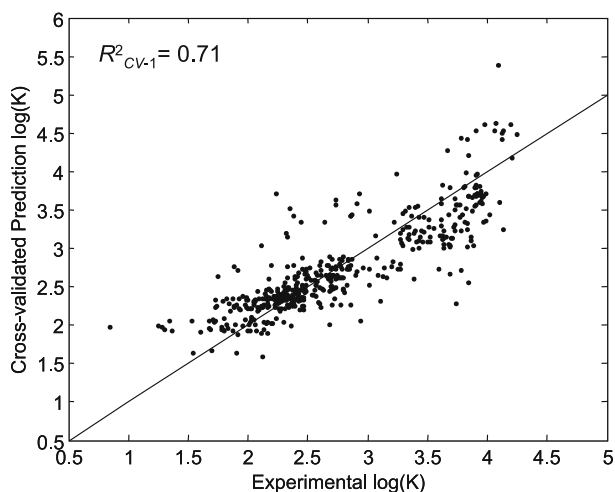


Fig. 21 Mathematical QSAR model correlating experimental vs predicted $\log(K_{\text{ass}})$

good quality of the fit. The mathematical model thus obtained was then used to predict the binding affinities of all possible tripeptide sequences in such a receptor, which can be obtained by permutation from all the 20 proteinogenic amino acids (library size $n = 8000$ members). This virtual library is 15 times larger than the initial experimental library of 512 receptors that we used for our screening. Out of the 7488 virtual receptors not yet synthesized, there were only 16 receptors that were predicted to bind better to the tetrapeptide EKAA than the most active receptors in our small library. However, the binding affinities are all in the same range and are not significantly larger than the ones already synthesized and analyzed. Therefore, the initial library size was completely sufficient to fully explore the chemical space for the given problem, the binding to this specific peptide target. An actual combinatorial synthesis of this much larger 8000-member library would not have paid off and would have required an unnecessary use of time and money. Hence, if the library is correctly designed for the question under study, small but focused libraries can provide the same results as much larger but random libraries. In contrast to the large libraries, the smaller libraries have the advantage that a full quantitative analysis of all library members is possible. This provides an additional wealth of information otherwise not obtainable.

2.2.6

Insights into Structure and Reactivity

A good example of the additional benefit that the information from the quantitative analysis of a whole library can provide is demonstrated in the follow-up work on an artificial peptide receptor, which shows not only significant

substrate selectivity but also a remarkable sequence-dependent stereoselectivity. An artificial receptor (CBS-KKF), which in other experiments showed high affinity to the peptidoglycan model peptide D-Glu-L-Lys-D-Ala-D-Ala-OH (vide supra), was further examined in a fluorescence screening against a combinatorial substrate library of 320 closely related tetrapeptides to get more information about its binding activity [92]. The substrates presented only three different side chains (Ala, Lys, and Glu) and differed only in the absolute configuration of one building block (D/L-Ala) or one chemical linkage (Ala vs Lac). The screening showed binding constants from $< 50 \text{ M}^{-1}$ up to $27\,000 \text{ M}^{-1}$ for the best substrate. These are already considerable differences for a library of such a moderate size. The quantitative evaluation resulted in a preference for substrates with anionic amino acids, as expected for a tris-cationic receptor. What was not expected, and would have been simply overlooked in a traditional combinatorial approach using the simple qualitative screening of a large library, was the sequence-dependent stereoselectivity of the receptor. The receptor showed a pronounced stereoselectivity between D- and L-alanine as well as a remarkable selectivity between D-alanine and D-lactate, *but only at certain positions within the complex*. This could be explained based on the conformational flexibility of the complex. Stereoselectivity requires a rather well defined complex structure, and is only possible when the position where the D-Ala/L-Ala exchange takes place is fixed at both sides by strong charge interactions between receptor and sub-

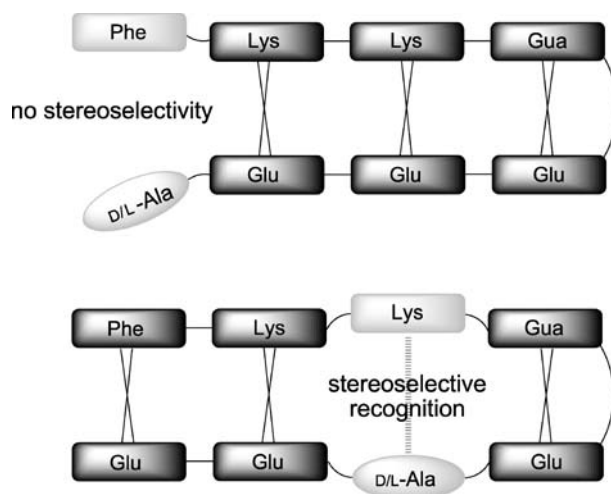


Fig. 22 Screening of a small focused library revealed a remarkable stereoselectivity between D-Ala and L-Ala, but only in certain sequences which allow the formation of overall well-defined complexes. This unexpected stereoselectivity is only observed when the position where the D-Ala/L-Ala exchange takes place is fixed *at both sides* by strong electrostatic interactions between receptor (*top*) and substrate (*bottom*)

strate. No stereoselectivity is observed, for example, when the alanine is in the N-terminal position (Fig. 22).

The results described above underline the potential of fully analyzable small libraries compared to large libraries resulting only in “yes or no” hits. This alternative approach allows for a fast and economic way to identify, e.g., potent receptors for a given target by using small but carefully composed combinatorial libraries. Hence, the pure size of a combinatorial library is not decisive for the outcome of the screening as long as the library contains the correct range of diversity for the given problem. Of course, the limited structural diversity of a small library requires careful design to provide the correct diversity needed to answer a certain question. But if composed correctly, a small but focused library can be as informative as a large but random library. It is not the pure size but the diversity that counts after all.

2.3

Dynamic Combinatorial Chemistry

Traditional combinatorial chemistry is based on libraries of prefabricated molecules synthesized by the essentially irreversible making and breaking of covalent bonds. Hence, the composition of the library is determined after its synthesis and before any screening or further study is performed. In contrast to this covalent approach, dynamic combinatorial chemistry relies on the reversible connection of building blocks to give access to libraries whose composition is not yet fixed but can change in response to its surroundings. If bond formation is reversible the library can rearrange, governed by the thermodynamics of the whole molecular ensemble [93–96]. For example, if a target molecule is added to such a dynamic library, the composition of the library will reequilibrate until the new thermodynamic minimum is reached. This can lead to an amplification of host molecules with high affinity to the added target molecule. Hence, the presence of a guest molecule induces the formation of an appropriate host molecule within the library. This approach has not yet been applied to identify peptide receptors, but other substrates such as inorganic anions have been used.

For example, Kubik and Otto applied this approach to optimize the anion affinity of bis(cyclopeptide) receptors (Fig. 23) [97]. They synthesized cyclopeptide dimer **26a** as starting material, which allowed them to employ disulfide exchange for the preparation of a dynamic combinatorial library. Disulfide exchange is a reversible reaction especially well suited to aqueous solution. Dimer **26a** was equilibrated with different dithiols (**26a–c**) in 33% H₂O/CH₃CN at pH 8–9. Under these conditions, a dynamic library was formed containing potential receptors in which two cyclopeptide rings are separated by different dithiol-derived spacers, or a combination of two or more spacers [97]. Adding different anions (i.e., iodide, bromide, sulfate) to this mixture led to the amplification of different bis(cyclopeptides). There-

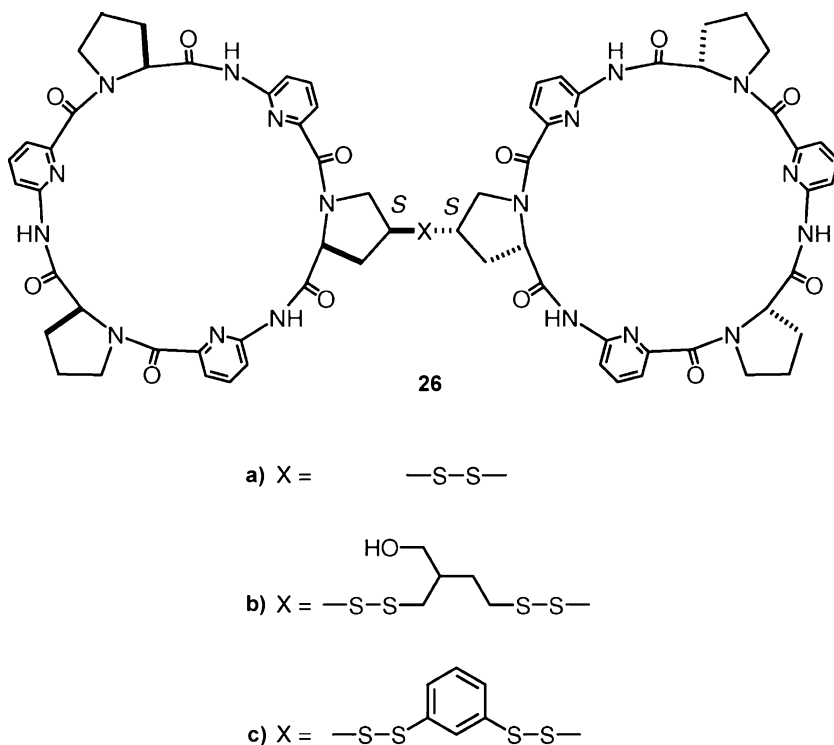


Fig. 23 Cyclopeptide dimers with variable disulfide-based linker can be used for the preparation of dynamic combinatorial libraries to recognize selective small anions

fore, the complex stability depends on the structure of the linker with which the two receptor moieties are connected.

However, there are several limitations of dynamic combinatorial chemistry, like the need for sufficient solubility of every single library member, the lack of suitable reversible chemistry, and the low level of reaction control. For example, nowadays most dynamic libraries are based on reversible chemistry such as imine or disulfide formation. This of course limits the scope of molecules that can be used to build a dynamic combinatorial library. Furthermore, it was recently shown with both theoretical simulations [98, 99] and by experiments [100, 101] that it is not necessarily the host with the highest affinity to a given target that is amplified the most within the library. Statistical reasons can demand the amplification of hosts with lower affinity. Nevertheless, even though the research in the field of dynamic combinatorial chemistry is still in an early stage, this technique makes a promising addition to the set of combinatorial methods. The next few years and the advent of more versatile reversible chemistry will surely reveal the full applicability of this approach.

3 Conclusion and Perspectives

We have demonstrated in this chapter that combinatorial chemistry is nowadays also a valuable tool in supramolecular chemistry. The screening of receptor libraries for binding of a given substrate has become a powerful method to identify selective artificial receptors for a variety of different substrates. Starting from large and random libraries, which can only be analyzed qualitatively, in recent times the focus has shifted more and more toward small and focused libraries that are specifically designed for a certain problem. This not only reduces the time and effort for synthesis and screening of the library, but also allows quantitative studies of the whole library (at least in cases where spatially separated libraries are present). In this way structure–activity relationships can be established which provide a much deeper insight into the supramolecular problem under question than the qualitative screening of large but random libraries. However, careful design of the library for each scientific problem is required. Since this new approach has now been validated for the finding of peptide receptors, we will most likely see a more extensive use of small but focused libraries in supramolecular chemistry in the future. The development of dynamic combinatorial chemistry for broader applications (e.g., in terms of reversible chemistry that can be used) will then surely provide the next significant methodological improvement in supramolecular chemistry. But as with any method, combinatorial approaches are just one among several others. As useful as they are, they also have their limitations and drawbacks. The clever use of all existing methods is still the best way to approach a scientific question.

References

1. Takeuchi I, Lauterbach J, Faselka MJ (2005) *Mater Today* 8:18
2. Koinuma H, Takeuchi I (2004) *Nat Mater* 3:429
3. Xiang XD, Sun X, Briceno G, Lou Y, Wang KA, Chang H, Wallace-Freedman WG, Chen S, Schultz PG (1995) *Science* 268:1738
4. Tietze FL, Rackelmann N, Sekar G (2003) *Angew Chem Int Ed* 42:4254
5. Hoveyda AH (1998) *Chem Biol* 5:R187
6. Krattiger P, McCarthy C, Pfaltz A, Wennemers H (2003) *Angew Chem Int Ed* 42:1722
7. Berkessel A (2003) *Curr Opin Chem Biol* 7:409
8. Sweeney MC, Wavreille AS, Park J, Butchar JP, Tridandapani S, Pei D (2005) *Biochemistry* 44:14932
9. Halkes KM, St Hilaire PM, Crocker PR, Meldal M (2003) *J Comb Chem* 5:18
10. Dolle RE (2001) *J Comb Chem* 3:477
11. van Regenmortel MHV (2000) *J Mol Recognit* 13:1
12. Schmuck C, Geiger L (2004) *J Am Chem Soc* 126:8898
13. Schneider HJ (1993) *Angew Chem Int Ed Engl* 32:848
14. Pecuh MW, Hamilton AD (2000) *Chem Rev* 100:2479

15. Srinivasan N, Kilburn JD (2004) *Curr Opin Chem Biol* 8:305
16. Galán A, Andreu D, Echavarren AM, Prados P, de Mendoza J (1992) *J Am Chem Soc* 114:1511
17. Hossain MA, Schneider HJ (1998) *J Am Chem Soc* 120:11208
18. Kelly JW, LaBrenz SR (1995) *J Am Chem Soc* 117:1655
19. Kelly JW, Kaul R, Angeles AR, Jäger M, Powers ET (2001) *J Am Chem Soc* 123:5206
20. Schmuck C, Heil M (2006) *Chem Eur J* 12:1339
21. Schmuck C, Heil M, Scheiber J, Baumann K (2005) *Angew Chem Int Ed* 44:7208
22. Schmuck C, Heil M (2003) *Chembiochem* 4:1232
23. Wright AT, Anslyn EV (2003) *Org Lett* 6:1341
24. Mizutani T, Wada K, Kitagawa S (2002) *Chem Commun* 1626
25. Rensing S, Schrader T (2002) *Org Lett* 4:2161
26. Sirish M, Schneider HJ (1999) *Chem Commun* 907
27. Davies M, Bonnat M, Guillier F, Kilburn JD, Bradley M (1998) *J Org Chem* 63:8696
28. Breslow R, Yang Z, Ching R, Trojandt G, Odobel F (1998) *J Am Chem Soc* 120:3536
29. Schmuck C, Geiger C (2004) *J Am Chem Soc* 126:8898
30. Schmuck C, Wienand W (2003) *J Am Chem Soc* 125:452
31. Gale PA (2003) *Coord Chem Rev* 240:191
32. Schmuck C (2000) *Chem Eur J* 6:709
33. Schmuck C (1999) *Chem Commun* 843
34. Schmuck C (1999) *Eur J Org Chem* 2397
35. Wehner M, Janssen D, Schäfer G, Schrader T (2006) *Eur J Org Chem* 138
36. Schrader T, Wehner M (2002) *Angew Chem Int Ed* 41:1751
37. McComas CC, Crowley BM, Boger DL (2003) *J Am Chem Soc* 125:9314
38. Nieto M, Perkins HR (1971) *Biochem J* 123:780
39. Walsh CT (2000) *Nature* 406:775
40. Williams DH, Bardsley B (1999) *Angew Chem Int Ed* 38:1172
41. Hartley JH, James TD, Ward CJ (2000) *J Chem Soc Perkin Trans I* 3155
42. Peczuł MW, Hamilton AD (2000) *Chem Rev* 100:2479
43. Collet A, Dutata JP, Lozach B, Canceill J (1993) *Top Curr Chem* 165:103
44. Collet A (1987) *Tetrahedron* 24:5725
45. Lam KS, Salmon SE, Hersh EM, Hruby VJ, Kazmierski WM, Knapp RJ (1991) *Nature* 354:82
46. Scott JK, Smith GP (1990) *Science* 249:386
47. Boyce R, Li G, Nestler HP, Suenaga T, Still WCJ (1994) *J Am Chem Soc* 116:7955
48. Gennari C, Nestler HP, Salom B, Still WC (1995) *Angew Chem Int Ed Engl* 34:1765
49. Shuttleworth SJ, Connors RV, Fu J, Liu J, Lizarzaburu ME, Qiu W, Sharma R, Wanska M, Zhang AJ (2005) *Curr Med Chem* 12:1239
50. Maly DJ, Huang L, Ellman JA (2002) *Chembiochem* 1:16
51. Cho CY, Moran EJ, Cherry SR, Stephans JC, Fodor SPA, Adams CL, Sundaram A, Jacobs JW, Schultz PG (1993) *Science* 261:1303
52. Uttamchandani M, Walsh DP, Yao SQ, Chang YT (2005) *Curr Opin Chem Biol* 9:4
53. Thompson LA, Ellman JA (1996) *Chem Rev* 96:555
54. St Hilaire PM, Meldal M (2000) *Angew Chem Int Ed* 39:1162
55. Furka A, Sebastyen F, Asgedom M, Dibo G (1991) *Int J Pept Protein Res* 37:487
56. Houghten RA, Pinilla C, Blondelle SE, Appel JR, Dooley CT, Cuervo JH (1991) *Nature* 354:84
57. Lam KS, Lebl M, Krchnak V (1997) *Chem Rev* 97:411
58. Borchardt A, Still WC (1996) *Acc Chem Res* 29:155
59. Lwik DWPM, Weingarten MD, Broekema M, Brouwer AJ, Still WC, Liskamp RMJ (1998) *Angew Chem* 110:1947

60. Lwik DPWM, Mulders SJE, Cheng Y, Shao Y, Liskamp RMJ (1996) *Tetrahedron Lett* 37:8253
61. Gennari C, Nestler HP, Salom B, Still WC (1995) *Angew Chem* 107:1894
62. Wennemers H, Yoon SS, Still WC (1995) *J Org Chem* 60:1108
63. Davies M, Bonnat M, Guillier F, Kilburn JD, Bradley M (1998) *J Org Chem* 63:8696
64. Torneiro M, Still WC (1997) *Tetrahedron* 53:8739
65. Monnee MCF, Brouwer AJ, Liskamp RMJ (2004) *QSAR Comb Sci* 23:546
66. Kelly JW, LaBrenz SR (1995) *J Am Chem Soc* 117:1655
67. Kelly JW, Kaul R, Angeles AR, Jäger M, Powers ET (2001) *J Am Chem Soc* 123:5206
68. Jensen KB, Braxmeier TM, Demarcus M, Kilburn JD (2002) *Chem Eur J* 8:1300
69. Srinivasan N, Kilburn JD (2004) *Curr Opin Chem Biol* 8:305
70. Shepherd J, Gale T, Jensen KB, Kilburn JD (2006) *Chem Eur J* 12:713
71. Xu R, Greiveldinger G, Marenus LE, Cooper A, Ellman JA (1999) *J Am Chem Soc* 121:4898
72. Chamorro C, Hofman JW, Liskamp RMJ (2004) *Tetrahedron* 60:8691
73. Wennemers H, Nold MC, Conza M, Kulicke KJ, Neuburger M (2003) *Chem Eur J* 9:442
74. Wennemers H, Conza M (2002) *J Org Chem* 67:2696
75. Krattiger P, Wennemers H (2005) *Synlett* 4:706
76. Schreiber SL, Burke MD (2004) *Angew Chem Int Ed* 43:46
77. Burke MD, Berger EM, Schreiber SL (2003) *Science* 302:613
78. Burke MD, Berger EM, Schreiber SL (2000) *Science* 287:1964
79. Breinbauer R, Vetter IR, Waldmann H (2002) *Angew Chem Int Ed* 41:2878
80. Stahl P, Kissau L, Mazitschek R, Huwe A, Furet P, Giannis A, Waldmann H (2001) *J Am Chem Soc* 123:11586
81. Stahl P, Kissau L, Mazitschek R, Giannis A, Waldmann H (2002) *Angew Chem Int Ed* 41:1174
82. Nicolaou KC, Pfefferkorn JA, Mitchell HJ, Roecker AJ, Barluenga S, Cao GQ, Afleck RL, Lillig JE (2000) *J Am Chem Soc* 122:9954
83. Xiao XY, Parandoosh Z, Nova MP (1997) *J Am Chem Soc* 62:6029
84. Czarnik AW (1997) *Curr Opin Chem Biol* 1:60
85. Borchardt A, Still WC (1994) *J Am Chem Soc* 116:373
86. Houghten RA (1985) *Proc Natl Acad Sci USA* 82:5131
87. Moran EJ, Sarshar S, Cargill JF, Shahbaz MM, Lio A, Mjalli AMM, Armstrong RW (1995) *J Am Chem Soc* 117:10787
88. Hirose K (2001) *J Inclusion Phenom Macrocyclic Chem* 39:193
89. Cheng Y, Suenaga T, Still WC (1996) *J Am Chem Soc* 118:1813
90. Connors KA (1987) *Binding constants*. Wiley, New York
91. Jarrett JT, Berger EP, Lansbury PT Jr (1993) *Biochemistry* 32:4693
92. Schmuck C, Wich P (2006) *Angew Chem Int Ed* 45:4277
93. Lehn JM (1999) *Chem Eur J* 5:2455
94. Otto S, Furlan RLE, Sanders JKM (2002) *Drug Discov Today* 7:117
95. Raymond JL (2004) *Angew Chem Int Ed* 43:5577
96. Otto S (2003) *Curr Opin Drug Discov Devel* 6:509
97. Otto S, Kubik S (2003) *J Am Chem Soc* 125:7804
98. Grote Z, Scopelliti R, Severin K (2003) *Angew Chem Int Ed* 42:3821
99. Severin K (2004) *Chem Eur J* 10:2565
100. Corbet PT, Sanders JKM, Otto S (2005) *J Am Chem Soc* 127:9390
101. Saur I, Severin K (2005) *Chem Commun* 1471

Calix[n]arenes as Protein Sensors

Anthony W. Coleman¹ (✉) · Florent Perret¹ · Aly Moussa² ·
Maryline Dupin³ · Yuping Guo³ · Hervi Perron³

¹Assemblages Moléculaire d'Intérêt Biologique, Université Lyon I, 7 passage du Vercors,
IBCP CNRS UMR 5086, 69367 Lyon cedex 07, France
aw.coleman@ibcp.fr

²Agence Française de Sécurité Sanitaire des Aliments, Site de Lyon, 69364 Lyon, France

³BioMérieux Advanced Technology Unit, R&D New Markers Discovery,
Chemin de L'Orme, 69280 Marcy L'Etoile, France

1	Introduction	32
2	Biological Properties	33
2.1	Complexation of Amino Acids	33
2.2	Complexation of Di- and Tripeptides	45
2.3	Protein Complexation	48
2.3.1	Tryptase Recognition	48
2.3.2	Lectin Complexation	48
2.3.3	Cytochrome C	50
2.3.4	Bovine Serum Albumin	53
2.4	Direct Biological Properties	56
2.4.1	Anti-tuberculosis Activity	56
2.4.2	Anti-viral Properties	57
2.4.3	Anti-bacterial Activities	57
2.4.4	Anti-cancer Activity	60
2.4.5	Anti-thrombotic Activity	61
2.4.6	Enzyme Inhibition	62
2.4.7	Ion Channels	62
3	Protein Sensing	64
4	Neurodegenerative Diseases	66
4.1	The Prion Protein	69
4.1.1	Diagnostic Tool for Prion-Related Diseases	72
4.1.2	Supramolecular Sensing for the PrP ^{SC} Form of the Prion	72
4.1.3	Streptomycin as a Reticulating Supramolecular System for the Prion Protein	73
4.2	<i>para</i> -Sulfonato Calix[n]arenes is Western Blot Detection of PrP	75
4.3	ELISA-Based Detection of PrP Using <i>para</i> -Sulfonato Calix[n]arenes as “Capture Antibodies”	78
4.3.1	Coupling the <i>para</i> -Sulfonato Calix[n]arenes to ELISA Plates	79
4.3.2	The Nature of the <i>para</i> -Sulfonato Calix[n]arene–Prion Interaction	84
4.4	The Test Set-Up	85
5	Conclusion	86
	References	86

Abstract The use of calix[n]arene derivatives for the sensing of proteins is described. Initially the properties of the calix[n]arenes are described. In order to better understand how the calix[n]arenes may be used for protein sensors, a detailed survey of the interactions between the molecules and amino acids and peptide is presented. The known complexes between proteins and various calix[n]arene derivatives is described and the biological activity of the molecules summarised. The use of calix[n]arenes as protein sensors observed by Schrader using amphiphilic calix[n]arenes shows that these molecules may allow nanomolar sensing. The major section of the work deals with the development of a *para*-sulfonato-calix[n]arene-based system for the prion protein responsible for bovine spongiform encephalitis and variant-Creutzfeldt–Jacobs disease(v-CJD) in humans. Initially, the development of the test was based on a Western Blot detection, however, the need for large scale testing after the discovery that blood transfusion may lead to infection with v-CJD led to the transfer of the technology to an ELISA-based test.

Keywords Calix[n]arenes · Creutzfeldt–Jacobs Disease · Prion · Proteins · Sensors

1

Introduction

The calix[n]arenes [1] are a class of macrocyclic organic host compounds, widely studied for their ability to complex a large range of ions and small molecules. The most widely studied molecules of the class are the synthetically readily available calix[4]arenes, calix[6]arenes and calix[8]arenes and their derivatives (Fig. 1).

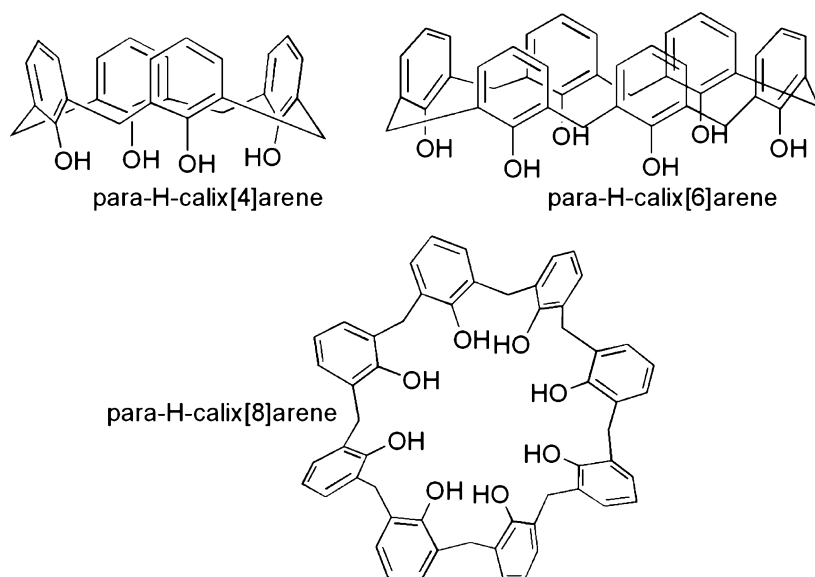


Fig. 1 General structures of the most common *para*-H-calix[n]arenes

Given that the calix[n]arenes possess widely divergent chemistries at the phenolic and *para*-aromatic faces, their use as molecular platforms for the coupling of different ligands, has proved much simpler to develop than the chemistry of the cyclodextrins. This development is further aided by a relative facility to modify regioselectively one or more position at either face of the molecular platform. This is particularly the case of the calix[4]arenes (Fig. 2).

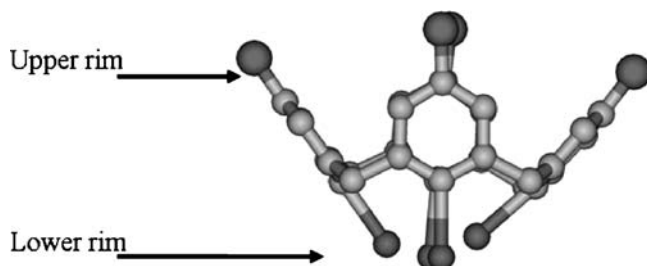


Fig. 2 Schematic of calix[4]arene showing the different chemistries at the opposing faces

One could then pose the question: why has the study of the biological properties of the calix[n]arenes seen a much slower development than that of the cyclodextrins?

The answer may come simply from the nature of the starting materials used and the reaction conditions involved in the initial synthesis of the two macrocyclic hosts. For the cyclodextrins, they are prepared by enzymatic degradation of amylose; while the calix[n]arenes are prepared from *para*-*t*-butyl-phenol and formaldehyde (MSDS number: 7040) in either diphenyl ether or toluene (MSDS numbers: 3077 and T3913) as solvent.

Strangely enough the cyclodextrins seem to present more problems of toxicity, particularly strong haemolytic properties, than the calix[n]arenes. In the case of the *para*-sulfonato-derivatives, there are no haemolytic effects at up to 50 g L⁻¹ [2]. No doubt as we probe further the biology of the calix[n]arenes some toxicological problems will emerge, although such toxicity may prove useful.

2 Biological Properties

2.1 Complexation of Amino Acids

In order to better understand how the calix[n]arenes interact with proteins and thus how to use them rationally as protein sensors, knowledge on how the

calix[n]arenes interact with the amino acid building blocks and with relevant short or longer peptide sequences is a necessary starting point.

Tables 1 to 5 summarise the known association constants observed by physical methods such as NMR, microcalorimetry, HPLC etc. for the complexation between amino acids and calixarenes.

For calix[n]arenes derivatives with the amino acids, we must caution the reader about apparent divergent results in some cases. However, the solvent conditions, pH values and buffers used can strongly influence the observed values.

The work has been extensively reviewed by Mutihac [3], Ludwig [4] and in two papers by ourselves [5, 6].

For the *para*-sulfonato calix[n]arenes, electrostatically driven interactions with the basic amino acids Lys and Arg, and di- and tripeptides of these amino acids lead to strong complexation [7–12].

However, mono-substitution at the lower rim by alkoxy carboxylic acid or amino moieties leads to some surprising modifications in the association constants, particularly with regard to binding of aspartic acid where the K_{ass} values rise from 510 M^{-1} for *para*-sulfonato calix[4]arene **1** to 2850 M^{-1} and 5620 M^{-1} for the *para*-sulfonato calyx[4]arene mono-methoxy carboxylic acid **1a** and mono-methoxy amino derivatives **1b**, respectively (Table 2).

Similar behaviour is observed for the calix[6]arene and calix[8]arene analogues (Tables 3 and 4).

For the phosphonato calixarene derivative **4**, reported by Kalchenko's group [13, 14] the driving forces in complexation seem to be dominated by hydrophobic interactions between lateral side chains and the cavity (Table 5) [15–17].

Table 1 Association constants (K_{ass}) between *para*-sulfonato-calix[4]arene and amino acids in solution

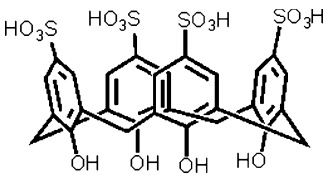
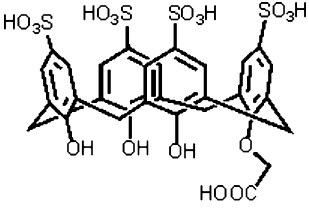
Guest	pH	Spectroscopic Study	Stoech.	K_{ass} (M^{-1})	Refs.
 <p style="text-align: center;">1</p>					
Gly	8	N.M.R.	1 : 1	30	[7]
	7	Microcal.	1 : 1	550	[8]
	2	RP HPLC	1 : 1	130	[9]

Table 1 continued

Guest	pH	Spectroscopic Study	Stoech.	K_{ass} (M^{-1})	Refs.
Ala	8	N.M.R.	1 : 1	80	[7]
	7	Microcal.	1 : 1	1660	[8]
	2	RP HPLC	1 : 1	680	[9]
Leu	8	N.M.R.	1 : 1	780	[7]
	7	Microcal.	1 : 1	1200	[8]
	7.3	N.M.R.	1 : 1	50	[10]
Pro	8	N.M.R.	1 : 1	1270	[7]
	2	RP HPLC	1 : 1	1140	[9]
Phe	8	N.M.R.	1 : 1	820	[7]
	7	Microcal.	1 : 1	1380	[8]
	7.3	N.M.R.	1 : 1	60	[10]
	2	RP HPLC	1 : 1	590	[9]
Trp	8	N.M.R.	1 : 1	260	[7]
	7	Microcal.	1 : 1	1350	[8]
	7.3	N.M.R.	1 : 1	30	[10]
	2	RP HPLC	1 : 1	1520	[9]
Tyr	2	RP HPLC	1 : 1	210	[9]
Asp	8	N.M.R.	1 : 1	510	[7]
	2	RP HPLC	1 : 1	110	[9]
Ser	8	N.M.R.	1 : 1	120	[7]
Lys	8	N.M.R.	1 : 1	1360	[7]
	8	Microcal.	1 : 1	740	[11]
	5	N.M.R.	1 : 1	600	[12]
	2	RP HPLC	1 : 1	1220	[9]
	1	N.M.R.	1 : 1	100	[11]
	1	Microcal.	1 : 1	1400	[12]
Arg	8	N.M.R.	1 : 1	1550	[7]
	8	Microcal.	1 : 1	1520	[11]
	5	N.M.R.	1 : 1	1700	[7]
	2	RP HPLC	1 : 1	2590	[9]
	1	N.M.R.	1 : 1	220	[7]
	1	Microcal.	1 : 1	2800	[11]
His	8	N.M.R.	1 : 1	500	[7]
	7.3	N.M.R.	1 : 1	20	[10]
	2	RP HPLC	1 : 1	720	[9]
Val	8	Microcal.	1 : 1	1585	[11]
	7.3	N.M.R.	1 : 1	20	[10]

Table 2 Association constants (K_{ass}) between *para*-sulfonato-calix[4]arene derivatives and amino acids in solution

Guest	pH	Spectroscopic Study	Stoech.	K_{ass} (M^{-1})	Refs.
 1a					
Gly	8	N.M.R.	1 : 1	50	[7]
Ala	8	N.M.R.	1 : 1	80	[7]
Leu	8	N.M.R.	1 : 1	490	[7]
Pro	8	N.M.R.	1 : 1	480	[7]
Phe	8	N.M.R.	1 : 1	390	[7]
Trp	8	N.M.R.	1 : 1	180	[7]
Asp	8	N.M.R.	1 : 1	2850	[7]
Ser	8	N.M.R.	1 : 1	3560	[7]
Lys	8	N.M.R.	1 : 1	890	[7]
Arg	8	N.M.R.	1 : 1	800	[7]
His	8	N.M.R.	1 : 1	310	[7]

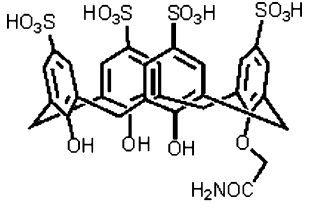
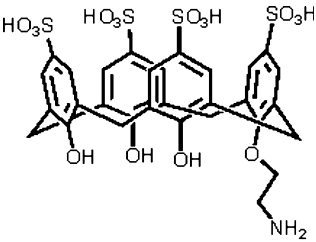
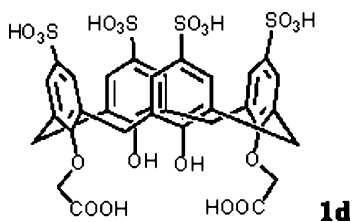
 1b					
Gly	8	N.M.R.	1 : 1	30	[7]
Ala	8	N.M.R.	1 : 1	100	[7]
Leu	8	N.M.R.	1 : 1	270	[7]
Pro	8	N.M.R.	1 : 1	370	[7]
Phe	8	N.M.R.	1 : 1	490	[7]
Trp	8	N.M.R.	1 : 1	210	[7]
Asp	8	N.M.R.	1 : 1	2250	[7]
Ser	8	N.M.R.	1 : 1	540	[7]
Lys	8	N.M.R.	1 : 1	580	[7]
Arg	8	N.M.R.	1 : 1	840	[7]
His	8	N.M.R.	1 : 1	210	[7]

Table 2 continued

Guest	pH	Spectroscopic Study	Stoech.	K_{ass} (M^{-1})	Refs.
 <p style="text-align: center;">1c</p>					
Gly	8	N.M.R.	1 : 1	40	[7]
Ala	8	N.M.R.	1 : 1	100	[7]
Leu	8	N.M.R.	1 : 1	310	[7]
Pro	8	N.M.R.	1 : 1	210	[7]
Phe	8	N.M.R.	1 : 1	280	[7]
Trp	8	N.M.R.	1 : 1	210	[7]
Asp	8	N.M.R.	1 : 1	5620	[7]
Ser	8	N.M.R.	1 : 1	420	[7]
Lys	8	N.M.R.	1 : 1	200	[7]
Arg	8	N.M.R.	1 : 1	450	[7]
His	8	N.M.R.	1 : 1	210	[7]



Val	7.3	N.M.R.	1 : 1	10	[10]
Leu	7.3	N.M.R.	1 : 1	79	[10]
Phe	7.3	N.M.R.	1 : 1	50	[10]
His	7.3	N.M.R.	1 : 1		[10]
Trp	7.3	N.M.R.	1 : 1	20	[10]

Table 2 continued

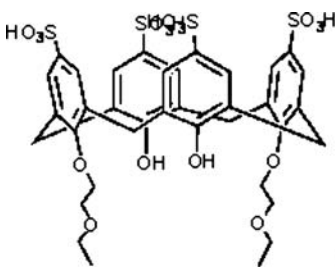
Guest	pH	Spectroscopic Study	Stoech.	K_{ass} (M^{-1})	Refs.
					
1c					
Val	7.3	N.M.R.	1 : 1		[10]
Leu	7.3	N.M.R.	1 : 1	8	[10]
Phe	7.3	N.M.R.	1 : 1	25	[10]
His	7.3	N.M.R.	1 : 1		[10]
Trp	7.3	N.M.R.	1 : 1	10	[10]

Table 3 Association constants (K_{ass}) between *para*-sulfonato-calix[6]arenes derivatives and amino acids in solution

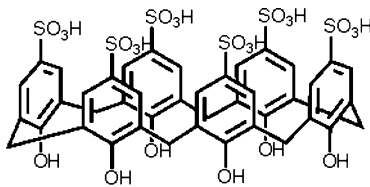
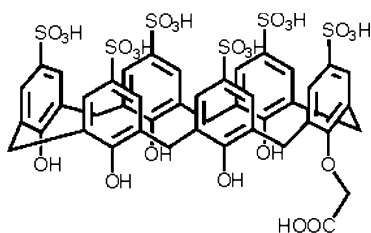
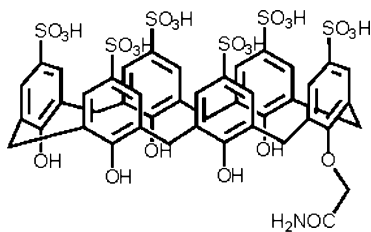
Guest	pH	Spectroscopic Study	Stoech.	K_{ass} (M^{-1})	Refs.
					
2					
Gly	8	N.M.R.	1 : 1	20	[7]
Ala	8	N.M.R.	1 : 1	70	[7]
Leu	8	N.M.R.	1 : 1	350	[7]
Pro	8	N.M.R.	1 : 1	170	[7]
Phe	8	N.M.R.	1 : 1	380	[7]
Trp	8	N.M.R.	1 : 1	1450	[7]
Asp	8	N.M.R.	1 : 1	350	[7]
Ser	8	N.M.R.	1 : 1	110	[7]

Table 3 continued

Guest	pH	Spectroscopic Study	Stoech.	K_{ass} (M^{-1})	Refs.
Lys	8	N.M.R.	1 : 1	2200	[7]
	8	Microcal.	1 : 1	94	[11]
	1	Microcal.	1 : 1	18	[11]
Arg	8	N.M.R.	1 : 1	3090	[7]
	8	Microcal.	1 : 1	1800	[11]
	1	Microcal.	1 : 1	45	[11]
His	8	N.M.R.	1 : 1	1930	[7]

**2a**

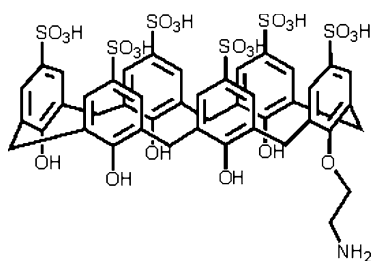
Gly	8	N.M.R.	1 : 1	40	[7]
Ala	8	N.M.R.	1 : 1	70	[7]
Leu	8	N.M.R.	1 : 1	110	[7]
Pro	8	N.M.R.	1 : 1	70	[7]
Phe	8	N.M.R.	1 : 1	90	[7]
Trp	8	N.M.R.	1 : 1	430	[7]
Asp	8	N.M.R.	1 : 1	3200	[7]
Ser	8	N.M.R.	1 : 1	170	[7]
Lys	8	N.M.R.	1 : 1	1710	[7]
Arg	8	N.M.R.	1 : 1	1480	[7]
His	8	N.M.R.	1 : 1	1040	[7]

**2b**

Gly	8	N.M.R.	1 : 1	50	[7]
Ala	8	N.M.R.	1 : 1	90	[7]
Leu	8	N.M.R.	1 : 1	140	[7]

Table 3 continued

Guest	pH	Spectroscopic Study	Stoech.	K_{ass} (M^{-1})	Refs.
Pro	8	N.M.R.	1 : 1	130	[7]
Phe	8	N.M.R.	1 : 1	370	[7]
Trp	8	N.M.R.	1 : 1	510	[7]
Asp	8	N.M.R.	1 : 1	2520	[7]
Ser	8	N.M.R.	1 : 1	240	[7]
Lys	8	N.M.R.	1 : 1	1250	[7]
Arg	8	N.M.R.	1 : 1	2020	[7]
His	8	N.M.R.	1 : 1	620	[7]

**2c**

Gly	8	N.M.R.	1 : 1	50	[7]
Ala	8	N.M.R.	1 : 1	130	[7]
Leu	8	N.M.R.	1 : 1	200	[7]
Pro	8	N.M.R.	1 : 1	360	[7]
Phe	8	N.M.R.	1 : 1	200	[7]
Trp	8	N.M.R.	1 : 1	2980	[7]
Asp	8	N.M.R.	1 : 1	5420	[7]
Ser	8	N.M.R.	1 : 1	180	[7]
Lys	8	N.M.R.	1 : 1	980	[7]
Arg	8	N.M.R.	1 : 1	670	[7]
His	8	N.M.R.	1 : 1	570	[7]

Table 4 Association constants (K_{ass}) between *para*-sulfonato-calix[8]arenes derivatives and amino acids in solution

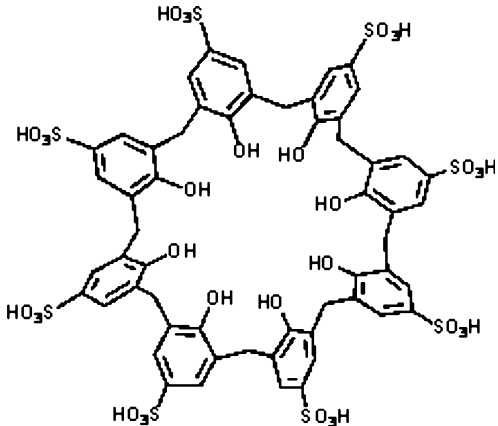
Guest	pH	Spectroscopic Study	Stoech.	K_{ass} (M^{-1})	Refs.
					
3					
Gly	8	N.M.R.	1 : 1	20	[7]
Ala	8	N.M.R.	1 : 1	70	[7]
Leu	8	N.M.R.	1 : 1	1110	[7]
Pro	8	N.M.R.	1 : 1	340	[7]
Phe	8	N.M.R.	1 : 1	2990	[7]
Trp	8	N.M.R.	1 : 1	3470	[7]
Asp	8	N.M.R.	1 : 1	610	[7]
Ser	8	N.M.R.	1 : 1	320	[7]
Lys	8	N.M.R.	1 : 1	4290	[7]
	8	Microcal.	1 : 1	400	[11]
	8	Microcal.	1 : 2	23	[11]
	1	Microcal.	1 : 1	140	[11]
	1	Microcal.	1 : 2	27	[11]
Arg	8	N.M.R.	1 : 1	10080	[7]
	8	Microcal.	1 : 1	350	[11]
	8	Microcal.	1 : 1	41	[11]
	1	Microcal.	1 : 1	73	[11]
	1	Microcal.	1 : 1	49	[11]
His	8	N.M.R.	1 : 1	2830	[7]

Table 4 continued

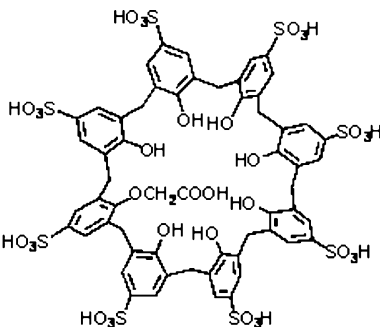
Guest	pH	Spectroscopic Study	Stoech.	K_{ass} (M^{-1})	Refs.
 <p style="text-align: center;">3a</p>					
Gly	8	N.M.R.	1 : 1	50	[7]
Ala	8	N.M.R.	1 : 1	80	[7]
Leu	8	N.M.R.	1 : 1	110	[7]
Pro	8	N.M.R.	1 : 1	50	[7]
Phe	8	N.M.R.	1 : 1	260	[7]
Trp	8	N.M.R.	1 : 1	1980	[7]
Asp	8	N.M.R.	1 : 1	ND	[7]
Ser	8	N.M.R.	1 : 1	ND	[7]
Lys	8	N.M.R.	1 : 1	2100	[7]
Arg	8	N.M.R.	1 : 1	3880	[7]
His	8	N.M.R.	1 : 1	1630	[7]

Table 5 Association constants (K_{ass}) between calix[4]arenes derivatives and amino acids in solution

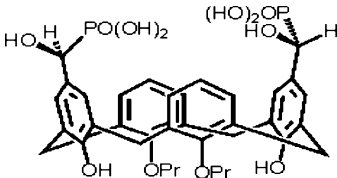
Guest	pH	Spectroscopic Study	Stoech.	K_{ass} (M^{-1})	Refs.
 <p style="text-align: center;">4</p>					
Gly	MeOH	Microcal.	1 : 1	6920	[13]
		N.M.R.	1 : 1	6920	[13]
		U.V.	2 : 1	740	[13]

Table 5 continued

Guest	pH	Spectroscopic Study	Stoech.	K_{ass} (M^{-1})	Refs.
Ala	MeOH	Microcal.	1 : 1	7760	[13]
		N.M.R.	1 : 1	7760	[13]
		U.V.	2 : 1	850	[13]
Val	MeOH	N.M.R.	1 : 1	13180	[13]
	MeOH	U.V.	2 : 1	1000	[13]
	3.40	Microcal.	1 : 1	8910	[14]
	4.52	Microcal.	1 : 1	12300	[14]
	7.29	Microcal.	1 : 1	13800	[14]
	9.25	Microcal.	1 : 1	6610	[14]
Leu	MeOH	Microcal.	1 : 1	15490	[13]
		N.M.R.	1 : 1	15490	[13]
		U.V.	2 : 1	1410	[13]
Ile	MeOH	N.M.R.	1 : 1	16980	[13]
	MeOH	U.V.	2 : 1	1580	[13]
	3.40	Microcal.	1 : 1	14450	[14]
	4.52	Microcal.	1 : 1	15140	[14]
	7.29	Microcal.	1 : 1	16980	[14]
	9.25	Microcal.	1 : 1	8910	[14]
Lys	MeOH	Microcal.	1 : 1	4370	[14]
Arg	MeOH	Microcal.	1 : 1	4680	[14]
His	MeOH	Microcal.	1 : 1	5250	[14]
Pro	MeOH	Microcal.	1 : 1	12880	[14]
OH-Pro	MeOH	Microcal.	1 : 1	10470	[14]
Phe	3.40	Microcal.	1 : 1	7240	[14]
	4.52	Microcal.	1 : 1	10230	[14]
	7.29	Microcal.	1 : 1	10480	[14]
	9.25	Microcal.	1 : 1	6030	[14]
Trp	MeOH	Microcal.	1 : 1	9770	[14]
Cys	MeOH	Microcal.	1 : 1	9330	[14]
Ser	MeOH	Microcal.	1 : 1	10720	[14]
Thr	MeOH	Microcal.	1 : 1	12880	[14]
Met	MeOH	Microcal.	1 : 1	16220	[14]

However, for analogous compounds where the phosphonate group is bound directly to the aromatic ring, strong complexation occurs again for the basic amino acids. The effect of an additional carbon between the negatively charged lead [16] group and the aromatic seems to mirror that observed for *para*-sulfonatomethyl calix[4]arene **6**, where the solid state structure slows construction of the cavity [18].

Table 5 continued

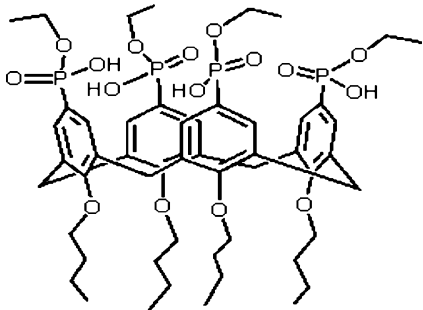
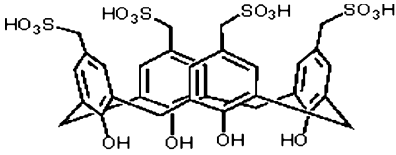
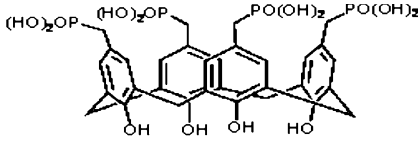
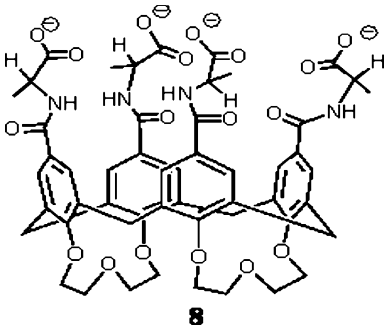
Guest	pH	Spectroscopic Study	Stoech.	K_{ass} (M^{-1})	Refs.
 5					
Ts-Arg-OMe	MeOH	N.M.R.	1 : 1	10000	[15]
H-Arg-OH	MeOH	N.M.R.	1 : 1	800	[15]
Ac-Lys-OMe	MeOH	N.M.R.	1 : 1	700	[15]
H-Lys-OH	MeOH	N.M.R.	1 : 1	3000	[15]
Ac-Val-OMe	MeOH	N.M.R.	1 : 1	< 10	[15]
Ac-Ser-OMe	MeOH	N.M.R.	1 : 1	< 10	[15]
 6					
 7					
Lys	7.5	Microcal.	1 : 1	100	[16]
Arg	7.5	Microcal.	1 : 1	40	[16]
N-AcLysNH ₂	7.5	Microcal.	1 : 1	260	[16]
LysNH ₂	7.5	Microcal.	1 : 1	1200	[16]
N-AcArgNH ₂	7.5	Microcal.	1 : 1	90	[16]
ArgNH ₂	7.5	Microcal.	1 : 1	460	[16]
Lys	7.5	Microcal.	1 : 1	140	[16]
Arg	7.5	Microcal.	1 : 1	150	[16]
N-AcLysNH ₂	7.5	Microcal.	1 : 1	520	[16]
LysNH ₂	7.5	Microcal.	1 : 1	1040	[16]
N-AcArgNH ₂	7.5	Microcal.	1 : 1	90	[16]
ArgNH ₂	7.5	Microcal.	1 : 1	360	[16]

Table 5 continued

Guest	pH	Spectroscopic Study	Stoech.	K_{ass} (M^{-1})	Refs.
 8					
L-Trp	7.3	N.M.R.	1 : 1	110	[17]
L-Trp-Me	7.3	N.M.R.	1 : 1	620	[17]
D-Trp-Me	7.3	N.M.R.	1 : 1	710	[17]
L-Phe	7.3	N.M.R.	1 : 1	70	[17]
L-Phe-Me	7.3	N.M.R.	1 : 1	400	[17]
D-Phe-Me	7.3	N.M.R.	1 : 1	430	[17]
L-Tyr	7.3	N.M.R.	1 : 1	< 20	[17]
L-Tyr-Me	7.3	N.M.R.	1 : 1	180	[17]
L-PheglyMe	7.3	N.M.R.	1 : 1	430	[17]
L-Leu	7.3	N.M.R.	1 : 1	< 20	[17]
L-Leu-Me	7.3	N.M.R.	1 : 1	290	[17]
L-Val	7.3	N.M.R.	1 : 1	no	[17]
L-Val-Me	7.3	N.M.R.	1 : 1	220	[17]
Gly	7.3	N.M.R.	1 : 1	no	[17]
Gly-Me	7.3	N.M.R.	1 : 1	no	[17]

2.2

Complexation of Di- and Tripeptides

Concerning complexation with peptides, it can be clearly seen in Table 6 that the sulfonato-calixarene derivatives **1** and **2** bind strongly with Arg and Lys di- and tripeptides with association constants up to $4.3 \times 10^4 M^{-1}$. The selectivity order (Arg > Lys > other amino acids) is kept in peptides. The stability increases when more binding sites interact, which is similar to natural host-guest systems.

In the case of **1**, the complexation is enthalpy-driven [19]. The larger calix[6]arene derivative **2** binds up to two di- and tripeptides. In the case of **2**, conformational rearrangement can occur, e.g. two KK (two Lys-Lys) are bound by the host in 1,2,3-alternate conformation.

Table 6 Association constants between calix[n]arenes derivatives and di- and tripeptides in solution

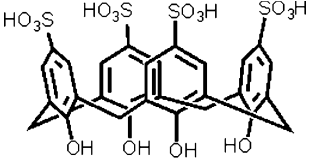
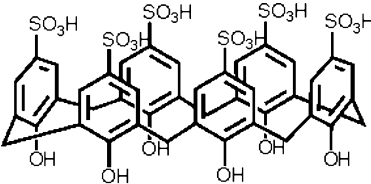
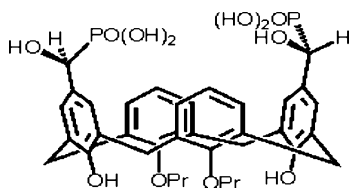
Guest	pH	Spectroscopic Study	Stoech.	K_{ass} (M^{-1})	Refs.
 1					
LysLys	8	N.M.R.	1 : 1	3400	[19]
	8	Microcal.	1 : 1	3800	[19]
LysLysLys	8	N.M.R.	1 : 1	30000	[19]
	8	Microcal.	1 : 1	30000	[19]
ArgArg	8	N.M.R.	1 : 1	7000	[19]
	8	Microcal.	1 : 1	7700	[19]
ArgArgArg	8	N.M.R.	1 : 1	33000	[19]
	8	Microcal.	1 : 1	35000	[19]
LysArg	8	N.M.R.	1 : 1	37000	[19]
	8	Microcal.	1 : 1	37000	[19]
ArgLys	8	N.M.R.	1 : 1	39000	[19]
	8	Microcal.	1 : 1	43000	[19]
GlyGly	7	Microcal.	1 : 1	980	[8]
GlyAla	7	Microcal.	1 : 1	1620	[8]
GlyVal	7	Microcal.	1 : 1	1740	[8]
GlyLeu	7	Microcal.	1 : 1	1660	[8]
LeuGly	7	Microcal.	1 : 1	1700	[8]
LeuAla	7	Microcal.	1 : 1	1700	[8]
GlyPhe	7	Microcal.	1 : 1	1700	[8]
GlyGlyGly	7	Microcal.	1 : 1	1290	[8]
LeuGlyGly	7	Microcal.	1 : 1	1320	[8]
 2					
LysLys	8	Microcal.	1 : 1	2300	[19]
	8	Microcal.	1 : 2	700	[19]

Table 6 continued

Guest	pH	Spectroscopic Study	Stoech.	K_{ass} (M^{-1})	Refs.
LysLysLys	8	Microcal.	1 : 1	3100	[19]
	8	Microcal.	1 : 2	3400	[19]
ArgArg	8	Microcal.	1 : 1	1200	[19]
	8	Microcal.	1 : 2	1200	[19]
ArgArgArg	8	Microcal.	1 : 1	1600	[19]
	8	Microcal.	1 : 2	11000	[19]
LysArg	8	Microcal.	1 : 1	1600	[19]
	8	Microcal.	1 : 2	730	[19]
ArgLys	8	Microcal.	1 : 1	1600	[19]
	8	Microcal.	1 : 2	730	[19]
GlyGly	7	Microcal.	1 : 1	1995	[8]
GlyAla	7	Microcal.	1 : 1	2950	[8]
GlyVal	7	Microcal.	1 : 1	1620	[8]
GlyLeu	7	Microcal.	1 : 1	1550	[8]
LeuGly	7	Microcal.	1 : 1	1620	[8]
LeuAla	7	Microcal.	1 : 1	1450	[8]
GlyPhe	7	Microcal.	1 : 1	1910	[8]
GlyGlyGly	7	Microcal.	1 : 1	1780	[8]
LeuGlyGly	7	Microcal.	1 : 1	1660	[8]

**4**

AlaAla	MeOH	Microcalo	1 : 1	26920	[14]
AlaLeu	MeOH	Microcalo	1 : 1	43650	[14]
AlaGlu	MeOH	Microcalo	1 : 1	37150	[14]
GlyTyr	MeOH	Microcalo	1 : 1	43650	[14]
ThrLeu	MeOH	Microcalo	1 : 1	39810	[14]

All the results concerning the ability of functionalised calix[n]arenes (amongst the *para*-sulfonato-calix[n]arenes) to form complexes, to act as extractants in liquid–liquid extraction and even to act as carriers in the transport of different biological amine compounds (amino acids, peptides etc.) have been recently reviewed by Mutihac et al. [3].

2.3

Protein Complexation

2.3.1

Tryptase Recognition

Consoli's group have developed a series of basic amino acid-derived calix[8]arene derivatives (Fig. 3) that act as new surface receptors with potent and selective inhibition activity for both human and recombinant lung β -tryptase [20]. Kinetic inhibition analysis on recombinant lung tryptase showed a time-dependent competitive inhibition with both initial and steady-state rate constants in the nanomolar range: respectively, 582 and 77 nm for 11, 283 and 2 nm for 12, 99 and 6 nm for 13 and 626 and 79 nm for 14.

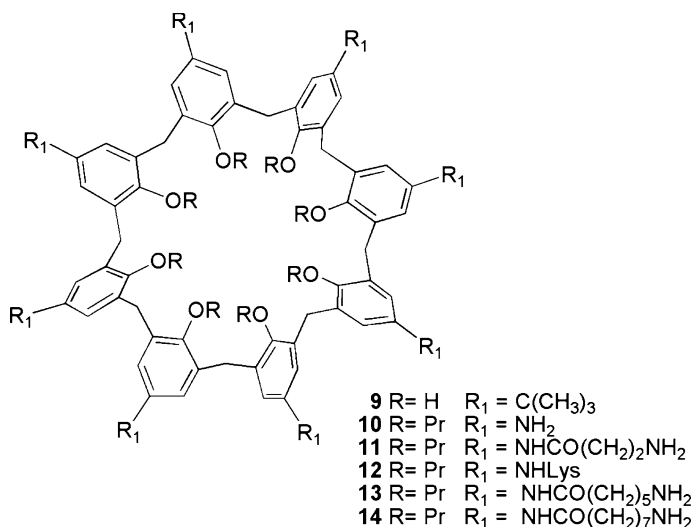


Fig. 3 Basic amino acid calix[8]arene derivatives showing tryptase inhibition

Human tryptase was indirectly inhibited due to the antagonist effect of derivatives 9–14 on the proteoglycan heparin. At the same time, competitive inhibition of recombinant human tryptase was also achieved, supporting the effectiveness of these surface binding receptors. This could outline a new approach to the design of artificial enzymatic inhibitors.

2.3.2

Lectin Complexation

The interactions between glycosylated-calixarenes (Fig. 4) and sugar-binding proteins such concanavalin A and other lectins have been investigated by Cas-

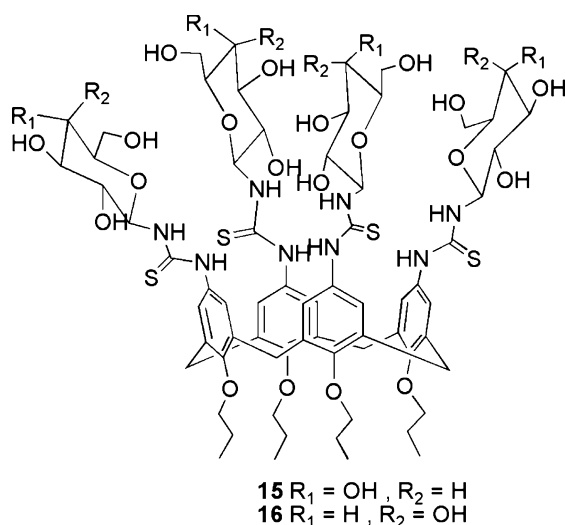


Fig. 4 Sugarcalixarenes complexing lectin

nati et al. [21]. They demonstrated the potential use of these glycosyl-cluster calixarenes as molecular delivery systems for transporting drugs or as probes interacting directly with a particular receptor site.

The tetra-functionalised receptors **15** and **16** also show the phenomenon of selective multivalency in their binding with two lectins, concanavalin A (Con A) and peanut lectin (PNA, *Arachis hypogaea*). Through a simple, qualitative turbidimetric analysis, they were able to demonstrate that the tetraglycosyl derivative causes microprecipitation of Con A, a known glucose and mannose binding protein. The multivalent interaction of glycolix[4]arene with several Con A molecules causes cross-linking and Con A agglutination. No microprecipitation was observed with the galactose binding lectin PNA, while a large excess of glucose partially inhibited the agglutination of Con A by **15**, demonstrating the binding specificity. Similar behaviour was shown by the tetragalactosyl derivative **16** toward PNA.

In both cases, the complexes of these “sugarcalixarenes” are more stable than those obtained between monomeric glucose or galactose and the respective lectin.

Consoli et al. [22] have developed a series of novel GlcNAc-presenting amino acid calixarenes (Fig. 5). Their specific lectin binding ability and amplified lectin affinity have been shown as well as the effects of the scaffold mobility and nature spacer. In particular, the best result obtained was a minimum inhibitory concentration (MIC) of 0.16 nM, 312-fold more potent than D-GlcNAc (MIC = 200 nM) used as control.

These compounds are novel “nanostructures”, useful in the study of recognition phenomena involving GlcNAc present at cell surfaces, and open per-

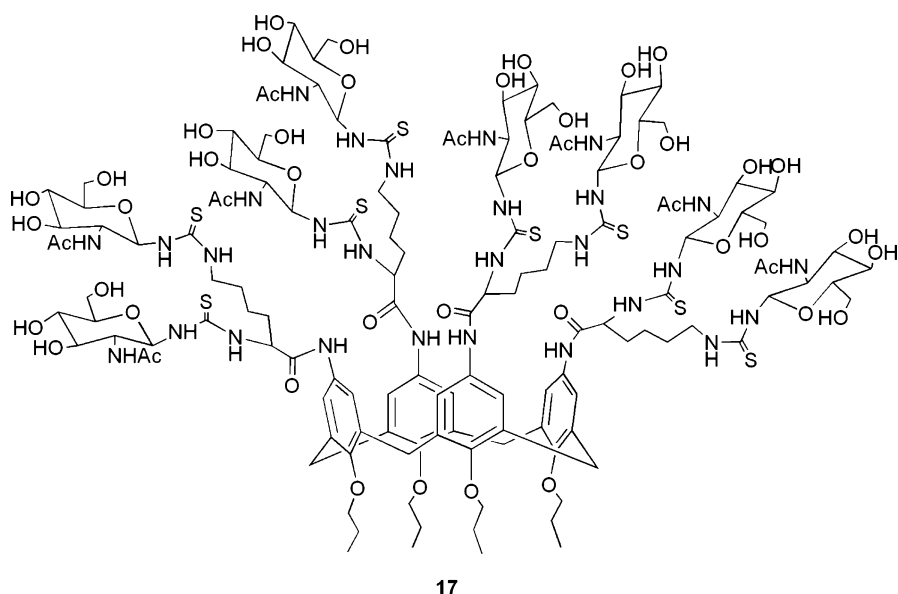


Fig. 5 One of the GlcNAc-calixarene derivatives studied by Consoli et al. [22]

spectives toward their application as drug delivery systems or inhibitors of GlcNAc-receptor binding involved in pathological events. Finally, since GlcNAc is a known substrate in glycosylation of natural glycoproteins, [23], the compounds appear to be interesting building blocks for the construction of more complex calixarene-based glycoconjugates.

2.3.3

Cytochrome C

Other water-soluble calix[n]arenes have also been demonstrated to possess biological activity. For example, Hamilton's group studied protein surface receptors based on calix[4]arenes carrying four constrained peptide loops (18–20, Fig. 6) [24–26].

They described the synthesis of a family of protein surface receptors based on calix[4]arene with four constrained cyclic peptides attached and observed a strong association between one of these receptors and cytochrome *c* (*Cc*) by means of affinity and gel permeation chromatography [26]. It was shown that this receptor inhibits the reduction of Fe(III)*Cc* by the ascorbate anion and, using a concentration-dependent analysis, they measured an association constant of $3.05 \times 10^6 \text{ M}^{-1}$. The nature of the substitution on the lower rim of the calixarene proved to be an essential element for strong binding to *Cc*, suggesting an important conformational role for this region of the receptor:

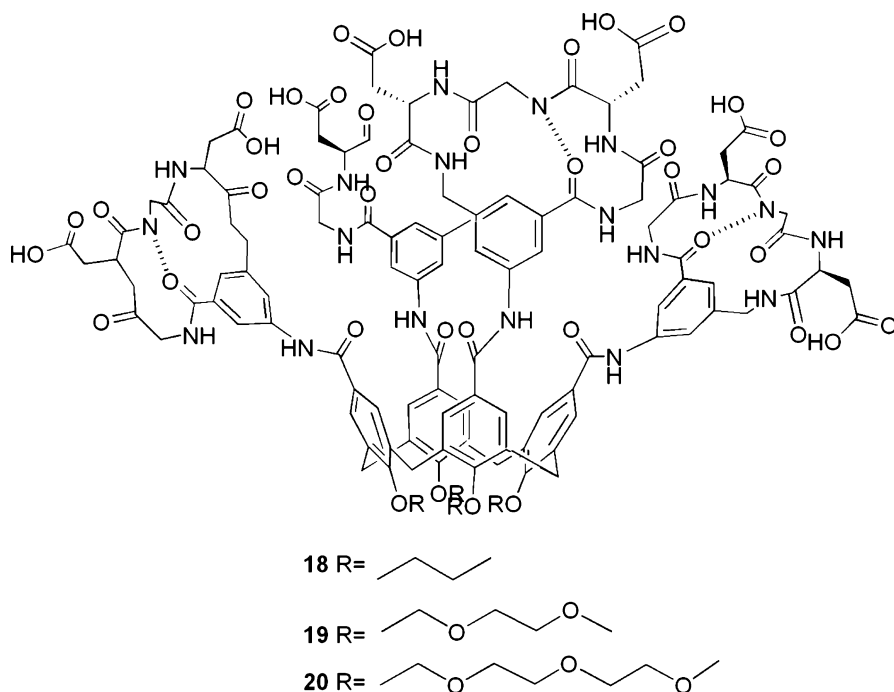


Fig. 6 Peptide loop containing calixarenes complexing cytochrome *c*

longer chains interfere with the binding at the upper rim either by inducing conformational changes or by backfolding.

Furthermore, the binding of the most active derivative (**18**) is strong enough to compete with natural receptors such as cytochrome *c* peroxidase (CcP) and Apaf-1. The 1 : 1 Cc–**18** complex, with a binding constant of $3 \times 10^8 \text{ M}^{-1}$, is strong enough to disrupt the Cc–Apaf-1 complex, a key adduct in apoptosis [27].

It is worth noting that this calixarene derivative also complexes α -chymotrypsin and inhibits its activity [28]. Due to opposite charges it binds to the protein surface in a two-step manner: slow binding, followed by enzyme isomerisation. The calixarene can displace α 1-trypsin inhibitor, thus it is considered to bind near the same site.

In other studies on the interaction of calix[n]arene derivatives with Cc, Oshima et al. used a series of anionic calix[n]arene derivatives (Fig. 7) [29].

Based on multiple electrostatic COO^- – NH_3^+ interactions, up to 20 calixarenes bind to one molecule of Cc. This is in good agreement with the 19 Lys residues known to be present on the surface of Cc (Fig. 8). Although this complexation encapsulates parts of Cc and renders the complex hydrophobic and extractable, the enzymatic activity is retained. The extractability decreases in the order: Cc(19) > guanidylated Cc(6) > lysosyme (4) and parallels the num-

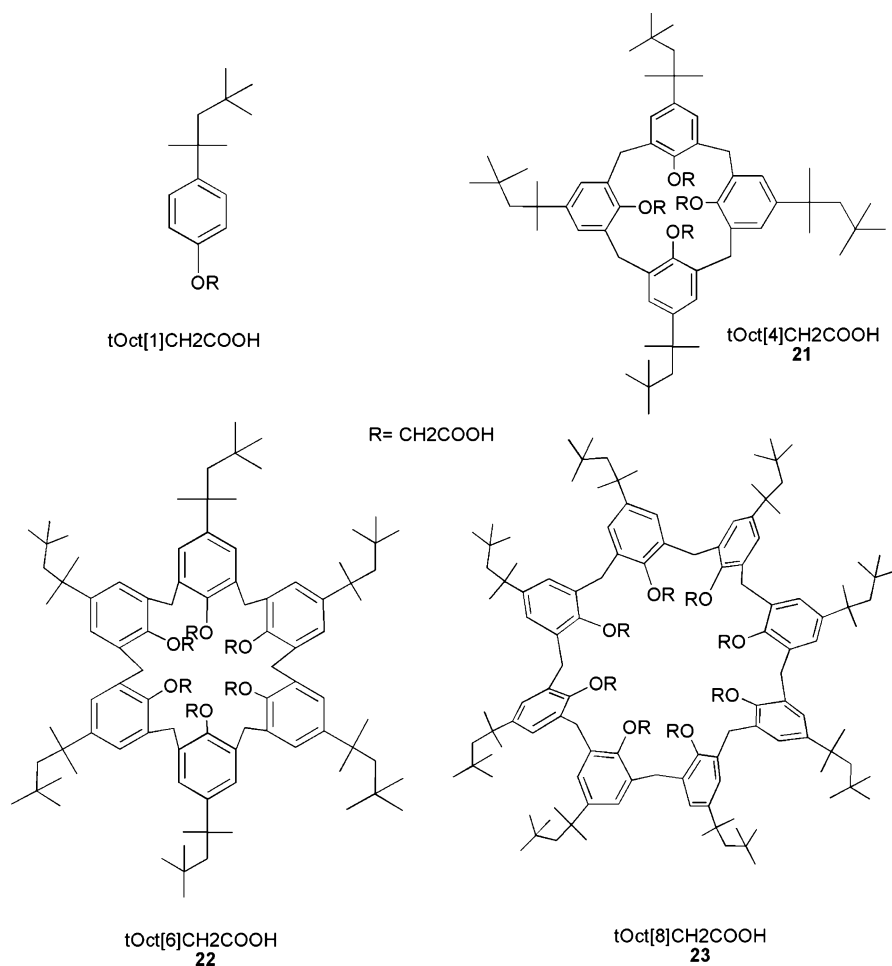


Fig. 7 Oshima's calixarenes

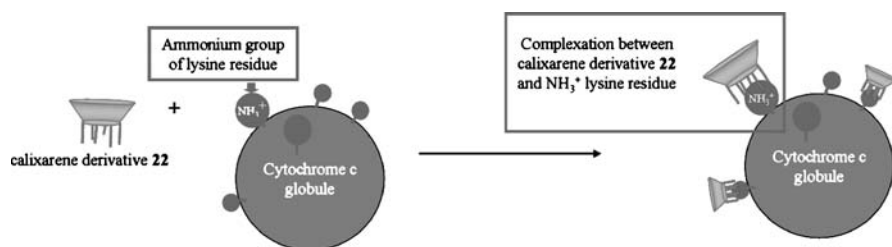


Fig. 8 Scheme of the phenomena of binding of Oshima's calixarenes to cytochrome c

ber of Lys groups (given in brackets). The extraction efficiencies of **23** and **22** are better than those of **21**.

2.3.4 Bovine Serum Albumin

The complexation of bovine serum albumin (BSA), an arginine- and lysine-rich protein, with *para*-sulfonato-calix[n]arenes has been demonstrated by our group [30] by means of electrospray mass spectrometry, dynamic light scattering and atomic force microscopy. It has been shown that with *para*-sulfonato-calix[4]arene **1**, one strong and two weaker binding sites can be detected (Fig. 9).

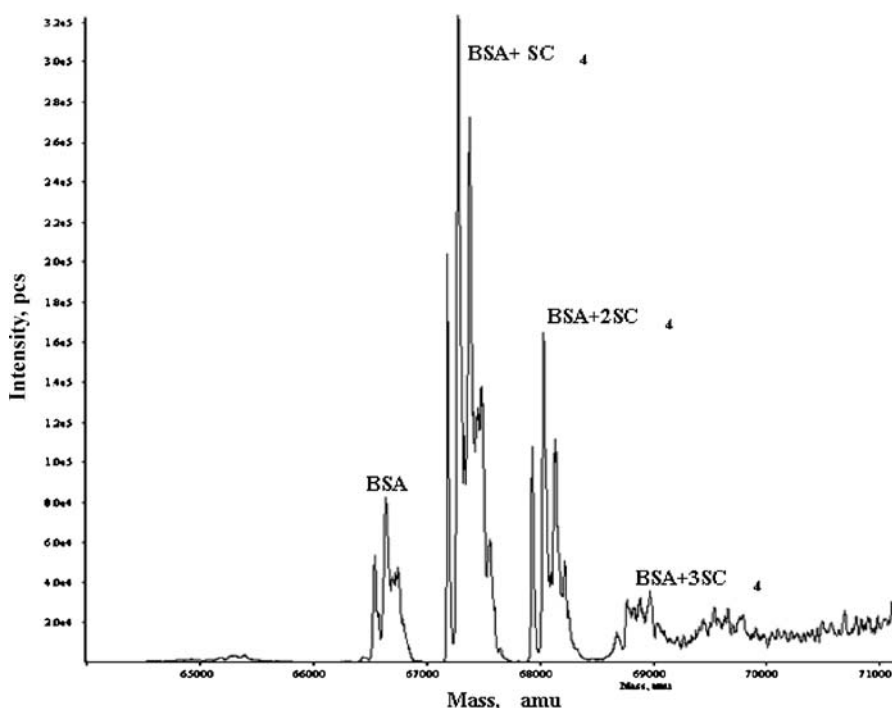


Fig. 9 View of mass spectra of the complexation of BSA with *para*-sulfonato calix[4]-arene **1**, at molar ratio 1 : 3 BSA/calixarene after deconvolution. At this molar ratio, BSA is present as the uncomplexed form and as three complexed forms with one, two and three molecules of **1**

The effects on the structure of thin films formed by surface deposition of BSA show that the *para*-sulfonato-calix[n]arenes act to reticulate the films and produce essentially planar systems.

In a more recent publication [31], we used electrospray ionisation mass spectrometry (ESI/MS) in order to determine the association constants (K_{ass}) and binding stoichiometries for parent *para*-sulfonato-calix[n]arenes and their derivatives with BSA. K_{ass} values were determined by titration experiments using a constant concentration of protein. It has been shown for the tetramer that **1** and **1c** interact strongly with BSA, showing three non-equivalent binding sites (Table 7).

Table 7 Association constants values derived from ES/MS data for the binding of parent *para*-sulfonato-calix[n]arenes and their derivatives to BSA

	K_{A1} (10^5 M^{-1})	K_{A2} (10^5 M^{-1})	K_{A3} (10^5 M^{-1})	R^2
1	7.69	3.85	0.33	0.987
1a	1.15	0.87	–	0.973
1b	1.72	2.33	–	0.998
1c	1.69	2.94	0.60	0.998
2	0.40	–	–	0.965
2a	0.29	–	–	0.972
2b	0.48	2.04	–	0.994
2c	2.08	0.48	–	0.940
2	0.07	–	–	0.945
2a	0.26	–	–	0.985
2b	0.14	–	–	0.970
2c	0.19	–	–	0.980

This table also shows that the strength of the interactions between the calixarene and BSA is inversely proportional to the size of macrocyclic ring: $n = 4 > n = 6 \gg n = 8$. It has been previously reported that BSA has three sites for anionic molecules and in particular for long chain fatty acids, salicylate, and some sulfonamides [32]. Binding of these anions involves, as expected, Arg or Lys residues with Lys-474 being implicated in the primary binding site, Lys-350 in the secondary site and Lys-116 in the weakest site. The three binding sites of BSA are present in domains I, II and III in order of increasing affinity [33]. The results obtained for the *para*-sulfonato-calix[n]arenes and their derivatives in this study are hence in agreement with previous biochemical studies of anion binding to BSA [32].

In other studies [34, 35], complexation between a diamide tetracid calix[4]-arene and a tetraamidotetraamine calix[4]arene (Fig. 10) with human serum albumin (HSA) has been demonstrated in the presence of gadolinium, Gd(III).

The metal ion is strongly bound by the diamide tetracid derivative **24** ($\log K_{\text{ass}} > 13$ in H_2O , pH 7). Only two ligating groups are involved and three water molecules remain hydrated to Gd^{3+} . Two of them are substituted by Asp

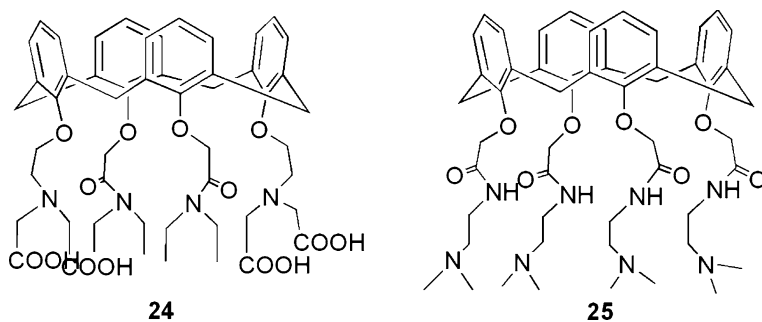


Fig. 10 Diamide tetracid calix[4]arene and tetraamidotetraamine calix[4]arene

or Glu groups when HAS is added. Additionally, HSA engages in hydrophobic interactions with the calixarene π -systems, resulting in $\log K_{\text{ass}} = 4.4$. Concerning the tetraamidotetraamine derivative **25**, although the association with Gd^{3+} through the carbonyl and ether oxygen atom is weaker than for the diamide tetracid derivative **24** ($\log K_{\text{ass}} = 5.3$), the non-covalent binding to HSA is clearly detected by changes in NMR relaxation time.

Finally, in our group, the interaction of solid lipid nanoparticles (SLN) based on amphiphilic calix[4]arenes (**26–28**, Fig. 11) with BSA has been investigated by proton correlation spectroscopy (PCS) and atomic force microscopy (AFM) [36]. The results have shown the formation of an albumin capping layer, one protein molecule thick on the surface of the SLNs. The lack of SLN aggregation, even at high concentration of BSA, opens the possibility of developing these transporters for intravenous administration.

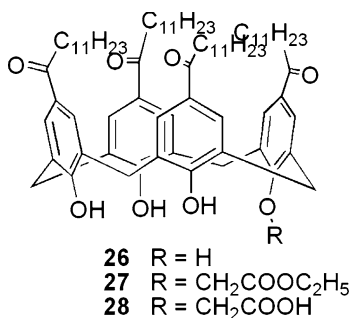


Fig. 11 Amphiphilic calix[4]arenes studied by our group

2.4 Direct Biological Properties

2.4.1 Anti-tuberculosis Activity

The first direct biological activity of calixarenes was reported by Cornforth et al. in 1955 [37]. *para*-Octyl-calix[8]arene having polyoxyethylene units at the lower rim of the calixarene was shown to be active as an anti-tuberculosis agent. Two derivatives were studied: Macrocyclon having one chain containing 12–13 ethyleneglycol units and HOC-60 having 60 ethyleneglycol units. The growth of *Mycobacterium tuberculosis* in infected macrophages (M phi) is inhibited by Macrocyclon and stimulated by HOC-60. The mechanism of action is completely different from that of other drugs currently used against tuberculosis and these compounds are promising since the resistance toward conventional chemio-therapeutic agents is increasing [37].

Also, triglyceride lipase obtained from M phi extracts and an extracellular phospholipase were inhibited by Macrocyclon and stimulated by HOC-60. This suggestion of a mechanism has been strengthened by the finding that M phi cultivated in monolayers and treated with Macrocyclon showed accumulation of lipids and little formation of fatty acid after incubation of killed cells. With HOC-60, lipid was depleted and a large quantity of fatty acids was found [38].

Fifty years later, Tascon's group [39] reproduced this work on Macrocyclon and on other *t*-butyl calix[6 and 8]arenes (29–31) with defined-length PEG chains (Fig. 12).

Their results led them to suggest that ring cavity size may be important when there is no functionalisation at the lower rim and that this is less critical, particularly for *t*-butylcalix[8]arenes and *t*-butylcalix[6]arenes when PEG chains are coupled at the lower rim.

In this study, they demonstrated that Macrocyclon is effective in controlling *M. tuberculosis* infections, and they provided evidence that its effect is partially mediated by an L-arginine-dependent mechanism of macrophage activation that involves the activity of the inducible nitric oxide synthase.

Understanding the final mechanisms involved in the control of bacterial infections by activated macrophages is of paramount importance for the treatment and control of infectious diseases. At present, it is not known whether Macrocyclon has any effects on other bacterial species. Similarly, a fundamental priority will be to investigate whether Macrocyclon is also effective in controlling mycobacterial infections by human macrophages.

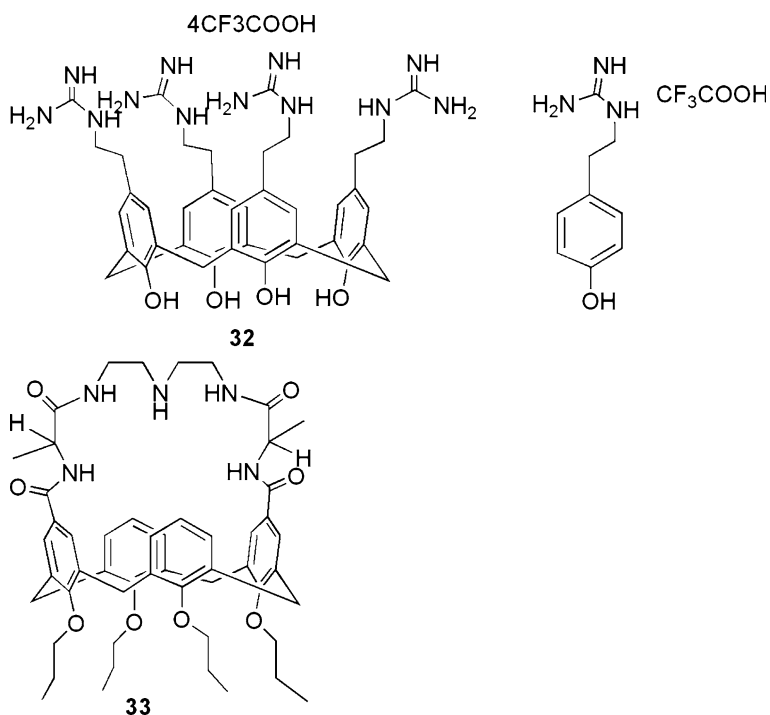


Fig. 12 Schematic structures of the calixarenes used by Tascon's group [39]

2.4.2

Anti-viral Properties

One of the interesting biological activities of the *para*-sulfonato-calix[n]-arenes (1–3) is their potential use in the treatment of viruses, such as HIV and herpes.

Hwang et al. [40] patented a method for inhibiting cell infection by an enveloped virus. The method involved administering to an infection site, a therapeutically effective amount of a calix[n]arene-derived compound, with polar substituents having a terminal carboxylate, phosphate or sulfonate group, including esters and amides that are cleavable *in vivo*. The mechanism of this action is proposed to be by interaction of the molecule with the viral envelope via electrostatic interactions, thus masking the recognition site for cells.

2.4.3

Anti-bacterial Activities

Recently, Regnouf de Vains and coworkers [41] evaluated the anti-bacterial activities of the tetra-*para*-guanidinoethylcalix[4]arene **32** and of its acyclic

monomer the *para*-guanidine-ethylphenol analogue (Fig. 13), on reference Gram-positive (*Staphylococcus aureus* ATCC 25923, *Enterococcus faecalis* ATCC 29212) and Gram-negative (*Escherichia coli* ATCC 25922, *Pseudomonas aeruginosa* ATCC 27853) bacteria.

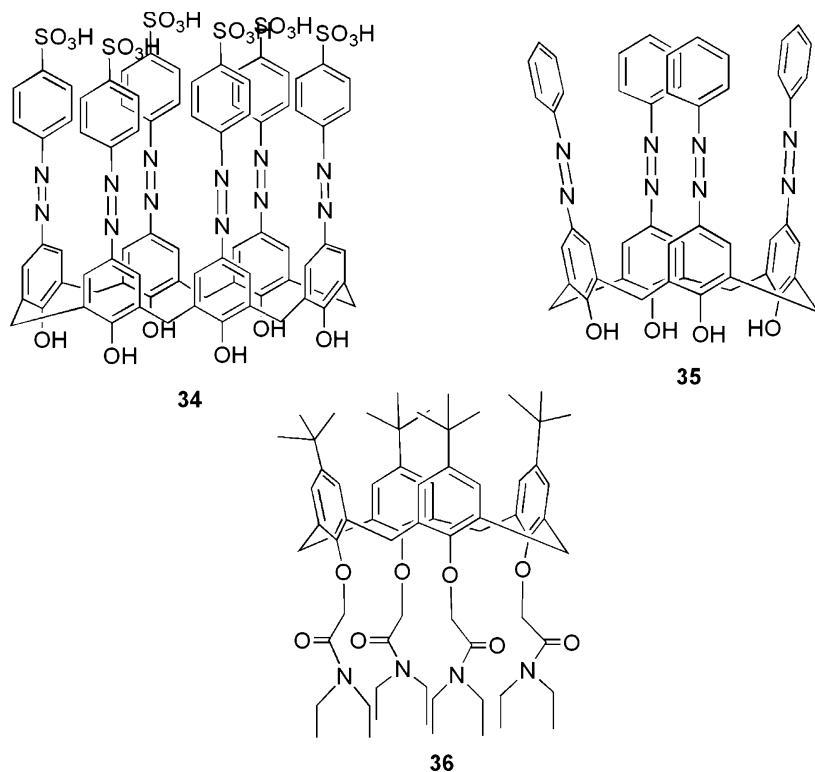


Fig. 13 Tetra-*para*-guanidinoethylcalix[4]arene 32 and its acyclic monomer the *para*-guanidine-ethylphenol

Antibiotic disk diffusion assays completed by the micromethod technique were employed to determine if a synergistic effect could be expected from the spatial organisation of the monomer into its cyclic tetrameric analogue.

All experiments revealed stronger anti-bacterial activity properties for the calixarene 32, with a real and important gain of activity with regards to the monomer: the results shown that the calixarene species is strongly active with inhibition at $16 \mu\text{g mL}^{-1}$ for *E. coli*, *S. aureus* or *E. faecalis*, and $64 \mu\text{g mL}^{-1}$ for *P. aeruginosa*. The monomer requires higher concentrations, at least $512 \mu\text{g mL}^{-1}$, for the same degree of activity. The calixarene appears thus incontestably more active than its monomer, from 32 (mass ratio) and 135 (molar ratio) times for *E. coli*, *S. aureus* and *E. faecalis*, to 8 and 34 times, respectively, for *P. aeruginosa*. The results obtained by Regnoul de

Vains and coworkers [41] showed a remarkable gain of anti-bacterial properties, without decrease of eukaryotic cell viability, from the monomeric *para*-guanidinoethyl phenol to its tetrameric cyclic isomer. As one of the possible explanations, it has been proposed that there is an important organisational role of the calixarene platform, which tethers close together and arrays at its upper rim four guanidinium groups, resulting in a synergistic effect in ionic interactions with the membrane targets.

In 1996, Casnati et al. [42] evaluated the anti-microbial activities of a calixarene derivative with a polyfunctional bridge containing D- or L-alanine units **33** and a diethylentriamine segment (Fig. 14).

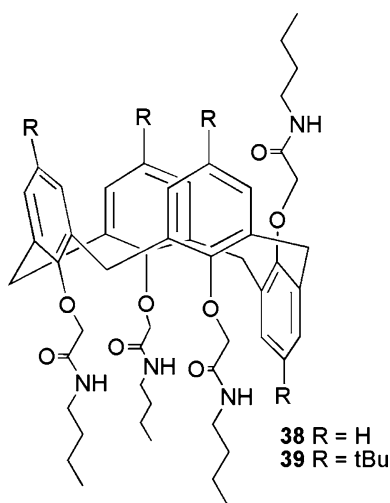


Fig. 14 Schematic structure of the bridged calix[4]arene used by Casnati et al. [42]

The evaluation of the anti-bacterial activity of these ligands (D, D and L, L), in comparison with vancomycin was conducted against selected Gram-positive bacteria (*S. aureus* 663; 853; 1131 *S. epidermidis*; *B. cereus*). The in-vitro activity was assessed by determination of minimum inhibitory concentration (MIC) values, which show an anti-Gram-positive activity from moderate to good ($64\text{--}4\text{ mg L}^{-1}$) although slightly inferior to vancomycin (2 mg L^{-1}).

It has been demonstrated that the combination of designed electrostatic, hydrogen bonding and possibly other weak interactions can stabilise complexes between the synthetic calixarene host **31** and amino acids and small peptides, leading to synthetic biologically active vancomycin antibiotic analogues.

Lamartine et al. [43] have also studied the anti-microbial activity of a series of water-soluble calixarenes. Preliminary screening of 57 calixarenes was conducted to assay their potential as anti-microbially active compounds

against *Corynebacterium*. Of these compounds, six calixarenes, were found to exhibit suitable anti-microbial activity: *para*-sulfonato-calix[n]arenes 1, 2 and 3 and other derivatives (34, 35, 36, Fig. 15). These six samples were then further tested to elucidate any anti-microbial activity they might have against additional species. After examining the growth and inhibition values of these selected compounds, 1, 2 and 3 were shown to also display anti-microbial activity against *Fusarium solani f. sp. Mori* [F.s.-26] with an inhibition range of approximately 60–70%. Additionally, all compounds exhibited excellent and selective anti-microbial activity against the fungal strains, *Rosellinia necatrix* [R-8], and *Colletotrichum dematium* [C.d.8901].

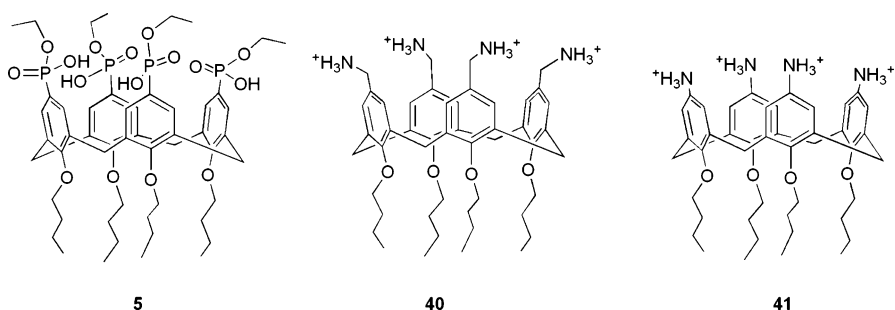


Fig. 15 Structures of the anti-bacterial active calix[n]arenes studied by Lamartine et al. [43]

2.4.4

Anti-cancer Activity

It has been shown by Hamilton's group [44], that the calixarene derivative 37 (Fig. 16) inhibits binding of vascular endothelial growth factor (VEGF) to its receptor, then blocks angiogenesis and tumourigenesis.

This calixarene derivative potently inhibits ^{125}I -VEGF binding to Flk-1 in Flk-1-overexpressing NIH 3T3 cells and human prostate tumour cells with an IC_{50} of 750 nm. This inhibition is highly selective for VEGF in that ^{125}I -platelet-derived growth factor binding to its receptor is not affected. 35 inhibits VEGF-stimulated Flk-1 tyrosine phosphorylation and subsequent activation of Erk1/2 mitogen-activated protein kinases. Furthermore, epidermal growth factor, platelet-derived growth factor, and fibroblast growth factor-dependent stimulation of Erk1/2 phosphorylation are not affected at concentrations as high as 10 μm . In vitro, this calixarene derivative inhibits angiogenesis; in vivo, it inhibits tumour growth and angiogenesis as measured by CD31 staining of A-549 human lung tumours in nude mice. Furthermore, this calixarene derivative is also effective at inhibiting tumour growth and metastasis to the lung of B16-F10 melanoma cells injected into immuno-

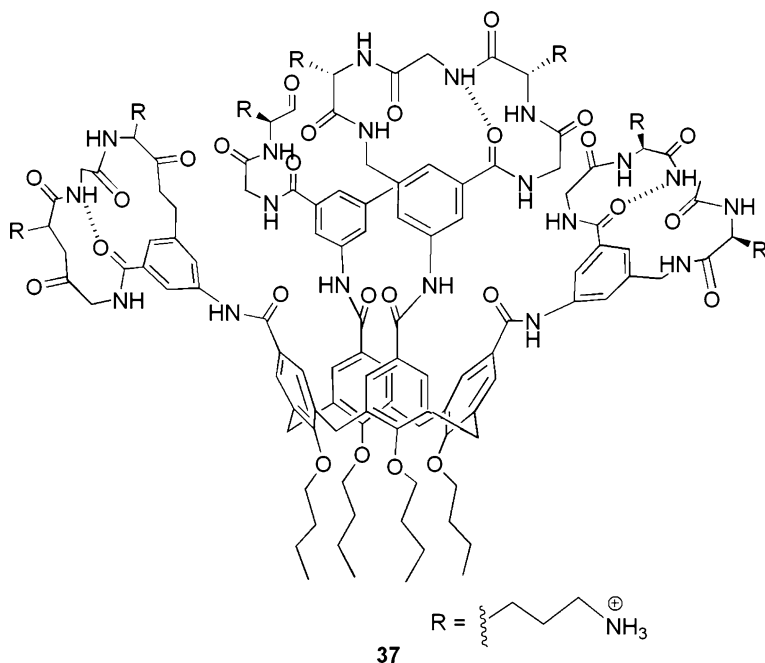


Fig. 16 Structures of the anti-cancerous active calix[n]arenes studied by Hamilton et al. [44]

competent mice. Taken together, these results demonstrate that a synthetic molecule capable of disrupting the binding of VEGF to its receptor selectively inhibits VEGF-dependent signalling and suppresses angiogenesis and tumourigenesis.

2.4.5

Anti-thrombotic Activity.

As noted before, we have done many experiments to study the complexation of *para*-sulfonato-calix[n]arenes with basic amino acids Lys and Arg and with di- and tripeptides composed of these amino acids. These experiments were undertaken in view of the previously observed increase of blood coagulation time in the presence of these macrocycles. In view of their chemical structure, their conformational flexibility and their number of SO₃ groups, these *para*-sulfonato-calix[n]arenes present analogies with glycosaminoglycans such as heparin [45, 46] Furthermore, Arg and Lys are the major amino acids present in the heparin recognition peptide sequences. This has lead us to study more deeply their anti-thrombotic activity [47].

The parent *para*-sulfonato-calix[n]arenes and six mono-O-substituted derivatives have been investigated in vitro for anti-coagulant activity. Dif-

ferent concentrations of calixarenes have been tested, showing that the compound **3a** has a significantly strong prolongation on the activated partial thromboplastin time (APTT) and on the thrombin time (TT) than the other calixarenes. Secondly, investigation of whether the anti-coagulant behaviour was via interaction with anti-thrombin (AT) or heparin cofactor II (HCII) was carried out. Thrombin inhibition mediated by AT and HCII activation has been investigated in comparison to the biological activators, heparin (Hep) and dermatan sulfate (DS). The results showed that **3a** and **2** produce activation of HCII at 500 μm comparable to that induced by DS at 100 μm . However, activation of AT by all of the investigated calixarenes is between 10 and 50 times lower than that observed in the presence of heparin. Mono-substitution of *para*-sulfonato-calix[n]arenes can lead to an increase in their anti-coagulant properties with the highest activity observed for the carboxylic pendant arm functionalised *para*-sulfonato-calix[8]arene **3a**. The mechanism of the anti-coagulant properties proceeds via interaction with the serine protease inhibitors HCII and AT. Chromogenic tests have indicated that interaction between the *para*-sulfonato-calix[n]arenes and HCII is the major factor in the activity of these molecules.

2.4.6

Enzyme Inhibition

para-Sulfonato-calix[n]arenes **1–3** have been used for the study of fibrolitic diseases of kidney, lung, liver and skin. L-Lysyl oxidase is an enzyme that assures the formation of covalent interactions between macromolecules of the extracellular matrix and the initiated reticulation by this enzyme is an essential factor in fibrolitic diseases in organs. Inhibition of L-lysyl oxidase by the *para*-sulfonato-calix[6]arene **2** has been reported by our group in a patent on the treatment, and cicatrisation of the skin [46]. The inhibition has been explained by the electrostatic interaction between the lateral chain of the basic amino acid of the active site of the enzyme (RADVRDYDHRVLLRFPQRVK) and the sulfonate group of the calixarene.

2.4.7

Ion Channels

Numerous calixarenes have been used, either as inhibitors of ionic channels or as biomimetic systems of ion channels.

For *para*-sulfonato-calix[n]arenes, Droogmans et al. [48] first carried out the study of the inhibition of the protein volume-regulated ionic channel (VRAC) present on endothelial cells, which allows the passage of ions depending on the membrane potential, using *para*-sulfonato-calix[4]arene **1** and its tetra-*O*-methyl derivative. Both induced a fast inhibition at positive potentials but were ineffective at negative potentials. Results have shown that

binding occludes VRAC at moderately positive potentials, but calix[4]arenes permeate the channel at more positive potentials. Their data suggest an open-channel blocking of VRAC by calix[4]arenes that also depends on the protonation of the binding site within the pore.

In complementary experimentation [49], they completed this work by studying the effect of *para*-sulfonato-calix[6]arene 2 and of *para*-sulfonato-calix[8]arene 3 on VRAC. At small positive potentials, the tetramer was a more effective inhibitor than the hexamer and the octamer, which became more effective at more positive potentials. 1, suramin and basile blue bind and occlude VRAC at moderate potentials, but permeate the channel at more positive potentials. *para*-Sulfonato-calix[6]arene 2 and *para*-sulfonato-calix[8]arene 3, however, do not permeate the channel.

Previously, in 1996, Atwood had patented a study concerning the inhibition of chloride-dependent channels in cells by calixarene sulfonates and other calixarenes with a *para*-acid functionality [50]. This study showed that the inhibition of the ionic channel increases with the size of the macrocycle ($3 \gg 2 \gg 1$).

Very recently, Davis and coworkers [51] reported a paper dealing with calixarenes that enable or inhibit transmembrane chloride transport.

They have shown that modest changes in the primary structure of a calix[4]arene amide (38–39, Fig. 17) lead to dramatic differences in the transport of chloride ion across phospholipid membranes. They explained these differences by comparing the solid state structures of the two derivatives. For the active H-derivative, the amide NH proton on the inverted arene is unavailable for intermolecular interactions. In contrast, for the inactive tBu-derivative, the NH proton is available. They finally suggested

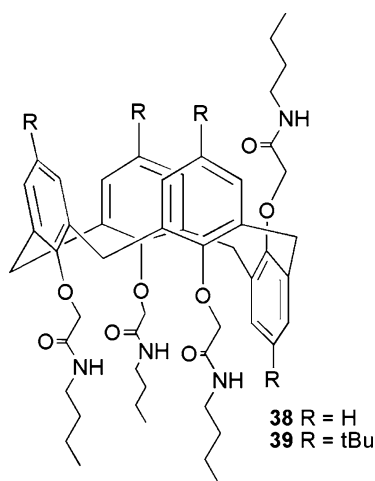


Fig. 17 Calixarene derivatives inhibiting transmembrane chloride transport

that self association and Cl^- ion transport activity might be controlled by the conformation of the side chain on the inverted arene of the partial cone.

3 Protein Sensing

In 2004, Koh's group immobilised BSA on gold surfaces by non-covalent interaction with calix[4]arene derivatives carrying carboxylate groups at their upper rims [52].

In 2005, Schrader's group introduced a new concept of protein sensing at the air-water interface, based on amphiphilic receptor molecules embedded in a lipid monolayer [15]. The process begins with incorporation of a small amount (0.13 equiv) of one or two different calix[4]arenes, adorned with charged functional groups at their upper rims (5, 40 and 41, Fig. 18), into a stearic acid monolayer. They mainly studied this phenomenon by Langmuir-Blodgett studies.

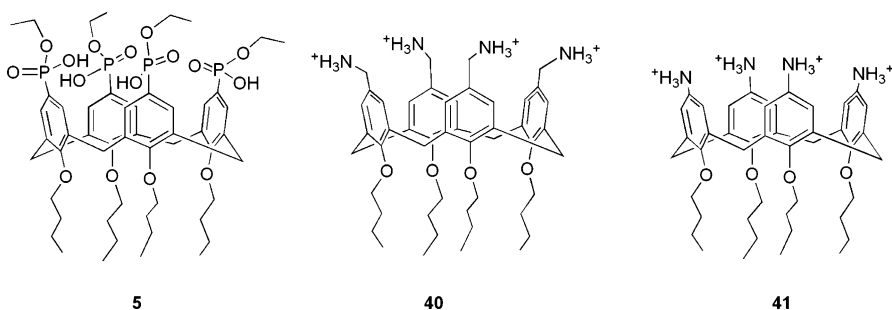


Fig. 18 Structures of the charged calixarene derivatives studied by Schrader's group [15]

These doped monolayers have been subsequently shown to attract peptides and proteins from the aqueous subphase. Depending on the host structure, the monolayers can be made selective for basic or acidic proteins. For example, the acidic calix[4]arene 5, known to have a high affinity in methanol for N/C-protected Arg ($\approx 10^4 \text{ M}^{-1}$) and Lys ($\approx 10^3 \text{ M}^{-1}$) derivatives [15], binds with the basic proteins proteinase K, thrombin, BSA, chymotrypsin, trypsin, cytochrome *c*, histone H1 and ferritin.

Oppositely charged calixarene derivatives do not form molecular capsules inside the monolayer, but rather remain separate inside the lipid layer, adopting a perpendicular orientation.

They combine their hydrogen bond donor and acceptor capacities, and thus markedly enhance the sensitivity of the sensor system toward proteins, pushing the detection limits to 10 pM concentrations. The response pattern

obtained from various receptor units inside the monolayer toward the same protein creates a fingerprint for this protein, which can hence be selectively detected at nanomolar concentrations (pattern recognition).

Recently, using these same calixarenes, Schrader's group achieved a "naked eye" colour detection of proteins by embedding these calixarene receptors within vesicles comprised of phospholipids and the chromatic polymer polydiacetylene [53]. Dramatic visible absorbance changes were induced through electrostatic interactions between the protein surface and the vesicle-incorporated hosts. The colorimetric responses could be induced by micromolar protein concentrations, and furthermore, specific protein fingerprints could be obtained by incorporating different receptors within the vesicles. This colorimetric assay constitutes a generic platform for high-sensitivity detection of soluble proteins and for evaluation of protein surface charge distribution.

The same group also used a calixarene derivative (42, Fig. 19) as a tool for highly sensitive detection and oriented immobilisation of proteins [54]. They employed a sandwich immunoassay for detection of specific interaction between prostate specific antigen and its antibody pairs as a model. When comparing the sensitivity of calixarene derivative with those of four other protein attachment agents, they shown that this calixarene had a superior sensitivity and a much lower detection limit than those of other protein chips. The superiority of the calixarene chip over the superaldehyde slide could be explained by the observation that protein immobilisation via ionic interac-

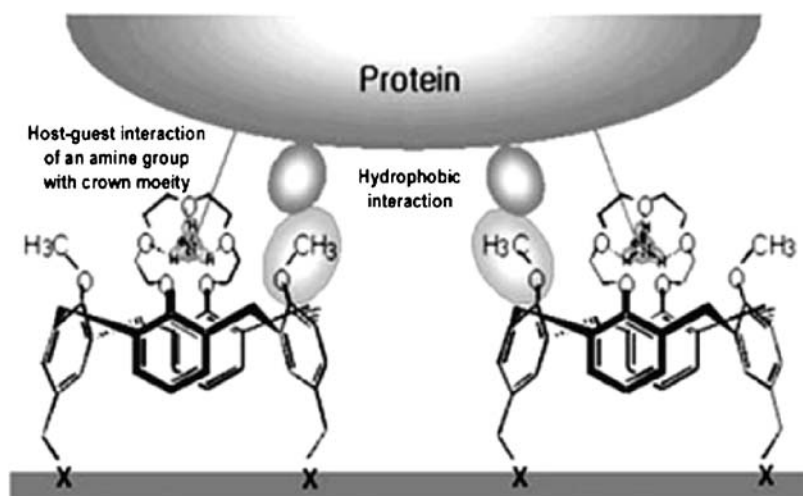


Fig. 19 A proposed mechanism of protein binding to calixcrown (42) molecular linkers. The major binding force could be attributed to the protonated amine groups of capture proteins, which bind to the crown moiety of the linker molecule by an ionic interaction

tion may maintain a better folding conformation and keeps the protein more functional, although the electrostatic charges present on the glass may lead to the denaturation of the proteins. Their study showed that this calixarene derivative chip can be used as a biological tool with a wide range of applications, including protein–protein interaction, protein–DNA interaction and an enzyme activity assay.

4

Neurodegenerative Diseases

A large number of neurodegenerative diseases involve in their pathology the formation of fibrillar plates, often termed amyloid fibres, as a result of conformational changes in the tertiary structures of proteins. The conformational shift from α -helical to β -sheet leads to exposure of hydrophobic surfaces on the proteins, followed by oligomerisation and formation of protofilament aggregation into amyloid fibres. Finally, aggregation of the amyloid fibres into larger structures causes cell disruption and degeneration of the brain tissue.

There exists a wide range of such neurodegenerative diseases [55] (see Table 8) and it can be seen that both intra- and extracellular proteins of widely different nature are involved in such diseases. One general feature of the proteins involved is the presence of a proteoglycan or glycosylamino glycan binding site, containing several basic amino acids.

Of these neurodegenerative diseases, those associated with the prion protein are, as of now, known to be infections. Generically termed transmissible spongiform encephalopathies, from the characteristic appearances of the brain of infected species, (see Fig. 20) they include in animals, scrapie (sheep and goats), chronic wasting disease (ruminants), feline spongiform encephalitis, and most particularly bovine spongiform encephalitis (BSE, mad cow disease).

In humans, several forms are known including fatal family insomnia, Creutzfeldt–Jacobs disease (genetic and new variant), Gerstmann–Straussler–Scheinker's syndrome and kuru.

While a number of prion-associated diseases, for example scrapie, have been well known for some hundreds of years, it was the appearance of BSE in the UK in 1986 which first brought the large scale health risks of these diseases to light [56]. In the BSE epidemic in Britain, it has been estimated that over 1 million cattle were infected, and that at least 180 000 animals, in general dairy cattle, died of the disease. The mean incubation time for BSE is in the order of 5 years, whilst meat cattle are generally slaughtered at the age of 2–3 years, which is well before symptoms are apparent. The epidemic came from the use of meat and bone meal prepared from the offal of various animals, including sheep and cattle. Changes in how the meat and bone meal was prepared in the 1970s may have been a factor in the cause of the epidemic.

Table 8 Neurodegenerative diseases characterized by filamentous lesions formed from aggregated peptides/proteins

Disease	Lesion/Components	Location
Alzheimer's disease (AD) ^a	Senile plaques/beta-amyloid, NAC Neurofibrillary tangles/PHFtau	Extracellular Intracytoplasmic
Amyotrophic lateral sclerosis (ALS)	Spheroids/NF subunits	Intracytoplasmic
Dementia with Lewy bodies (DLB) ^b	Lewy bodies/NF subunits, alpha-synuclein	Intracytoplasmic
Lewy body variant Alzheimer's disease (AD + DLB) ^b	Senile plaques/beta-amyloid, NAC Neurofibrillary tangles/PHFtau	Extracellular Intracytoplasmic
Multiple system atrophy (MSA) ^b	Lewy bodies/NF subunits, alpha-synuclein	Intracytoplasmic
Neuronal intranuclear inclusion disease	Glial cell inclusions/alpha-synuclein	Intracytoplasmic
Parkinson's disease (PD) ^b	Inclusions/Expanded polyglutamine tracts Lewy bodies/NF subunits, alpha-synuclein	Intranuclear Intracytoplasmic
Prion diseases	Amyloid plaques/prion	Extracellular
Tauopathies ^a	Neurofibrillary tangles/AD-like PHFtau	Intracytoplasmic
Tri-nucleotide repeat diseases	Inclusions/expanded polyglutamine tracts	Intranuclear

This table summarizes neurodegenerative disorders characterized by filamentous brain lesions in the extracellular space or within neurons or glia
^a AD is a heterogeneous dementing disorder, and one of several tauopathies. Other tauopathies are: progressive supranuclear palsy, disease, corticobasal degeneration, FTDP-17 and Guam amyotrophic lateral sclerosis/Parkinsonism dementia complex
^b Synuclein are implicated in diverse disorders known as synucleinopathies, of which AD is one (from [55])

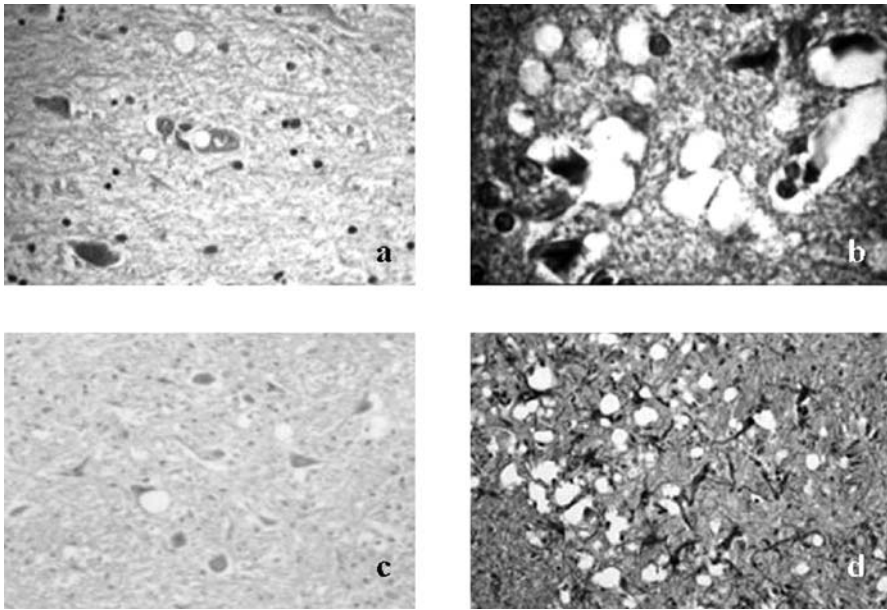


Fig. 20 Spongiform encephalopathies in the brain of infected species: **a** CJD – human; **b** kuru – human; **c** BSE – cow; **d** scrapie – sheep

Two possible causes for the epidemic exist, either through cross-species transfer of the scrapie prion or through accumulation of bovine prion in the meat and bone meal.

In July 1988, the use of meat and bone meal as cattle food was banned. There is now statistical evidence that this ban coupled with the radical culling of infected herds is leading to the disappearance of BSE (see Table 9) [57].

Table 9 Indigenous cases of BSE arranged by country and order of first occurrence [56]

Country	1985– 1989	1990– 1994	1995– 1999	2000	2001	2002	Total
United Kingdom	10181	136574	32640	1443	1202	534	182574
Rep. of Ireland	10	78	347	149	246	254	1084
France		10	69	161	274	177	691
Portugal		12	362	149	110	49	682
Switzerland		118	215	33	42	12	420
Germany				7	125	83	215
Spain				2	82	109	193

The major interspecies crossover of the prion-related diseases is associated with the transmission of BSE to humans.

In Great Britain in 1994, the first cases in teenagers and young adults of Creutzfeldt–Jacobs disease (CJD) were observed. The ages of the affected patients were much younger than previously associated with CJD and the neuropathology was characterised by numerous PrP amyloid plaques associated with a halo of intense spongiform degeneration in the brain, as a result of these differences. The disease was eventually labelled variant-CJD (v-CJD) or new variant-CJD (nv-CJD). From the nature of the outbreak, the possibility of interspecies crossover was first proposed and eventually became an accepted fact.

In fact, only about 150–200 known cases of nv-CJD have occurred up to this date. Given this relatively small incidence of infection and the effective reduction in the incidence of BSE, nv-CJD seemed to be a disease that would soon vanish.

However, in 2004 the first cases of inter-human transmission of nv-CJD were confirmed in Great Britain, with the infection occurring through blood transfusion. Other confirmed cases of infection via blood transfusion now exist. Perhaps more seriously, there are now known to be over 400 people known to have received blood or derived products from these known cases.

Research in the Great Britain has established that there is probably a pool of over 10 000 people carrying nv-CJD in the latent state.

Finally, in the summer of 2006, the World Health Organisation declared blood to be a carrier for nv-CJD.

TSE diseases, both in humans and animals present a certain number of characteristics:

1. An extremely long latency period with no visible symptoms, which can range from 16 months to over 40 years
2. The appearance of clinical signs reflects exclusively the arrival of destruction of the central nervous system
3. They are associated with an absence of other biochemical or cellular anomalies, other than the aggregation of the prion
4. A lack of reaction of the immune system
5. The lesions are located uniquely in the central nervous system

It is clear from the above that diagnosis of such diseases at an early stage of the disease requires a method for selective detection of the pathogenic form of the prion protein.

4.1

The Prion Protein

The normal cellular prion protein (PrP^C) is normally expressed in neuronal and lymphoid tissues. It contains ca. 210 amino acids, possesses a C-ter-

minal glycosylphosphatidylinositol (GPI) anchor and two N-glycosylation sites [56].

While there is wide conservation of the peptide sequence, both the GPI lipid anchor structure and in particular the glyco form structures have been shown to vary widely.

The structure of PrP^C is rich in α -helical content, however, there is a conformational shift on changing to the pathogenic PrP^{SC} form associated with a decrease in the α -helical content and an increase in the β -sheet content. This shift in conformation is associated with two changes in the biochemical properties (Table 10).

Table 10 Structural differences between PrP^C and PrP^{SC} (adapted from [56])

Property	PrP ^C	PrP ^{SC}
Protease resistance	No	Stable core containing residues 90–231
Disulfide bridge	Yes	Yes
Molecular mass after deglycosylation	16kD (rPrP 90–231)	16 kD (PrP 27–30)
Glycosylation	2N-linked sugars	2N-linked sugars
Glycoforms	Mixture of un-, mono-, and di-glycosolated forms	Mixture of un-, mono-, and di-glycosolated forms
Secondary structure	Dominated by α -helices	Rich in β -structure
Sedimentation properties	Consistent with monomeric species	Multimeric aggregated species (PrP 27–30)

The core residues 90–231 become resistant to protease cleavage and the protein tends to aggregate into plaques.

The three dimensional structure of PrP^C from various animal sources and recombinant forms has been widely studied by NMR, X-ray crystallography or combinations of both methods. Most recently the structure of the core region (123–230) of the bovine sheep prion was reported by Bayley's group [58] (Fig. 21). As with other studies, the structure is composed of three α -helical regions with two β -sheet regions positioned around the first α -helical.

The N-terminal region (residues 23–124) shows high disorder. Of particular interest in the work that follows is the presence of binding sites for the heparan sulfate glycofragments present on cell surface proteoglycans and the 37-kDA/67-kDA laminin receptor protein (LRP). From the amino acid sequence of PrP, shown in Fig. 22, two putative binding sites for heparan sulfate may be identified: 99–113 and 148–161 [6].

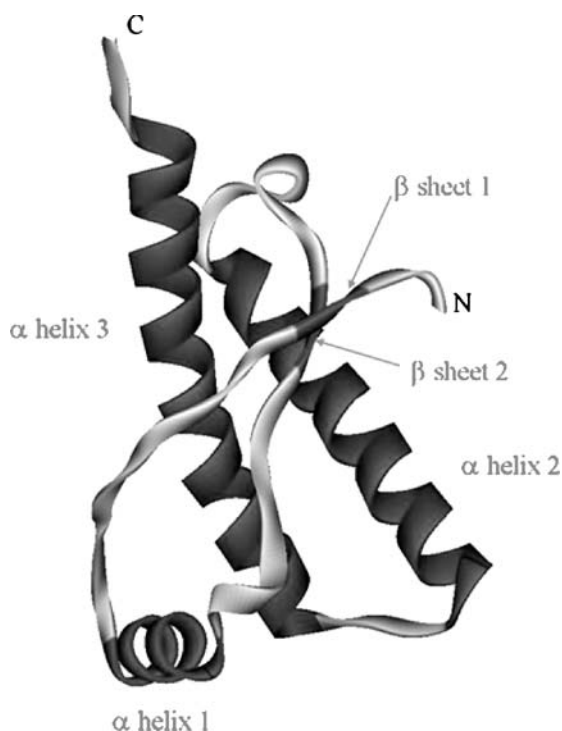


Fig. 21 Stereo view of residues 123–230 of the crystal structure of the globular domain of sheep PrP

```
MVKSHIGSWILVLFVAMWSDVGLCKKRPKPGGGWNTGGSRYPGQGSPG
GNRYPPQGGGGWGQPHGGGWGQPHGGGWGQPHGGGWGQPHGGGW
GQPHGGGGWGQGGTHGQWNKPSKPKTNMKHVAGAAAAGAVVGLGGY
MLGSAMSRPLIHFGSDYEDRYRENMHRYPNQVYYRPVDQYSNQNNFVH
DCVNITVKEHTVTTTTKGENFTETDIKMMERVVEQMCITQYQRESQAYYQR
GASVILFSSPPVILLISFLIFLIVGG
```

Fig. 22 Amino acid sequence of the bovine PrP protein, SAF84 epitope in *black*, putative binding sites for *para*-sulfonato-calix[n]arene derivatives *underlined*(99–113 and 148–161)

Both sites are rich in Lys and Arg, positively charged amino acids, as shown by modelling the charge surface of the protein (Fig. 23).

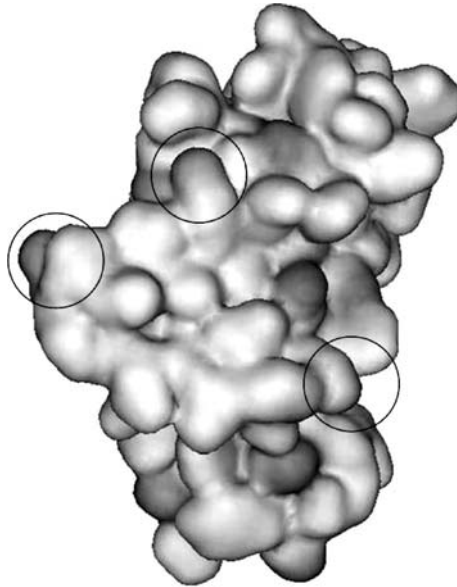


Fig. 23 Charge surface of the fragment 125–231 of the PrP. *Encircled* are the positively charged parts of the surface

4.1.1

Diagnostic Tool for Prion-Related Diseases

From the above, we can start to define the basis of a diagnostic tool for prion related diseases:

1. Ante-mortem detection
2. Detection for easily accessible physiological sources, e.g. spinal fluid or blood
3. Selective concentration of the prion protein to allow presymptomatic detection
4. Proteolytic removal of the cellular form PrP^C
5. Capture of the prion by a system resistant to proteolytic cleavage
6. Highly efficient detection of the prion.
A final condition must be added if the diagnostic test is to be used for large scale screening of populations:
7. Use of a test suitable for industrialisation

4.1.2

Supramolecular Sensing for the PrP^{SC} Form of the Prion

In the following sections we will follow the development of a “working test” for PrP^{SC}. In fact, the test is based on two sets of supramolecular interactions:

firstly, aggregation of PrP is achieved via hydrogen bonding between a suitable basic molecule and the negatively charged sites on PrP and secondly, suitable calix[n]arene derivatives are used to both amplify antibody detection of PrP^{SC} and to replace the capture antibody in an ELISA-based test.

4.1.3

Streptomycin as a Reticulating Supramolecular System for the Prion Protein

A screening experiment on the interactions between a number of antibiotics and PrP^{SC} showed that streptomycin (Fig. 24) caused an increase in the molecular weight of PrP^{SC} (Fig. 25). All three glycoforms of PrP^{SC} showed the same increase in mass, which was proportional to the quantity of streptomycin added. Approximately 10–12 molecules of streptomycin were observed by the mass increase to bind to PrP^{SC}. However, higher molecular ratios caused aggregation and flocculation of the protease K-resistant ovine PrP^{SC} [59].

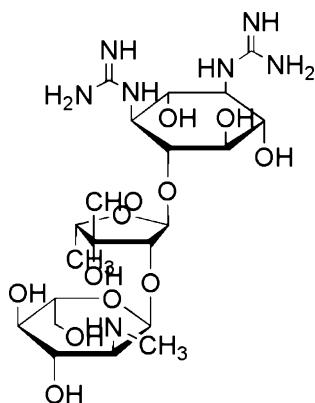


Fig. 24 Molecular structure of streptomycin

Further experiments showed that streptomycin was capable of precipitating aggregates of PrP^{SC} from cattle, mice and later human brain tissues.

The use of which gave similar results, ruling out an initial hypothesis that a Schiff-base reaction was not the cause of the aggregation. The work was extended to include other small molecules with at least two basic functions and we may generalise and state that the combination of at least two ammonium, pyridinium or guanadinium groups allowed precipitation of PrP^{SC}.

The proposed mechanism is via hydrogen bond salt bridges between the basic groups of streptomycin and acidic amino acids present on the surface of PrP (see Fig. 26).

Thus, via supramolecular interactions, a method for concentrating PrP^{SC} present in biological samples by the use of streptomycin as a precipitating

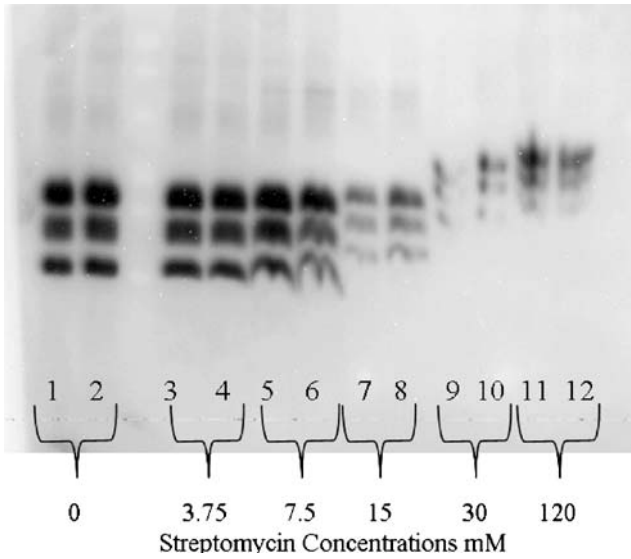


Fig. 25 Western blot: 10 μ L of the non-soluble fraction of PrP^{Sc} extracted from 2 mg of scrapie-infected sheep brain tissue per tube, and increasing concentrations of streptomycin

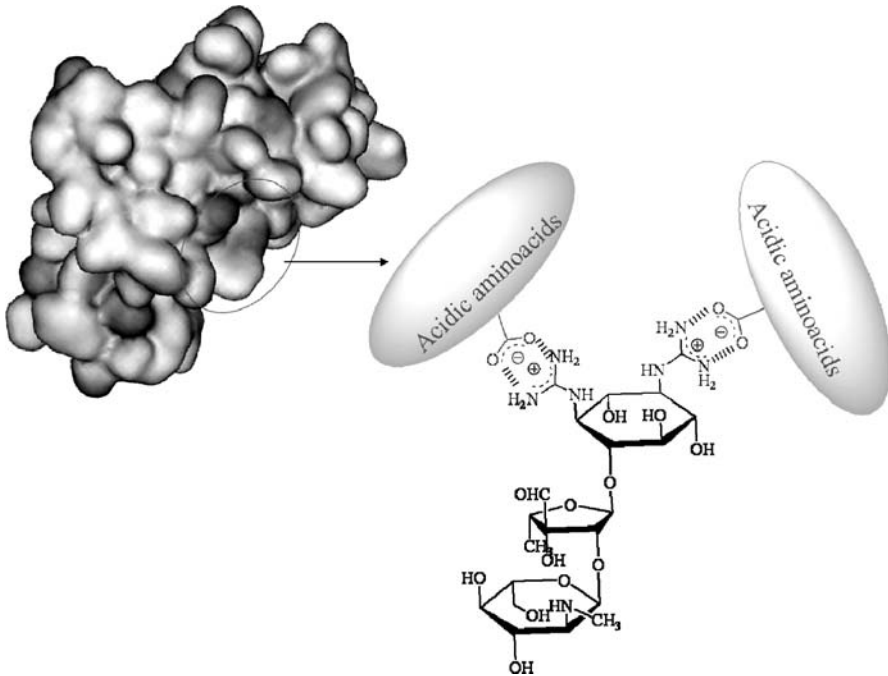


Fig. 26 Hydrogen bond salt bridges occurring between the basic groups of streptomycin and acidic amino acids of PrP

agent has been obtained. This enabled us to obtain one of the key steps in the development of a working test for prion-based diseases.

4.2

para-Sulfonato Calix[n]arenes is Western Blot Detection of PrP

The analogy between the *para*-sulfonato calix[n]arenes and the glycosyl-amino-glycans suggested that in view of the known heparan sulfate binding sites present in PrP these molecules should interact with PrP [60–62].

The series of *para*-sulfonato calix[n]arenes tested are shown in Fig. 27.

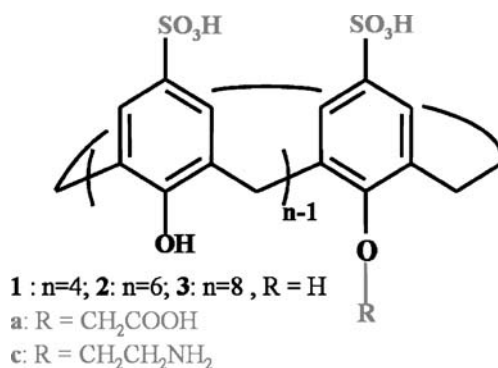


Fig. 27 Structure of *para*-sulfonato-calix[n]arene and their mono-functionalised derivatives

While there was little effect observed for the parent *para*-sulfonato calix[n]arenes 1, 2 and 3, the mono-substituted derivatives having either *O*-methoxycarbonylic acid (a) or *O*-ethoxyamine (c) functions at the lower rim showed considerable amplification of the Western Blot detection of PrP^{SC} (Fig. 28). As can be seen clearly, the detection limit was lowered by a factor of ten under optimised conditions. The antibody used here was SAF84, which has an epitope situated between 126 and 170 in the PrP sequence.

In the case of the Western Blot experiments, *para*-sulfonato calix[6]arene 2a was used in all further work. It was confirmed that 2a also amplified detection of PrP^{SC} from scrapie-infected goats and sheep (Fig. 29) in a similar manner to the bovine detection.

It is evident that whilst enhanced detection of PrP^{SC} was then desirable, if this had been accompanied by false positive or false negative results, the effective use of the *para*-sulfonato calix[n]arenes would have been limited or zero. In order to verify that this was not the case, two sets of experiments were undertaken. The first concerned showing a lack of false positives. Here, brain tissue from calves of less than 6 months, known not to be infected, were tested using Western Blots in the presence of 2a (Fig. 30).

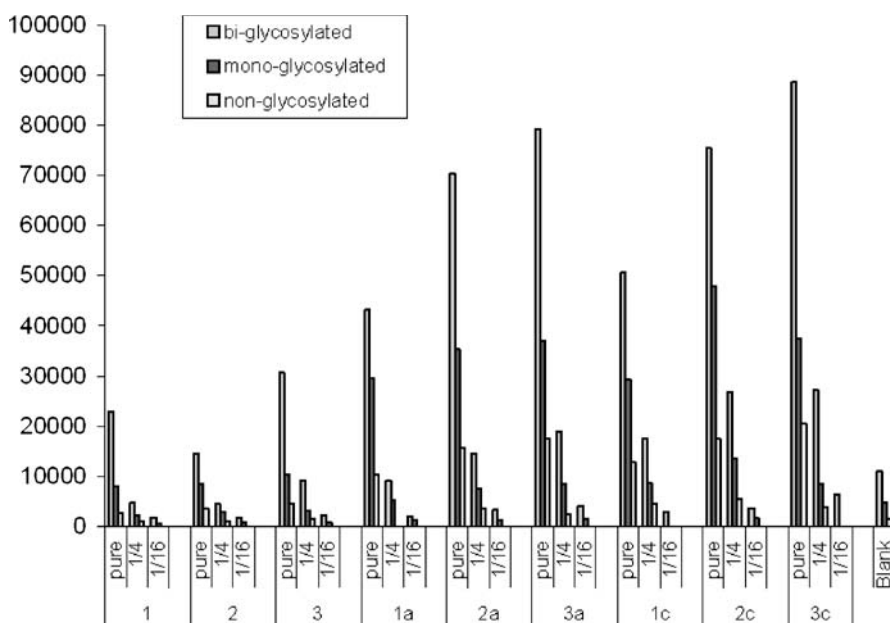


Fig. 28 Comparative Amplification of PrP^{SC} detection in presence of calix[n]arene derivatives

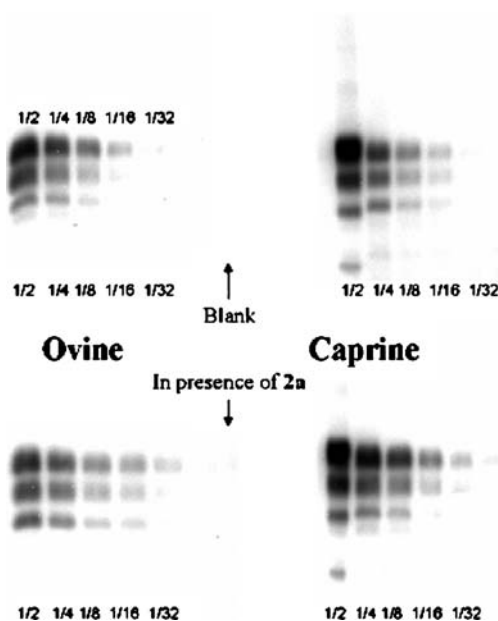


Fig. 29 Western Blot detection of ovine PrP^{SC} (left) and caprine PrP^{SC} (right) diluted at 1/2, 1/4, 1/8, 1/16 and 1/32 with addition of *para*-sulfonato-calix[6]arene derivative 2b. The blank was carried in absence of calixarene

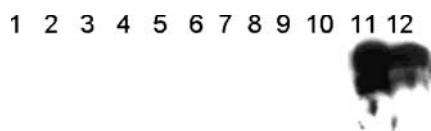


Fig. 30 Western blot detection of PrP^{SC} present in brains of calves aged 6 months (lanes 1–10) and from confirmed positive BSE cattle brains (lanes 11 and 12) in the presence of 1 μ L of a 0.1 M solution of *para*-sulfonato-calix[6]arene derivative **2a**

There are clearly no positive results in the lanes corresponding to the calf samples, whilst clear detection is observed for the lanes corresponding to two known positive samples.

In the second experiments, results of the use of **2a**, were compared to those obtained using the official AFSSA methodology (Fig. 31). Both methods detected three suspected cases (lanes 12, 13 and 14).

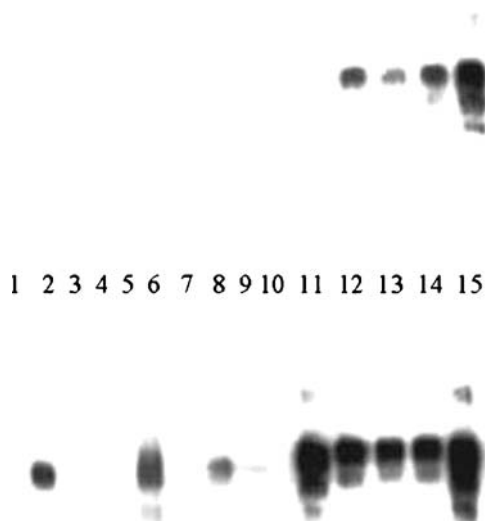


Fig. 31 Western blot detection of 13 BSE suspected field samples in absence (upper) and in presence (lower) of 1 μ L of 0.1 M *para*-sulfonato-calix[6]arene derivative **2a**. Two confirmed BSE positive controls were loaded onto lane 11 lower well and in lane 15 upper and lower wells. Buffer was load in the lane 11 upper well

However, for three cases (lanes 2, 6 and 8), whilst the “official” method showed negative results, the use of **2a** implied that these three cases were in fact weakly positive. Further immunohistochemical testing confirmed the fact these were indeed positive cases.

Summarising at this stage, mono-O-substituted *para*-sulfonato calix[n]-arenes interact with PrP^{SC} in such a manner that the detection of the pathogenic protein is amplified by up to ten times. Equally importantly, the

use of **2a** in the Western Blot detection of PrP^{SC} led neither to false positive nor to false negative results. Furthermore, cases not detected by standard methods were detected by **2a**-enhanced Western Blots.

4.3

ELISA-Based Detection of PrP Using *para*-Sulfonato Calix[n]arenes as “Capture Antibodies”

As we remarked earlier, the major aim of this work was to develop a test for the prion capable of use for screening millions of samples per year.

As such, although completely successful as a laboratory test, the Western Blot assays based on **2a**-induced amplification of PrP detection were not suitable for scale-up to such a level [61, 62].

The most widely used biological assays for proteins are based on the ELISA concept, either through (i) direct adsorption of a protein at a surface (Fig. 32a) followed by detection using antibodies, firstly a primary antibody specific to the detected protein and secondly an antibody containing an optical signal, or (ii) via a sandwich, which differs only in the use of a surface-coupled antibody to specifically capture the desired protein (Fig. 32b).

The use of a protease, generally proteinase K, to proteolytically cleave all other proteins than the resistant PrP^{SC} effectively removes both of these op-

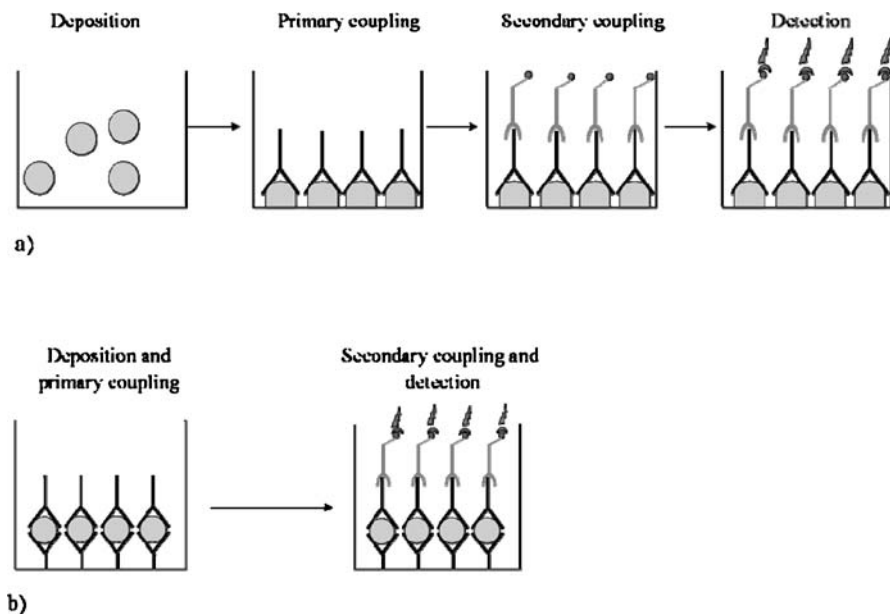


Fig. 32 The ELISA concept: **a** “classic type”, **b** “sandwich type”

tions. In the first case, there will be non-specific adsorption of the many peptide fragments remaining, blocking adsorption of PrP^{SC}. In the second case, either total removal of proteinase K must be achieved or proteolysis of the capture antibody will occur again and again and PrP^{SC} will not be held at the surface.

It is here that the advantage of the *para*-sulfonato calix[n]arene derivatives arises. If they could be successfully covalently coupled to the surface of the plastic 96-well titre plate used in ELISA, whilst still keeping their ability to capture PrP^{SC}, a replacement for the sandwich ELISA resistant to proteinase K would be available.

4.3.1

Coupling the *para*-Sulfonato Calix[n]arenes to ELISA Plates

A second advantage of the mono-substituted *para*-sulfonato calix[n]arenes, now comes into view, for not only are these compounds more active in the amplification of signal for the detection of PrP^{SC} but they also present a reactive handle for covalent grafting to suitably activated surface.

The most evident chemistry was via amide coupling either via activated carboxylate functions at the polymer surface or via activation of the carboxylate group on the calixarene for coupling to an amine activated surface (Figs. 33a and 33b, respectively).

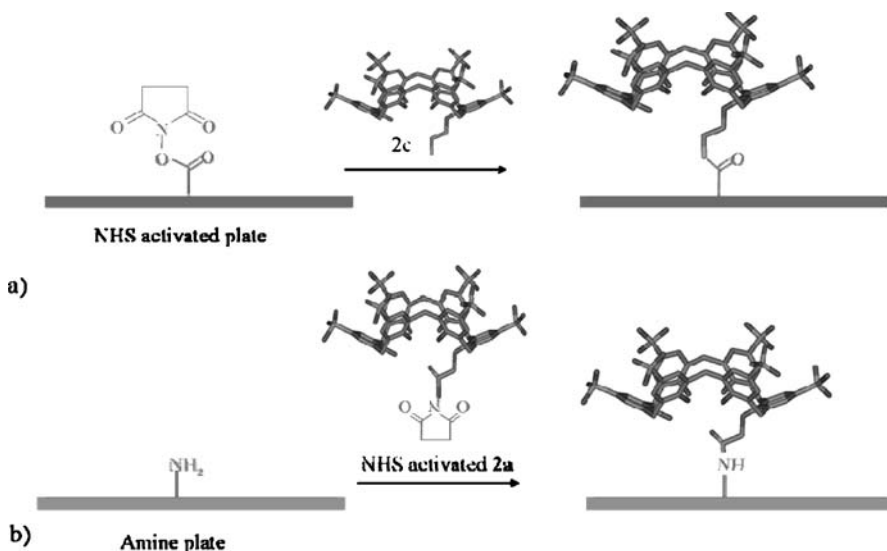


Fig. 33 Two ways of grafting calixarene derivatives on a surface: **a** via activated carboxylate functions at the polymer surface, or **b** via activation of the carboxylate group on the calixarene

Both methods were attempted but, unexpectedly, NHS-activation of the carboxylate function of **2a** proved totally impossible. (This led us to try various other agents for the activation of this carboxylic acid, but no success has so far been achieved; we consider that the function must be masked either sterically or via hydrogen bonding.) However, coupling of **2c** to an NHS-activated carboxylic acid was successful. However, not all commercially available titre plates, either NHS- or maleic anhydride-activated proved usable. Evidently the surface chemistry for coupling to small molecules such as calix[n]arenes differs strongly from that for protein coupling.

Another alternative for coupling calixarenes to microplates was then explored: biotinylated calixarenes and streptavidin-coated microplates. Thus, calixarenes were synthesised and grafted on the lower ring with a chemical spacer itself linked to a biotin molecule. Under these conditions, the biotinylated calixarenes revealed appropriate for PrP^{SC} detection. Figure 34

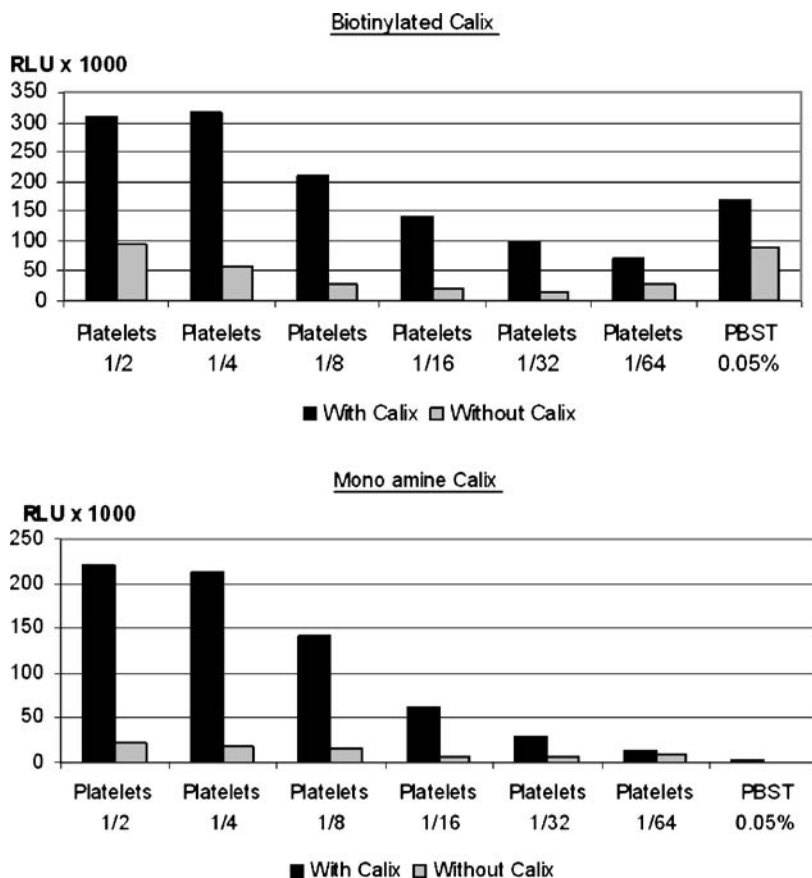


Fig. 34 Capture of platelet PrP on calixarene microplates: **a** streptavidin microplates with biotinylated calixarenes, **b** NHS microplates with NH₂ calixarenes

illustrates this property and compares the performance of biotinylated versus NH_2 -calixarenes on NHS-activated and streptavidin-coated microplates, respectively. Here, we used as source of antigen the non-infectious standard with PrP^{C} that has been long experienced in our studies to mimic PrP^{SC} aggregates, i.e. a suspension of sonicated human platelets cleared of large cellular debris by low-speed centrifugation.

Interestingly, the NH_2/NHS system provided the best detection conditions, given the ratio of OD between “with” and “without” calixarenes and, most of all, between specific signal and background noise, illustrated by that of PBST (phosphate buffer saline with 0.05% Tween 20).

The above success led us to develop a spectroscopic method for detection of *para*-sulfonato calix[n]arenes at the surface. This was based on the case of DMMB, as we had previously demonstrated the detection of these molecules in solution [63]. The differential signals, whilst very small, were sufficient to detect qualitatively *para*-sulfonato calix[n]arenes **2c** coupled to the titre well plates (Fig. 35).

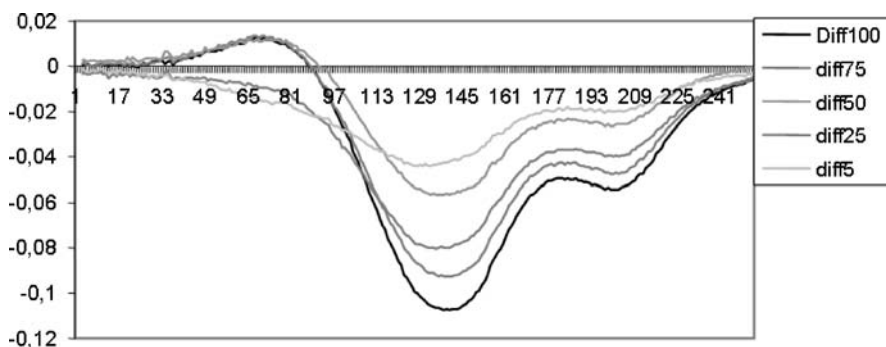


Fig. 35 Detection of *para*-sulfonato calix[n]arenes **2c** coupled to the titre well plates

The NHS-activated 96-well titre plates were designed for use in aqueous buffer; however, given the strong acidity of **2c**, there were some concerns about hydrolysis. Given this, the coupling reaction was carried out using three solvent systems: $\text{H}_2\text{O}/\text{PBS}$ (from P0 to P50), MeOH/NET_3 (from M0 to M50) and EtOH/NET_3 (from E0 to E50). The results in Fig. 36 show clearly that optimum coupling for the detection of platelet PrP occurred using the MeOH/NET_3 solvent system.

The use of platelet PrP as the test system arose from two points: (i) the very small quantities of PrP^{SC} available ruled out its use for optimisation of the test and (ii) the readily available recombinant PrP does not correspond to the behaviour of PrP^{SC} in these tests.

Having, pre-optimised the test system, confirmation of its utility for testing of PrP^{SC} in various types of biological sample was required. Figures 37, 38 and

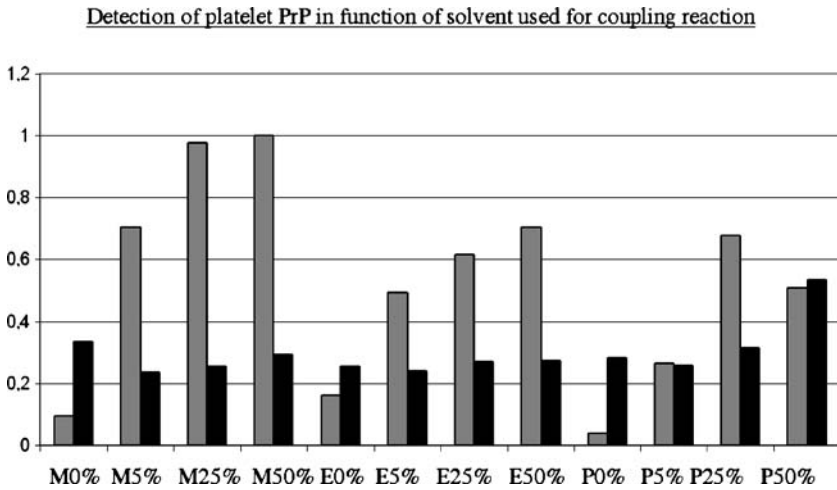


Fig. 36 Coupling as a function of the solvent system: *M* MeOH/NET₃, *E* EtOH/NET₃, *P* H₂O/PBS, grey “platelet”, black blank

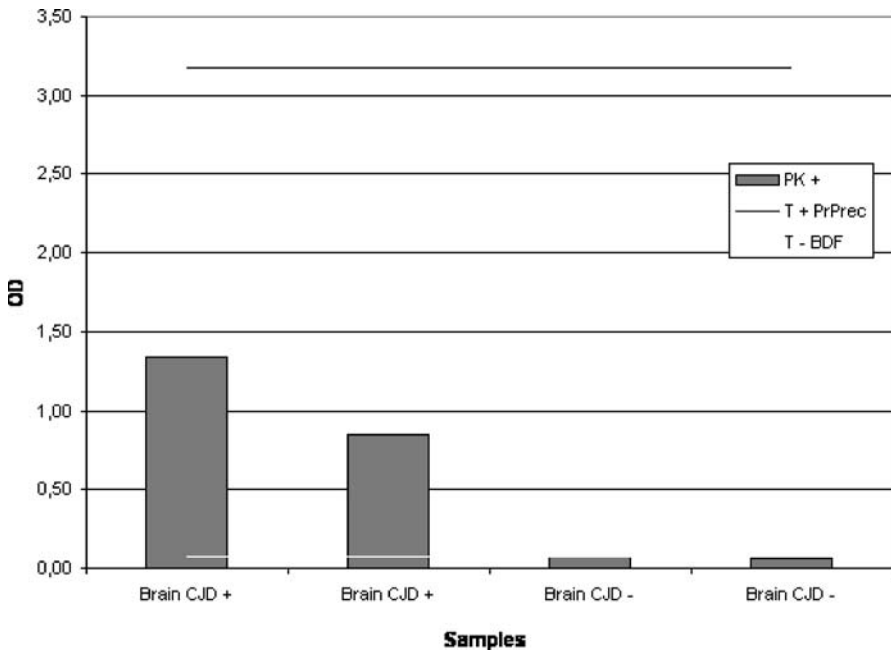


Fig. 37 Detection of PrP^{SC} in human CJD brain tissues

39 show the results for tests on brain tissue of CJD patients, spinal fluid from positive cases and finally plasma samples from known negative and positive bovine samples, respectively.

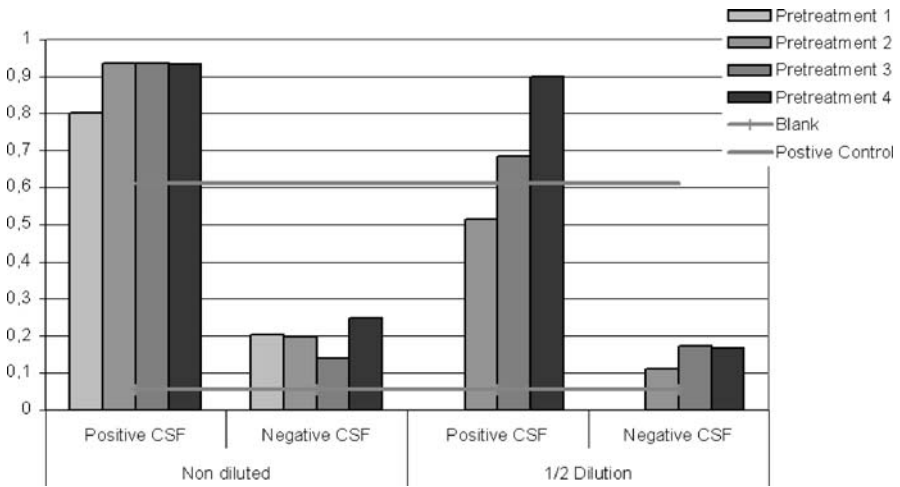


Fig. 38 Detection of PrP^{SC} in spinal fluid

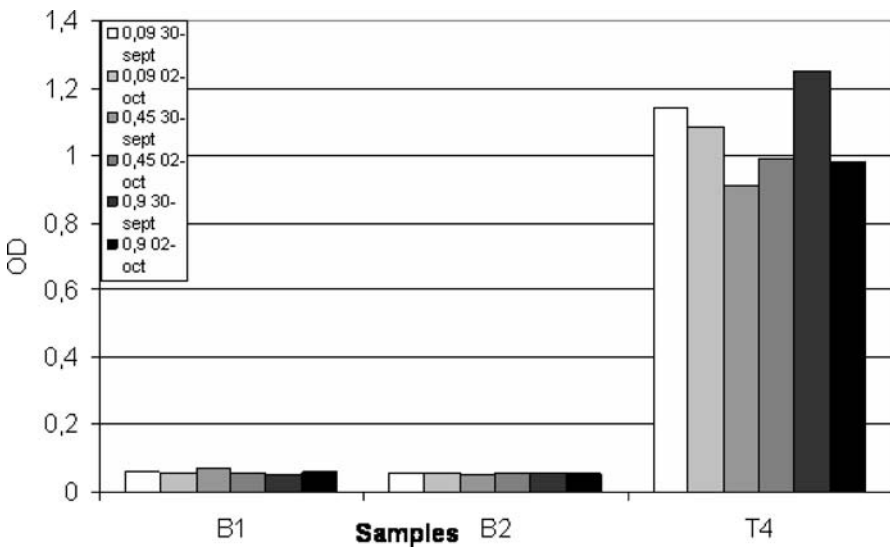


Fig. 39 Detection of PrP^{SC} (with repeatability over different experiments at different dates) in bovine plasma and BSE-infected ovine plasma: *B1* and *B2* are known to be negative samples, *T4* is known to be a positive sample (plasma from BSE-infected ovine)

It is clear that in all three types of biological sample there is clear discrimination between known positive cases and known negative cases. Moreover, the test, initially conceived using bovine PrP^{SC}, can also be used to detect human PrP^{SC} from brain tissue.

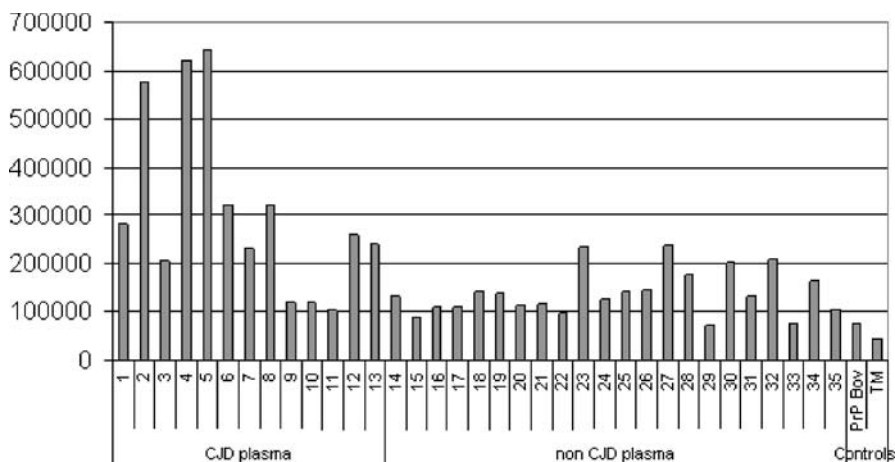


Fig. 40 Detection of PrP^{SC} in human CJD and non-CJD plasma

Moreover, we could thereafter set up a first prototype test for human plasma (here, not optimised for sensitivity and specificity), as illustrated in Fig. 40 with plasma samples from CJD and non-CJD (other dementias and blood donors) individuals. This first prototype test has nonetheless confirmed the feasibility of PrP^{SC} detection in human blood and has opened the avenue to further ongoing optimisations for a routine “PrP^{SC} screening” blood test in humans.

4.3.2

The Nature of the *para*-Sulfonato Calix[n]arene–Prion Interaction

Whilst a working test was the main objective of the work, a fundamental question remained. Where and how did the *para*-sulfonato calix[n]arenes interact with the prion protein.

As previously mentioned, two putative binding sites, 99–113 and 148–161, in the peptide sequence possess a high percentage of the basic amino acids Lys and Arg. In order to probe the possible interactions, the corresponding peptides were synthesised and their interaction with various *para*-sulfonato calix[n]arenes investigated using electrospray mass spectrometry, which we had previously shown to be a useful tool for the study of calix[n]arene–protein interactions.

Whilst the formation of complexes was observed (see Fig. 41) the results proved inconclusive as to which was the preferred site.

Pathogenicity of the prion protein is associated with conformational changes in the structure of the protein with presence of β -sheets increasing. However, ¹H NMR studies by Prusiner showed that while the sequence 124–231 is structured as an α -helix, the sequence 90–123 is unstructured [64]. The

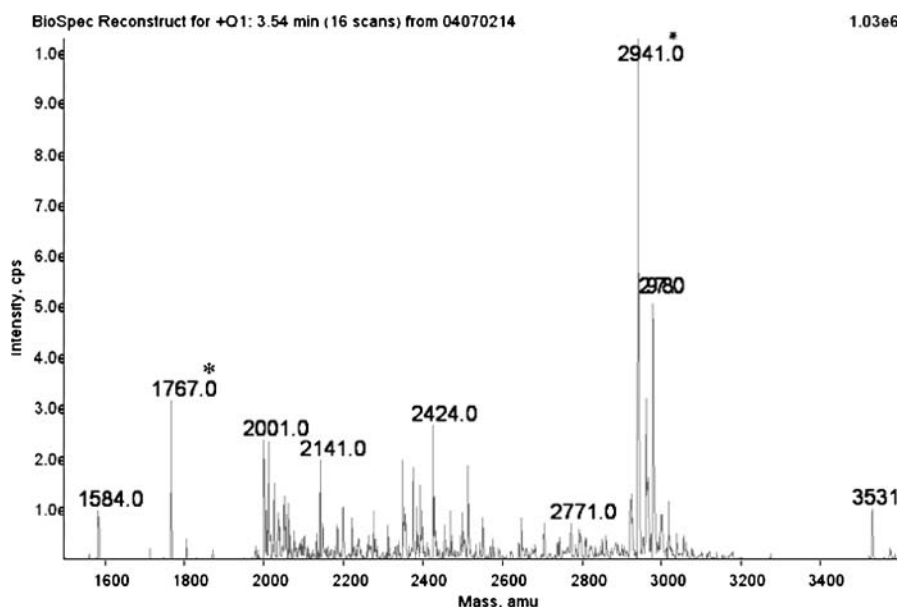


Fig. 41 ES/MS spectra of complexation of calixarene **2a** with peptide 99–113. The peak at 1767 UMA corresponds to peptide, the peak at 2941 UMA corresponds to the complex

presence of mobile peptide segments in the amyloid-associated HET-s prion, also containing Lys and Arg amino acids, has also recently been reported by Meier's group [65].

4.4

The Test Set-Up

The current, as of published results, set-up for the detection test for PrP^{SC} is summarised in Fig. 42.

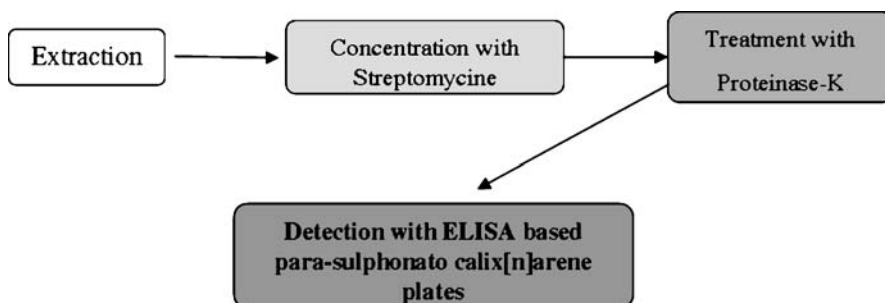


Fig. 42 Set-up for the detection of PrP^{SC}

Evidently, certain questions have not been answered in this review but the main one remaining is: can this test be transferred to an automated blood test for detection of PrP^{SC} at an early stage in human blood?

5 Conclusion

In conclusion, in spite of their non-biological origins the calix[n]arenes have proved to be of considerable interest due to their interactions with proteins.

In the case of the prion protein, we hope that a working diagnostic test based on capture of the pathogenic protein by a *para*-sulfonato-calix[n]arene will soon be available on a large scale, permitting screening for nv-Creutzfeldt–Jacobs disease and preventing infection by blood transfusion.

Acknowledgements One of us (FP) acknowledges financial support from the CNRS. We wish to express our gratitude for the help of Michele Granger and Sandrine Magnetto (SPV, CNRS, DR Rhine-Auvergne) without whom the prion project would never have been achieved. We also wish to thank Charlotte Veyssier for her help in preparing the manuscript.

References

1. Gutsche CD (1998) Calixarenes revisited: monographs in supramolecular chemistry. The Royal Society of Chemistry, Cambridge
2. Da Silva E, Shahgaldian P, Coleman AW (2004) *Int J Pharm* 273:57
3. Mutihac L, Buschmann H-J, Mutihac R-C, Schollmeyer E (2005) *J Inclu Phenomena Macrocycl Chem* 51:1
4. Ludwig R (2005) *Microchim Acta* 152:1
5. Da Silva E, Lazar AN, Coleman AW (2004) *J Drug Delivery Sci Technol* 14:3
6. Perret F, Lazar AN, Coleman AW (2006) *Chem Comm*, p 2425
7. Da Silva E, Coleman AW (2003) *Tetrahedron* 59:7357
8. Buschmann HJ, Mutihac L, Schollmeyer E (2003) *J Inclu Phenomena Macrocycl Chem* 46:133
9. Kalchenko OI, Perret F, Morel-Desrosiers N, Coleman AW (2001) *J Chem Soc, Perkin Trans* 2:258
10. Arena G, Contino A, Gulino FG, Magri A, Sansone F, Sciotto D, Ungaro R (1999) *Tetrahedron Lett* 40:1597
11. Douteau-Guevel N, Coleman AW, Morel J-P, Morel-Desrosiers N (1999) *J Chem Soc, Perkin Trans* 2:629
12. Douteau-Guevel N, Coleman AW, Morel J-P, Morel-Desrosiers N (1998) *J Phys Org Chem* 11:693
13. Zielenkiewicz W, Marcinowicz A, Poznanski J, Cherenok S, Kalchenko V (2006) *J Inclu Phenomena Macrocycl Chem* 55:11
14. Zielenkiewicz W, Marcinowicz A, Cherenok S, Kalchenko VI, Poznanski J (2006) *Supramol Chem* 18:167

15. Zadmard R, Schrader T (2005) *J Am Chem Soc* 127:904
16. Perret F (2002) Etudes thermodynamique et structurale de la complexation d'acides aminés et de molécules modèles par des calixarènes hydrosolubles. Université Blaise Pascal
17. Sansone F, Barbosio S, Casnati A, Sciotto D, Ungaro R (1999) *Tetrahedron Lett* 40:4741
18. Perret F, Guiret S, Danylyuk O, Suwinska K, Coleman AW (2006) *J Mol Struct* 797:1
19. Douteau-Guevel N, Perret F, Coleman AW, Morel J-P, Morel-Desrosiers N (2002) *J Chem Soc* 2:524
20. Mecca T, Consoli GML, Geraci C, Cunsolo F (2004) *Bioorg Med Chem* 12:5057
21. Casnati A, Sansone F, Ungaro R (2003) *Acc Chem Res* 36:246
22. Consoli GML, Cunsolo F, Geraci C, Sgarlata V (2004) *Org Lett* 6:4163
23. Leray E, Parrot-Lopez H, Auge C, Coleman AW, Finance C, Bonaly R (1995) *Chem Comm*, p 1019
24. Hamuro Y, Calama MC, Park HS, Hamilton AD (1997) *Angew Chem, Int Edn (in English)* 36:2680
25. Lin Q, Hamilton AD (2002) *Comptes Rendus Chimie* 5:441
26. Lin Q, Park HS, Hamuro Y, Lee CS, Hamilton AD (1998) *Biopolymers* 47:285
27. Wei Y, McLendon GL, Hamilton AD, Case MA, Purring CB, Lin Q, Park HS, Lee CS, Yu TN (2001) *Chem Comm*, p 1580
28. Park HS, Lin Q, Hamilton AD (1999) *J Am Chem Soc* 121:8
29. Oshima T, Goto M, Furusaki S (2002) *Biomacromolecules* 3:438
30. Memmi L, Lazar A, Brioude A, Ball V, Coleman AW (2001) *Chem Comm*, pp 2474–2475
31. Da Silva E, Rousseau CF, Zanella-Clion I, Becchi M, Coleman AW (2006) *J Incl Phenomena Macrocycl Chem* 54:53
32. Peters TJ (ed) (1996) All about albumin: biochemistry, genetics and medical applications. Academic, San Diego
33. Reed RG (1986) *J Biol Chem* 261:15619
34. Aime S, Barge A, Botta M, Casnati A, Fragai M, Luchinat C, Ungaro R (2001) *Angew Chem-Int Edn* 40:4737
35. Bryant LH, Yordanov AT, Linnoila JJ, Brechbiel MW, Frank JA (2000) *Angew Chem-Int Edn* 39:1641
36. Gualbert J, Shahgaldian P, Coleman AW (2003) *Int J Pharm* 257:69
37. Cornforth JW, D'Arcy Hart P, Nicholls GA, Rees RJW, Stock JA (1955) *Brit J Pharm Chemotherapy* 10:73
38. Hart PD, Armstrong JA, Brodaty E (1996) *Infection Immunity* 64:1491
39. Colston MJ, Hailes HC, Stavropoulos E, Herve AC, Herve G, Goodworth KJ, Hill AM, Jenner P, Hart PD, Tascon RE (2004) *Infection Immunity* 72:6318
40. Hwang KM, Qi YM, Liu SY, Choy W, Chen J (1995) (Genelabs, USA) US Patent 5 441 983
41. Mourer M, Duval RE, Finance C, Regnouf-de-Vains J-B (2006) *Bioorg Med Chem Lett* 16:2960
42. Casnati A, Fabbi M, Pelizzi N, Pochini A, Sansone F, Ungaro R, DiModugno E, Tarzia G (1996) *Bioorg Med Chem Lett* 6:2699
43. Lamartine R, Tsukadab M, Wilson D, Shirata A (2002) *C R Chimie* 5:163
44. Sun JZ, Blaskovich MA, Jain RK, Delarue F, Paris D, Brem S, Wotoczek-Obadia M, Lin Q, Coppola D, Choi KH, Mullan M, Hamilton AD, Sebt SM (2004) *Cancer Res* 64:3586
45. Hwang KM, Qi YM, Liu SY, Lee TC, Choy W, Chen J (1995). (Genelabs, USA). US Patent 5 409 959

46. Hulmes D, Coleman A, Aubert-Foucher E (1999) World Patent 99-FR1922
47. Da Silva E, Ficheux D, Coleman AW (2005) *J Incl Phenom Macrocyclic Chem* 52:201
48. Droogmans G, Prenen J, Eggermont J, Voets T, Nilius B (1998) *Am J Physiol* 275:C646
49. Droogmans G, Maertens C, Prenen J, Nilius B (1999) *Brit J Pharm* 128:35
50. Atwood JL, Bridges RJ, Juneja RK, Singh AK (1996). (The University of Alabama At Birmingham Research Foundation, USA). US Patent 5 489 612
51. Seganish JL, Santacroce PV, Salimian KJ, Fettinger JC, Zavalij P, Davis JT (2006) *Angew Chem-Int Edn* 45:3334
52. Lee M, An WG, Kim J-H, Choi H-J, Kim S-H, Han M-H, Koh K (2004) *Mater Sci Eng, C: Biomimetic Supramolecular Sys* C24:123
53. Kolusheva S, Zadnarm R, Schrader T, Jelinek R (2006) *J Am Chem Soc* 128:13592
54. Oh SW, Moon JD, Lim HJ, Park SY, Kim T, Park J, Han MH, Synyder M, Choi EY (2005) *FASEB J* 19:1335
55. Trojanowski JQ, Goedert M, Iwatsubo T, Lee VM-Y (1998) *Cell Death Diff* 5:832
56. Prusiner SB (ed) (2004) *Prion biology and diseases*, 2nd edn. Cold Spring Harbor Laboratory, New York
57. World Organisation for Animal Health (OIE) (2003) http://www.oie.int/eng/info/en_esbmonde.htm, last visited: 8 Mar 2007
58. Haire LE, Whyte SM, Vasisht N, Gill AC, Verma C, Dodson EJ, Dodson GG, Bayley PM (2004) *J Molecular Biol* 336:1175
59. Moussa A, Coleman AW, Bencsik A, Leclere E, Perret F, Martin A, Perron H (2006) *Chem Comm*, p 973
60. Coleman AW, Perret F, Cecillon S, Moussa A, Martin A, Dupin M, Perron H, Leclere E (2007) *New J Chem* DOI:10.1039/b615523p
61. Bencsik RA, Coleman AW, Da Silva E, Dupin M, Leclere E, Martin A, Moussa A, Perron H, Ronzon F (2005). (Biomerieux S.A., Fr.; Agence Francaise de Securite Sanitaire des Aliments AFSSA; Centre National de la Recherche Scientifique CNRS; Universite Claude Bernard Lyon I). FR Patent 004/00492, 2004
62. Moussa A, Coleman AW, Shahgaldian P, Da Silva E, Martin A (2004). (Agence Francaise De Securite Sanitaire Des Aliments Afssa, Fr.; Centre National De La Recherche Scientifique Cnrs; Universite Claude Bernard Lyon I). PCT/FR03/03857, 2003
63. Rousseau CF, Cecillon S, da Silva E, Freyria A-M, Herbage D, Leclere E, Coleman AW (2005) *J Incl Phenomena Macrocycl Chem* 53:9
64. Prusiner SB (1991) *Science* 252:1515
65. Siemer AB, Arnold AA, Ritter C, Westfeld T, Ernst TM, Riek R, Meier BH (2006) *J Am Chem Soc* 128:13224

Polypeptide Conjugate Binders for Protein Recognition

Lars Baltzer

Department of Biochemistry and Organic Chemistry, Uppsala University, BMC, Box 576,
75123 Uppsala, Sweden
Lars.Baltzer@biorg.uu.se

1	Introduction	90
2	Molecular Recognition of Proteins	91
2.1	The Design Challenge	91
2.1.1	Forces Between Biomolecules in Aqueous Solution	91
2.1.2	The Entropy Problem in Molecular Recognition	92
2.2	The Design Strategy	92
2.3	The Synthesis Challenge	93
2.4	A Chemical Approach to Protein Recognition	94
3	A Polypeptide Conjugate Binder for Protein Recognition	95
3.1	Human Carbonic Anhydrase II – a Model Target Protein	95
3.2	The Helix-Loop-Helix Motif - a Versatile Multifunctional Scaffold	96
3.2.1	The Solution Structure of the Helix-Loop-Helix Dimer	98
3.2.2	The Functionalization of the Helix-Loop-Helix Dimer	99
4	The Binding of Human Carbonic Anhydrase II	99
4.1	KE2-PL Binds HCAII Selectively and With High Affinity	99
4.1.1	The Affinity Depends Critically on Spacer Properties and Length	100
4.2	Characterizing Binding by NMR Spectroscopy	101
4.3	KE2-PL Binds HCAII As a Monomer	103
4.4	Biosensing With KE2-PL	103
5	Polypeptide Conjugates as Agents in Protein Recognition	104
	References	105

Abstract A new class of hybrid molecules for protein recognition is presented, where polypeptides are covalently linked to small organic molecules to form polypeptide conjugates that bind proteins with high affinity and selectivity. To illustrate the concept, a binder for human carbonic anhydrase II with a dissociation constant of 4 nM is described. The affinity of the polypeptide conjugate arises from cooperativity in binding between a benzenesulfonamide residue, with a dissociation constant of 1.5 μ M, and the polypeptide scaffold with a dissociation constant of < 1 mM. The combination of a ligand with moderate affinity for a target protein with a polypeptide relaxes considerably the need for high affinity on the part of the polypeptide, and thus the need for structural complexity and preorganization. At the same time, the requirement for high affinity on the part of ligand is relaxed. As a consequence, the time for development of robust, high affinity, selective binder is shortened. The chemical approach to protein recognition provides well-defined molecular entities that are conveniently handled, stored and site-specifically functionalized.

Keywords Affinity · Conjugate · Molecular recognition · Polypeptide · Protein

Abbreviations

HCAI	Human carbonic anhydrase I
HCAII	Human carbonic anhydrase II
KE2	42-residue polypeptide KE2
KE3	42-residue polypeptide KE3
KE2-P	KE2 with covalently attached fluorophor
KE2-PL	KE2 with covalently attached fluorophor and benzenesulfonamide ligand

1

Introduction

Protein-mediated molecular recognition events control innumerable important functions in the living cell. The recognition and binding of proteins is the key to capitalizing on the rapid progress in the field of proteomics. Molecules capable of discriminating between tens of thousands of proteins in complex biological media such as whole blood, serum and plasma are required for today's and tomorrow's diagnostic and therapeutic applications in the health care sector. From a fundamental point of view, the design of molecules capable of recognizing and binding proteins represents a considerable challenge and an important goal in testing our understanding of molecular recognition and design.

While molecular recognition remains a buzzword in chemistry, with the exception of small molecule drugs, surprisingly few attempts have been reported by chemists aimed at designing and synthesizing molecules capable of recognizing and binding proteins [1]. Strategies emanating from molecular biology and immunology largely dominate the field, mainly antibodies [2, 3], aptamers [4] and peptides/proteins from phage-display generated libraries [5]. These "biologically generated" binders for proteins, especially the antibodies, are extensively used as tools in biomedical and biotechnological research laboratories, and as components in clinical diagnostic tests. Several antibodies are in clinical trials to be evaluated for pharmaceutical use. While the use of antibody technologies has enabled numerous applications and antibodies have proven to be extremely useful reagents in biotechnology and biomedicine, new molecular concepts need to be developed to meet the requirements of the future. Of special interest are robustness, the elimination of batch-to-batch variation and access to several directly addressable molecular handles that can be used to combine multiple functions, with ease and reproducibly, in well-defined scaffolds. Synthetic organic chemistry has developed over many years to meet those requirements as well as many others, and the application of chemical strategies to the design and synthesis of recognition elements for proteins is long overdue.

In this article we describe the design and function of a new type of “chemically generated” recognition element or “binder” for proteins in which the properties of polypeptides are combined with those of small molecules to form robust, efficient and selective polypeptide conjugates with high affinity and selectivity for proteins.

2

Molecular Recognition of Proteins

The design of binders for proteins needs to take into account how to obtain affinity and selectivity in aqueous solution, and how to balance flexibility versus rigidity in the binder structure.

2.1

The Design Challenge

From a fundamental perspective, at the molecular level, the recognition of proteins represents a considerable challenge due to the weak non-covalent interactions of amino acid functional groups in aqueous solution. In addition, proteins are moving targets due to the dynamic nature of protein structures. Molecules exhibiting “nM to pM affinities” for proteins (i.e. dissociation constants of the protein–binder complexes in the nM to pM region) in combination with the capacity to discriminate between tens or even hundreds of thousands of proteins, some of which are in very large abundance, represent an ambitious level in molecular design.

2.1.1

Forces Between Biomolecules in Aqueous Solution

The side chains of amino acids are, in principle, monofunctional and form non-covalent bonds through salt bridges and hydrogen bonds as well as through hydrophobic interactions. The strengths of these interactions have been measured and are now well understood [6]. A salt bridge in aqueous solution contributes 0.5 kcal/mol of binding free energy [7]. A single hydrogen bond in aqueous solution may contribute little or no free energy since both the donor and the acceptor are solvated before forming the hydrogen bond and the net change in the number of hydrogen bonds may be zero [8]. The magnitude of hydrophobic interactions is directly proportional to the buried surface area and contributes $50 \text{ cal}/\text{\AA}^2$, corresponding typically to 2–3 kcal/mol for a leucine side chain [9]. It follows that individual interactions are weak and that multidentate binders are required for high affinities if they are based exclusively on amino acids. In order to orientate several

functional groups in three-dimensional space, complex structures need to be formed.

2.1.2 The Entropy Problem in Molecular Recognition

Amino acid side chains have rotatable bonds and the binding event is linked to an entropic penalty, approximately 0.9 kcal/mol per bond [10], assuming that the amino acid binds in only one conformation. The peptide backbone can adopt at least two conformations per amino acid residue [11] and the entropic penalty becomes severe when unordered peptides are to bind in a single conformation to a protein target. The same considerations apply to any molecule with many rotatable bonds. Binding of proteins by linear peptides is nevertheless observed, although with moderate affinities, showing that the accessible binding energy inherent in amino acid functional groups that bind cooperatively is considerable, provided that the binding surfaces in the complex are reasonably shape and charge complementary. It is a reasonable assumption that some affinity of a polypeptide for a protein surface should be achievable with relative ease, and possibly also that a polypeptide with moderate complexity, say 42 amino acid residues as discussed below, should have the potential for forming weak complexes with several proteins, adopting different conformations in each case.

2.2 The Design Strategy

While evolution has selected to build our immune system upon binders based on many individually weak interactions to ensure selectivity and affinity, it is an open question whether such complex structures are actually required or even optimal for efficient recognition and binding. In contrast to what is observed for biooligomers and biopolymers, small organic molecules used as drugs (i.e. enzyme inhibitors, receptor agonists or antagonists) bind to binding sites with high affinities in spite of the fact that they have molecular weights of less than 500 and relatively few functional groups. A precise fit and a high degree of rigidity is undoubtedly part of the reason for the efficient binding and it is tempting to hypothesize that in general, rigid, multifunctional residues would be expected to have higher propensities for binding to proteins than the side chains of the common amino acids. While small molecules with drug-like affinities would be very useful tools in protein recognition, they are not easy to come by. In contrast, small molecules with dissociation constants in the range from high to low micromolar are relatively abundant and often observed in the screening of combinatorial libraries. This suggests that a faster route towards efficient binders would be to covalently link small molecules with modest affinities in a scaffold.

The incorporation of small molecules with moderate affinities into polypeptide scaffolds provides an attractive alternative to biologically generated binders since peptide chemistry is well-developed and since the peptide scaffold itself has the capacity to contribute to the overall binding interaction. Such conjugate molecules would be expected to have considerably improved binding properties over those of each of its components, provided that there is charge and shape complementarity between binder and protein. They would also be expected to have better binding properties than those based on the common amino acids since each individual interaction is stronger. The use of residues with higher inherent propensities for molecular interactions with protein surfaces or binding sites than those of the common amino acids would furthermore be expected to reduce the number of interactions needed with the target to achieve similar or better selectivity, and to relax significantly the demand for structural complexity and rigidity of the binder. The methodology for the synthesis of such conjugate molecules is well developed and polypeptide conjugate molecules may be produced rapidly as well as combinatorially.

2.3

The Synthesis Challenge

The time taken to prepare a binder will be an important factor in deciding whether synthetic strategies will be of general interest as an alternative to antibodies and aptamers. The technologies needed to develop antibodies, aptamers and phage-display generated peptides and proteins are well developed. The fact that synthetic binders will most often require multistep preparative operations raises the question of whether polypeptide conjugate molecules are in fact at all practical alternatives for protein recognition on a global scale. Peptide chemistry is, however, now well developed and peptide synthesis is for most purposes automated and fast. The synthesis of non-natural amino acids is cumbersome and time-consuming but, fortunately, there are convenient strategies for functionalizing directly the side chains of amino acids of polypeptides without the need for protection group strategies. Methods and reagents for the incorporation of fluorophores, linkers, metal complexes etc. chemoselectively and site-selectively into peptides and proteins have been developed that can be used to introduce virtually any functional group using very simple chemistry. The methods of peptide and protein chemistry will thus ensure fast access to multifunctionalized peptides with non-native residues linked to the side chains of serine, threonine, tyrosine, lysine, cysteine, glutamic acid and aspartic acid residues. The rate-limiting step will be the synthesis of the small molecule derivatives to be conjugated to the polypeptide scaffolds and will vary from binder to binder.

2.4 A Chemical Approach to Protein Recognition

As the first step towards developing a general strategy for the preparation of synthetic binders for proteins based on this concept, the incorporation of benzenesulfonamide, a small molecule inhibitor with $1.5 \mu\text{M}$ affinity for human carbonic anhydrase II (HCAII) [12] into a polypeptide scaffold was attempted, Fig. 1. The goal was to form a polypeptide conjugate molecule in which the combination of affinities from the polypeptide and the inhibitor could be expected to give rise to high overall affinity. Selectivity was ex-

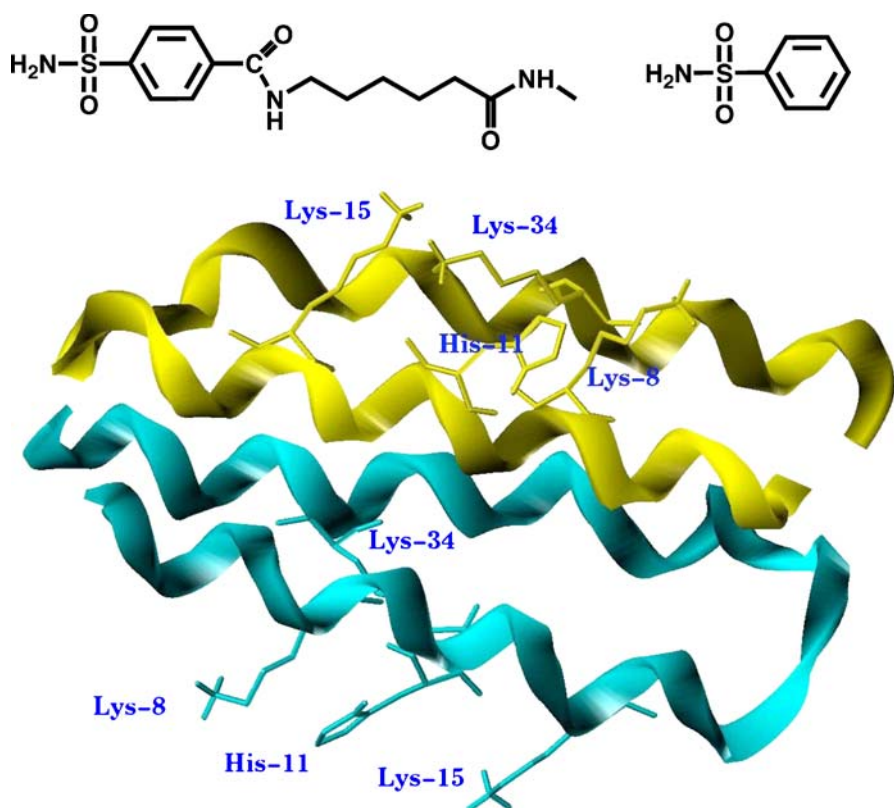


Fig. 1 Illustration of the concept of polypeptide conjugation for protein recognition. Benzenesulfonamide is a known inhibitor of HCAII, with a dissociation constant of $1.5 \mu\text{M}$ [12]. Chemical modification of the aromatic ring makes it possible to attach a bi-functional spacer, here aminohexanoic acid, to covalently link the benzenesulfonamide residue to a lysine residue side chain in the polypeptide scaffold. In this case, an active ester was reacted directly with the lysine residue in a site-selective functionalization reaction

pected to arise from the combined selectivities of the benzenesulfonamide, which binds to the Zn ion in the active site, and of the scaffold, which was expected to bind to the surface of the protein in the neighbourhood of the active site. In a semi-rational approach, a suitable spacer would have to be found to allow simultaneous binding of the benzenesulfonamide and of the scaffold. In addition to the ligand, a fluorophore was incorporated into the scaffold to enable quantification of interactions, under the assumption that the molecular environment of the fluorophore would change upon complexation. The incorporation of fluorophores provides a convenient strategy for the screening of binder libraries and of automated measurements of affinities.

3

A Polypeptide Conjugate Binder for Protein Recognition

In a proof-of-principle demonstration HCAII was selected as the target protein and the helix-loop-helix dimer KE2 was chosen as scaffold for functionalization with a known small molecule inhibitor for HCAII.

3.1

Human Carbonic Anhydrase II – a Model Target Protein

Human carbonic anhydrase II (HCAII) was selected as a target for the design of a polypeptide conjugate binder. HCAII is a 29 kD enzyme that catalyses the interconversion of carbon dioxide and bicarbonate in the respiratory system [13]. The active site is located in a 15Å deep cleft and the most important component of the catalytic machinery is a Zn ion to which sulfonamide inhibitors have been shown to bind. Crystal structures of HCAII, and of HCAII complexed to ligands, have been determined several times [14–16] and the NMR spectrum has been assigned [17]. In addition, the folding properties of HCAII have been studied extensively [18] and several inhibitors are known [19,20]. A binder for HCAII was designed by attaching a derivative of benzenesulfonamide, a 1.5 μM inhibitor of HCAII [12], via an aliphatic spacer to a helix-loop-helix motif under the assumption that the combined affinities of the inhibitor, the spacer and the polypeptide scaffold would give rise to a high overall affinity [21]. According to the design, the inhibitor residue should bind to the Zn ion in the active site, and the scaffold should form contacts with the surface area in close proximity to the active site. The binding site contains several hydrophobic residues capable of interacting with the aliphatic spacer [22] and contributions from the spacer might also add to the overall affinity. An illustration of how binding could be envisioned to occur is shown in Fig. 2.

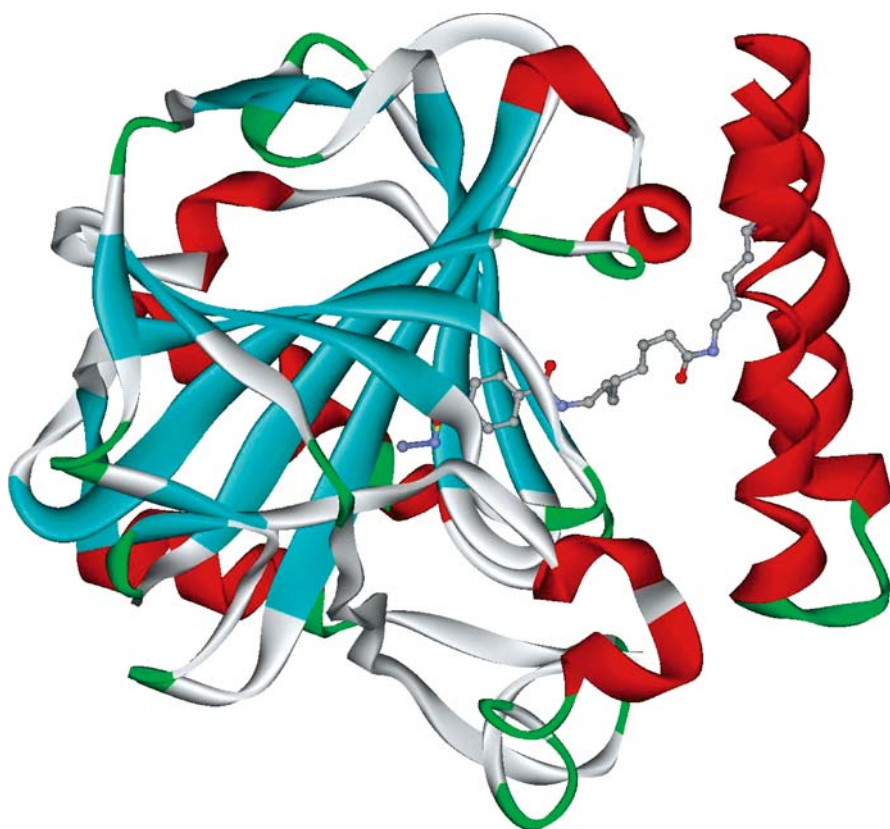


Fig. 2 Illustration of how binding might occur, based on the crystal structure of HCAII crystallized in the presence of benzenesulfonamide modified with an aliphatic substituent [16]. The structure of the helix-loop-helix motif equipped with an aminooctanoic acid spacer has been modelled into the crystal structure. The overall affinity of the binder arises from contacts between the benzenesulfonamide group as well as the interactions between scaffold and protein. It has been experimentally verified that the conjugate binds as a monomer [29] and that there are interactions between scaffold and HCAII surface residues [28]

3.2

The Helix-Loop-Helix Motif - a Versatile Multifunctional Scaffold

A de novo designed 42-residue polypeptide that folds into a helix-loop-helix motif and dimerizes to form a four-helix bundle was selected as the scaffold [23]. It can be site-selectively functionalized with relative ease using a variety of methods and reagents [6,24]. The helical segments are amphiphilic with one hydrophobic and one hydrophilic face, enabling hydrophobic as well as charge-charge interactions with the target protein. The se-

NBADJEAAIKALAEHJBAK	GPVD	BAQJAEQLAKAFEAFARBG	SA42
NAADLEAAIRHLAEKLAAR	GPVD	AAQLAEQLAKKFEAFARAG	KE2
NAADLEAKIRHLAEKLAAR	GPCD	AAQLAEQLARRFEAFARAG	KE3

Fig. 3 Amino acid sequences of SA42, KE2 and KE3

quence KE2, Fig. 3, was based upon that of SA-42, a well characterized de novo designed helix-loop-helix dimer [25], and differed by 13 residues from the parent polypeptide. Four Aib residues were replaced by alanines, three norleucine residues were replaced by leucines and two lysines were replaced by arginines. Four sequence modifications were related to function. The design principles of the helix-loop-helix dimer have been described in detail [23, 25]. In short, helix segments were designed based on amino acid propensities for helix formation and the incorporation of amino acid residues capable of salt bridge formation, helix dipole neutralization and capping to stabilize the folded helical state. A short loop, Gly-Pro-Val-Asp, was used to connect the helical sequences. Amphiphilicity was introduced using combinations of hydrophobic and hydrophilic amino acid residues, in a pattern conveniently described in terms of the heptad repeat $(abcdefg)_n$. The *a* and *d* residues are hydrophobic and form the hydrophobic core, the *b* and *e* residues are charged and control the mode of dimerization at the helix interfaces, and the *g* and *c* residues are used to incorporate recognition and reporting groups (Fig. 4). Folding is driven mainly by hydrophobic interactions between the hydrophobic faces of the amphiphilic helices. The size of the scaffold was chosen on the assumption that it should be able to interact with proteins without perfect structural complementarity, yet contain enough inherent binding energy to enhance the affinity of the

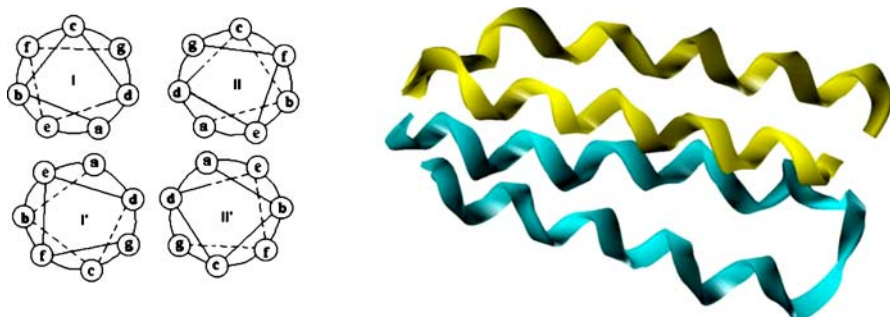


Fig. 4 Heptad repeat pattern adapted to an antiparallel helix-loop-helix dimer, to illustrate the formation of a hydrophobic core from *a* and *d* residues, and the accessibility of *c* and *g* residues for modification in aqueous solution in the folded state

conjugate above that of the small molecule ligand. The dynamic nature of the helix-loop-helix motif suggested that it should be able to adapt to several protein surfaces [25]. It should not be non-specific but promiscuous in its interactions with proteins.

3.2.1

The Solution Structure of the Helix-Loop-Helix Dimer

KE2 dissociates to form unordered monomers at low μM concentration, as revealed by the low negative value of the mean residue ellipticity at 222 nm, Θ_{222} [25]. The value of Θ_{222} at higher μM concentrations tends towards $-20\,000\text{ deg cm}^2\text{ dmol}^{-1}$, which is typical of related and well-characterized helix-loop-helix dimers. Surprisingly, polypeptides functionalized with fluorophores and small molecule ligands showed higher helical contents than unmodified ones (see Table 1). KE2 does not form a uniquely folded bundle structure but populates several conformations in fast exchange. The ^1H NMR spectrum of the sequence LA42h, which differs from that of KE2 in only three positions (two norleucines and one lysine in LA42h were replaced by two leucines and one alanine in KE2) showed broadened lines and poorly dispersed chemical shifts [24]. In combination with well-developed secondary structures, this is typical of molten globule-like folds. Analytical ultracentrifugation of the parent peptide SA-42 showed that it forms a clean helix-loop-helix dimer at sub-millimolar concentrations without further aggregation, and it is likely that the same applies to KE2 [25]. In the family of polypeptides derived from SA-42 the hydrophobic core remains constant, and it is mainly functional residues in *g* and *c* positions that have been modified or replaced. Since the binding interface is largely conserved, polypeptides from the family of sequences are expected to be able to form heterodimers, unless electrostatic repulsion prevents it.

Table 1 Mean residue ellipticities of polypeptides and polypeptide conjugates in aqueous solution

Polypeptide	Conc. (μM)	Θ_{222} ($\text{deg cm}^2\text{ dmol}^{-1}$)
SA42	93	- 25 000
KE2	1	- 14 600
KE2-P	1	- 19 800
KE3-P	1	- 17 300
KE2-PL	1	- 18 200
KE3-PL	1	- 24 700

P dansyl, *L* benzensulfonamide spacers with aminohexanoic acid

3.2.2

The Functionalization of the Helix-Loop-Helix Dimer

The scaffold was prepared by solid phase peptide synthesis, using Fmoc protection group strategies, and functionalized on the solid phase after selective deprotection of the Alloc group by Pd(PPh₃)₄ by reacting it with dansyl chloride [21]. After cleavage from the solid support and purification by HPLC the polypeptide was reacted with an active ester derivative of benzenesulfonamide to form an amide at the side chain of Lys-34. The reactivity of Lys-34 has been analysed in detail, and is due to a combination of pKa depression and proximity to His-11, which acts as an intramolecular acyl-transfer reagent [26]. The identity of the functionalized polypeptide was confirmed by MALDI-TOF mass spectrometry. As a control a second scaffold, KE3, was synthesized and functionalized (Fig. 3) in which the ligand was attached to a lysine residue in position 8. The synthesis was carried out in a manner fully analogous to that of KE2. In the nomenclature used here, KE2-P refers to a sequence in which a fluorophore has been covalently incorporated, and KE2-PL refers to a sequence in which both a fluorophore and a ligand have been covalently incorporated.

4

The Binding of Human Carbonic Anhydrase II

The polypeptide KE2-PL, covalently linked to a benzenesulfonamide group via an aliphatic spacer, binds HCAII as a monomer, with high affinity and selectivity. The overall affinity for HCAII is derived from cooperativity between scaffold and benzenesulfonamide.

4.1

KE2-PL Binds HCAII Selectively and With High Affinity

The fluorescence emission intensity of 1 μ M KE2-PL in buffer solution at pH 7 with aminohexanoic acid as the spacer, was increased by the addition of 50 μ M HCAII, whereas in a control experiment KE2-P, with no benzenesulfonamide attached, showed no response to the addition of HCAII, demonstrating that KE2-PL binds to HCAII with high affinity and that the binding depends on the presence of the benzenesulfonamide residue [21]. Titration of a solution of 1 μ M of KE2-PL with HCAII gave rise to a sigmoid curve, which after analysis provided a dissociation constant of 20 nM. The affinity for HCAII of benzenesulfonamide has been reported previously to be 1.5 μ M [12]. Under the experimental conditions, assuming that within the experimental accuracy a maximum of 5% complexation occurred between HCAII and KE2-P, an upper limit of 1 mM affinity can be esti-

mated for the unsubstituted scaffold. Consequently, the scaffold and the benzenesulfonamide both contribute to binding, and the observed affinity is higher than that of each of the components. The overall design goal was therefore fulfilled: to construct a binder from molecular building blocks that cooperatively bound the target protein. The sequence KE3-PL, where a lysine residue was incorporated by replacing Ala-8 and functionalized with the benzenesulfonamide group, showed a similar behaviour as KE2-PL. Upon addition of HCAII the intensity was also increased, but less so than for KE2-PL. Only KE2-PL was therefore characterized further. There is no correlation between intensity variation and affinity, and the affinity of KE3-PL for HCAII may well be higher than that of KE2-PL. The observation demonstrated that the position of the fluorophor affects the fluorescence intensity.

4.1.1

The Affinity Depends Critically on Spacer Properties and Length

In order to explore the dependence of the affinity of KE2-PL for HCAII on spacer length, several KE2 conjugates were synthesized in which the number of methylene groups in the spacer was systematically varied (Fig. 5) [27]. Titration of the binders with HCAII and determination of the dissociation constants demonstrated that the affinity was crucially dependent on spacer length and therefore on the ability of HCAII to accommodate simultaneous binding of the benzenesulfonamide residue and the polypeptide scaffold. For binders with no spacer, or spacers shorter than aminohexanoic acid, the dissociation constants were determined to be between 0.7 and 3 μM . The difference between using aminopentanoic acid or aminohexanoic acid as the spacer, a difference of only a single methylene group, amounted to a factor of 40 in affinity, with dissociation constants of 800 and 20 nM, respectively. Precise alignment is required for optimal binding. A further increase in spacer length gave even higher affinities, but not as dramatically as in the change from aminopentanoic acid to aminohexanoic acid. The use of aminooctanoic acid provided a binder with 4 nM affinity for HCAII [28]. Longer spacers than aminooctanoic acid gave rise to lower apparent affinities, but with a binding situation that became more complex. The measured dissociation constants for spacers longer than that of aminooctanoic acid increase in agreement with a model where cooperativity between benzenesulfonamide and scaffold is an important factor in determining affinity. As the spacer length is increased, there is less restriction on the degrees of freedom of the binder in the bound state and cooperative effects are reduced in significance. However, the measurement of affinities for the longer spacers was hampered by the fact that the state of aggregation, and thus the stoichiometry of the complex, was poorly defined (see below).

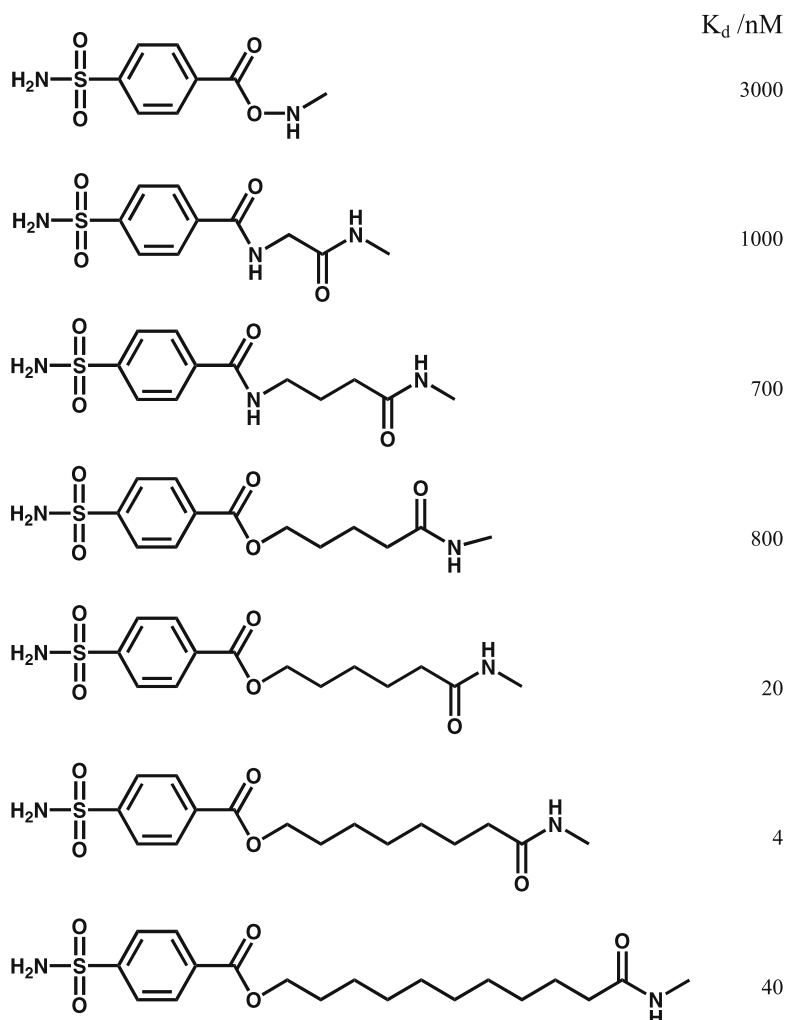


Fig. 5 Dissociation constants of KE2-PL as a function of spacer. The highest affinity is observed for an aminooctanoic acid spacer, while for an even longer spacer the affinity decreases. Note the dramatic jump in affinity between the aminopentanoic acid and aminohexanoic acid spacers

4.2

Characterizing Binding by NMR Spectroscopy

No crystal structure of a complex between HCAII and a conjugate binder has yet emerged, but NMR spectroscopy is a powerful tool for identifying binding interfaces. The ^1H and ^{15}N NMR spectra of HCAII have been as-

signed [17] and the $^1\text{H} - ^{15}\text{N}$ HSQC spectrum of HCAII at various concentrations close to $100\ \mu\text{M}$ using cryoprobe technology, in the presence of several binders, was used to identify amide groups perturbed upon binding [28]. The binder without spacer and a dissociation constant of $3\ \mu\text{M}$ did not perturb the amide groups of HCAII, in spite of the fact that the dissociation constant strongly suggested that the benzenesulfonamide residue bound to the Zn ion in the active site of the enzyme. Inspection of the crystal structure of HCAII suggests that the binding site is relatively narrow and incapable of accommodating a folded helix-loop-helix motif. It appears that the Zn-sulfonamide interaction dominates the binding and that the helix-loop-helix motif unfolds and adopts an unordered conformation in order to fit in the active site of HCAII. The ligand was attached to the side chain of Lys-34, only eight residues from the C-terminus. It is possible to accommodate this short fragment of the 42-residue sequence in the $15\ \text{\AA}$ deep cleft if it is unfolded. In contrast to what is observed for the “short” conjugated polypeptide, a helix-loop-helix motif without benzenesulfonamide affected the resonances of the backbone amide groups to form a hairpin image on the surface of HCAII in close proximity to the active site. It is clear that the scaffold binds to the protein surface although with weak affinity. The binder with the aminohexanoic acid spacer and $20\ \text{nM}$ affinity perturbs the amide groups of HCAII severely in the vicinity of the active site (Fig. 6).

For longer spacers a decrease in intensity in the one-dimensional ^1H NMR spectrum was observed that was interpreted as a sign of further complexation. The aminooctanoic acid-spacer binder reduced the intensity

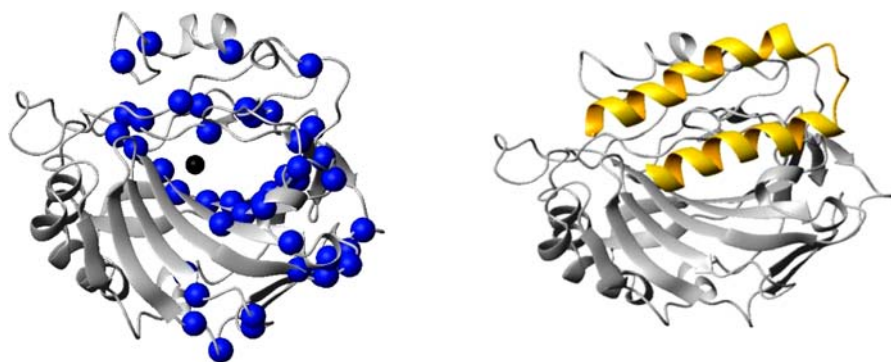


Fig. 6 Mapping of binding interaction between KE2-PL with aminohexanoic acid spacer and HCAII determined by NMR spectroscopy [28]. The $^1\text{H} - ^{15}\text{N}$ HSQC spectrum of ^{15}N -labelled HCAII in the presence and absence of binder provides information about which amide group chemical shifts are affected by the binding event, here shown in *blue*. For comparison, the relative sizes of binder and target protein are illustrated in a modelled complex. The size of the helix-loop-helix motif approximately matches the perturbation on the surface of HCAII

significantly, whereas the aminoundecanoic acid-spacer binder reduced it severely [28]. A reduction in signal intensity is most likely due to an increased relaxation rate resulting in line broadening as a result of decreased tumbling rates. Complexation and increased apparent molecular weight has exactly this effect. It appears that a long hydrophobic spacer induces further aggregation, including at least two HCAII molecules.

4.3

KE2-PL Binds HCAII As a Monomer

The ability of KE2 to form heterodimers with alternative but similar polypeptides was used to determine the number of polypeptides in the complex with the target protein. Labelling KE2 with two fluorophores, dansyl and methoxycoumarin, using double orthogonal protocols, led to a fluorescence spectrum with intensities at the wavelength maxima of both fluorophores that were severely reduced, apparently due to internal quenching [29]. A comparison between intensities of a solution containing 1 μM KE2-PL, and a solution of 1 μM KE2-PL in the presence of 100 μM of KE2, showed a fourfold higher intensity for the latter in spite of the fact that KE2 has no fluorescently active groups. A 100-fold dilution of KE2-PL with a fluorescently silent version of the polypeptide makes it statistically unlikely that KE2-PL will form a homodimer, and the increase in fluorescence intensity upon dilution clearly demonstrated that self-quenching occurred in the homodimer. A comparison of the intensity of 1 μM KE2-PL and that of KE2-PL in the presence of excess HCAII showed an almost identical response pattern. The self-quenching of the homodimer disappeared upon introduction of HCAII, proving that there are no homodimers of KE2-PL in the complex with HCAII. A control experiment using KE2 labelled with a fluorescence quencher, KE2-Q, gave the same result. Here, the complex of KE2-PL with excess KE2-Q gave almost no fluorescence in the free state and a strong light-up effect upon addition of HCAII. Consequently, KE2-PL binds to the target protein as a monomer. The binding mode is in good agreement with a model in which the hydrophobic components of the helix-loop-helix motif interact with hydrophobic patches of the biomolecular target, and thus cannot form a homodimer.

4.4

Biosensing With KE2-PL

The concentration of polypeptide determines to what extent it exists as an unordered monomer or folded dimer in aqueous solution and whether the binding to the target protein requires folding of the monomer or dissociation of the dimer prior to the binding event. Which situation is the more beneficial, or less detrimental, thermodynamically remains an open question. Spectroscopic studies revealed that the fluorophore is buried in the hydropho-

bic interior of the helix-loop-helix motif, probably due to its hydrophobic nature and to the fact that the helix-loop-helix dimer was not perfectly packed [30]. This observation suggested that the fluorescence response upon binding could be an increase as well as a decrease in intensity, as the fluorophore might experience a transition from hydrophobic environment buried in the core of the four-helix bundle, to a less hydrophobic environment, depending on the structure of the complex with the biological target, or vice versa. This was also shown to be the case [31]. For biosensing purposes it is irrelevant whether binding is associated with an increase or a decrease of fluorescent intensity, but an observation of zero change in intensity could in principle be falsely interpreted as a non-binding event and give rise to a false negative interpretation. Binding should probably be tested at two different concentrations in the case of negative responses.

5

Polypeptide Conjugates as Agents in Protein Recognition

A new type of binder for proteins based on conjugated polypeptides has been developed and the molecular properties investigated. The ease of modification of the polypeptide scaffold and the ability of the scaffold to enhance the affinity of the polypeptide conjugate over that of the small molecule ligand by several orders of magnitude has been demonstrated in the case of HCAII. Affinities of the polypeptide conjugates for HCAII are tunable and comparable to those of antibodies. Polypeptides are more robust than folded proteins and antibodies with regards to handling as well as to storage. The crucial question is whether the discriminating power of polypeptide conjugates is comparable to or better than that of biologically generated binders. While this question remains an open one, due to the limited amount of data that is so far available for synthetic binders, the selectivity inherent in a scaffold binder has been tested in the case of carbonic anhydrases. Human carbonic anhydrase I and II, HCAI and HCAII, are both Zn-dependent enzymes that bind benzenesulfonamide. Their sequences are not identical but approximately 70% homologous. Their folds are virtually identical. The affinities of KE2-PL with an aminohexanoic spacer for HCAI and HCAII were measured and found to differ by almost three orders of magnitude [27]. The dissociation constant of the KE2-PL-HCAII complex was 20 nM whereas that of KE2-PL-HCAI was 10 μ M, a ratio of of 500:1. While KE2-PL binds weakly to HCAI, virtually no HCAI would bind at the concentrations used in clinical diagnostics, and thus in a biosensor experiment little or no signal would be detected. From a practical point of view such a binder would be considered specific.

The discrimination of the benzenesulfonamide group between HCAI and HCAII is small and the selectivity thus has its origin in the polypeptide scaf-

fold. While a binder that is selective for HCAI has not yet been selected, a comparison between the two scaffolds, and the obtained affinities, would be very interesting. The observation of considerable selectivity of the polypeptide conjugate binder in discriminating between the two carbonic anhydrases suggests that the concept is a powerful one for protein recognition. In comparison with antibodies or folded proteins the structural complexity is modest. The concept has therefore been shown to be promising.

An important aspect of using binders for proteins is how they respond to immobilization on surfaces or in hydrogels. Synthetic binders based on polypeptide scaffolds have been immobilized on gold particles and in hydrogels and shown to retain their functional integrity [32, 33].

The rate-limiting step in the preparation of a binder of the type described here is the design and synthesis of the small molecule ligand, whereas the peptide synthesis and functionalization by today's standards is straightforward, and automatable. The conjugation reaction, too, is automatable. The observation so far that selectivity between highly homologous proteins with identical prosthetic groups can be obtained by chemical tools much less complex than those observed in the living cell gives reasons for optimism that, in the future, synthetic binders optimized for a variety of tasks will be rapidly available. The selection of the small molecules to be conjugated will be a critical part of the process, as it affects affinities and most likely, in most cases, also the selectivity. In addition, the selection of a ligand that requires a complicated synthesis may add many months to the development of a binder, whereas a smart choice of ligand will ensure a rapid process.

The elucidation of which small molecules provide the best protein recognition is expected to provide fundamental insights into molecular recognition in biology. The concept presented here is a general one and the ligand need not be an inhibitor of an enzyme but could be any group that binds to a protein, or for that matter several groups that in combination bind to proteins. It demonstrates the power of chemical approaches and the concept is therefore most likely one of several future routes to protein recognition and binding in a field that is currently under rapid development.

Acknowledgements Financial support from the Swedish Research Council and from the Foundation for Strategic research is gratefully acknowledged.

References

1. Fletcher S, Hamilton AD (2005) *Curr Opin Chem Biol* 9:632
2. Carter PJ (2006) *Nat Rev Immunol* 6:343
3. Haab BB (2006) *Curr Opin Biotechnol* 17:415
4. Ng EWM, Shima DT, Calias P, Emmett T, Cunningham ET Jr, Guyer DR, Adamis AP (2006) *Nat Rev Drug Discov* 5:123
5. Schlehuber S, Skerra A (2005) *Drug Discov Today* 10:23

6. Fersht AR (2002) Structure and mechanism in protein science, 4th edn. W.H. Freeman, New York
7. Lyu PC, Gans PJ, Kallenbach NR (1992) *J Mol Biol* 223:343
8. Fersht AR, Shi JP, Knill Jones J, Lowe DM, Wilkinson AJ, Blow DM, Brick P, Carter P, Waye M, Winter G (1985) *Nature* 314:235
9. Fersht AR, Jackson SE, Serrano L (1993) *Phil Trans R Soc London Ser A* 345:141
10. Page MI, Jencks WP (1971) *Proc Natl Acad Sci USA* 68:1971
11. Levinthal C (1968) *J Chim Phys* 85:44
12. Taylor PW, King RW, Burgen ASV (1970) *Biochemistry* 9:2638
13. Liljas A, Håkansson K, Jonsson B-H, Xue YF (1994) *Eur J Biochem* 219:1
14. Eriksson AE, Kylsten PM, Jones TA, Liljas A (1988) *Proteins* 4:283
15. Håkansson K, Carlsson M, Svensson LA, Liljas A (1992) *J Mol Biol* 227:1192
16. Boriack PA, Christianson DW, Kingerywood J, Whitesides GM (1995) *J Med Chem* 38:2286
17. Venters RA, Farmer BT, Fierke CA, Spicer LD (1996) *J Mol Biol* 5:1101
18. Carlsson U, Jonsson B-H (2000) In: Chegwidden WR, Carter ND, Edwards YH (eds) *The carbonic anhydrases: new horizons*. Birkhäuser, Basel
19. Krebs HA (1948) *Biochem J* 43:525
20. Miller WH, Dessert AM, Roblin RO (1950) *J Am Chem Soc* 72:4893
21. Enander K, Dolphin GT, Andersson LK, Liedberg B, Lundström I, Baltzer L (2002) *J Org Chem* 67:3120
22. Jain A, Whitesides GM, Alexander RS, Christianson DW (1994) *J Med Chem* 37:2100
23. Baltzer L, Nilsson H, Nilsson J (2001) *Chem Rev* 101:3153
24. Andersson LK, Dolphin GT, Baltzer L (2002) *Chem Bio Chem* 3:741
25. Olofsson S, Johansson G, Baltzer L (1995) *J Chem Soc Perkin Trans 2*, p 2047
26. Andersson LK, Casparsson M, Baltzer L (2002) *Chem Eur J* 8:3687
27. Enander K, Dolphin GT, Liedberg B, Lundström I, Baltzer L (2004) *Chem Eur J* 10:2375
28. Andersson T, Lundquist M, Dolphin GT, Enander K, Jonsson B-H, Nilsson JW, Baltzer L (2005) *Chem Biol* 12:1245
29. Enander K, Dolphin GT, Baltzer L (2004) *J Am Chem Soc* 126:4464
30. Becker HC, Lignell M, Enander K, Baltzer L (2005) *Abstr Pap Am Chem Soc* 230:U2925
31. Enander K (2003) *Folded polypeptide scaffolds for biosensor and biochip applications – design, synthesis, functionalisation and characterisation*. Linköping Studies in Science and Technology, Dissertation 848, Linköping
32. Enander K, Aili D, Baltzer L, Lundström I, Liedberg B (2005) *Langmuir* 21:2480
33. Aili D, Enander K, Rydberg J, Lundström I, Baltzer L, Liedberg B (2006) *J Am Chem Soc* 128:2194

Saccharide-Selective Boronic Acid Based Photoinduced Electron Transfer (PET) Fluorescent Sensors

Tony D. James

Department of Chemistry, University of Bath, Bath BA2 7AY, UK
t.d.james@bath.ac.uk

1	Introduction	108
2	Complexation of Boronic Acids with Saccharides	110
3	Fluorescent Sensors	115
3.1	Photoinduced Electron Transfer (PET) Systems	116
3.2	Systems with Selectivity for Specific Saccharides	118
4	Amine–Boron (N–B) Interactions	119
5	The Importance of Pyranose to Furanose Interconversion	122
5.1	The Preference of Monoboronic Acids for D-Fructose	125
6	Modular Fluorescent Sensors	128
6.1	The Design Rationale	128
6.2	Modular Systems	130
6.2.1	Linker Dependence	131
6.2.2	Energy Transfer Systems	135
6.2.3	Fluorophore Dependence	138
6.3	Other Approaches	145
6.3.1	Wang and Coworkers	145
6.3.2	Hall and Coworkers	146
7	Conclusions	148
	References	149

Abstract The ability to monitor the presence of analytes within physiological, environmental and industrial systems is of crucial importance. However, due to the scale at which recognition events occur on the molecular level, gathering this information poses a non-trivial challenge. Therefore, robust chemical molecular sensors with the capacity to detect chosen molecules selectively and to signal this presence have attracted considerable attention over recent years.

Of particular interest is the real-time monitoring of saccharides in aqueous systems, such as D-glucose in blood. To this end the covalent pair-wise interaction between boronic acids and saccharides has been exploited.

Keywords Boronic acid · Carbohydrate · Fluorescent sensor · Photoinduced electron transfer · Saccharide

1 Introduction

The recognition of a target molecule by a synthetically prepared receptor has captured the imagination of supramolecular chemists. Since its inception, research in this area has been instrumental in elucidating the mode of action of a great many biological events concerning recognition and catalysis [1]. The importance of this work was underlined with the award of the Nobel Prize in Chemistry to Cram, Lehn and Peterson in 1987 “for their development and use of molecules with structure-specific interactions of high selectivity” [2]. Since then the diversity of compounds studied under the umbrella of supramolecular chemistry has grown significantly. Of particular interest are chemical molecular sensors, single molecules with the ability to both recognise and signal analytes in real time [3, 4].

Molecular recognition lies at the very heart of sensor chemistry. The process itself involves the interaction between two substances, often termed: a host and a guest, a lock and a key or a receptor and a substrate. Importantly, recognition is not just defined as a binding event but requires selectivity between the host and the guest.

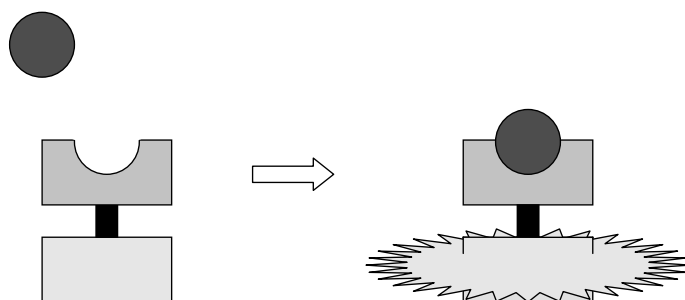
Selectivity between host and guest is a premise of compatibility. It arises between compounds with carefully matched electronic, geometric and polar elements. For synthetic receptors the potential therefore exists to engineer receptors for any chosen analyte through judicious structural design and functional group complementarity. The power of this concept is illustrated within Nature. Biological systems have evolved with exquisitely constructed active binding sites, sequestering guest molecules with near perfect selectivity.

Nevertheless, for the recognition event at a receptor to be of practical use, a further element is required. A channel of communication must be established between the receptor and the outside world. This additional quality converts a receptor into a sensor (Scheme 1).

For a sensor to function it must therefore permit selective binding to occur between host and guest and also report these binding events by generating a tangible signal. By performing these two fundamental tasks sensors have the potential to relay information on the presence and location of important species in a quantifiable manner, bridging the gap between events occurring at the molecular level and our own.

Chemical sensors can be broadly categorised as either biosensors, or synthetic sensors. Biosensors make use of existing biological elements for recognition. Many of the physiologically important analytes already have corresponding biological receptors with intrinsically high selectivity and if these receptors can be connected to a signal transducer a biosensor can be developed [5].

Synthetic sensors incorporate a synthetically prepared element for recognition. Whilst biomimetic receptors have been prepared, with synthetic

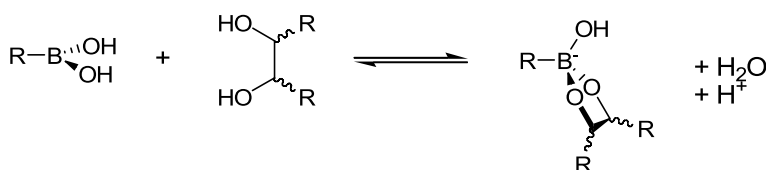


Scheme 1 Complementary interaction between a guest analyte and a host binding pocket, illustrated here by a *dark-grey* guest and *grey* host, allows selective binding to occur between two elements. Incorporation of a unit capable of generating a physical signal in response to this binding event, converts the receptor into a sensor. In this cartoon an optical “off-on” response is depicted from an appended fluorophore, illustrated in *light-grey*, typical of the systems covered within this chapter

receptors mimicking the active sites in naturally occurring biological molecules, synthetic receptors can, and often are, designed entirely from first principles.

The development of coherent strategies for the selective binding of target molecules, by rationally designed synthetic receptors, remains one of chemistry’s most sought-after goals. The research conducted to this end is driven by a fundamental inquisitiveness and need to monitor compounds of industrial, environmental and biological significance.

Within our research group we have exploited the interaction between boronic acids and diols. The primary interaction of a boronic acid with a diol is covalent and involves the rapid and reversible formation of a cyclic boronate ester (Scheme 2). The array of hydroxyl groups present on saccharides provides an ideal scaffold for these interactions and has led to the development of boronic acid based sensors for saccharides [6–19].



Scheme 2 Rapid and reversible formation of a cyclic boronate ester

Many synthetic receptors developed for neutral guests have relied on non-covalent interactions, such as hydrogen bonding, for recognition. It is the case, however, that in aqueous systems neutral guests may become heavily solvated. Whilst biological systems have the capacity to expel water from their binding pockets and sequester analytes wholly, using non-covalent in-

teractions, synthetic monomeric receptors have not yet been designed where hydrogen bonding has been able to compete with bulk water for low concentrations of monosaccharides [20]. However, it should be pointed out that progress is being made in this area and recently Davis reported a hydrogen bonding receptor capable of binding D-glucose in water with a weak but significant stability constant [21].

The capacity of boronic acid receptors to function effectively in water is reflected by the number of published sensory systems designed around them. The most popular class of the fluorescent boronic acid based sensors utilise an amine group proximal to boron. The Lewis acid–Lewis base interaction between the boronic acid and the neighbouring tertiary amine has a dual role. First, it enables molecular recognition to occur at neutral pH. Second, it can be used to communicate binding by modulating the intensity of fluorescence emission through photoinduced electron transfer (PET), introducing an “off-on” optical response to the sensor.

2

Complexation of Boronic Acids with Saccharides

In a pioneering series of papers spanning the 29 years from 1911 to 1940, Böeseken and coworkers elucidated the absolute structural configuration of a panoply of saccharides and other hydroxyl-containing compounds [22]. The configurations were determined, in large part, from the known ability of boric acid to complex diols. As boric acid complexes formed in solution, with hydroxyl groups in favourable 1,2- and sometimes 1,3-configurations, a rise was observed in both acidity and conductivity. By tracking the changes in conductivity of boric acid solutions as saccharides were added, the relative configurations of the hydroxyl groups could be inferred. This method was employed in 1913 to conclusively determine the structure of the pyranose and furanose forms of D-glucose. Changes in conductivity revealed the relative *cis*- and *trans*-orientations of the vicinal C1 and C2 hydroxyl groups, thus permitting the absolute structural configuration of the α - and β -pyranose and furanose anomers to be attributed [23] (Fig. 1).

Given the significance of boric acid in the determination of saccharide configurations, it is perhaps surprising that the same properties were not ob-

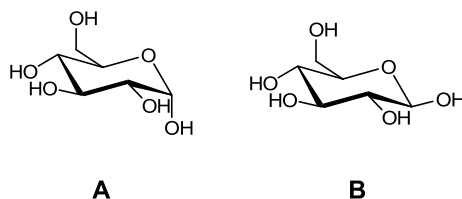
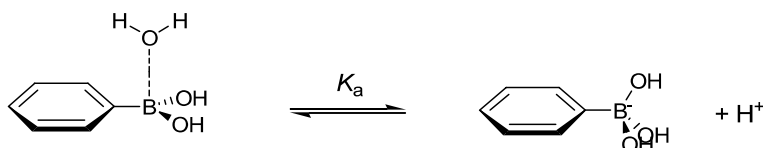


Fig. 1 Pyranose anomers of D-glucose: A α -D-glucopyranose and B β -D-glucopyranose

served in boronic acids until 1954 [24]. During a course of investigations into aromatic boronic acids, Kuivila and coworkers observed a new compound being formed on addition of phenylboronic acid to a solution of saturated mannitol, correctly postulating the formation of a cyclic boronic ester analogous to the one known to form between boric acid and polyols.

A number of publications followed examining the properties and synthesis of boronic acids [25–27], with the first quantitative investigation into the interactions between boronic acids and polyols in 1959 [28]. In a study to clarify the disputed structure of the phenylboronate anion, Lorand and Edwards added a range of polyols to solutions of phenylboronic acid. The pH of the solutions was adjusted such that there was an equal speciation of phenylboronic acid in its neutral and anionic forms; the pH matching the pK_a . As diol was added the pH of the systems decreased, allowing binding constants to be determined through the technique of pH depression.

From these experiments Lorand and Edwards concluded that the conjugate base of phenylboronic acid has a tetrahedral, rather than trigonal structure. The dissociation of a hydrogen ion from phenylboronic acid occurs from the interaction of the boron atom with a molecule of water. As the phenylboronic acid and water react a hydrated proton is liberated, thereby defining the acidity constant K_a (see Hartley, Phillips and James [29]). This is depicted in Scheme 3 by considering an explicit water molecule associated with the Lewis acidic boron. The reported pK_a s of phenylboronic acid fluctuate between ~ 8.7 and 8.9 [30–35], with a recent in-depth potentiometric titration study refining this value to 8.70 in water at 25°C [36].



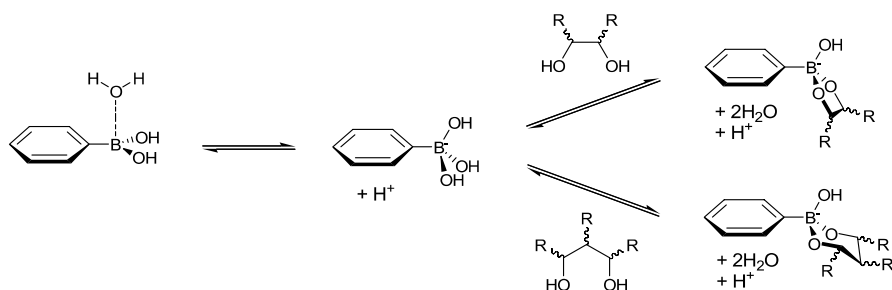
Scheme 3 Acid-conjugate base equilibrium for phenylboronic acid in water

Whilst one explicitly associated molecule is shown in a number of illustrative schemes for clarity, water should be considered to be in rapid exchange on the Lewis acidic boron in much the same way that hydrated Lewis acidic metal ions exchange bound water. A pertinent comparison can be found with the ionisation of Zn^{2+} in water, the reaction $\text{Zn} - \text{OH}_2 \rightarrow \text{Zn} - \text{OH} + \text{H}^+$ having a pK_a of 8.8 [37].

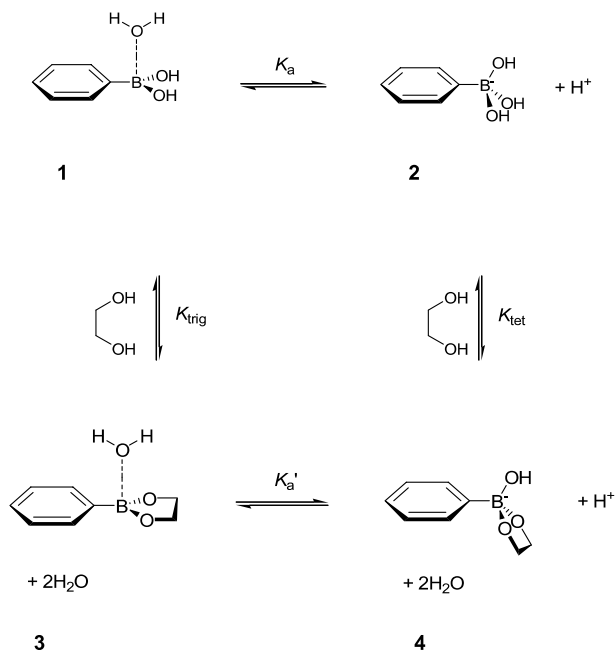
Boronic acids have been reported to rapidly and reversibly [38] interact with dicarboxylic acids [39, 40], α -hydroxy carboxylic acids [34, 40–42] and diols [28] to form esters in aqueous media [43]. The most common interaction is with 1,2- and 1,3-diols to form five- and six-membered rings, respectively. From experimental observations it is well known that the kinetics of this interconversion are fastest in aqueous basic media where the boron

is present in its tetrahedral anionic form [44]. Typically differences in rate of 10^4 are observed between boron in its trigonal and tetrahedral forms [43].

Whilst the boronate anion does account for the strongest binding of diols in aqueous media the interaction between diols and the neutral boronic acid should not be ignored. In considering these interactions the equilibria in Scheme 4 can be readily expanded to form a thermodynamic cycle, as illustrated in Scheme 5.



Scheme 4 Interaction of the phenylboronate anion with 1,2- and 1,3-diols to form diol-phenylboronate complexes with five- and six-membered rings, respectively



Scheme 5 The equilibria for boronate ester formation couple to generate a thermodynamic cycle. The acidity constant of the unbound complex is defined as K_a and the acidity constant of the bound complex is defined as K'_a , where it is observed that $pK_a > pK'_a$

Considering Scheme 5 we define the formation of the diol boronate anion complex as K_{tet} and the formation of the diol boronic acid complex as K_{trig} , where it is observed that $K_{\text{tet}} > K_{\text{trig}}$. For instance the logarithm of these constants for phenylboronic acid binding fructose in 0.5 M NaCl in water is $\log K_{\text{tet}} = 3.8$ whereas $\log K_{\text{trig}} < -1.4$. This difference in the value of the binding constant between K_{tet} and K_{trig} is typical, with differences of up to \sim five orders of magnitude being commonplace [36]. It is also known that the neutral boronic acid becomes more acidic upon binding. The acidity constant of the bound complex is defined by K'_a , where it is observed that $\text{p}K'_a > \text{p}K_a$. For instance the $\text{p}K_a$ of phenylboronic acid is 9.0 in 0.1 M NaCl 1 : 2 (v/v) methanol/water, under the same conditions the $\text{p}K'_a$ of phenylboronic acid bound to fructose is 5.2; in other words the boronic ester is more acidic than the boronic acid [36].

The final point to be considered in boronic acid–saccharide binding is the predisposition of boronic acids to interact with different kinds of diols. The stability constants (K) between various polyols and boronic acids were first quantified by Lorand and Edwards and it is the case that the trends established now appear inherent in all monoboronic acids [28].

It is well known that boronic acids readily form five-membered rings with vicinal *cis*-diols in basic aqueous media. It is also the case that six-membered rings can be formed with *trans*-1,3-diol groups, although the stability of these cyclic diesters is somewhat lower than their five-membered counterparts [44–48].

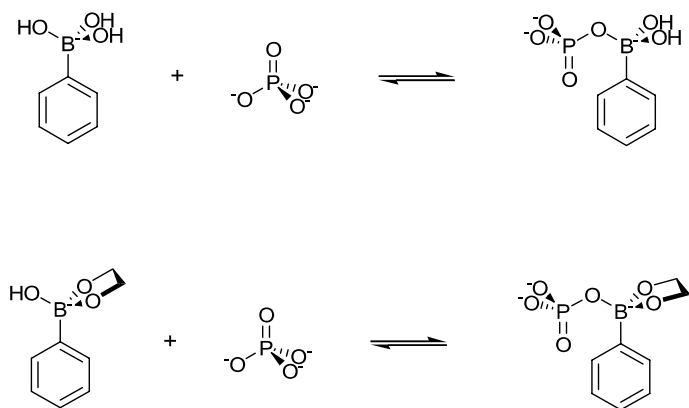
Table 1 Binding constants calculated by Lorand and Edwards for phenylboronic acid in water at 25 °C [28]

Polyol	Binding constant K (mol^{-1})
1,3-Propanediol	0.88
Ethylene glycol	2.80
Propylene glycol	3.80
3-Methoxy-1,2-propanediol	8.50
D-Glucose	110
D-Mannose	170
D-Galactose	280
Pentaerythritol	650
Mannitol	2300
D-Fructose	4400
Catechol	18 000

The four monosaccharides most routinely used in the evaluation of sensors for saccharides are highlighted in bold

These trends have been heavily utilised in the design of new sensors and it has been found that the apparent values determined for monoboronic acid sensors concur with the trends of the equilibrium constants reported in Table 1. Apparent values depend heavily on the environments in which the sensors have been studied and are influenced by factors such as: pH, buffer, solvent composition, the concentration of the reactants and the presence of any Lewis basic components.

In response to the growing demand for an accurate interpretation of the complex multi-component equilibria involved in these systems, an extensive investigation was conducted using the potentiometric titration technique [36]. The refined values for the acidity and binding constants displayed a good match with previously published data. Nevertheless, it became clear from the results that the thermodynamic cycle in Scheme 5 is somewhat of a simplification. Stable complexes were found to form readily between boronic acids and Lewis bases. This represents a significant finding in sensor design as Lewis bases such as the conjugate bases of phosphate, citrate and imidazole are commonly used to buffer the pH of solutions during the spectrophotometric evaluation of sensors, adding a new degree of sophistication to the understanding of the species present in solution (see Scheme 6).



Scheme 6 In addition to the pair-wise interaction of boronic acids with polyhydroxyl species discussed, boronic acids also form stable complexes with buffer conjugate bases. These complexes can be formed between both the free boronate anion and Lewis bases as well as between saccharide boronate complexes and Lewis bases. Not recognised until 2004, these species persist into acidic solution and under certain stoichiometric conditions can become the dominant component in the solution. The two modes of interaction between the phenylboronate anion and phosphate are illustrated here

It was shown that in buffered solutions binary (boronate–Lewis base) complexes as well as ternary (boronate–Lewis base–saccharide) complexes will be formed. Under acidic conditions these ternary complexes are significant and

under certain stoichiometric conditions can become the dominant components in solution.

When conducting fluorescence experiments in solutions buffered with a Lewis basic component there is therefore a “medium dependence” related to the formation of Lewis base adducts [31]. These complexes reduce the free boronate and boronic acid concentrations, diminishing the observed stability constants (K_{obs}).

From an experimental perspective this characteristic means that strongly Lewis basic components should be avoided by researchers in the future study of boronic acid appended systems. With care, buffers can be chosen so as not to overwhelm the system being investigated. For example, phosphate buffer (pH 7.5) was found not to make a significant contribution to the observed fluorescence intensity or alter significantly the binding constants of the excited state complex under investigation.

Therefore, so long as one is aware of the conditions that K_{obs} has been determined under and the effect that is induced by Lewis basic components in solution, these spectrophotometrically determined constants do provide an accessible, useful and valid measure in the development of boronic acid based sensory systems.

3 Fluorescent Sensors

The use of light to transfer information on events occurring between molecules is particularly advantageous; it provides researchers with a natural interface between events occurring at the molecular level and the macroscopic one. As optical signals convey information through space, fluorescent sensors can be absorbed into dynamic systems such as living tissue and relay information remotely. Sub-millisecond response times are typical, allowing information to be communicated in real-time and, if targeted correctly, fluorophores can be located with sub-nanometre accuracy, in effect permitting real-space monitoring [49]. Fluorescence also demonstrates an exceptionally high sensitivity of detection; under controlled conditions modern instrumentation has allowed analysts to detect responses from single fluorescent molecules [50–52] and in the case of fluorescent sensors, from single guest molecules [53].

As fluorescent sensors are capable of reporting on a wealth of physical information at low concentrations (micromolar concentrations are typical), they can operate with the minimum of disturbance to the system being investigated. From an analytical perspective these characteristics are attractive and commercially the parsimonious quantities of compound required can be used to offset synthetic costs.

Fluorescent sensors can be found in many recent analytical advances, such as the continuous monitoring systems developed by immobilising fluorescent sensors onto fibre optic sensing arrays [54], or the live imaging of analytes within cells through confocal microscopy [55]. Commercial examples of the use of fluorescent sensors include clinical tools such as the blood gas analysers that are now commonplace within hospital high-dependency wards and ambulances allowing point-of-care diagnostic monitoring [56–59], or the glucose-responsive contact lenses currently being pioneered by the Lakowicz research group [60]. These examples highlight the robust and versatile nature of fluorescent sensors, which in turn permit rapid and accurate analyte diagnosis by portable devices.

The use of boronic acids in the development of fluorescent sensors for saccharides is a comparatively young area of research. The first publication on the subject was made by Czarnik in 1992 [61]. D-Glucose selectivity was achieved 2 years later in 1994 by James [62] within Shinkai's industrious research group, who followed this up with enantioselective saccharide recognition a year later [63]. In the intervening decade the field has blossomed and hundreds of publications on boronic acid–saccharide recognition now embellish the scientific press.

Across the diverse range of boronic acid based fluorescent sensors developed, two distinct design principles predominate in the scientific literature: internal charge transfer (ICT) and photoinduced electron transfer (PET). In both cases successful signalling of the binding event arises from alternative low energy pathways being discretely offered to either the bound or unbound sensors, these processes affecting defined spectral changes in the emission band.

3.1

Photoinduced Electron Transfer (PET) Systems

In the case of fluorescent PET sensors the design is often discussed in terms of a receptor and a fluorophore separated by a spacer so as to match the donor–bridge–acceptor motif (Fig. 2). To permit the recognition of saccharides via boronic acid complexation, the interaction between *o*-methylphenylboronic acids (Lewis acids) and proximal tertiary amines (Lewis bases) has been exploited (Fig. 3).

Whilst the precise nature of the amine base–boronic acid (N–B) interaction has been debated, it is clear that an interaction does exist and that it provides two distinct advantages.

The first, proposed by Wulff [64], is that the interaction between a boronic acid and proximal amine lowers the pK_a of the boronic acid. This effect is sufficient to allow binding to occur at neutral, i.e. physiological, pH.

The second, relates to the contraction of the O–B–O bond angle of a boronic acid on complexation with a saccharide and the associated increase

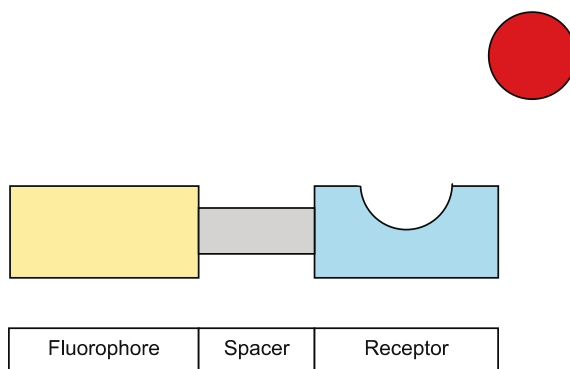


Fig. 2 Schematic representation of the fluorophore–spacer–receptor design assembly for fluorescent PET sensory systems

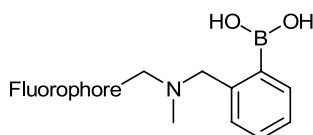
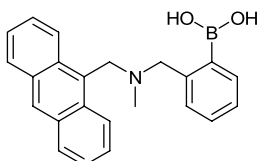


Fig. 3 Generic design of fluorescent PET sensors with the *N*-methyl-*o*-(aminomethyl)phenyl-boronic acid recognition unit

in acidity at the boron centre. This increase in acidity of the already Lewis acidic boron augments the N – B interaction and in turn disrupts PET. The reduction in pK_a at boron on saccharide binding therefore has the net effect of modulating fluorescence emission intensity, via the amine group, and introducing a digital “off-on” response from the fluorophore, indicative of the boronic acid receptor being unbound or bound, respectively.

The first fluorescent PET sensor for saccharides to employ the *N*-methyl-*o*-(aminomethyl)phenylboronic acid fragment was reported by James et al. in 1994 [65, 66]. Illustrated in Fig. 4, sensor 5 functioned remarkably well; a large



5

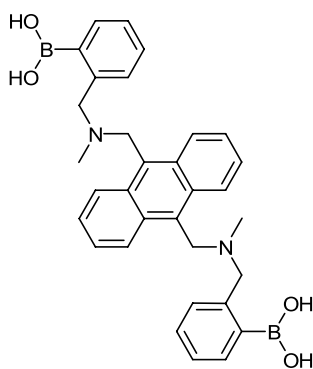
Fig. 4 First fluorescent PET sensor for saccharides to have been rationally designed. In this illustration the fluorophore–spacer–receptor construction is readily apparent; anthracene represents the fluorophore, methylene the spacer and *N*-methyl-*o*-(aminomethyl)phenylboronic acid the receptor

increase in fluorescence on addition of saccharide was observed, as well as the capacity to function over a broad range of pH. Noticeably the monoboronic acid **5** displayed the same inherent trend in selectivity for saccharides as had been documented by Lorand and Edwards for phenylboronic acid 35 years earlier, a trend that appears to be inherent to all monoboronic acid receptors of this type. Qualitatively, binding constants (K) with monoboronic acids increase in the order: D-glucose < D-galactose < D-fructose [28].

3.2

Systems with Selectivity for Specific Saccharides

The D-fructose-selective monoboronic acid based sensor **5** was enhanced by James in 1995 with the introduction of a second boronic acid group to form the diboronic acid sensor **6** [62, 66] (Fig. 5). This receptor-spacer-fluorophore-spacer-receptor system retained the advantage of utilising PET to modulate an off-on response to saccharides whilst introducing an advanced recognition site. The co-operative action of two boronic acid receptors permitted a number of possible binding modes to occur with saccharides. However, for fluorescence to be restored both boronic acid moieties must be complexed, which requires either an acyclic 2 : 1 or cyclic 1 : 1 (saccharide/sensor) complex to form.



6

Fig. 5 First rationally designed boronic acid based fluorescent PET sensor to display selectivity for D-glucose. The receptor-spacer-fluorophore-spacer-receptor assembly requires binding to occur at both receptors in order to restore fluorescence

The modification proved successful and fortuitously the spacing of the two boronic acid groups provided an effective binding pocket for D-glucose. D-Glucose complexation occurred with a 1 : 1 stoichiometry with the saccharide binding to form a macro-cyclic ring. Whilst the inherent selectivity of monoboronic acids is for D-fructose, in this compound the stabilisation de-

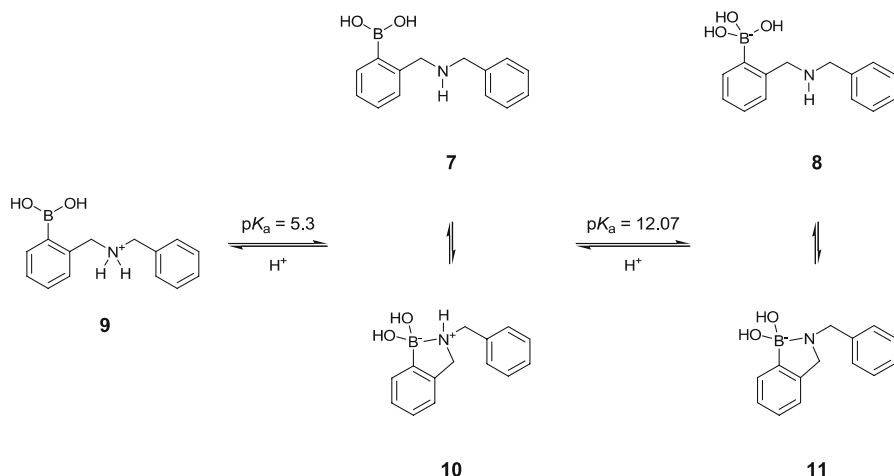
rived from the rigid macro-cyclic ring produces a D-glucose selective system, allowing diboronic acid systems to be tuned for saccharides. The K_{obs} for sensor **6** were 320 M^{-1} with D-fructose, 4000 M^{-1} with D-glucose and 160 M^{-1} with D-galactose in 33 wt % methanol in aqueous buffer at pH 7.77.

4

Amine–Boron (N–B) Interactions

The so-called coordinative or dative, nitrogen to boron (N–B or alternatively N \rightarrow B) bonds have been studied for more than 100 years. The strength of N–B bonds depend greatly on the substituents at both atoms; electron withdrawing groups increase the Lewis acidity of boron, whilst electron donating groups increase the Lewis basicity at nitrogen. In considering the bond strength it is necessary to balance these electronic factors against the counteracting steric requirements of these same substituents. An investigation of 144 compounds with coordinative N–B bonds concluded that steric interactions as well as ring strain (in the case of cyclic diesters) weaken and elongate the N–B bond, which occurs with a concurrent reduction in the tetrahedral geometry of the boron centre [67].

The *N*-methyl-*o*-(phenylboronic acid)-*N*-benzylamine **7** system has been investigated separately by Wulff, Anslyn and within the T.D. James research group [36, 64, 68]. Scheme 7 depicts a general model where, at one extreme, the acyclic forms (**7** and **8**) illustrate no N–B interaction and at the other,



Scheme 7 The extent of the interaction between nitrogen and boron is illustrated within the upper and lower bounds of possible contact, depicted as the cyclic and acyclic forms [36]

the cyclic forms (10 and 11) illustrate a full N – B interaction; the species existing in equilibrium. Species 9 involves a protonated nitrogen, therefore the ammonium cation precludes any N – B interaction.

The energy of the N – B interaction has been calculated from the stepwise formation constants of potentiometric titrations. Based on the relative stabilities of ternary phosphate complexes it was calculated that the upper and lower limits of the N – B interaction must be bound between approximately 15 and 25 kJ mol⁻¹ in *N*-methyl-*o*-(phenylboronic acid)-*N*-benzylamine [36]. This value is in good agreement with computational data, which estimated the N – B interaction to be 13 kJ mol⁻¹ or less in the absence of solvent [69]. To qualify this in terms of familiar bonding motifs the energy of the N – B interaction is about the same as that of a hydrogen bond.

As we have discussed, the strength of this interaction is a central feature in many fluorescent PET sensors, where the N – B interaction plays a pivotal role in signalling the binding event. If the interaction were much stronger, then the binding of a diol would not be able to disrupt the N – B interaction sufficiently so as to modulate a change in fluorescence. By the same token, if the interaction were much weaker then there would be no significant intramolecular N – B interaction to disrupt in the first place.

For some time the formation of a direct bond between nitrogen and boron was assumed to be responsible for the fluorescence enhancement seen when boronic acids bound diols. This interpretation does, however, raise certain questions.

The fluorescence revival in these systems functions as a digital off-on response. Fluorescence emission returns to the same maximal value regardless of the observed stability constant (K_{obs}) of the ligand or the $\text{p}K'_a$ of the resulting boronate ester. It is known that the acidity of boron in other systems directly influences the strength of the N – B bond. Therefore, if a direct N – B bond did modulate PET we might necessarily expect the fluorescence response to vary as a function of the degree of acidity or strength of complexation, but this is not the case [70]. Moreover, the numerical values do not agree with the interpretation of a direct N – B bond [36].

A recent evaluation of the first fluorescent diboronic acid sensor to be reported as a single-crystal X-ray structure both in its bound and unbound state has recently been published [71]. In the case of the unbound receptor the geometry at boron is trigonal planar. This is important as the absence of deviation from planarity implies that there is no direct N – B Lewis base–Lewis acid bond at boron.

When bound to tartaric acid, the complex was crystallised from a methanol and dichloromethane solution. In the tartrate complex two molecules of methanol, one at each boron centre are bound through their oxygen atoms to their respective boron centres. Whilst the hydrogen atoms of methanol were not directly located it is not unreasonable to infer from the geometry that each oxygen atom will concurrently bind to the boron centre and hydrogen

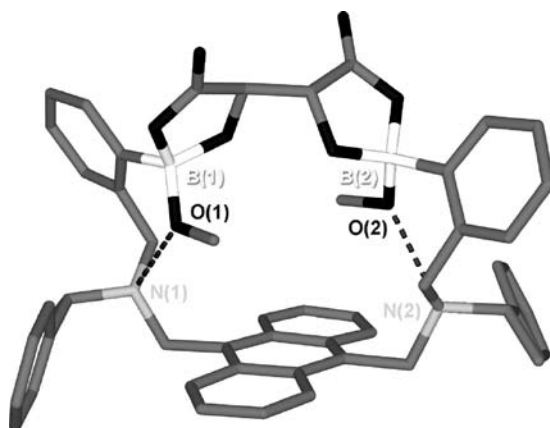


Fig. 6 The single-crystal X-ray structure of the *S,S*-diboronic acid–*L*-tartaric acid complex isolated by James and coworkers [71]. Whilst the hydrogen atoms of methanol were not directly located it can be inferred that the geometry between the bound and unbound receptors will be similar, each oxygen atom will therefore concurrently bind to the boron centre and hydrogen bond to the nitrogen atom. Oxygen to nitrogen bond distances of around 2.7 Å were reported [N(1)...O(1) = 2.655 Å and N(2)...O(2) = 2.693 Å]. Atoms marked in *black* represent oxygen, *white* boron, *dark-grey* carbon and *light-grey* nitrogen. For clarity hydrogen atoms are not displayed. The *dotted lines* represent hydrogen bonds

bond to the adjacent nitrogen atom. Oxygen to nitrogen bond distances of around 2.7 Å were reported in this case (Fig. 6).

Whilst speculative, this structural interpretation of the interaction between boronic acid and the proximal tertiary amine through a bound protic solvent molecule (solvent insertion into the N – B bond) corresponds well with contemporary computational and potentiometric titration data, in which the formation of intramolecular seven-membered rings should not be ignored [31, 36, 72, 73]. The values for the bond length (from the X-ray crystal structure) and for the bond strength (from the potentiometric titrations) are those that would be expected for a hydrogen bonding interaction manifested through a bound solvent molecule at the boron centre.

The idea postulated is by no means a new one. An infrared study into the interaction between nitrogen and boron in a similar system came to a similar “tentative conclusion” in 1964 [74]. The experimental rationale was based on comparing two emergent peaks in infrared spectra to similar peaks in known model systems. The results indicated that in carbon tetrachloride the interaction between the nitrogen and boron of 8-quinolineboronic acid could be modulated by either water or phenol bound to the boron centre at oxygen (Fig. 7).

Anslyn recently performed a detailed structural investigation of the N – B interaction in *o*-(*N,N*-dialkyl aminomethyl) arylboronate systems [75]. From detailed ^{11}B -NMR measurements (and X-ray data) it was shown that in an

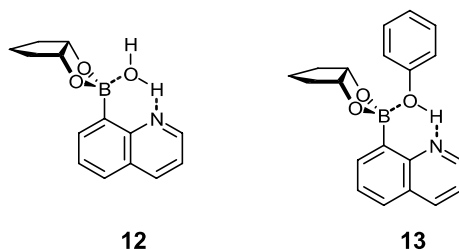
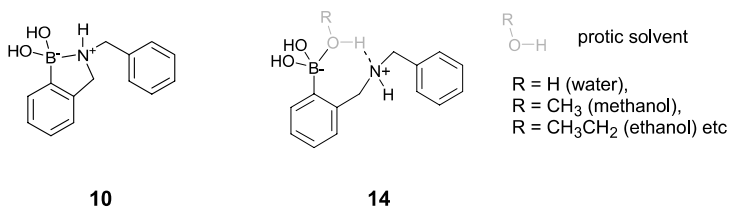


Fig. 7 Morrison's proposed complexes of the *cis*-1,2-cyclopentanediol ester of 8-quinolineboronic acid with solvent water and phenol molecules bridging the nitrogen and boron centres [74]. *Bold dashed* bonds are used to represent dative bonding

aprotic solvent, the N – B dative bond is usually present. However, in a protic media, solvent insertion of the N – B, occurs to afford a hydrogen-bonded zwitterionic species.

So what is the take-home message about the N – B interaction (in these systems)? Until recently we would have been reluctant to make any sweeping statements but thanks to the seminal publication from Anslyn [75] and current works from a number of other groups [36, 69, 70, 75] the N – B interaction can be ascribed to a hydrogen bonding interaction mediated through a bound solvent molecule. In other words, the N – B interaction in protic media such as water or methanol should not be represented as **10** but, rather the solvent-inserted form **14**.



From a design perspective, even though the mechanism responsible for conferring binding information from boron to nitrogen is indirect, what can be said with certainty is that this recognition unit is an effective one in saccharide recognition and should continue to be incorporated into sensory systems.

5 The Importance of Pyranose to Furanose Interconversion

In refining the selectivity of boronic acid sensors for saccharides the structure of the guest species must be addressed. Although there is a long history of

research into the structural character of boronic acid–saccharide complexes, the rapid isomerisation of monosaccharides in water precludes the description of a simple generic binding motif. The hemiacetal ring of a monosaccharide is readily cleaved in water, often reforming rings of different sizes and anomeric configurations. The equilibrium between linear, pyranose and furanose configurations as well as the α and β -anomers of the pyranose and furanose rings, substantially increases the number of possible structures that may be formed on complexation.

Sensor 6 provided the first structural elucidation of a diboronic acid sensor with D-glucose complexed within the binding site. The ^1H NMR spectrum of this complex indicated that in deuterated methanol the D-glucose was bound in the α -pyranose form at the 1,2 and 4,6 positions, as in Fig. 8 [66].

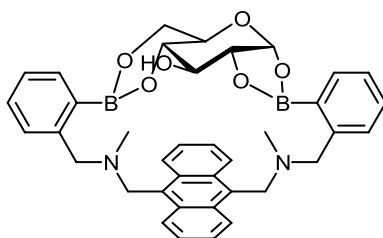


Fig. 8 Initial 1,2:4,6 complex formed between sensor 6 and D-glucose in MeOD [66]

A re-examination of this work was conducted by Norrild and Eggert [76]. Employing ^{13}C -1 and ^{13}C -6 labelled D-glucose the $^1\text{J}_{\text{C}1-\text{C}2}$ and $^1\text{J}_{\text{C}5-\text{C}6}$ coupling constants were monitored. Exploiting the observed reduction in the $^1\text{J}_{\text{CC}}$ value upon formation of a five-membered boronic ester [77], the analysis determined that the previous ^1H NMR assignment was correct, but that the interpretation was only valid as the initial complex formed under anhydrous conditions. With time the α -D-glucopyranose isomerised to the α -D-glucofuranose form. In deuterated methanol this process was slow, 20 h elapsed before the emergence of new NMR peaks became clear, with a complete disappearance of the original α -D-glucopyranose signals occurring after 8 days. However, if water was introduced to the system, isomerisation was accelerated dramatically and after 10 min in a 1 : 2 water/methanol solution isomerisation had gone to completion.

In the case of sensor 6 it was concluded that once formed the complex in Fig. 8 rearranges to the thermodynamically more stable 1,2:3,5,6 bound α -D-glucofuranose complex, Fig. 9, as a function of time and the water content of the medium. This binding pattern is comparable with that of other known structures, such as the commercially available diacetone-D-glucose 15.

Indeed the furanose form of the ring is the one that might be intuitively expected. For an O–B–O fragment to bridge the gap between conformationally locked synclinal (axial and equatorial) hydroxyl groups on a pyranose ring,

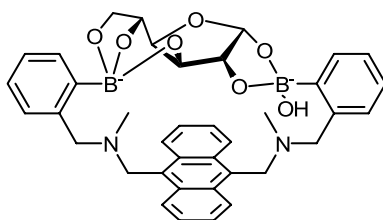
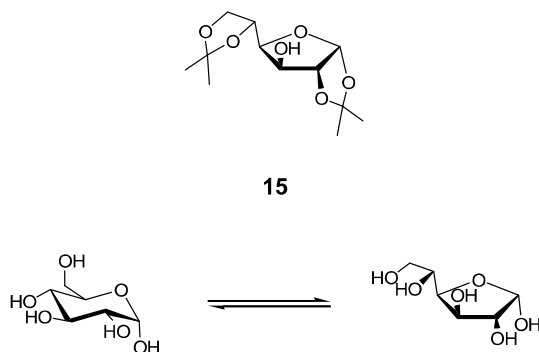


Fig. 9 Thermodynamically stable 1,2:3,5,6 complex observed to form between sensor **6** and D-glucose in basic aqueous media (given the current understanding of N – B interactions the boron bound at the 1,2 position is illustrated as a tetrahedral boronate) [76]

a substantial degree of torsional strain would be induced across the newly formed cyclic diester. In an effort to understand the significance of this torsional strain Nicholls and Paul undertook the molecular modelling of a series of boronic acid–cyclic saccharide complexes to determine the structure of the thermodynamically stable boronate esters formed [78]. It was found that the vicinal diols involved in complexation must possess, or at least be able to adopt, a syn-periplanar arrangement.

Anti-periplanar hydroxyl groups therefore fail to form boronic acid–diol complexes. Synclinal hydroxyl groups can adopt syn-periplanar geometry in instances when the energy lost due to induced distortions in the saccharide ring are outweighed by the energetic stability gained from complexation. But generally the most stable boronic acid–diol complexes occur between boronic acids and the conformationally locked syn-periplanar hydroxyl groups on furanose rings (Scheme 8) [78].



Scheme 8 The conformationally locked C1,C2-syn-periplanar diol group of the α -D-glucopyranose ring provides an ideal binding site for boronic acids [78]

This relationship is consistent with previously reported observed stability constants (K_{obs}) and was illustrated by Norrild and Eggert in a study of the complexation of *p*-tolylboronic acid with D-glucose. The study provided convincing evidence of a clear preference for the furanose form of the hemiacetal

ring at a stoichiometric ratio of 2 : 1 (boronic acid/D-glucose) [77]. The extent of the thermodynamic stability of this complex becomes apparent if one recalls that α -D-glucopyranose accounts for a mere 0.14% of the total speciation of equilibrated D-glucose in water yet becomes the dominant species in solution when complexed to monoboronic acids [79].

5.1

The Preference of Monoboronic Acids for D-Fructose

Drawing these observations together we indicate that the apparent dependence of the stability constants (K) of monoboronic acids on the ability of the vicinal diols of saccharides to conform to a syn-periplanar arrangement could be used to explain the heightened stability of D-fructose over other monosaccharides (see Lorand and Edwards' results in Table 1).

The furanose form of D-fructose with an available syn-periplanar anomeric hydroxyl pair (C2–C3) is β -D-fructofuranose (D in Fig. 10). At equilibrium this species accounts for an enormous 25% of the total speciation of D-fructose in deuterated water at 31 °C [80]. This value can be contrasted with that of the furanose form of D-glucose with an available syn-periplanar anomeric hydroxyl pair, α -D-glucopyranose, which accounts for 0.14% of the equilibrated forms of D-glucose in deuterated water at 27 °C [79]. In the presence of phenylboronic acid, the stability constants (K) reported by Lorand and Edwards were 4400 M⁻¹ with D-fructose and 110 M⁻¹ with D-glucose [28] (Table 1).

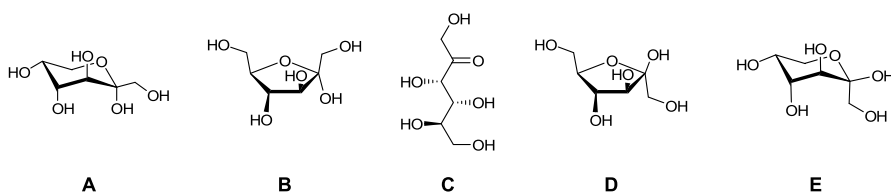
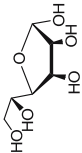

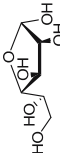
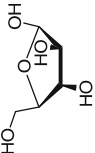
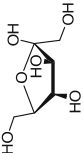


Fig. 10 D-Fructose in its various configurations and the percentage composition at equilibrium of each form of the sugar in D₂O at 31 °C: A α -pyranose, 2.5%; B α -furanose, 6.5%; C acyclic form, 0.8%; D β -furanose, 25%; E β -pyranose, 65% [80]

From a simplistic viewpoint we indicated that a very general statistical trend appears to exist between the natural speciation of saccharide forms containing the syn-periplanar anomeric hydroxyl pair arrangement (a premise of the form's stability) and the qualitative trend observed for their stability constants (K) with monoboronic acids (Table 2).

Unfortunately the complexity and extensive number of possible binding motifs precludes such a simplistic approach from providing anything other than a statistical rule-of-thumb guide.

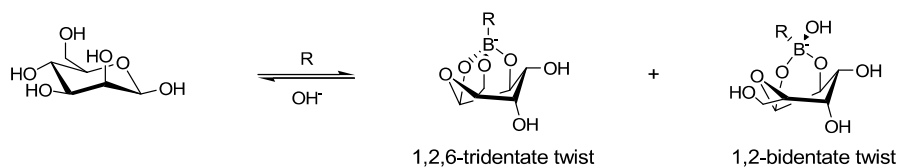
Table 2 Saccharide structures containing a syn-periplanar anomeric hydroxyl pair, equilibrated percentages in D₂O and stability constants with phenylboronic acid

Saccharide (furanose form with syn-periplanar arrangement of the anomeric hydroxyl pair)	Structure	Relative percentage (of the total composition in D ₂ O) (%)	K_{obs} (with phenylboronic acid) [28] (dm ³ mol ⁻¹)
D-Glucose (α-D-glucofuranose)		0.14 ^a	110
D-Mannose (β-D-mannofuranose)		0.3 ^b	170
D-Galactose (α-D-galactofuranose)		2.5 ^b	280
D-Arabinose (β-D-arabinofuranose)		~2 ^b	340
D-Fructose (β-D-fructofuranose)		25 ^b	4400

^a Following equilibration in D₂O at 27 °C [79]

^b Following equilibration in D₂O at 31 °C [80]

The furanose form of a saccharide may not necessarily always be the one favoured for binding. For example NMR data suggests that D-mannose may be preferentially complexed by monoboronic acids in a pyranose twist conformation, Scheme 9 [78].



Scheme 9 The probable twist isomers of the β -D-mannopyranose boronate esters, where R = *m*-nitro phenylboronic acid [78]

Furthermore, bidentate and tridentate complexation is known to occur, with *endo*- and *exo*-orientations of the substituents affecting the thermodynamic stability of the bidentate species, Fig. 11.

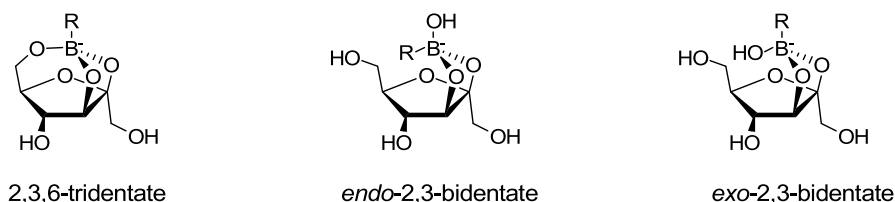


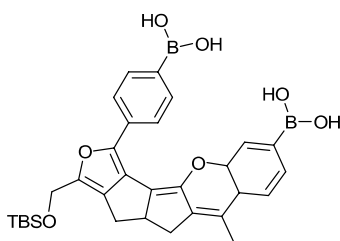
Fig. 11 Structures assigned to D-fructose at a 1 : 1 *p*-tolylboronic acid/D-fructose ratio [81]

This was illustrated in an examination into the complexation of *p*-tolylboronic acid with D-fructose [81]. From these two compounds, in aqueous alkaline solution, seven different complexes were afforded. Notably, the abundance of the major species within the system fluctuated as a function of solvent, pH and boronic acid concentration.

From the pragmatic viewpoint of designing diboronic acid sensors with selectivity for D-glucose, many receptors have relied on an approximate spacing of the two boronic acid units such that the dimensions of the binding pocket mimic that of other established systems.

Whilst the binding sites for the second boronic acid (at the 3,5,6 or 3,4,6 positions of D-glucose) depend on the experimental conditions and the particular boronic acid being investigated [77, 82], there is agreement that the strongest interaction between monoboronic acids and D-glucose occurs with the syn-periplanar hydroxyls on the 1 and 2 positions of α -D-glucofuranose [77, 78, 83, 84]. Given these observations and the known importance of pyranose to furanose interconversion, it has been suggested that in the future design of diboronic acid sensors for saccharides, the pyranose form should not be considered in aqueous systems [82].

Despite these observations, Drueckhammer and coworkers successfully used a computer-guided approach to engineer sensor **16**, a receptor specifically designed to complex α -D-glucopyranose at the 1,2 and 4,6 positions [85]. The computational approach produced a rigid molecular scaffold anchoring the two boronic acid groups precisely in space. Defined spatial architecture led the receptor to exhibit a 400-fold greater affinity for D-glucose over any of the other saccharides the receptor was evaluated against. Significantly, ^1H NMR confirmed that D-glucose was formed and retained as a stable complex in its pyranose form. Sensor **16** demonstrates that where two point binding is achieved between boronic acids of fixed distances and enforced geometries, different isomeric forms of a saccharide guest may be witnessed within the binding cleft than would have otherwise been predicted from the simple monoboronic acid structural analogues discussed above.

**16**

In refining the selectivity of boronic acid appended sensors for saccharides it therefore seems that pre-empting the structure of the guest species or the thermodynamic complex that it will form is non-trivial. It is known that only saccharides with the ability to interconvert between pyranose and furanose forms with an available anomeric hydroxyl pair have so far been reported to interact strongly with boronic acids. It is also generally the case that in aqueous solutions the furanose form of the saccharide will be thermodynamically favoured. However, as illustrated by Drueckhammer and others, in the case of recognition sites with two linked boronic acid fragments this is a function of substrate structure and geometry.

6

Modular Fluorescent Sensors

6.1

The Design Rationale

In the design of boronic acid based sensory systems it has been established that two receptor units are required if selectivity is to be achieved

for specific saccharides [66]. It has been demonstrated that the *N*-methyl-*o*-(aminomethyl)phenylboronic acid fragment is particularly effective at signalling these binding events via PET when correctly positioned alongside a suitable fluorophore [9].

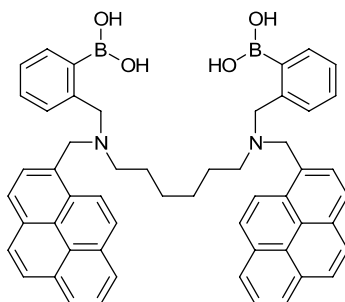
Retaining the same dual boronic acid recognition units throughout, it was thought advantageous to develop a modular system in which the linker and fluorophore units of these sensors could be modified independently. It was postulated that this approach would afford information on the effect of altering the dimensions of the binding pocket, permit the emission wavelength of the systems to be altered and provide clear data on the role of these individual variables by allowing them to be altered in a controlled manner.

In designing a range of modular sensors from which quantitative trends are to be derived, a generic scaffold must be established at the start of the project and adhered to throughout, if a meaningful comparison is to be obtained across the series.

Whilst sensors developed around the anthracene core unit (e.g., **6**) have proved to be selective for saccharides such as D-glucose, the rigid core unit (functioning as the scaffold, linker and fluorophore) limits the modifications that can be made to any one part of the system without influencing the sensor as a whole. Perusing the literature it appears that this limitation holds for a great many sensors.

In adopting a modular approach it was deemed important to design a system in which the receptor, linker and fluorophore units could be connected to the molecular scaffold in such a way as to permit these subunits to be varied independently.

Reported in 1995 compound **17** provides an example of a fluorescent PET sensor with clear compartmentalisation of the receptor, linker and fluorophore subunits [86]. Documented by Sandanayake, James and Shinkai, it was found that the stoichiometry of saccharide binding with sensor **17** (i.e. 1 : 1 or 2 : 1 saccharide/sensor) could be correlated with a decrease in



the fluorescence emission due to the excited state dimer (excimer) complex formed between the two pyrene residues, broad peak ~ 470 nm. Moreover, the saccharide concentration could be monitored via the usual increase in fluorescence emission intensity from the LE state of pyrene as a function of PET, peaks at 370, 397 and 417 nm. The K_{obs} for **17** was 2000 M^{-1} with D-glucose and 790 M^{-1} with D-galactose in 33 wt % methanol in water [86].

Appleton and Gibson investigated the effect of longer linker units between the two receptor units in this system [87]. 1,6-Diaminohexane, 1,7-diaminoheptane, 1,8-diaminooctane, 1,12-diaminododecane and 4,4'-diamino dicyclohexylmethane were introduced, with the observation that six- and seven-carbon linkers conferred the highest selectivity towards D-glucose whereas extended linkers lost the selectivity derived from the cooperative action of the dual recognition units.

Compound **17** was re-synthesised by the James group and the fluorescence properties re-evaluated [8]. The fluorescence titrations of compound **17** ($7.5 \times 10^{-7} \text{ mol dm}^{-3}$, $\lambda_{\text{ex}} = 342 \text{ nm}$) with different saccharides were carried out in a pH 8.21 aqueous methanolic buffer solution [52.1 wt % methanol (KCl, $10.00 \times 10^{-3} \text{ mol dm}^{-3}$; KH_2PO_4 , $2.752 \times 10^{-3} \text{ mol dm}^{-3}$; Na_2HPO_4 , $2.757 \times 10^{-3} \text{ mol dm}^{-3}$)]. The K_{obs} with coefficient of determination (r^2) was calculated by the fitting of emission intensity versus saccharide concentration using custom-written non-linear (Levenberg–Marquardt algorithm) curve fitting [88]. The errors reported are the standard errors obtained from the best fit. Relative fluorescent enhancements (I/I_0) are also reported. The results for **17** with D-glucose were $K_{\text{obs}} = 260 \pm 15 \text{ M}^{-1}$ ($r^2 = 1.00$), $I/I_0 = 4.9$; with D-galactose $K_{\text{obs}} = 237 \pm 6 \text{ M}^{-1}$ ($r^2 = 1.00$), $I/I_0 = 4.2$; with D-fructose $K_{\text{obs}} = 244 \pm 26 \text{ M}^{-1}$ ($r^2 = 0.99$), $I/I_0 = 3.4$ and with D-mannose $K_{\text{obs}} = 32 \pm 3 \text{ M}^{-1}$ ($r^2 = 0.99$), $I/I_0 = 3.2$.

6.2

Modular Systems

Six carbons separate the two amino nitrogens in the D-glucose selective compound **17**, the same number as separate the two amino nitrogens in the D-glucose selective sensor **6**. The boronic acid groups appended to the two nitrogens of sensor **17** (and **6**) must both take part in a binding event to allow the full fluorescence emission of the system to be restored. The dual recognition sites and their separation are therefore key to the observed saccharide selectivity. With this in mind it was decided that a generic template based on sensor **17** would prove effective. The general design assembly proposed is illustrated in Fig. 12.

This design retains the two boronic acid groups required for selectivity but allows the separation between them to be varied by altering the linker. It also permits the fluorophore to be varied independently and by using only one fluorophore overcomes the problems that may arise from excimer

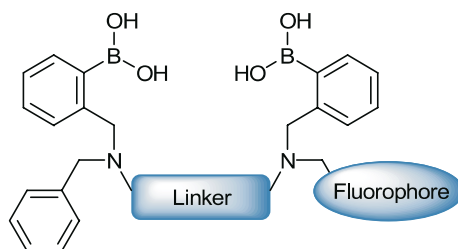


Fig. 12 Receptor and spacer groups remained unchanged throughout. Two *N*-methyl-*o*-(aminomethyl)phenylboronic acid groups functioned as the receptor units with a methylene spacer modulating PET

emission,¹ insolubility, excessive hydrophobicity and steric crowding at the binding pocket.

6.2.1

Linker Dependence

The modular PET sensors **18**_(*n*=3) – **23**_(*n*=8) contained two phenylboronic acid groups, a pyrene fluorophore and a variable linker (Fig. 13). The linker was varied from trimethylene **18**_(*n*=3) to octamethylene **23**_(*n*=8). The aim of this research was to elucidate the optimum linker length required for maximum D-glucose selectivity [89–91].

The fluorescence titrations of **18**_(*n*=3) – **23**_(*n*=8) and **24**_(pyrene) (1.0×10^{-7} mol dm⁻³) with different saccharides were carried out in a pH 8.21 aqueous methanolic buffer solution, as described above [92]. The fluorescence intensity of sensors **18**_(*n*=3) – **23**_(*n*=8) and **24**_(pyrene) increased with increasing saccharide concentration. The observed stability constants (K_{obs}) of PET sensors **18**_(*n*=3) – **23**_(*n*=8) and **24**_(pyrene) were calculated by fitting the emission intensity at 397 nm versus saccharide concentration and are given in Table 3.

To help visualise the trends in K_{obs} documented in Table 3, the K_{obs} of the diboronic acid sensors **18**_(*n*=3) – **23**_(*n*=8) are reported in Fig. 14 divided by (i.e. relative to) the K_{obs} of their equivalent monoboronic acid analogue **24**_(pyrene). In most cases, the K_{obs} with diboronic acid sensors **18**_(*n*=3) – **23**_(*n*=8) are higher than for the monoboronic acid sensor **24**_(pyrene).

It is known that D-glucose and D-galactose will bind to diboronic acids readily using two sets of diols, thus forming stable, cyclic 1 : 1 complexes. The allosteric binding of the two boronic acid groups is clearly illustrated by the relative difference between the K_{obs} of the equivalent di- and monoboronic

¹ Whilst excimer emission can be used to visually determine the stoichiometry of the binding event and advantageously red shifts the fluorescence emission, the comparatively small changes in fluorescence emission intensity do not lend this part of the emission band to accurate signalling of saccharide concentrations. It is also generally the case that sensors with two fluorophore units have observed binding constants (K_{obs}) ~ four times lower than their mono-fluorophore counterparts.

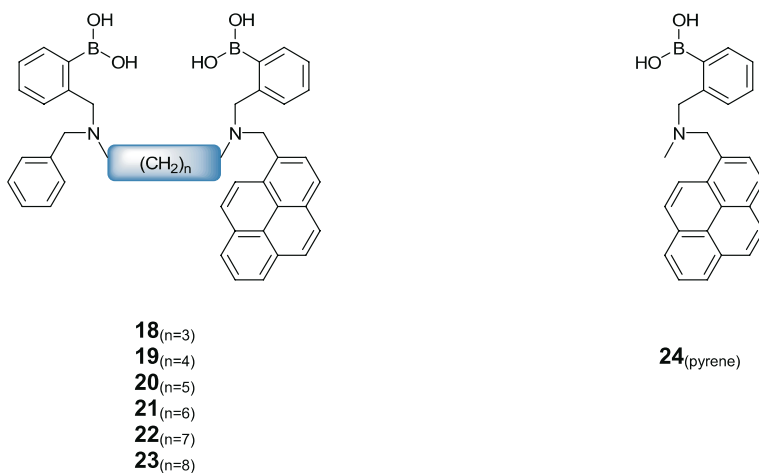


Fig. 13 Modular PET sensors **18**_(n=3) – **23**_(n=8) with monoboronic acid reference compound **24**_(pyrene)

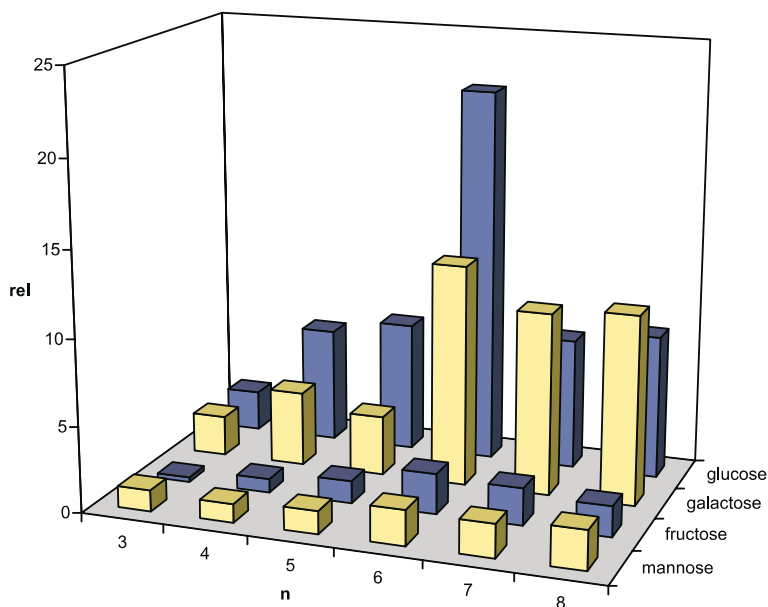


Fig. 14 Observed stability constants (K_{obs}) of **18**_(n=3) – **23**_(n=8) divided by K_{obs} of **24**_(pyrene), to yield relative values with saccharides. The D-configuration of the monosaccharides was used throughout this evaluation

acid compounds. The K_{obs} of the diboronic acid sensors are up to ~ 22 times larger than with their monoboronic acid counterparts (see Fig. 14).

The K_{obs} for the diboronic acid sensors with D-fructose and D-mannose are, at most, twice as strong as with the monoboronic acid sensor **24**_(pyrene).

Table 3 Quantum yield (qFM), observed stability constant (K_{obs})(coefficient of determination, r^2) and fluorescence enhancement for compounds **18**_(n=3) – **23**_(n=8) and **24**_(pyrene)

Sensor	D-Glucose			D-Galactose		
	qFM ^a (dm ³ mol ⁻¹)	$K_{\text{obs}}(r^2)^{\text{b}}$	Fluorescence enhancement ^b	$K_{\text{obs}}(r^2)^{\text{b}}$ (dm ³ mol ⁻¹)	Fluorescence enhancement ^b	
18 _(n=3)	0.16	103 ± 3 (1.00)	3.9	119 ± 5 (1.00)	3.5	
19 _(n=4)	0.16	295 ± 11 (1.00)	3.3	222 ± 17 (1.00)	3.7	
20 _(n=5)	0.20	333 ± 27 (1.00)	3.4	177 ± 15 (1.00)	3.0	
21 _(n=6)	0.24	962 ± 70 (0.99)	2.8	657 ± 39 (1.00)	3.1	
22 _(n=7)	0.16	336 ± 30 (0.98)	3.0	542 ± 41 (0.99)	2.9	
23 _(n=8)	0.19	368 ± 21 (1.00)	2.3	562 ± 56 (0.99)	2.3	
24 _(pyrene)	0.17	44 ± 3 (1.00)	4.5	51 ± 2 (1.00)	4.2	

Sensor	D-Fructose			D-Mannose		
	qFM ^a (dm ³ mol ⁻¹)	$K_{\text{obs}}(r^2)^{\text{b}}$	Fluorescence enhancement ^b	$K_{\text{obs}}(r^2)^{\text{b}}$ (dm ³ mol ⁻¹)	Fluorescence enhancement ^b	
18 _(n=3)	0.16	95 ± 9 (0.99)	3.6	45 ± 4 (1.00)	2.7	
19 _(n=4)	0.16	266 ± 28 (0.99)	4.2	39 ± 1 (1.00)	3.4	
20 _(n=5)	0.20	433 ± 19 (1.00)	3.4	48 ± 2 (1.00)	3.0	
21 _(n=6)	0.24	784 ± 44 (1.00)	3.2	74 ± 3 (1.00)	2.8	
22 _(n=7)	0.16	722 ± 37 (1.00)	3.3	70 ± 5 (1.00)	2.7	
23 _(n=8)	0.19	594 ± 56 (0.99)	2.3	82 ± 3 (1.00)	2.2	
24 _(pyrene)	0.17	395 ± 11 (1.00)	3.6	36 ± 1 (1.00)	3.7	

The system with the highest K_{obs} is highlighted in bold

^a In the absence of saccharides

^b With monosaccharides

Each D-fructose and D-mannose molecule will only bind to one boronic acid unit through one diol. This allows complexes to form with overall 2 : 1 (saccharide/sensor) stoichiometry. The relative values of ca. 2 are indicative of two independent saccharide binding events on each sensor, with no increase in stability derived from cooperative binding.

The highest K_{obs} for D-glucose within these systems was obtained by sensor **21**_(n=6). The flexible six carbon linker provided the optimal selectivity for D-glucose over other saccharides. This is in agreement with the observed selectivity of compounds **6** and **17**, which also have linkers containing six carbon atoms.

Curiously there is an inversion in the selectivity displayed by these systems on going from a six to a seven carbon linker. From Fig. 14 it is clear that the trimethylene linked **18**_(n=3) shows little specificity between D-glucose and D-galactose. Increasing the size of the binding pocket, tetramethylene **19**_(n=4) through to hexamethylene **21**_(n=6), induces a clear selectivity for D-glucose, with **21**_(n=6) providing the strongest binding by far. However, there is an inversion in this selectivity on increasing the linker length to heptamethylene

$22_{(n=7)}$ and octamethylene $23_{(n=8)}$, with the enlarged binding pocket being D-galactose selective.

This facet was initially ascribed to the difference in configuration of these diastereomers [91]. The 1,2- and 4,6-diols of D-glucose point in the same direction (down), but in D-galactose (the 4-epimer of D-glucose), the 1,2-diol is down and the 4,6-diol is up, as illustrated in Fig. 15. Therefore, not only are the inter-diol distances of D-galactose slightly longer than in D-glucose but the diols are also on opposite faces of the saccharide ring. On this basis it seemed reasonable to expect better complementarity for D-galactose with a larger inter-receptor distance than for D-glucose.



Fig. 15 α -D-Pyranose forms of glucose and galactose with the 1,2- and 4,6-diols highlighted in *light-grey*

As discussed above, current thinking requires that we consider saccharidic forms where a syn-periplanar arrangement of the anomeric hydroxyl pair can be attained. Generally this requires formation of the furanose form of the saccharide. However, computational work has shown that in the case of D-galactose the α -D-furanose form of the saccharide is not the only species that can be considered with a syn-periplanar alignment of the anomeric hydroxyl pair [78].

On complexation of a boronic acid to the diol in the 1,2-position of α -D-galactopyranose a reorientation of the saccharide can afford an acetal ring with a boat or twist boat conformation (Fig. 16). This reorientation permits a second boronic acid group to bind with the diol in the 3,4-position producing an energetically stable complex with the pyranose form of the saccharide.

In light of this new data it seems plausible that the preference of D-galactose for a slightly larger binding pocket than D-glucose can be ascribed to

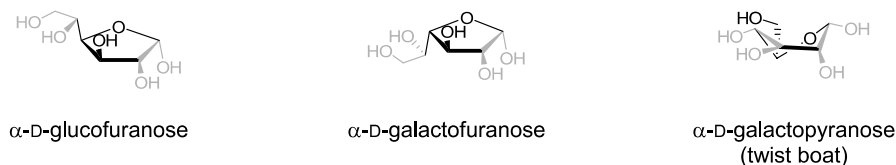


Fig. 16 α -D-Furanose forms of glucose and galactose with the 1,2- and 5,6-diols highlighted in *light-grey*, as well as the twist-boat conformation of the α -D-pyranose form of galactose with the 1,2- and 3,4-diols highlighted in *light-grey*

the stability of the preferred ring form. D-Galactose can generate complexes with boronic acids in its pyranose form, whereas D-glucose will prefer the smaller furanose ring form.

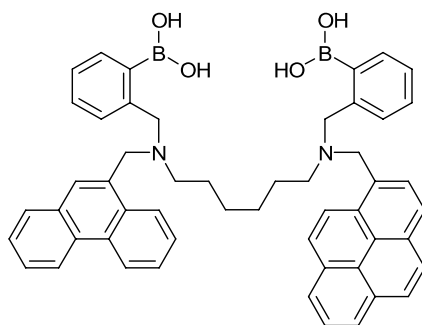
6.2.2

Energy Transfer Systems

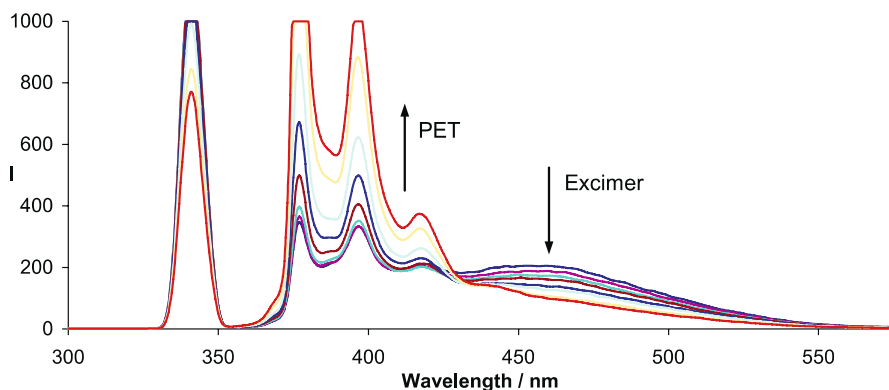
Fluorescence energy transfer is the transfer of excited-state energy from a donor to an acceptor. The transfer occurs as a result of transition dipole-dipole interactions between the donor-acceptor pair [93]. The fluorescent sensor investigated, **25**_(phenanthrene-pyrene), had two phenylboronic acid groups, a hexamethylene linker and two different fluorophore groups: phenanthrene and pyrene [94].

The purpose of constructing sensor **25**_(phenanthrene-pyrene) was to investigate the efficiency of energy transfer from phenanthrene to pyrene as a function of saccharide binding. A similar concept had previously been employed in the construction of a fluorescent calix[4]arene sodium sensor [95]. The excitation and emission wavelengths of the phenanthrene (donor) are 299 nm and 369 nm, respectively, while the excitation and emission wavelengths of the pyrene (acceptor) are 342 nm and 397 (or 417) nm, respectively. The emission wavelength of phenanthrene (369 nm) and excitation wavelength of pyrene (342 nm) overlap. These observations led to the postulation that intramolecular energy transfer from phenanthrene to pyrene could take place in sensor **25**_(phenanthrene-pyrene).

Using light of 342 nm (the λ_{ex} of pyrene) to excite sensor **25**_(phenanthrene-pyrene) leads to long wavelength excimer emission due to π - π interactions between phenanthrene and pyrene (Scheme 10 broad peak \sim 470 nm). PET-modulated emission is also observed from the LE state of pyrene, the three distinctive peaks of the emission band visible in Scheme 10 at 370, 397 and 417 nm. The intense peak in Scheme 10 at 342 nm is due to Raleigh scattering of the exciting radiation.



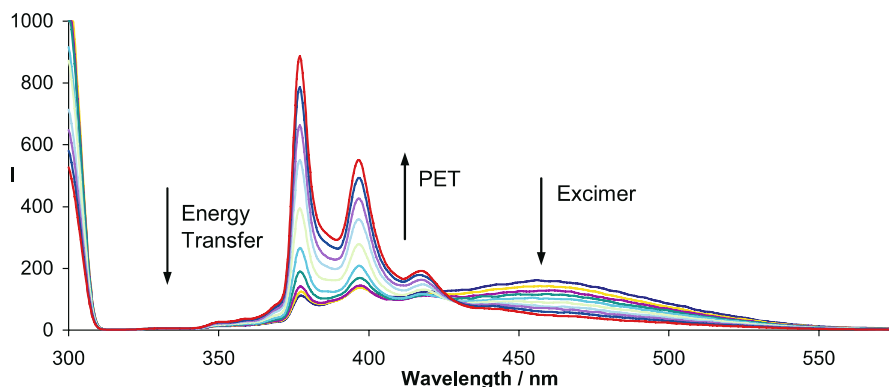
25 (phenanthrene-pyrene)



Scheme 10 Fluorescence intensity versus wavelength for sensor $25_{(\text{phenanthrene-pyrene})}$ ($2.5 \times 10^{-6} \text{ mol dm}^{-3}$) displaying photoinduced electron transfer and excimer emission with increasing concentrations of D-glucose (from 0 to $1.0 \times 10^{-1} \text{ mol dm}^{-3}$) in 52.1 wt % MeOH pH 8.21 phosphate buffer. $\lambda_{\text{ex}} = 342 \text{ nm}$

If light of 299 nm was used (the λ_{ex} of phenanthrene) to excite sensor $25_{(\text{phenanthrene-pyrene})}$, the fluorescence emission spectrum did not display an emission band around 369 nm as would be expected for phenanthrene (Scheme 11). Instead the resulting emission band had an emission maximum at 417 nm and was identical to the emission observed when pyrene was excited directly, as in Scheme 10. This result can be ascribed to energy transfer from the phenanthrene to the pyrene fluorophore.

The fluorescence titrations of sensor $25_{(\text{phenanthrene-pyrene})}$ ($2.5 \times 10^{-6} \text{ mol dm}^{-3}$, $\lambda_{\text{ex}} = 299 \text{ nm}$ for phenanthrene and $\lambda_{\text{ex}} = 342 \text{ nm}$ for pyrene) with



Scheme 11 Fluorescence intensity versus wavelength for sensor $25_{(\text{phenanthrene-pyrene})}$ ($2.5 \times 10^{-6} \text{ mol dm}^{-3}$) displaying energy transfer, photoinduced electron transfer and excimer emission with increasing concentrations of D-glucose (from 0 to $1.0 \times 10^{-1} \text{ mol dm}^{-3}$) in 52.1 wt % MeOH pH 8.21 phosphate buffer. $\lambda_{\text{ex}} = 299 \text{ nm}$

different saccharides were carried out in a pH 8.21 aqueous methanolic buffer. Absorption versus concentration plots of sensor **25**_(phenanthrene-pyrene) and the monoboronic acid reference compounds **24**_(pyrene) and **31**_(phenanthrene) confirmed that the π - π stacking of sensor **25**_(phenanthrene-pyrene) was solely intramolecular. The fluorescence intensity of sensor **25**_(phenanthrene-pyrene) at 417 nm increased with added saccharide when excited at both 299 and 342 nm, while the excimer emission at 460 nm decreased with added saccharide. The change in excimer emission indicates that the π - π interaction between phenanthrene and pyrene is disrupted on saccharide binding.

The observed stability constants (K_{obs}) of sensor **25**_(phenanthrene-pyrene) (with $\lambda_{\text{ex}} = 299$ nm and $\lambda_{\text{ex}} = 342$ nm) were calculated by fitting the emission intensities at 417 nm versus concentration of saccharide curves and are given in Table 4. The K values were analysed in KaleidaGraph using non-linear (Levenberg–Marquardt algorithm) curve fitting. The errors reported are the standard errors obtained from the best fit. The K_{obs} for the diboronic acid sensor **25**_(phenanthrene-pyrene) ($\lambda_{\text{ex}} = 299$ and 342 nm) with D-glucose were enhanced relative to those of the monoboronic acid reference compounds **24**_(pyrene) and **31**_(phenanthrene), while the K_{obs} for the diboronic acid sensor **25**_(phenanthrene-pyrene) ($\lambda_{\text{ex}} = 299$ and 342 nm) with D-fructose were reduced relative to those for the monoboronic acid reference compounds **24**_(pyrene) and **31**_(phenanthrene).

Table 4 Observed stability constants (K_{obs}) (coefficient of determination, r^2) and fluorescence enhancements for compounds **17** and **25**_(phenanthrene-pyrene) with saccharides

Sensor	D-Glucose		D-Galactose	
	K_{obs} ($\text{dm}^3 \text{mol}^{-1}$)	Fluorescence enhancement	K_{obs} ($\text{dm}^3 \text{mol}^{-1}$)	Fluorescence enhancement
17	260 ± 15 (1.00)	4.9	237 ± 6 (1.00)	4.2
25 _(phenanthrene-pyrene) ^a	142 ± 12 (0.99)	3.9	74 ± 7 (0.99)	2.2
25 _(phenanthrene-pyrene) ^c	108 ± 10 (0.99)	2.4	81 ± 8 (0.99)	2.6
Sensor	D-Fructose		D-Mannose	
	K_{obs} ($\text{dm}^3 \text{mol}^{-1}$)	Fluorescence enhancement	K_{obs} ($\text{dm}^3 \text{mol}^{-1}$)	Fluorescence enhancement
17	244 ± 26 (0.99)	3.4	32 ± 3 (0.99)	3.2
25 _(phenanthrene-pyrene) ^a	76 ± 10 (0.98)	1.7	– ^b	– ^b
25 _(phenanthrene-pyrene) ^c	125 ± 11 (0.99)	3.5	8 ± 1 (1.00)	3.5

^a $\lambda_{\text{ex}} = 299$ nm, $\lambda_{\text{em}} = 417$ nm

^b K_{obs} and fluorescence enhancement could not be determined because of the small changes in fluorescence

^c $\lambda_{\text{ex}} = 342$ nm, $\lambda_{\text{em}} = 417$ nm

Sensor **25**_(phenanthrene-pyrene) was particularly noteworthy in that the difference between the observed fluorescence enhancements obtained when excited at phenanthrene ($\lambda_{\text{ex}} = 299 \text{ nm}$) and pyrene ($\lambda_{\text{ex}} = 342 \text{ nm}$) can be correlated with the molecular structure of the saccharide-sensor complex via PET (see Table 4). The fluorescence enhancement of sensor **25**_(phenanthrene-pyrene) with D-glucose was 3.9 times greater when excited at 299 nm and 2.4 times greater when excited at 342 nm. With D-fructose the enhancement was 1.9 times greater when excited at 299 nm and 3.2 times greater when excited at 342 nm. This is to say that the selectivity between D-fructose and D-glucose within the same complex is in fact inverted, dependant on the excitation wavelength used. This result arises from the fact that energy transfer from phenanthrene to pyrene is far more efficient in the 1 : 1 cyclic saccharide-diboronic acid complex than in the alternative 2:1 acyclic complex. This approach finally allows for efficient discrimination between saccharides based on their binding motif (i.e. the formation of a 1 : 1 or a 2 : 1 complex).

6.2.3

Fluorophore Dependence

Given the understanding developed in the previous section regarding the influence of the linker length in modular PET sensors for saccharides, as well as the advantages of using energy transfer to determine selectivity, the next structural feature to be evaluated was the fluorophore appended to the modular sensor, see Arimori et al. [96].

The fluorophores chosen are all commercially available as their aldehyde derivatives, comparatively inexpensive and have similar photophysical properties.

Sensors **26**_(pyrene) – **30**_(2-naphthalene) all utilise the same general structural motif, this is illustrated in Fig. 17. The two phenylboronic acid receptors introduce saccharide selectivity while the hexamethylene linker governs the dimensions of the binding cleft, with a proven bias towards D-glucose selectivity.

In order to determine the binding stoichiometry of the complexes formed within the binding sites of the diboronic acid based sensors **26**_(pyrene) – **30**_(2-naphthalene) and elucidate the benefits gained from allosteric interactions, these systems must be contrasted against analogous monoboronic acid reference compounds (Fig. 18). These reference compounds **24**_(pyrene), **31**_(phenanthrene) – **34**_(2-naphthalene) shall be discussed first.

The fluorescence titrations of the monoboronic acid reference compounds **24**_(pyrene), **31**_(phenanthrene) – **34**_(2-naphthalene) and the diboronic acid sensors **26**_(pyrene) – **30**_(2-naphthalene) with D-glucose, D-galactose, D-fructose and D-mannose were carried out in an aqueous methanolic buffer solution [52.1 wt % methanol at pH 8.21 (KCl, $10.00 \times 10^{-3} \text{ mol dm}^{-3}$; KH_2PO_4 ,

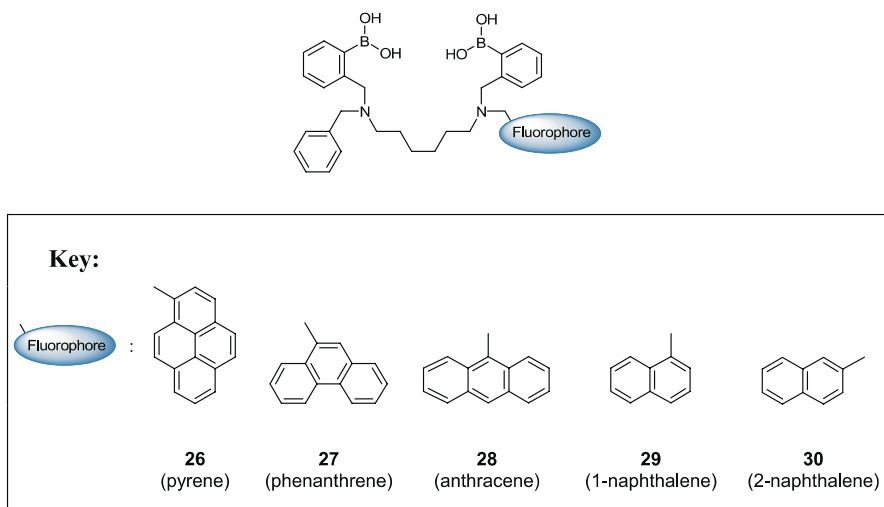


Fig. 17 Generic template for the five diboronic acid sensors with variable fluorophore units **26**(pyrene) – **30**(2-naphthalene)

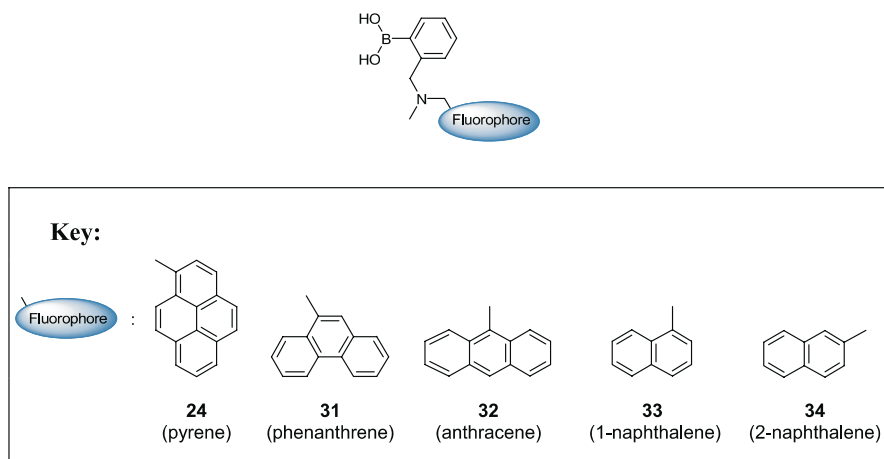


Fig. 18 Generic template for the five monoboronic acid reference compounds with variable fluorophore units **24**(pyrene) – **34**(2-naphthalene)

$2.752 \times 10^{-3} \text{ mol dm}^{-3}$; Na_2HPO_4 , $2.757 \times 10^{-3} \text{ mol dm}^{-3}$] [92]. The fluorescence intensity of the diboronic acid sensors **26**(pyrene) – **30**(2-naphthalene) increased with increasing saccharide concentration. The observed stability constants (K_{obs}) of PET sensors **26**(pyrene) – **30**(2-naphthalene) and **24**(pyrene), **31**(phenanthrene) – **34**(2-naphthalene) were calculated by the fitting of emission in-

Table 5 Observed stability constants (K_{obs}) (coefficient of determination, r^2) and fluorescence enhancements for the saccharide complexes of sensors $24_{(\text{pyrene})}$, $31_{(\text{phenanthrene})}$ – $34_{(2\text{-naphthalene})}$ and $26_{(\text{pyrene})}$ – $30_{(2\text{-naphthalene})}$

Sensor	D-Glucose		D-Galactose	
	K_{obs} ($\text{dm}^3 \text{mol}^{-1}$)	Fluorescence enhancement	K_{obs} ($\text{dm}^3 \text{mol}^{-1}$)	Fluorescence enhancement
$26_{(\text{pyrene})}$	962 ± 70 (0.99)	2.8	657 ± 39 (1.00)	3.1
$24_{(\text{pyrene})}$	44 ± 3 (1.00)	4.5	51 ± 2 (1.00)	4.2
$27_{(\text{phenanthrene})}$	325 ± 58 (0.97)	1.5	611 ± 101 (0.97)	1.4
$31_{(\text{phenanthrene})}$	30 ± 7 (0.98)	1.5	77 ± 12 (0.98)	1.4
$28_{(\text{anthracene})}$	441 ± 76 (0.98)	3.2	536 ± 31 (1.00)	3.1
$32_{(\text{anthracene})}$	61 ± 3 (1.00)	3.4	93 ± 6 (1.00)	3.0
$29_{(1\text{-naphthalene})}$	417 ± 60 (0.98)	6.1	1072 ± 68 (0.99)	5.4
$33_{(1\text{-naphthalene})}$	52 ± 1 (1.00)	5.7	78 ± 5 (1.00)	5.0
$30_{(2\text{-naphthalene})}$	532 ± 57 (0.99)	4.2	894 ± 66 (0.99)	4.1
$34_{(2\text{-naphthalene})}$	35 ± 2 (1.00)	4.5	49 ± 4 (1.00)	4.3

Table 6 Observed stability constants (K_{obs}) (coefficient of determination; r^2) and fluorescence enhancements for the saccharide complexes of sensors $24_{(\text{pyrene})}$, $31_{(\text{phenanthrene})}$ – $34_{(2\text{-naphthalene})}$ and $26_{(\text{pyrene})}$ – $30_{(2\text{-naphthalene})}$

Sensor	D-Fructose		D-Mannose	
	K_{obs} ($\text{dm}^3 \text{mol}^{-1}$)	Fluorescence enhancement	K_{obs} ($\text{dm}^3 \text{mol}^{-1}$)	Fluorescence enhancement
$26_{(\text{pyrene})}$	784 ± 44 (1.00)	3.2	74 ± 3 (1.00)	2.8
$24_{(\text{pyrene})}$	395 ± 11 (1.00)	3.6	36 ± 1 (1.00)	3.7
$27_{(\text{phenanthrene})}$	1013 ± 126 (0.98)	1.4	134 ± 18 (0.98)	1.4
$31_{(\text{phenanthrene})}$	548 ± 55 (0.99)	1.4	58 ± 8 (0.98)	1.4
$28_{(\text{anthracene})}$	1000 ± 69 (0.99)	3.0	111 ± 6 (1.00)	2.8
$32_{(\text{anthracene})}$	713 ± 35 (1.00)	3.0	61 ± 3 (1.00)	3.0
$29_{(1\text{-naphthalene})}$	964 ± 41 (1.00)	5.5	101 ± 3 (1.00)	5.0
$33_{(1\text{-naphthalene})}$	529 ± 45 (0.99)	5.4	46 ± 1 (1.00)	5.2
$30_{(2\text{-naphthalene})}$	1068 ± 63 (1.00)	3.8	98 ± 4 (1.00)	3.5
$34_{(2\text{-naphthalene})}$	399 ± 34 (0.99)	4.6	40 ± 2 (1.00)	3.8

tensity versus saccharide concentration curves [97]. The K_{obs} calculated are reported in Table 5 and Table 6.

To help visualise the trends of K_{obs} in Table 5 and Table 6, the stability constants of the diboronic acid sensors $26_{(\text{pyrene})}$ – $30_{(2\text{-naphthalene})}$ are reported in Fig. 19 divided by the stability constants of the analogous monoboronic acid reference compounds $24_{(\text{pyrene})}$, $31_{(\text{phenanthrene})}$ – $34_{(2\text{-naphthalene})}$.

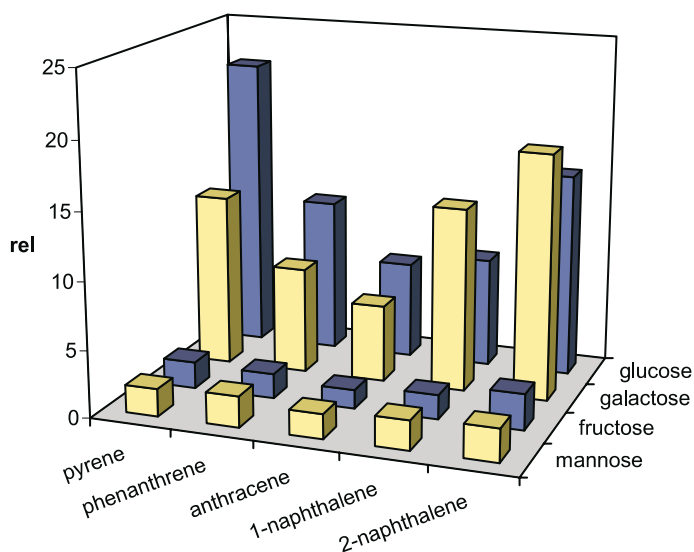


Fig. 19 Observed stability constants (K_{obs}) of the diboronic acid sensors **26**_(pyrene) – **30**_(2-naphthalene) divided by K_{obs} of the corresponding monoboronic acid reference compounds **24**_(pyrene), **31**_(phenanthrene) – **34**_(2-naphthalene) to yield relative values with saccharides. The D-configuration of the monosaccharides was used throughout this evaluation

6.2.3.1 Inference

It could be thought that altering the appended fluorophore on the modular diboronic acid systems would simply lead to fluorescent sensors with different emission and excitation wavelengths. As can be readily observed from the bar graph in Fig. 19 this was not the case.

The relative stabilities clearly illustrate that an increase in selectivity is obtained by cooperative binding through the formation of 1 : 1 cyclic systems. The large enhancement of the relative stability observed for the 1 : 1 cyclic systems (formed with D-glucose and D-galactose) are clearly contrasted with the small twofold enhancement observed for the 2 : 1 acyclic systems (formed with D-fructose and D-mannose).

The results in Fig. 19 indicate that the best match between receptor and guest is for sensors **26**_(pyrene), **31**_(phenanthrene) and **28**_(anthracene) with D-glucose and for sensors **29**_(1-naphthalene) and **30**_(2-naphthalene) with D-galactose.

The bar graph in Fig. 19 describes a saddle-like trend from pyrene through to 2-naphthalene with a change in selectivity from D-glucose to D-galactose occurring in the middle of the series. To account for such a trend these results must be a function of more than one variable.

6.2.3.2 Solvation

The first factor to be considered was the size of the fluorophore's π surface. From Fig. 19 it can be observed that the largest relative value was for sensor **26**_(pyrene) with D-glucose. Pyrene, with four fused benzene rings, represents the largest fluorophore in the series and as such endows sensor **26**_(pyrene) with the largest planar aromatic π surface of any of the sensors **26**_(pyrene) – **30**_(2-naphthalene). As the size of the fluorophore is reduced to three fused benzene rings in phenanthrene and anthracene the relative values are seen to diminish. As the fluorophore size decreases further still to the two fused benzene rings in 1- and 2-naphthalene there is a distinct change in the direction of the trend. The relative values increase, with a concomitant change in selectivity from D-glucose to D-galactose. Given the proximity of the fluorophore's planar aromatic π surface to the binding pocket it seemed reasonable to infer that the hydrophobicity within the binding pocket would be a function of the size of the fluorophore. If so, sensor **26**_(pyrene) would therefore have the most hydrophobic environment within the binding pocket of any of the sensors **26**_(pyrene) – **30**_(2-naphthalene), this environment being observed to have the best D-glucose selectivity across the series.

To rationalise these observed changes in terms of the complementarity between the hydrophobicities of the monosaccharides and sensors **29**_(1-naphthalene) – **30**_(2-naphthalene) the reported hydration values for the monosaccharides were examined. From the literature it appears that establishing the hydration characteristics of monosaccharides such as D-glucose and D-galactose is non-trivial; however, there is general agreement that D-galactose is slightly more hydrophobic than D-glucose [98–100]. The opposite of what we would expect based on the above observations.

The interactions between aromatic hydrocarbons and monosaccharides in aqueous solutions have been determined. Janado et al. documented that aqueous solutions of D-galactose were found to dissolve more benzene, naphthalene and biphenyl than the equivalent aqueous solutions of D-glucose [101, 102]. A result consistent with D-galactose being the more hydrophobic of the two saccharides.

In attempting to establish a rationale for the values displayed in Fig. 19 a number of factors have to be considered: the size, orientation and proximity of the fluorophores in sensors **26**_(pyrene) – **30**_(2-naphthalene) to the binding pocket; the hydrophobicities of the monosaccharides in their relative compositions and the manner in which complexation with boronic acids will change this (as discussed above D-glucose will predominantly favour the α -D-glucopyranose form and D-galactose will favour an α -D-galactopyranose or α -D-galactopyranose (twist-boat) form) [79, 80] as well as the covalent interactions of the saccharide hydroxyl groups with the diboronic acid receptors on binding. Rationalising these trends in a quantitative manner would

therefore require a considerable computational effort given the complex and dynamic nature of these systems. However, in considering these experimental observations a number of important features come to light.

Since Emil Fischer's seminal article of 1894 in which the hydrated polar groups within yeast's binding site were described as a locked gate that could only be opened by the key polar groups of α -glucosides (and not β -glucosides) much work has been done on understanding the cause of such well-defined stereospecific recognition [103, 104]. Whilst the physical fit of the "key" within the "lock" could be intuitively understood, further research demonstrated that selectivity was not just a facet of enthalpic stabilisation but relied intimately on the increase in entropy that occurred when water was displaced from the binding site. In turn this entropic stabilisation had to be played off against the decrease in entropy that occurred when the perturbed solvent shell surrounding the saccharide was displaced.

For most of the hexoses and pentoses there is little overall difference in hydrophobicity, nevertheless, it is the case that very slight differences in the stereochemical configuration of the monosaccharide hydroxyl groups can lead to significant changes in solvation properties. One of the most significant deviations from the general trend within the hexoses is the presence of an axial C4 hydroxyl group [99, 105]. This facet has been documented as causing D-galactose to have a substantially diminished fit in water compared to D-glucose. As such, the two monosaccharides have been categorised as having markedly different hydration properties (i.e. whilst their observed hydrophobicities may appear to be similar, the degree of disorder they introduce to the water molecules surrounding them is quite different) [98, 100, 106].

Water molecules are therefore crucial in controlling the selective recognition of saccharides within aqueous systems and it is the case that the restructuring of perturbed surface water provides an important force in controlling these molecular associations [107]. Therefore if correctly approached the solvation effects observed within our simple diboronic acid sensors may provide the impetus for a more refined discrimination between the molecular recognition of D-glucose and D-galactose in aqueous systems through careful control of the hydrophobicity of the binding pocket.

This observation may prove of particular interest not only in sensor design but also in regard to the significant work being undertaken on saccharide transport through organic membranes (such as lipid bilayers) via boronic acid carriers. In these systems D-galactose is noticeable by its absence as, to date, no data has been reported regarding the transport of D-galactose through hydrophobic membranes using boronic acid carriers [108–113].

6.2.3.3 Steric Crowding

If the size of the fluorophore's π surface was the only factor to be considered, little difference would be expected between the results observed for sensors **29**_(1-naphthalene) and **30**_(2-naphthalene). This was not the case. In comparing sensors **29**_(1-naphthalene) and **30**_(2-naphthalene) there was no difference in size between the fluorophore's hydrophobic π surfaces, only a difference in connectivity and therefore in the relative alignment of the fluorophores with regard to the binding cleft. In explaining the difference between the relative values, the number of *peri*-hydrogens on the fluorophores was considered. The fluorophore with the highest number of *peri*-hydrogens is anthracene with two, then pyrene, phenanthrene and 1-naphthalene with one each and then 2-naphthalene with none.

This ties in well with the observed results in the bar graph of Fig. 19. Anthracene with the greatest number of *peri*-hydrogens displays the lowest relative stability. These *peri*-hydrogens can be considered to increase the steric crowding within the binding pocket and as such this hypothesis seems quite reasonable. It also fits the increase in sensitivity observed for 2-naphthalene over 1-naphthalene.

6.2.3.4 Denouement

These results demonstrate that in a fluorescent PET saccharide sensor with two phenylboronic acid groups, a hexamethylene linker and a fluorophore, the choice of the fluorophore is crucial. The fluorophore not only defines the emission wavelength but also influences the environment within the binding site, with the overall selectivity being fluorophore-dependent.

An informed decision will therefore have to be taken in the future design of fluorescent sensors, such that the polarity of the chosen guest species complements the solvation within the binding pocket. Whilst not a direct premise of complementarity between hydrophobicity of the appended fluorophore of the sensor and the pyranose form of the guest monosaccharide, it appears to be the case that boronic acids display enhanced selectivity for D-glucose over D-galactose when the hydrophobicity of the binding pocket is increased.

In addition to considering solubility, a minimisation of the *peri*-hydrogens should reduce steric crowding within the binding pocket and, as demonstrated with D-glucose and D-galactose, increase the relative stability of complexes formed with diboronic acid sensors.

6.3

Other Approaches

Following publication of the modular construct used by our research group in the design of boronic acid based fluorescent PET sensors in 2001 [90], two research groups have published further data on libraries of sensors assembled in a modular fashion.

6.3.1

Wang and Coworkers

Recently Wang and coworkers have documented a range of diboronic acid sensors (a–z in Fig. 20) [114–116]. It can be seen by examining the generic template used that the sensors are designed around the known core of sensor **6**, the first diboronic acid sensor to display selectivity for D-glucose.

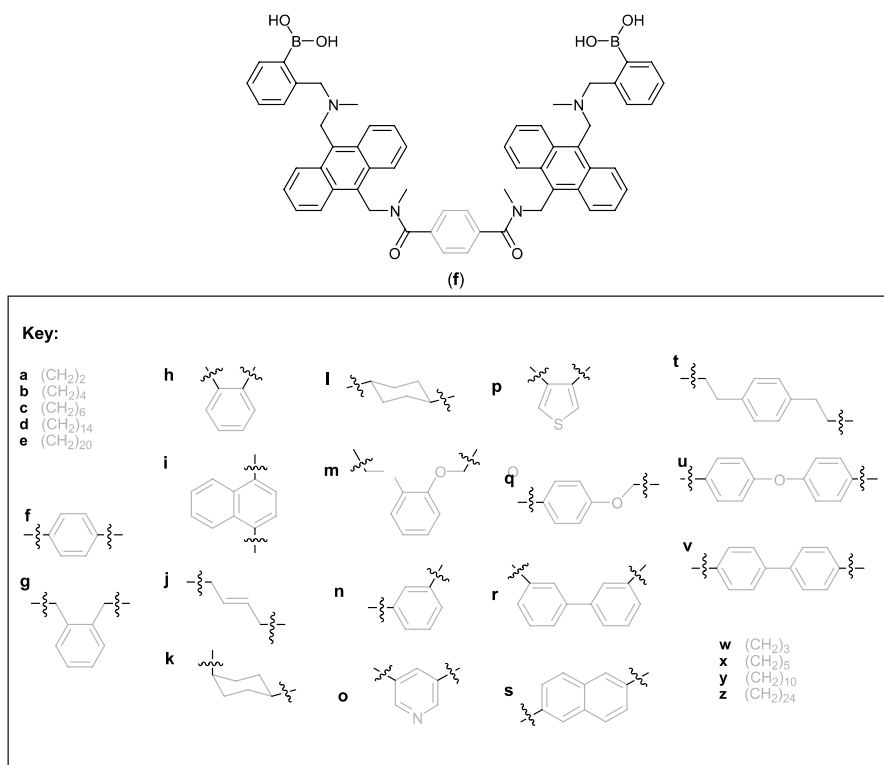


Fig. 20 Range of diboronic acid sensors (a–z) with the interchangeable linker fragments highlighted in light-grey. Sensor **f** displayed selectivity for sialyl Lewis X and **g** displayed selectivity for D-glucose

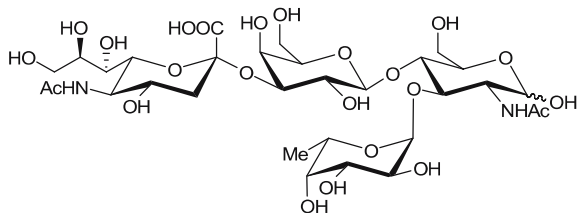
In this construct the number of carbon atoms from one *N*-methyl-*o*-(aminomethyl)phenylboronic acid nitrogen atom to the other is increased substantially. Six carbon atoms separate each of the adjacent amine–amide nitrogen atoms with anthracene cores rigidifying this section of the molecule and introducing possible interactions through either π – π stacking or steric encumbrance. The variable linkers examined augment the length of these rigid linkers further still. Sensor f (Fig. 20) with the *para*-benzene linker was found to be selective for sialyl Lewis X [114, 116]. Sensor g with the *ortho*-xylene linker was found to be selective for D-glucose [115]. In replacing the *ortho*-xylene linker of sensor g with the flexible butyl linker of sensor b the number of carbon atoms in the linker remained the same but the structural rigidity of the linker was lost. This led to a halving of the observed stability constant (K_{obs}). In reintroducing the rigidity but changing the geometry and spacing of the core unit to the *ortho*-benzene linker (sensor h) K_{obs} was seen to decrease further still.

The K_{obs} for the selected sensors in Fig. 20 were: sensor g, 34 M^{-1} with D-fructose, 1470 M^{-1} with D-glucose and 30 M^{-1} with D-galactose; sensor b, 80 M^{-1} with D-fructose, 640 M^{-1} with D-glucose and 110 M^{-1} with D-galactose; sensor h, 280 M^{-1} with D-fructose, 180 M^{-1} with D-glucose and 30 M^{-1} with D-galactose in a solution of 1 : 1 (v/v) methanol/0.1 M aqueous phosphate buffer solution at pH 7.4. The K_{obs} for sensor sensor f with sialyl Lewis X was not reported.

6.3.2

Hall and Coworkers

In an article published in 2004, Hall and coworkers documented the first parallel, solid phase synthesis of modular boronic acid based sensors [117]. The series was developed from a range of common components allowing the rapid assembly of a library of compounds, with the use of semi-preparative high performance liquid chromatography (HPLC) to ensure sensors of satisfactory purity. This approach allowed the structures of the inter-amine linkers to be altered (selectivity was once again found for D-glucose with a linker



sialyl Lewis X

six carbon atoms in length). However, the investigation went on to assess the potential role of a third boronic acid receptor moiety in the recognition of disaccharides (Fig. 21) and the effect of introducing unencumbering electron-withdrawing and electron-donating groups *para* to the arylboronic acid (Fig. 22).

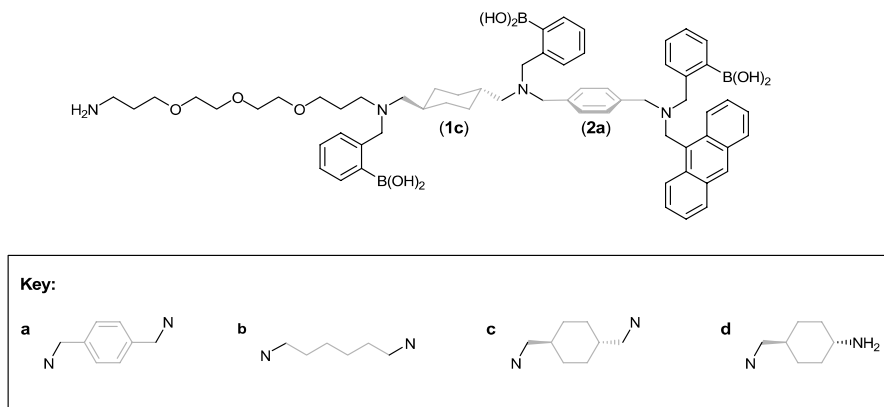


Fig. 21 Triboronic acid sensors assembled via combinatorial synthesis to evaluate the potential of increased allosteric binding effects through three-point binding (the interchangeable linker units are highlighted in *light-grey*)

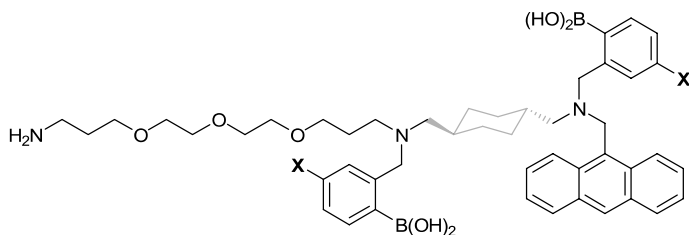


Fig. 22 Diboronic acid modular systems with an interchangeable linker section (highlighted in *light-grey*) and interchangeable electron-withdrawing and electron-donating groups *para* to the arylboronic acid (highlighted in *bold*)

The triboronic acid sensors were titrated against four disaccharides: lactulose, melibiose, turanose and trehalose. Across the range of sensors and guests examined no benefit was found from three (versus two) boronic acid receptor units. For example, the K_{obs} of triboronic acid (1c and 2a in Fig. 21) with lactulose was 200 M^{-1} , this value can be contrasted with the value obtained for the analogous diboronic acid (2a derivative) that displayed a K_{obs} of 220 M^{-1} with lactulose in $10 \times 10^{-3} \text{ mol dm}^{-3}$ phosphate buffer at pH 7.8 in a 1 : 1 water/methanol mixture.

Table 7 Observed stability constants (K_{obs}) for the general structure illustrated in Fig. 22 with lactulose

X	Linker ^a	σ_{p}	$K_{\text{obs}}^{\text{b}}$ ($\text{dm}^3 \text{mol}^{-1}$)
OMe	c	- 0.12	150
F	c	0.15	585
CN	c	0.70	1020
CN	b	0.70	1870

^a Structures are shown in Fig. 22

^b Determined in $10 \times 10^{-3} \text{ mol dm}^{-3}$ phosphate buffer at pH 7.8 in a 1 : 1 water/methanol mixture

Building on these observations, Hall and coworkers examined the dependence of complexation on the electronic characteristics of the arylboronic acid receptors. By altering the Lewis acidity at boron it was believed that two main features in the molecular recognition event could be altered: the strength of the binding interaction with the saccharides and the strength of the N – B interaction controlling the fluorescence intensity. This hypothesis was tested by introducing electron-withdrawing and electron-donating groups at the *para* position of the arylboronic acid ring.

Five substituent groups were considered in all: methoxy, fluoro, methoxycarbonyl, cyano and nitro, with *para*-substituent parameters σ_{p} of - 0.12, 0.15, 0.44, 0.70 and 0.81, respectively [118]. If Fig. 22 is considered and lactulose is used as the model disaccharide, the binding measurements display a qualitative trend that electron-poor phenylboronic acids are preferable for binding (Table 7). This observation was rationalised on the basis that on increasing the Lewis acidity at boron the N – B interaction becomes stronger developing more of a tetrahedral character at boron. This in turn reduces the ring strain in the developing boronic ester. In addition to this, acidifying boron and reducing its $\text{p}K_{\text{a}}$ also provides the substantial benefit of allowing the sensor to function at lower pH.

In enhancing K_{obs} the use of methoxycarbonyl, cyano and nitro groups appeared to be particularly effective. Overall, the largest K_{obs} reported with lactulose was with the diboronic acid with a hexamethylene linker and a *para*-cyano electron withdrawing group (illustrated in Fig. 22) [117].

7

Conclusions

The development of coherent strategies for the selective binding of saccharides, by rationally designed synthetic receptors, remains one of chemistry's most sought after goals. The research conducted to this end is driven by

a fundamental inquisitiveness and need to monitor saccharides of industrial, environmental and biological significance.

Since the first publication on glucose-selective diboronic acid based PET sensors a decade ago, these systems have proved their worth and have come to find application at the cutting edge of medical care.

On complexation of a saccharide to a boronic acid there is a contraction of the O–B–O bond angle with a concomitant increase in the acidity of the boron species. Boronic acid–diol complex formation is heavily pH-dependent. Rate and stability constants increase by around four and five orders of magnitude, respectively, at a pH above the pK_a of the boronic acid.

The introduction of a carefully located tertiary amine proximal to the boron centre of a fluorescent sensor permits the sensor to function at lower pH and introduces an off–on optical response to the system via photoinduced electron transfer (PET). The tertiary amine–boronic acid (N–B) interaction in a boronic acid based PET sensor has a strength in the range 15–25 kJ mol⁻¹. In an aprotic solvent, the N–B dative bond is usually present. However, in a protic media, solvent insertion of the N–B occurs to afford a hydrogen-bonded zwitterionic species.

The use of two boronic acid receptors within a binding site introduces saccharide selectivity, permitting saccharides such as D-glucose to be specifically targeted. Computational data and observed experimental results indicate that strong binding between boronic acids and saccharides occurs preferentially with saccharides that have an available anomeric hydroxyl pair, which has the capacity to conform to a syn-periplanar alignment. In the vast majority of cases this requires formation of the furanose form of the saccharide.

These observations clearly show that the many challenges of saccharide recognition can be conquered by using boronic acids.

References

1. Desiraju GR (2001) *Nature* 412:397
2. Malmström BG (1997) Nobel lectures in chemistry (1991–1995). World Scientific, Singapore
3. de Silva AP, Gunaratne HQN, Gunnlaugsson T, Huxley AJM, McCoy CP, Rademacher JT, Rice TE (1997) *Chem Rev* 97:1515
4. Czarnik AW (1993) *Fluorescent chemosensors for ion and molecule recognition*. American Chemical Society Books, Washington DC
5. Jelinek R, Kolusheva S (2004) *Chem Rev* 104:5987
6. James TD, Linnane P, Shinkai S (1996) *Chem Commun*, p 281
7. James TD, Sandanayake KRAS, Shinkai S (1996) *Angew Chem, Int Ed Engl* 35:1911
8. Phillips MD, James TD (2004) *J Fluoresc* 14:549
9. James TD, Shinkai S (2002) *Top Curr Chem* 218:159
10. Davis AP, James TD (2005) In: Schrader T, Hamilton AD (eds) *Functional synthetic receptors*. Wiley, Weinheim, p 45

11. James TD (2005) In: Hall DG (ed) Boronic acids in organic synthesis and chemical biology. Wiley, Weinheim, p 441
12. Striegler S (2003) *Curr Org Chem* 7:81
13. Wang W, Gao X, Wang B (2002) *Curr Org Chem* 6:1285
14. Cao H, Heagy MD (2004) *J Fluoresc* 14:569
15. Fang H, Kaur G, Wang B (2004) *J Fluoresc* 14:481
16. Granda-Valdes M, Badia R, Pina-Luis G, Diaz-Garcia ME (2000) *Quim Anal* 19:38
17. Moschou EA, Sharma BV, Deo SK, Daunert S (2004) *J Fluoresc* 14:535
18. Shinkai S, Takeuchi M (2004) *Biosens Bioelectron* 20:1250
19. Shinkai S, Takeuchi M (2005) *Bull Chem Soc Jpn* 78:40
20. Davis AP, Wareham RS (1999) *Angew Chem Int Ed* 38:2978
21. Klein E, Crump MP, Davis AP (2004) *Angew Chem Int Ed* 44:298
22. Böeseken J (1949) *Adv Carbohydr Chem* 4:189
23. Böeseken J (1913) *Chemische Berichte* 46:2612
24. Kuivila HG, Keough AH, Soboczenski EJ (1954) *J Org Chem* 19:780
25. Wolf from MI, Solms J (1956) *J Org Chem* 21:815
26. Lappert MF (1956) *Chem Rev* 56:959
27. Torssel K (1957) *Ark Kemi* 10:473
28. Lorand JP, Edwards JO (1959) *J Org Chem* 24:769
29. Hartley JH, Phillips MD, James TD (2002) *New J Chem* 26:1228
30. Soundararajan S, Badawi M, Kohlrust CM, Hageman JH (1989) *Anal Biochem* 178:125
31. Springsteen G, Wang B (2002) *Tetrahedron* 58:5291
32. Yuchi A, Tatebe A, Kani S, James TD (2001) *Bull Chem Soc Jpn* 74:509
33. Juillard J, Gueguen N (1967) *Comp Rend Acad Sci C* 264:259
34. Friedman S, Pace B, Pizer R (1974) *J Am Chem Soc* 96:5381
35. Edwards JO, Sederstrom RJ (1961) *J Phys Chem* 65:862
36. Bosch LI, Fyles TM, James TD (2004) *Tetrahedron* 60:11175
37. Martell AE, Smith RM (1976) *Critical stability constants*. Plenum, New York
38. DiCesare N, Lakowicz JR (2001) *Anal Biochem* 294:154
39. Friedman S, Pizer R (1975) *J Am Chem Soc* 97:6059
40. Pizer R, Selzer R (1983) *Inorg Chem* 23:3023
41. Kustin K, Pizer R (1969) *J Am Chem Soc* 91:317
42. Babcock L, Pizer R (1980) *Inorg Chem* 19:56
43. Pizer R, Tihal C (1992) *Inorg Chem* 31:3243
44. Ferrier RJ (1978) *Adv Carbohydr Chem Biochem* 35:31
45. Shinkai S, Tsukagoshi K, Ishikawa Y, Kunitake T (1991) *J Chem Soc, Chem Commun*, p 1039
46. Finch A, Gardner PJ, McNamara PM, Wellum GR (1970) *J Chem Soc A*, p 3339
47. Tsukagoshi K, Shinkai S (1991) *J Org Chem*, p 4089
48. Kondo K, Shiomi Y, Saisho M, Harada T, Shinkai S (1992) *Tetrahedron*, p 8239
49. Bissell RA, Desilva AP, Gunaratne HQN, Lynch PLM, Maguire GEM, Sandanayake KRAS (1992) *Chem Soc Rev* 21:187
50. Böhmer M, Enderlein J (2003) *Chem Phys Chem* 4:793
51. Moerner WE, Fromm DP (2003) *Rev Sci Instrum* 74:3597
52. Ambrose WP, Goodwin PM, Jett JH, Van Orden A, Werner JH, Keller RA (1999) *Chem Rev* 99:2929
53. Sauer M (2003) *Angew Chem Int Ed* 42:1790
54. Epstein JR, Walt DR (2003) *Chem Soc Rev* 32:203
55. Fehr M, Lalonde S, Ehrhardt DW, Frommer WB (2004) *J Fluoresc* 14:603

56. de Silva AP, Gunaratne HQN, Gunnlaugsson T, Nieuwenhuizen M (1996) *Chem Commun*, p 1967
57. He HR, Mortellaro MA, Leiner MJP, Young ST, Fraatz RJ, Tusa JK (2003) *Anal Chem* 75:549
58. Tudos AJ, Besselink GAJ, Schasfoort RBM (2001) *Lab Chip* 1:83
59. Schlebusch H, Paffenholz I, Zerback R, Leinberger R (2001) *Clin Chim Acta* 307:107
60. Badugu R, Lakowicz JR, Geddes CD (2004) *Bioorg Med Chem* 13:113
61. Yoon J, Czarnik AW (1992) *J Am Chem Soc* 114:5874
62. James TD, Sandanayake KRAS, Shinkai S (1994) *Angew Chem, Int Ed Engl* 33:2207
63. James TD, Sandanayake KRAS, Shinkai S (1995) *Nature* 374:345
64. Wulff G (1982) *Pure Appl Chem* 54:2093
65. James TD, Sandanayake K, Shinkai S (1994) *J Chem Soc, Chem Commun*, p 477
66. James TD, Sandanayake KRAS, Iguchi R, Shinkai S (1995) *J Am Chem Soc* 117:8982
67. Höpfl H (1999) *J Organomet Chem* 581:129
68. Wiskur SL, Lavigne JJ, Ait-Haddou H, Lynch V, Hung Chiu Y, Canary JW, Anslyn EV (2001) *Org Lett* 3:1311
69. Franzen S, Ni W, Wang B (2003) *J Phys Chem B* 107:12942
70. Ni WJ, Kaur G, Springsteen G, Wang BH, Franzen S (2004) *Bioorg Chem* 32:571
71. Zhao J, Davidson MG, Mahon MF, Kociok-Köhn G, James TD (2004) *J Am Chem Soc* 126:16179
72. Bhat KL, Braz V, Laverty E, Bock CW (2004) *THEOCHEM J Mol Struct* 712:9
73. Bhat KL, Howard NJ, Rostami H, Lai JH, Bock CW (2005) *THEOCHEM J Mol Struct* 723:147
74. Morrison JD, Letsinger RL (1964) *J Org Chem* 29:3405
75. Zhu L, Shabbir SH, Gray M, Lynch VM, Sorey S, Anslyn EV (2006) *J Am Chem Soc* 128:1222
76. Bielecki M, Eggert H, Norrild JC (1999) *J Chem Soc, Perkin Trans 2*, p 449
77. Norrild JC, Eggert H (1995) *J Am Chem Soc* 117:1479
78. Nicholls MP, Paul PKC (2004) *Org Biomol Chem* 2:1434
79. Angyal SJ (1991) *Adv Carbohydr Chem Biochem* 49:19
80. Angyal SJ (1984) *Adv Carbohydr Chem Biochem* 42:15
81. Norrild JC, Eggert H (1996) *J Chem Soc, Perkin Trans 2*, p 2583
82. Eggert H, Frederiksen J, Morin C, Norrild JC (1999) *J Org Chem* 64:3846
83. Cooper CR, James TD (1998) *Chem Lett*, p 883
84. Nagai Y, Kobayashi K, Toi H, Aoyama Y (1993) *Bull Chem Soc Jpn* 66:2965
85. Yang W, He H, Drueckhammer DG (2001) *Angew Chem Int Ed* 40:1714
86. Sandanayake KRAS, James TD, Shinkai S (1995) *Chem Lett*, p 503
87. Appleton B, Gibson TD (2000) *Sens Actuators B* 65:302
88. Cooper CR, James TD (2000) *J Chem Soc, Perkin Trans 1*, p 963
89. Phillips MD (2000) *Fluorescent phosphate sensors*. M NatSc (Chem) Dissertation, The University of Birmingham, UK
90. Arimori S, Bell ML, Oh CS, Frimat KA, James TD (2001) *Chem Commun*, p 1836
91. Arimori S, Bell ML, Oh CS, Frimat KA, James TD (2002) *J Chem Soc, Perkin Trans 1*, p 803
92. Perrin DD, Dempsey B (1974) *Buffers for pH and metal ion control*. Chapman Hall, London
93. Lakowicz JR (1999) *Principles of fluorescence spectroscopy*. Plenum, New York
94. Arimori S, Bell ML, Oh CS, James TD (2002) *Org Lett* 4:4249
95. Jin T (1999) *Chem Commun*, p 2491
96. Arimori S, Consiglio GA, Phillips MD, James TD (2003) *Tetrahedron Lett* 44:4789

97. Barboiu M, Supuran CT, Scozzafava A, Briganti F, Luca C, Popescu G, Cot L, Hovnarian N (1997) *Liebigs Ann Chem*, p 1853
98. Galema SA, Blandamer MJ, Engberts J (1990) *J Am Chem Soc* 112:9665
99. Fabri D, Williams MAK, Halstead TK (2005) *Carbohydr Res* 340:889
100. Galema SA, Blandamer MJ, Engberts J (1992) *J Org Chem* 57:1995
101. Janado M, Yano Y (1985) *Bull Chem Soc Jpn* 58:1913
102. Yano Y, Tanaka K, Doi Y, Janado M (1988) *Bull Chem Soc Jpn* 61:2963
103. Fischer E (1894) *Ber Dtsch Chem Ges* 27:2985
104. Lemieux RU, Spohr U (1994) *Adv Carbohydr Chem Biochem* 50:1
105. Warner DT (1962) *Nature* 196:1055
106. Walkinshaw MD (1987) *J Chem Soc, Perkin Trans 2*, p 1903
107. Lemieux RU (1996) *Acc Chem Res* 29:373
108. Westmark PR, Smith BD (1994) *J Am Chem Soc* 116:9343
109. Draffin SP, Duggan PJ, Duggan SAM (2001) *Org Lett* 3:917
110. Gardiner SJ, Smith BD, Duggan PJ, Karpa MJ, Griffin GJ (1999) *Tetrahedron* 55:2857
111. Westmark PR, Gardiner SJ, Smith BD (1996) *J Am Chem Soc* 118:11093
112. Riggs JA, Litchfield RK, Smith BD (1996) *J Org Chem* 61:1148
113. Morin GT, Hughes MP, Paugam ME, Smith BD (1994) *J Am Chem Soc* 116:8895
114. Yang W, Gao S, Gao X, Karnati VVR, Ni W, Wang B, Hooks WB, Carson J, Weston B (2002) *Bioorg Med Chem Lett* 12:2175
115. Karnati VV, Gao X, Gao S, Yang W, Ni W, Sankar S, Wang B (2002) *Bioorg Med Chem Lett* 12:3373
116. Yang W, Fan H, Gao X, Gao S, Karnati VVR, Ni W, Hooks WB, Carson J, Weston B, Wang B (2004) *Chem Biol* 11:439
117. Stones D, Manku S, Lu XS, Hall DG (2004) *Chem Eur J* 10:92
118. Carey FA, Sundberg RJ (2000) *Advanced organic chemistry*. Kluwer Academic/Plenum, New York

Part II
Creative Detection Techniques

Biomolecular Sensing with Colorimetric Vesicles

Raz Jelinek (✉) · Sofiya Kolusheva

Department of Chemistry and Ilse Katz Center for Nanotechnology,
Ben Gurion University, Beer Sheva, Israel
razj@bgu.ac.il

1	Introduction	156
2	Vesicle-Based Chromatic Sensors	157
3	Colorimetric Polydiacetylene-Based Sensors	158
3.1	Polydiacetylene Vesicles	158
3.2	Lipid/PDA Vesicles	161
3.2.1	Colorimetric Detection of Enzymatic Catalysis	163
3.2.2	Colorimetric Detection of Peptide–Membrane Interactions	164
3.2.3	Colorimetric Vesicles for Pharmaceutical Screening	165
3.2.4	Bacterial Sensing with Lipid/PDA Vesicles	167
3.3	Lipid/PDA Vesicles Incorporating Recognition Elements	168
3.3.1	Ion Discrimination by Ionophore/Lipid/PDA Vesicles	170
3.3.2	Antibody Detection by Epitope/Lipid/PDA Vesicles	171
3.3.3	Artificial Receptors Embedded in Lipid/PDA Vesicles	172
4	Conclusions	175
	References	176

Abstract This chapter summarizes recent studies employing colorimetric vesicle-based systems for biomolecular sensing. Vesicular aggregates exhibit an important advantage as a biological sensing platform in that they mimic the cell membrane—the site of molecular docking, ligand–receptor binding, and other important processes that can be exploited as a means of signal generation. Particularly attractive for sensing applications is the use of colour changes visible to the naked eye or detected spectroscopically as the signal transduction mechanism.

Vesicle assemblies comprising polydiacetylene (PDA)—a chromatic polymer that undergoes blue–red transformations in response to varied biological analytes and processes—are the primary focus of this chapter. We discuss the features of PDA that make it a promising constituent in biosensing platforms, in particular its self-assembly properties, the rigid framework allowing incorporation of varied lipid constituents, and the chromatic transformations induced by reactions with biological analytes.

Recent studies depicting distinct vesicle assemblies are summarized. Vesicles comprising chemically modified PDA, in which receptor units are attached to the polymer-surface head groups, have been employed for detection of chemical and biological toxins, viruses, and bacteria. Mixed vesicles in which lipid bilayer domains are incorporated within the PDA matrix have also been extensively used as colorimetric biomimetic membrane platforms for studying diverse membrane processes and cell-surface phenomena. The PDA-embedded lipid bilayers further facilitate anchoring of varied molecular markers and recognition modules.

Keywords Biomimetic sensors · Chromatic polymers · Colour biosensors · Polydiacetylene · Vesicle biosensors

Abbreviations

CR Colorimetric response
DMPC Dimyristoylphosphatidylcholine
ELISA Enzyme-linked immunosorbent assay
PDA Polydiacetylene

1

Introduction

Development of chemical approaches for the detection and screening of biological molecules is an important and highly active field of research because of the scientific and practical significance of biosensors. Numerous bioanalytical technologies have been developed for the identification and study of biological compounds [1–5]. The utilization of *colour* as the transduction mechanism in biosensor technologies is particularly attractive. Besides the obvious advantage of identification of colour changes with the naked eye, colorimetric transitions can also be easily recorded using conventional apparatuses such as spectrophotometers or ELISA plate readers. An additional feature of colour detection is the possibility of coupling the colorimetric sensor with existing optical technologies, such as optical fibres, optical signal processing, and others. Examples of colour-based sensor technologies include monosaccharide detection by boronic acid derivatives [6], colour sensors based on active interference filters constructed from silicon-compatible materials [7], vapo-chromic detection of organic compounds using optical fibres [8], optical thin-film waveguide ion sensors [9], flow-through cell detectors based on colour-changing organic compounds [10], colorimetric toxin detection [11], and other molecular dye applications [12–15].

This chapter focuses on *vesicle-based* colorimetric sensor systems. We limit discussion here to a somewhat narrow definition of vesicles: aggregates that self-assemble in aqueous solutions and contain organized amphiphathic molecules, generally lipids but also polymers. This definition precludes broad areas of sensing applications using other types of molecular aggregates, such as nanoparticles and quantum dots [16], which are beyond the scope of this chapter. However, we do refer to systems in which organized lipid and/or polymeric structures were combined with other chemical entities for creation of sensor assemblies.

Vesicular particles have been employed in diverse applications in biological research, mostly due to their relative ease of preparation and variability in composition. In addition, vesicles are often perceived as closely mimicking the cell membrane, thus functioning as convenient biomimetic platforms.

These properties have promoted the use of vesicles in biosensor assemblies. In this chapter we summarize recent developments in chromatic vesicle-based biosensor applications. We particularly emphasize the contribution of *chromatic polydiacetylene-based vesicles* as a vehicle for the detection and analysis of biological analytes.

2

Vesicle-Based Chromatic Sensors

Vesicular particles can be useful sensing platforms due to their defined molecular organizations, ease of preparation, and overall robustness and stability. Nevertheless, actual biosensor devices and applications employing vesicles are rare, mostly due to the necessity for maintaining vesicles in aqueous solutions (rather than in solid morphologies), their insufficient homogeneity, lack of complete control of their composition and organization, and inadequate means for incorporation of signal-generating modules in vesicles. In addition, introducing *specificity* into vesicle-based sensors, for example through incorporation of biological recognition elements, is challenging; one has to accomplish efficient insertion of the desired receptor molecule into the vesicle bilayer without adversely impacting the biological properties and molecular recognition capabilities of the receptor, while in addition retaining vesicle stability.

Several studies have presented innovative applications of vesicles in sensors and biological assays. Fluorescence-doped vesicles have often been used in neurobiology assays [17], or for studying the pH effect of excitory proteins [18]. Oxygen sensors based on phospholipid vesicles doped with fluorescent markers have been reported [19]. Vesicles have been used as components in immunosensors [20–22] and for other biochemical applications [23–25]. Other applications of vesicle-based sensors include taste sensors [26], molecular recognition [27], and transport through thermo-responsive substances [28].

The use of *colorimetric* vesicles in sensor platforms has been particularly challenging because of the additional requirement for the inclusion of optical reporter molecules within the vesicular aggregates. The optical probe merocyanine 540 was incorporated within unilamellar vesicles, and changes in its absorption spectra were used to monitor bilayer interactions of surfactant molecules [29]. An immunoassay based on liposome migration, optically detected by employing vesicles encapsulating a coloured dye, was also described [30, 31]. That work underlined one of the drawbacks of colour-based biosensing techniques—the limited capability of the human eye to differentiate between mixed colours and shades. This limitation is generally remedied by the use of spectroscopy or even digital scanning, facilitating better discrimination of real signals.

3 Colorimetric Polydiacetylene-Based Sensors

3.1 Polydiacetylene Vesicles

Conjugated polydiacetylene (PDA) is a remarkable polymeric system which exhibits unique chromatic properties. PDA is formed through 1,4 addition of aligned diacetylenic monomers, initiated by ultraviolet (UV) irradiation [32] (Fig. 1). The resulting polymer is intensely blue to the eye, due to electronic

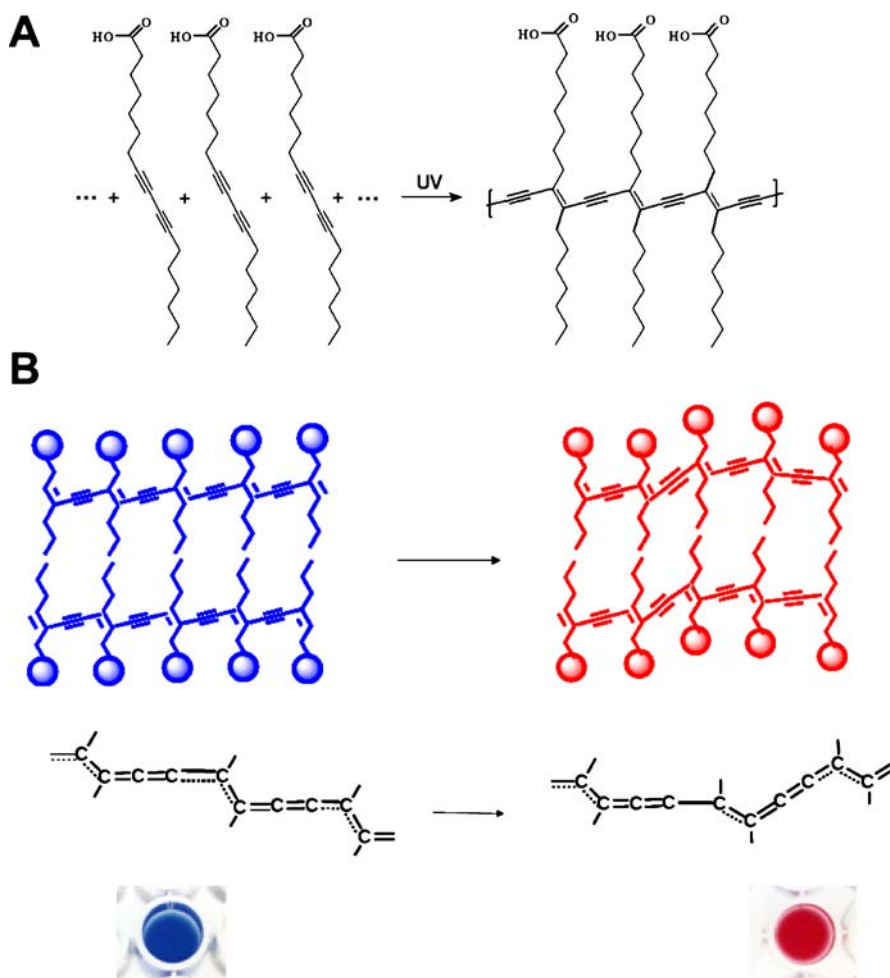


Fig. 1 Structural features of polydiacetylene. **a** Creation of the polymerized backbone from the diynoic acid monomers; **b** induction of the blue–red colour transitions

delocalization within the conjugated framework, giving rise to absorption at around 650 nm in the visible region of the electromagnetic spectrum. Importantly, PDA can undergo rapid blue–red colorimetric transitions due to a variety of external perturbations, such as temperature changes [33–36], pH, and surface pressure [37]. The molecular mechanism corresponding to the colour change is believed to be an irreversible stress-induced structural transition of the conjugated backbone of the polymer [38, 39]. This externally induced conformational transformation of the PDA backbone essentially shortens the effective conjugation network, giving rise to an appearance of the polymer as a *red* substance. The structural transition of the backbone is believed to be primarily affected by surface perturbations to the pendant side chains of the PDA assemblies [36, 39]. The colorimetric transformations of supramolecular PDA assemblies are *irreversible*; however, there have been reports describing the introduction of colour-change reversibility via chemical modification of the polymer head groups, thus altering the molecular packing and topochemical transformations within the polymer modules [40, 41].

The lipidomimetic structural features of PDA, i.e. hydrophobic tail (terminated by a methyl group) and hydrophilic head group (carboxylate), result in the formation of biomimetic membrane assemblies, such as monolayers at the air/water interface and vesicular aggregates in aqueous solutions. These organizations have facilitated utilization of the unique optical properties of PDA for varied biological sensing applications. In a sense, PDA assemblies could combine the role of both the cytoskeleton, through stabilization of various natural proteins and other molecules in the biomimetic polymer layers, as well as mimicking the lipid scaffolding of the cellular membrane [32]. Indeed, the proliferation of biological applications utilizing PDA assemblies is based upon the ability to induce structural modifications, and thus colorimetric transitions, within the polymeric PDA framework through perturbations induced by binding of biological analytes onto the surface of the vesicle bilayer [42, 43]. Such interfacial disruption could occur through biological recognition processes, which correspondingly affect the pendant side chains of PDA, leading to the colorimetric transitions observed [40, 42–48].

Bilayer configurations are not the only self-assembled structures utilized for exploiting the chromatic properties of PDA for biosensing applications. PDA bolaamphiphiles (containing polar head groups at both sides) were shown to form stable vesicles [49]. Interestingly, these vesicles exhibited dramatic colorimetric responses to varied external stimuli, suggesting that both head-group and side-chain organization within PDA systems affect the conjugated framework and contribute to the structural and colorimetric transformations. Intriguing “dendrimer scaffolds” that might facilitate construction of colorimetric PDA vesicle sensors were recently described [50]. In such systems polyamidoamine (PAMAM) dendrimers were employed to display the PDA moieties, putatively amplifying the signals induced by varied stimuli [50]. Similarly, PDA covalently attached to silica nanocomposites exhibited

very high colorimetric sensitivity, stability, and reversibility pointing to potentially superior properties for practical biosensing applications [51].

Many reports have appeared in recent years depicting biosensing applications of PDA vesicles [47, 50, 52–55]. Most such applications involved chemical modification of the PDA head groups [53, 56, 57] for incorporation of functional and biomolecular recognition units at the PDA surface (Fig. 2). A generic example of this concept has been the utilization of diacetylene monomers displaying biotin in vesicle frameworks [58]. The high affinity between soluble streptavidin and the PDA–biotin complex gave rise to the blue–red transition, accompanied by vesicle aggregation due to the multimeric interactions involving streptavidin and four biotin units.

Experiments depicted in the literature have demonstrated diverse avenues for colorimetric detection of proteins, nucleic acids, and whole microorganisms through covalent binding of specific receptor units to the PDA vesicle framework. Detection of influenza virus was achieved through attachment of sialic acid residues to the surface of PDA vesicles [52, 54, 59–61]. Colour sensing of DNA strains through PDA functionalized with oligonucleotides was also illustrated [62, 63]. The design utilized the structural/chromatic transformations of PDA as a vehicle for amplification of the oligonucleotide recognition signal. An original “bacterial fingerprinting” approach has relied on vesicles constructed from different ratios of diacetylene monomers functionalized with indole or phenol units [64]. The different affinities of bacterially expressed lipopolysaccharide (LPS) to the functionalized liposomes facilitated identification of distinct fingerprints for bacterial species through a combination of vesicles having different compositions.

Immobilization of colorimetric PDA vesicles onto or within various solid supports was demonstrated, enhancing the potential of PDA systems as practical biosensing solutions. PDA vesicles have been immobilized on solid

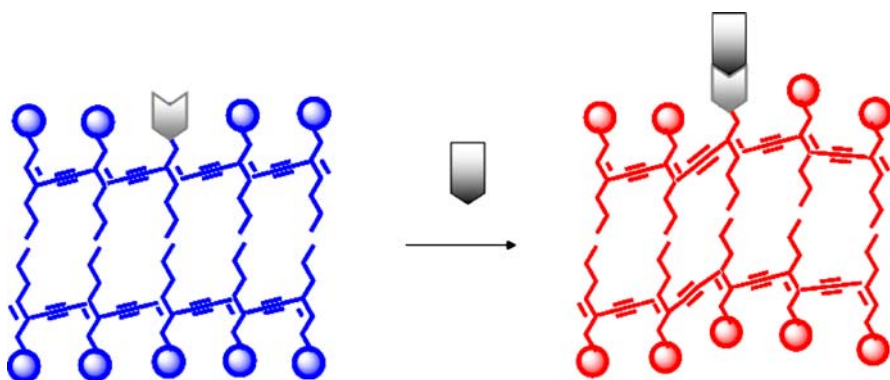


Fig. 2 Colorimetric detection of molecular recognition using modified PDA. Introducing recognition units through chemical modification of the PDA head group

surfaces while still retaining their colorimetric properties [65, 66]. Sol–gel matrixes were also employed as hosts for PDA vesicles displaying surface recognition groups [60]. The enhanced stability of sol–gel materials, their optical transparency, and feasibility of analyte diffusion within the porous substance point to powerful advantages for immobilization of the PDA vesicles and construction of viable biosensors.

3.2

Lipid/PDA Vesicles

An important development enhancing the applicability of the colorimetric PDA technology for biological and pharmaceutical sensing systems has been the construction of *mixed lipid/PDA vesicles*, comprising both the polymer and phospholipids and/or other constituents of the cell membrane. The advantages of such mixed assemblies stem from the observation that the PDA framework can act as “scaffolding” for the stabilization of additional lipophilic dyes and/or recognition elements that can be incorporated into the vesicles (rather than covalently attached to the polymer). In particular, the inclusion of additional molecular components into the vesicles creates a “modular” molecular architecture facilitating diverse biomolecular recognition capabilities, without the need to resort to often cumbersome and technically difficult synthetic manipulation of the PDA framework.

Early examples of lipid/PDA vesicle biosensor systems were the incorporation of gangliosides into the PDA vesicle framework, exploiting the affinity between the ganglioside head group and cholera toxin for viral detection [55, 67–70]. Another example of the implementation of novel sensing schemes using lipid/PDA vesicles is the incorporation of cholesterol moieties as a “bait” for colorimetric sensing of pore-forming toxins produced by bacteria [71]. That scheme has been further expanded, employing fluorescently labelled lipid insertion into the vesicles for bacterial sensing [72].

A particularly important feature of lipid/PDA vesicle systems is the feasibility of incorporating a significant concentration of lipid constituents within the PDA matrix—up to 50% (mole ratio). This architecture is designed to better mimic the cell surface and is radically different from PDA systems containing smaller quantities of lipid “dopants”, both in structure as well as functionality. Essentially, such mixed vesicles comprise distinct lipid domains embedded within the polymer framework that still retains its structural and chromatic properties [43, 44, 48, 73]. Figure 3 depicts a schematic description of lipid/PDA vesicles. Previous studies indicated that the lipids and PDA most likely form interspersed microscopic phases within the vesicles [48]. The phospholipids incorporated within the PDA matrix adopt a bilayer structure, the dominant lipid organization within cellular membranes. Published data further point to the contribution of changes in fluidity within the lipid domains in inducing the blue–red transitions [43, 48].

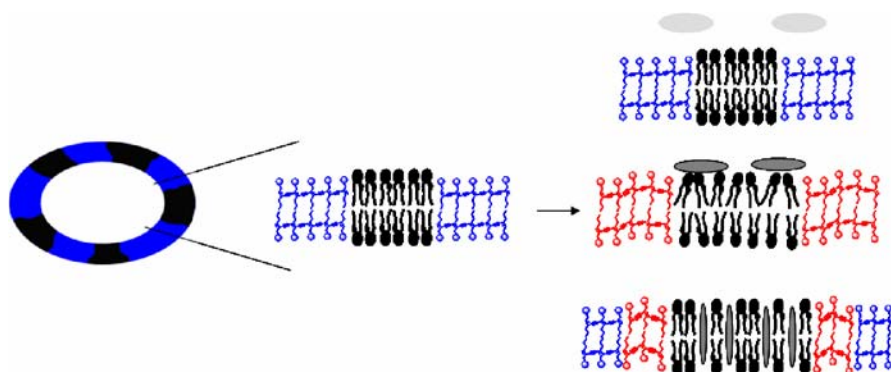


Fig. 3 Colorimetric sensing with lipid/PDA vesicles. Structural/colorimetric transformations of PDA (*blue*) induced by molecules (*grey ovals*) interacting with the lipid bilayer domains (*black*)

The observation that the lipid components in the mixed vesicles form distinct bilayer domains is significant in the context of biosensing applications; such vesicles could then closely mimic the membrane surface of a cell. Enhancing the utilization of lipid/PDA vesicles for biological applications has been the capability of incorporating within the vesicles varied synthetic and natural phospholipids, glycolipids, lipopolysaccharides, cholesterol, or total membrane extracts, essentially mimicking the lipid compositions of different membranes and cellular systems [74].

Utilization of lipid/PDA vesicles for biosensing applications has been based upon the observation that numerous biological analytes primarily interacting with the *lipid* domains can still give rise to the blue–red transformations of the polymer. This phenomenon means that PDA in the mixed vesicles essentially constitutes a reporter module for lipophilic or membrane-active molecules. In that regard, the generic affinity of varied biological molecules, drug compounds, viruses, and microorganisms to lipid assemblies could make lipid/PDA vesicles a powerful biosensing platform. In the subsections below we summarize several biosensor applications of the system.

The mechanisms accounting for the induction of colorimetric transformations in lipid/PDA vesicle systems by lipid-bound biomolecules have not been fully elucidated; however, several studies have shed light on the factors contributing to the blue–red changes [44, 48]. Specifically, previous studies determined that the PDA framework in the mixed lipid/PDA vesicles retains its conjugated backbone structure, accounting for the initial blue colour of the vesicles. The externally induced colorimetric transformations are a consequence of structural and dynamical perturbations within the lipid domains which affect the PDA through the lipid/polymer interfaces [43, 44, 48, 73].

Molecular events occurring and affecting the vesicle *surface* are the principal biological phenomena which trigger the colour transitions. Indeed,

correlation was detected between the extent of lipid bilayer surface perturbation induced by membrane-active compounds and the degree of colorimetric transformations [42]. This interpretation is based on the observation that molecules that preferably interact with and disrupt the lipid head group region were shown to induce more pronounced colour transitions, while deeper penetration into the hydrophobic lipid core generally gave rise to more moderate blue–red transformations [42].

The colorimetric transitions of the lipid/PDA vesicles can also be *quantified*, making the system a useful bioanalytical tool. Enumeration of the blue–red transformations is carried out through computing the relative intensities of the “blue” and “red” components, respectively, in the visible spectra of the solutions. The parameter commonly used for quantifying the colour change was denoted %CR, i.e. percentage colorimetric response, defined as [75]:

$$\text{CR} = \frac{\text{PB}_0 - \text{PB}_1}{\text{PB}_0} \cdot 100\% ,$$

where $\text{PB} = \frac{A_{\text{blue}}}{A_{\text{blue}} + A_{\text{red}}}$, and A is the absorbance of either the blue component in the UV–Vis spectrum (peak at 640 nm) or the red component (550 nm). (Note: blue and red refer to the visual appearance of the material, not its actual absorbance.) PB_0 is the red/blue ratio of the control blue sample, while PB_1 is the value obtained after colour change occurred. In principle, a higher CR value indicates a greater reddish appearance of the solution, compared to the blue control sample (the initial blue solution yields, by definition, a zero %CR).

3.2.1

Colorimetric Detection of Enzymatic Catalysis

An important property of lipid/PDA vesicles is the feasibility of incorporation of varied lipid species. This versatility facilitates the application of the colorimetric assay for detection and analysis of lipophilic enzyme hydrolysis [44, 76] (Fig. 4). Figure 4a schematically depicts a colorimetric enzyme screening experiment. Vesicles containing different lipid molecules were exposed to lipophilic enzymes; a colorimetric reaction occurred only when the enzyme recognized its lipid substrate embedded within the vesicles. The colorimetric response has been ascribed to binding and cleavage of the lipid substrate by the enzyme that overall induce structural perturbation of the polymer and the corresponding colorimetric transformation.

Representative data presented in Fig. 4b clearly demonstrate that the colour transitions induced by particular enzymes are directly related to the lipid composition of the vesicles. For example, the enzyme phospholipase A2 gave rise to a strong blue–red transition when the PDA matrix contained phosphatidylcholine, but this enzyme did not induce colorimetric transitions

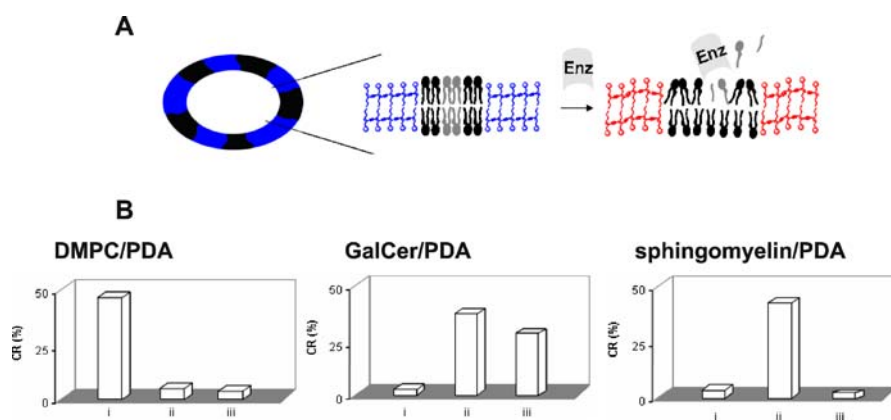


Fig. 4 Colorimetric detection of lipophilic enzyme catalysis. **a** Schematic description of the experiment in which the blue–red colour transitions are induced by enzymatic hydrolysis of vesicle-embedded lipid molecules. **b** Colorimetric response induced by different enzymes following mixing with lipid/PDA vesicles having the indicated compositions: *i*—phospholipase A2; *ii*—sphingomyelinase; *iii*—galactocerebrosidase

when other types of lipids were present within the vesicles (Fig. 4b, bars *i*). Another demonstration of the specificity of the assay was the absence of significant colorimetric transitions induced in pure PDA vesicles (where no lipid molecules were incorporated) [76]. In general, Fig. 4 demonstrates that the lipid/PDA vesicle assay can constitute a useful platform for screening enzymes and molecules with putative enzymatic properties. Importantly, the strategy based on the colorimetric vesicles does not require additional chemical reagents or post-cleavage chemical analysis. The “one-step” approach can be easily applied, for example, for identifying enzyme inhibitors through simply monitoring colour changes of the vesicle suspensions in standard multiwell plates.

3.2.2

Colorimetric Detection of Peptide–Membrane Interactions

Interactions between peptides and lipid membranes play major roles in numerous physiological processes, such as signalling, formation of ion channels, cytolysis, and cellular recognition. Furthermore, membrane permeation plays a crucial role in determining the activity of antimicrobial peptides [73]. Several reports have demonstrated that lipid/PDA vesicles undergo colour changes upon binding of antimicrobial peptides [42, 73, 77–80]. Moreover, studies have shown that important biophysical parameters, such as the degree of penetration of the peptides into lipid bilayers and mechanisms of peptide–lipid binding, affect the extent and dynamics of the colorimetric transitions. Figure 5 depicts an example of colour changes induced by different pep-

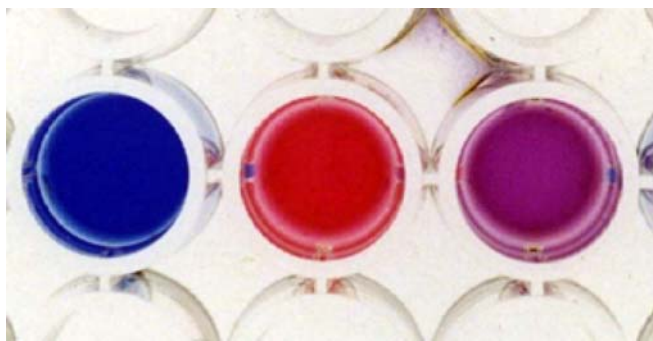


Fig. 5 Colour transitions induced by membrane-associated antimicrobial peptides. *Left*: control vesicle solution; *center*: cryptdin-4 added; *right*: melittin added. Peptide concentrations were 0.1 mM

tides (at identical concentrations) in lipid/PDA vesicle solutions. The distinct colours are indicative of the purported mode of membrane interaction of the peptides: stronger interfacial association of the positively charged beta-sheet structured cryptdin-4 yielded a more pronounced red colour ascribed to surface perturbations induced by the peptide [79, 80], while melittin, a helical antibacterial peptide that inserts into lipid bilayers, is expected to give rise to a more moderate colour change, as is indeed observed in Fig. 5.

Investigations employing the lipid/PDA vesicle assay for screening and analysis of antimicrobial peptides have been reported, including evaluation of the contribution of specific lipid molecules in the bilayer to peptide adsorption and penetration [77, 78, 80, 81], comparative study of the contributions of specific residues within antimicrobial peptide sequences to their membrane interactions [42, 73, 79], and membrane binding of pre-fibrillar assemblies and its significance to amyloid toxicity [82]. The observation of rapid colorimetric transitions induced by antimicrobial peptides opens the way for using lipid/PDA vesicles as a useful bioanalytical tool. The assay could be applied as a vehicle for rapid colorimetric screening of bilayer interactions and membrane binding of antimicrobial compounds, or the absence of such interactions.

3.2.3

Colorimetric Vesicles for Pharmaceutical Screening

A significant part of pharmaceutical research and development efforts entails the evaluation of interactions and penetration of tested substances and formulations through hydrophobic physiological barriers, such as the blood-brain barrier (BBB) [83–85]. In that regard, lipid/PDA vesicles might become a useful platform for evaluation of membrane interactions of pharmaceutical materials [86]. That work demonstrated colorimetric screening of a large

number of common pharmaceutical compounds by lipid/PDA vesicle solutions. The important feature of the vesicle assay apparent in that study was the observation that the tested molecules could be distinguished according to the *extent* of colorimetric response elicited following their addition to DMPC/PDA vesicles (Fig. 6). Specifically, the analysis showed that the concentration ranges in which the blue-red transformations were induced varied significantly among the molecules. Roughly, three groupings could be distinguished: compounds inducing colour changes at *micromolar* ranges, substances affecting transitions at *millimolar* concentrations, and those that did not affect the chromatic vesicles even at much higher concentrations (Fig. 6).

The different colorimetric dose-response curves in Fig. 6 correspond to the types of interactions of the pharmaceutical compounds with the lipid/PDA vesicles. Specifically, molecules that preferably aggregate at the *lipid/water interface* (rather than penetrate or cross through the lipid barrier) give rise to pronounced surface perturbations, thus inducing colour changes even at very low, micromolar concentrations (curve i, Fig. 6). Another grouping encompasses compounds that tend to *insert into the bilayer*. Such interaction would give rise to smaller surface perturbations, leading to higher, millimolar concentrations inducing the blue-red transitions (curve ii, Fig. 6). A third group of compounds distinguished by the colorimetric vesicle assay are molecules that *do not bind or interact with lipid membranes*, thus not inducing noticeable colorimetric transitions (curve iii, Fig. 6).

The phospholipid/PDA vesicle assay exhibits important practical advantages for application as a generic tool for drug screening. The vesicle solutions can be placed and stored for long periods in conventional 96-well (or 384-well) plates. The colorimetric transitions are induced within a very short time (seconds) after mixing the reagents. The colorimetric technique is robust and easy to apply, and data for large compound libraries can be obtained in a few

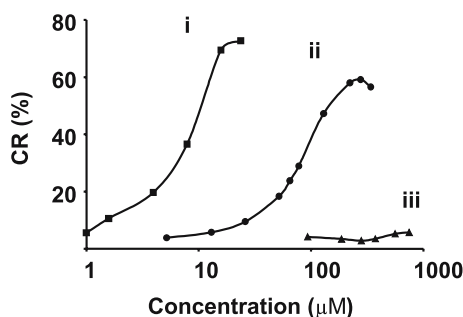


Fig. 6 Colorimetric screening of pharmaceutical compounds. Representative colorimetric dose-response curves induced by pharmaceutical compounds: *i*—imipramine; *ii*—lidocaine; *iii*—theophylline

minutes. The lipid/PDA vesicle assay can thus become a useful tool for predicting membrane interactions and bilayer permeation at early stages of drug development and profiling.

3.2.4

Bacterial Sensing with Lipid/PDA Vesicles

The observation that colour changes could be induced within lipid/PDA vesicles by interactions with amphiphilic and membrane-associated molecules opens the way for other sensing applications. An intriguing recent avenue has been the utilization of lipid/PDA vesicles as a vehicle for bacterial detection [87]. In that new sensing approach, microorganisms are detected through the blue–red change induced in lipid/PDA vesicles by the *amphiphilic and membrane-active molecules* they secrete to their environment [88–90]. Figure 7a depicts the schematic arrangement of the bacterial sensor, in which phospholipid/PDA vesicles were embedded in agar scaffolding containing bacterial-growth medium [87]. The *agar matrix* serves as an amplification vehicle. It facilitates bacterial multiplication, thereby promoting the release of secreted substances by the bacteria. Essentially, molecules released by bacteria that proliferate on the agar surface diffuse through the semi-porous agar substrate and induce chromatic changes in the agar-embedded vesicles, thus reporting on the bacterial presence.

Figure 7b depicts a representative scanned image of a DMPC/PDA/agar plate showing the colour transitions induced by bacteria (*Salmonella typhimurium*). The picture in Fig. 7b clearly shows that red hollows form

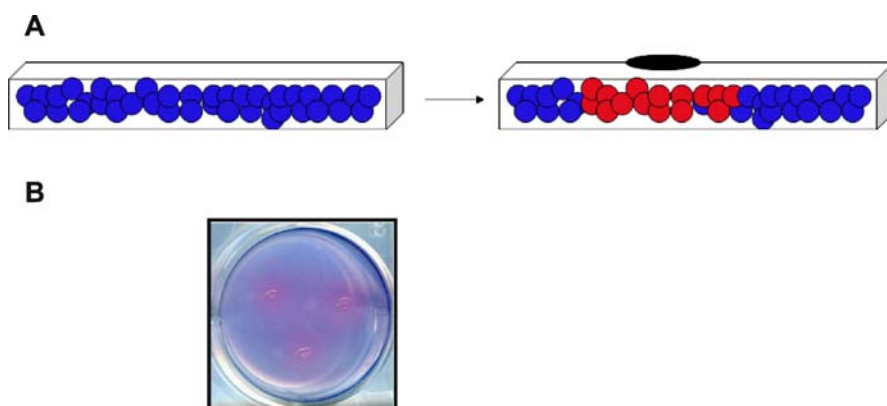


Fig. 7 Bacterial sensing with lipid/PDA vesicles. **a** Schematic description of the lipid/PDA vesicles (*blue circles*) embedded in an agar matrix (*white box*). Bacterial proliferation and colony formation (*black oval*) results in the blue–red transformation of the vesicles. **b** An example of the colour transformations induced by bacterial colonies (*S. typhimurium*) on a DMPC/PDA/agar plate

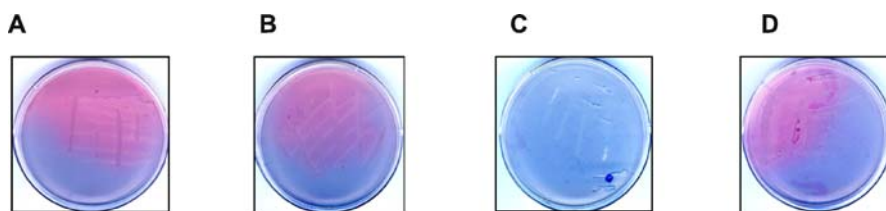


Fig. 8 Colorimetric screening of bacterial resistance. Scanned images of DMPC/PDA/agar plates further containing antibiotic substances onto which different bacterial strains were streaked. **a** *E. coli* K-12 C600 streaked on DMPC/PDA/agar not containing antibiotics; **b** *E. coli* C600 *pMRIInv* streaked on DMPC/PDA/agar not containing antibiotics; **c** *E. coli* K-12 C600 streaked on DMPC/PDA/agar that contained kanamycin; **d** *E. coli* C600 *pMRIInv* streaked on DMPC/PDA/agar containing kanamycin

around the bacterial colonies following incubation (note that the apparent “doublets” in Fig. 7b are due to the reflection of the scanner light). The blue–red transformation of the matrix was directly related to bacterial proliferation; each colony was surrounded by an area in which the blue agar matrix changed colour to red, while the remaining agar matrix stayed blue. The dispersion of red regions under and around the bacterial colonies indicates that the colour transitions were due to diffusion of substances released by the bacteria into the surrounding matrix.

Figure 8 demonstrates an application of the lipid/PDA/agar assay for evaluation of antibiotic resistance of bacterial strains [87]. In the experiment shown in Fig. 8, *Escherichia coli* strains exhibiting different antibiotic resistance were streaked onto plates containing lipid/PDA/agar matrix that further incorporated antibiotic compounds. The striking colour transitions shown in Fig. 8 appeared only in plates in which the genotype of the streaked bacteria exhibited resistance to the antibiotic included within the matrix. For example, a red colour (corresponding to transformed vesicles) appeared in a plate containing kanamycin/DMPC/PDA/agar onto which the kanamycin-resistant *E. coli* C600 *pMRIInv* strain [91, 92] was streaked (Fig. 8d), while no colour change occurred when *E. coli* K-12 C600 strain was streaked—a bacterium that cannot grow on kanamycin-containing substrates [91, 92] (Fig. 8c).

3.3

Lipid/PDA Vesicles Incorporating Recognition Elements

Incorporation of natural and artificial receptors within lipid/PDA assemblies (Fig. 9) has been a particularly important development in the utilization of the chromatic vesicles for colorimetric detection of biological analytes. The design of new systems for rapid detection of interfacial biomolecular interactions has to fulfil two main objectives. First, the chemical construct should

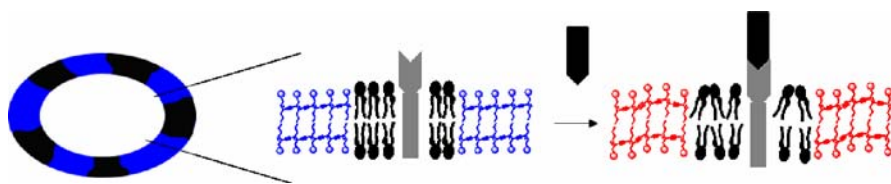


Fig. 9 Colorimetric molecular recognition using lipid/PDA vesicles. Recognition elements (grey) are embedded within the lipid moieties, and the colorimetric transformations are induced following ligand–receptor binding at the vesicle surface

allow physical access and binding between the receptor and the ligand in an aqueous solution. The second requirement is that the ligand–receptor interactions could be reported through easily detected chemical or physical transformations within the system. Lipid/PDA vesicles embedding recognition elements adhere to the above requirements. In such vesicles the phospholipid framework is exploited as an anchoring platform for receptors containing hydrophobic moieties, overall facilitating display of the recognition elements at the vesicle surface.

Colorimetric detection of ligand–receptor interactions through *physical incorporation* of receptors within lipid/PDA vesicles presents important advantages over *chemical attachment* of recognition units to the PDA itself, discussed above. First, chemical derivatization of PDA can be technically demanding, and the organic synthesis procedures limit the scope of this approach. Furthermore, attaching additional chemical units onto the diacetylene monomers often disrupts the organization and self-assembly of the monomers and adversely affects polymerization. Consequently, the abundance of recognition modules in previously reported derivatized PDA vesicles is low [61, 67]. Such limitations are generally not encountered in *lipid/PDA* vesicles incorporating recognition elements. No chemical modification of the diacetylene monomers is needed because the lipid moieties constitute the scaffolding modules for anchoring the receptor modules. In addition, a higher number of receptors can be incorporated in the vesicles because of the high mole ratio—almost 50%—of the lipids in the mixed lipid/PDA vesicles [43, 93]. Another noteworthy feature of the lipid/PDA system as a vehicle for receptor display is the generic nature of this approach; in principle, attachment of appropriate lipophilic residues is the only precondition for displaying any receptor unit at the vesicle surface.

Incorporation of biological receptor modules in PDA-based vesicles can be combined with other scaffolding systems for the creation of versatile sensing modules. For example, sol–gel assemblies comprising phospholipid/PDA vesicles that further contained immunoglobulins were shown to respond to the presence of specific antigens through visible blue–red changes [93]. Below we describe several sensor systems utilizing receptor/lipid/PDA vesicles for specific molecular recognition.

3.3.1 Ion Discrimination by Ionophore/Lipid/PDA Vesicles

An early study reported the construction of an ion sensor through incorporation of *ionophores* in phospholipid/PDA vesicles [94] (Fig. 10). Selective colorimetric response to ions depended on the different affinities between the soluble ions and vesicle-embedded ionophores. The mechanism of colorimetric changes in this vesicle system has been ascribed to the structural transformations and mobility of the ionophores within the lipid bilayers, induced by ion binding [94].

Figure 10b depicts representative colour changes observed in DMPC/PDA vesicles incorporating different ionophores. The ionic selectivity demonstrated in Fig. 10b is consistent with the established binding affinities of these particular ionophores. Valinomycin, for example, binds potassium ions with much higher affinity compared to sodium cations [95]. On the other hand, the more pronounced blue–red colour change within the monensin/DMPC/PDA vesicles is induced by addition of *sodium* cations to the solution, reflecting the higher affinity of monensin to Na^+ ions. Another important observation in the ionophore/phospholipid/PDA system was the capability of the system

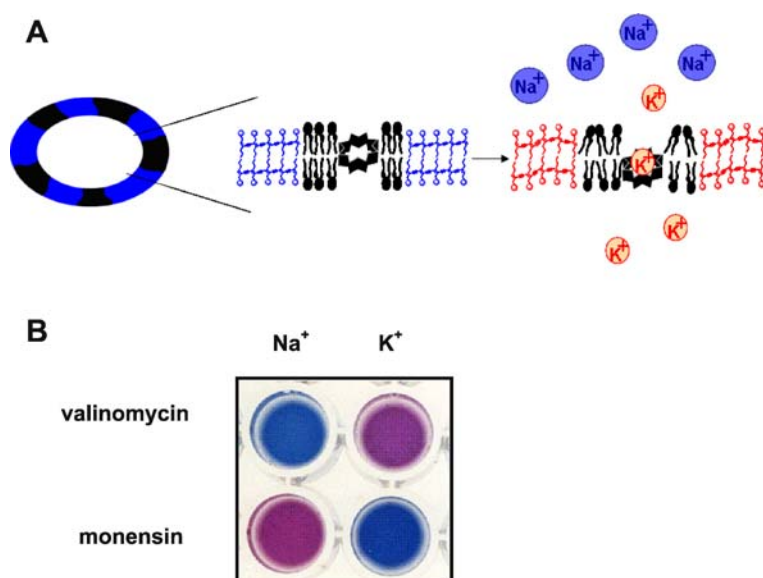


Fig. 10 Ion sensing by ionophore/lipid/PDA vesicles. **a** Schematic description of colorimetric ion sensing by lipid/PDA vesicles embedding ionophores. The ionophore (macrocyclic unit) is incorporated in the lipid domains (*black*); ion binding to the ionophore gives rise to the blue–red transformation of the PDA scaffold. **b** Representative colour transitions induced by ion–ionophore binding. *Top row*: valinomycin incorporated in vesicles; *bottom row*: monensin

to *distinguish* among ions in a mixture, depending on the specific ionophore incorporated within the vesicles [94]. Overall, the assay might be applied to rapid determination of physiological ionic species, investigation of intra- and extra-cellular ion concentrations, and evaluation of the performance and selectivity of putative ion-binding compounds and metal-binding peptides.

3.3.2 Antibody Detection by Epitope/Lipid/PDA Vesicles

An innovative approach designed to accomplish biomolecular recognition using lipid/PDA vesicles has been introduced through implanting *epitopes* within the phospholipid scaffolding [97]. The vesicle system is schematically shown in Fig. 11a. Vesicular particles of PDA and phospholipids further incorporated peptide epitopes covalently attached to the N-termini of hydrophobic amino acid sequences. This configuration facilitated display of the epitope at the surface of the phospholipid bilayer that essentially served for anchoring the hydrophobic peptide moiety.

The design shown in Fig. 11a assures that specific antibody–epitope interactions at the vesicle surface would affect structural perturbations of the PDA and consequent colorimetric transformations. Figure 11b depicts representative colorimetric data recorded with the epitope/lipid/PDA assemblies. The hydrophobic sequence employed for anchoring the epitope was an Ala-Leu re-

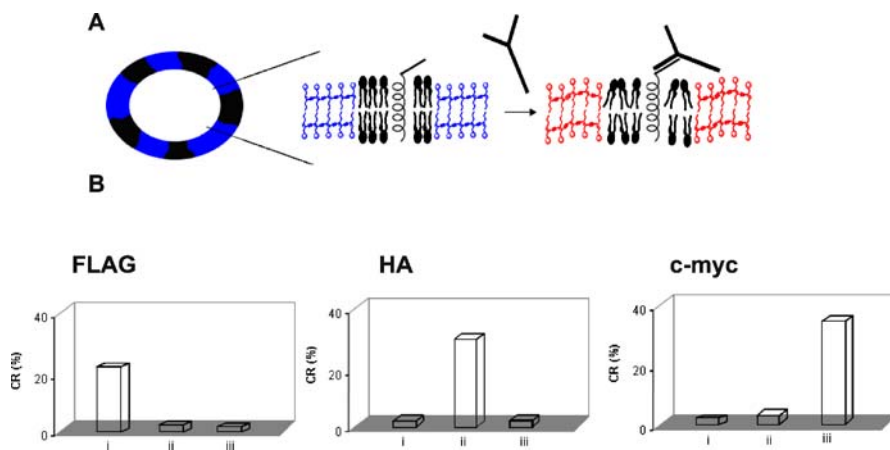


Fig. 11 Colorimetric detection of antibodies using epitope/lipid/PDA vesicles. **a** Schematic description of the antibody-induced colour transitions. The epitope is attached to a helical peptide sequence embedded within the lipid bilayer; binding of the specific antibody gives rise to the blue–red transition of the polymer. **b** Colorimetric response (%CR) induced by specific antibody–epitope binding; each graph summarizes colorimetric data recorded for a specific epitope/lipid/PDA assembly: *i*—anti-FLAG antibody added; *ii*—anti-HA antibody added; *iii*—anti-c-myc antibody added

peat, flanked by Lys residues designed for anchoring the hydrophobic sequence at both sides of the bilayer [98,99]. Epitopes that were displayed include the c-myc epitope [100], the FLAG epitope (amino acid sequence DYKD-DDDK [101]), which is widely used in epitope tagging experiments, and the HA epitope (YPYDVPDYA), derived from the human influenza virus haemagglutinin protein [102]. The colorimetric data in Fig. 11b clearly demonstrate that pronounced colorimetric transitions occurred *only* when the displayed epitopes were recognized by their specific antibodies. The colour changes induced by *non-specific* interactions between the antibodies and the lipid-polymer particles were considerably smaller than the real signal.

Figure 11 confirms the correlation between colorimetric response and the occurrence of specific epitope-antibody interactions at the vesicle interface. In particular, binding between the antibodies, which are relatively big macromolecules, and the epitopes displayed at the vesicle surface is expected to result in significant surface-induced perturbations of the pendant side chains of the polymer, giving rise to the structural transformation and observed colour changes within the PDA matrix.

3.3.3

Artificial Receptors Embedded in Lipid/PDA Vesicles

Indirect induction of chromatic signals within the polymer matrix by specific ligand-receptor binding can be further extended to include *synthetic* receptor systems. A generic approach for high-sensitivity and specific detection of catecholamine ligands through implanting synthetic hosts within phospholipid/PDA vesicles has been recently described [103]. The system is depicted schematically in Fig. 12, showing a representative artificial receptor designed to recognize catecholamines with high specificity embedded in a phospholipid/PDA vesicle; complexation of the catecholamine ligand triggers the blue-red transformation.

The schematic structure in Fig. 12a shows the phospholipid-flanked cavity which is open to the aqueous solution, available for binding the catecholamine guests. Figure 12b depicts an image of a receptor/lipid/PDA vesicle solution before and after addition of two catecholamine ligands. The colour response of the vesicles clearly echoes the specific binding between the catecholamine ligand (noradrenaline) and the synthetic host designed to bind the molecule [104]. Published data further demonstrated that *chromatic selectivity* is achieved in these vesicle systems; for example, the inclusion of noradrenaline-binding host in DMPC/PDA vesicles could discriminate between noradrenaline and adrenaline—a highly similar ligand—in a solution mixture of the two compounds.

Protein sensors based on synthetic receptors embedded within lipid/PDA vesicles have also been recently demonstrated [106]. Protein sensing by artificial molecules is a challenging endeavour, especially if the recognition

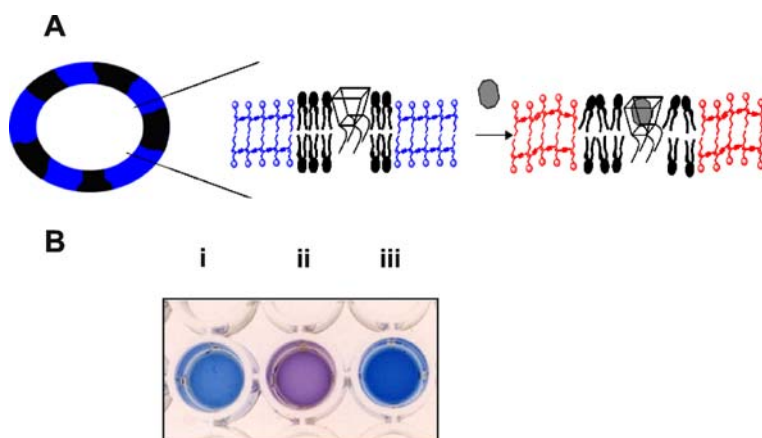


Fig. 12 Colorimetric detection of ligands through vesicle-embedded receptors. **a** Schematic description of the experiment: ligand–receptor recognition between soluble ligand and embedded receptor gives rise to the colorimetric transformation of PDA. **b** Scanned image of lipid/PDA vesicles incorporating a synthetic host designed to specifically bind noradrenaline [104]: *i*—control vesicle (no ligand added); *ii*—noradrenaline added; *iii*—adrenaline added

event is desired to be coupled to a simple quantifiable readout. The innovative scheme for colorimetric determination and fingerprinting of proteins through electrostatic interactions with vesicle-embedded calixarene derivatives is depicted in Fig. 13. Specifically, the hydrophobic calixarene hosts were incorporated within the lipid bilayers, while their charged moieties bound soluble proteins through multivalent electrostatic interactions with charged protein surfaces [105].

Figure 13b presents UV–Vis spectra of DMPC/PDA vesicle solutions, and the effect of protein–host interactions. It shows that addition of pepsin to lipid/PDA vesicles not containing additional receptors did not give rise to a noticeable colour transformation (the solution remained blue, Fig. 13b, ii) due to the fact that both pepsin ($pI = 1$) and the PDA surface display a negative charge in the pH conditions employed in the experiment. However, adding pepsin to DMPC/PDA vesicles to which a positively charged calixarene was pre-added gave rise to a distinct blue-to-purple colour change, clearly reflected in the visible spectrum of the solution mixture (Fig. 13b, iii).

The differences in colour changes induced after addition of proteins to lipid/PDA vesicles containing the calixarene hosts can also be quantified according to the %CR formula shown above. Specifically, the *net colorimetric response* (ΔCR) can be calculated for each protein and vesicle-embedded receptor [106]. ΔCR corresponds to the difference between the colour response induced by a tested protein added to lipid/PDA vesicles containing the calixarene receptor and vesicles that did not include the receptor. Interestingly, the set of ΔCR values obtained for different proteins makes possible *protein*

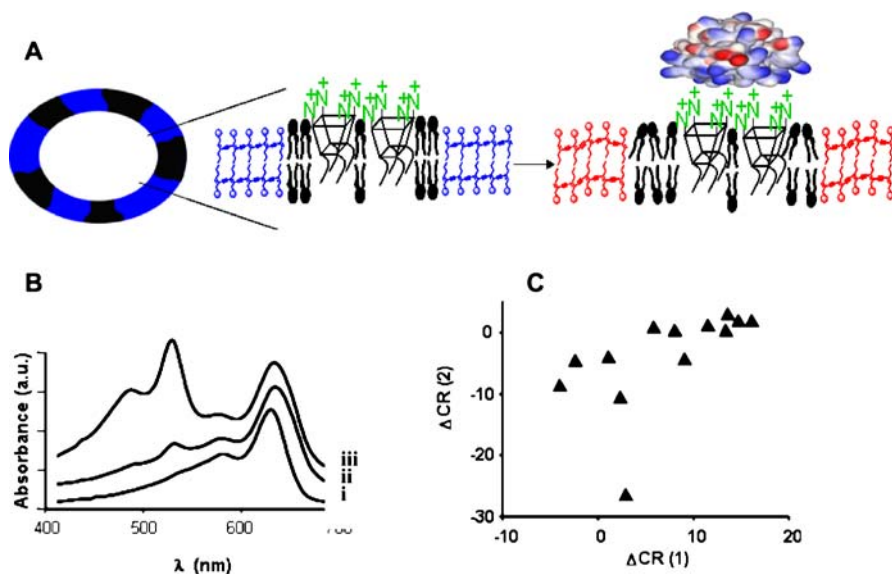


Fig. 13 Protein fingerprinting by charged receptors incorporated within lipid/PDA vesicles. **a** Schematic description of a lipid/PDA vesicle incorporating a synthetic host which binds a protein molecule through electrostatic attraction. **b** Visible spectra depicting protein sensing by the receptor/lipid/PDA vesicles: *i*—control vesicles (no protein added); *ii*—pepsin (a negatively charged protein, $pI = 1.0$) added to lipid/PDA vesicles *not containing* the receptor; *iii*—pepsin added to lipid/PDA vesicles that also incorporate a positively charged synthetic host. **c** “Protein fingerprinting”: each triangle corresponds to a specific protein; x and y axes represent the changes in %CR recorded after embedding receptors 1 and 2, respectively, within the vesicles prior to protein addition [106]

fingerprinting (Fig. 13c). Specifically, proteins can be distinguished, in principle, by a combination of net colorimetric effects recorded by using *different* vesicle-embedded receptors.

The protein fingerprinting concept is shown in Fig. 13c [105]. Each data point in the two-dimensional graph represents a protein for which ΔCR values were recorded by using positively-charged calixarene (x axis) or negatively-charged calixarene (y axis). The dispersion of protein data points is particularly large for either acidic or basic proteins, which is an expected outcome since the platform relies on *electrostatic interactions* between the proteins and the calixarene hosts. Specifically, when *negative* proteins were added to vesicles containing the positively charged calixarene host 1, more pronounced colour changes were recorded (positive ΔCR) due to the enhanced binding of the negative proteins to the vesicles. On the other hand, when *positive* proteins were added to lipid/PDA vesicles containing negative hosts, *negative* ΔCR values were obtained due to binding of proteins to the receptor rather than the negative PDA framework [105]. Overall, the distribution map in Fig. 13c indicates that, in principle, the construction of

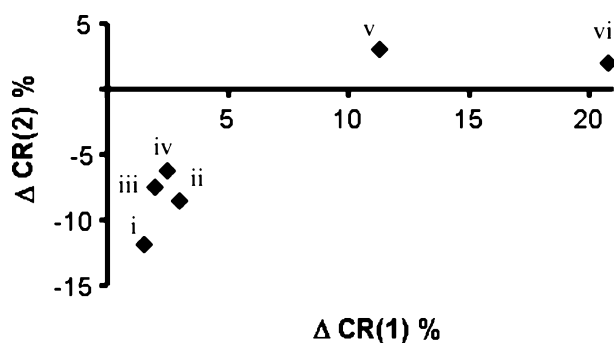


Fig. 14 Colorimetric fingerprinting of small molecules by receptor/lipid/PDA vesicles. Net colorimetric responses (ΔCR) recorded for several biological and pharmaceutical molecules added to lipid/PDA vesicles containing the positively charged receptor 1 and the negatively charged receptor 2: *i*—amitriptyline (pI = 9.4); *ii*—maprotiline (10.5); *iii*—promethazine (9.1); *iv*—nortriptyline (9.7); *v*—nicotinamide adenine dinucleotide (NADH, 4.8); *vi*—adenosine triphosphate (ATP, 4.2)

a sufficiently broad colorimetric protein database would allow identification of proteins by combining information on their molecular weights with the colorimetric assay.

The concept of colorimetric fingerprinting based upon electrostatic affinity between vesicle-embedded receptors and charged species in aqueous solutions can be broadened to also include detection of small biological analytes and not only proteins. Figure 14 depicts the net colorimetric response graph of small biomolecules and pharmaceutical compounds following their addition to lipid/PDA vesicles incorporating a positively charged calixarene (1) and a negatively charged host (2) [105]. Similar to the situation encountered for proteins (Fig. 13), the insertion of a positively charged host into the vesicles gave rise to more pronounced colorimetric transformations when adding *negative* analytes to the vesicles, and lesser colour changes when *positive* compounds were added.

4

Conclusions

This chapter discussed biosensor platforms and applications employing colorimetric vesicles as the signal-generating module. Most vesicle systems presented are based on polydiacetylene (PDA)—a polymer that self-assembles in water into vesicle bilayers, and that further exhibits dramatic blue–red transformations. Important features of the vesicle arrangements that were emphasized include their generic nature, simplicity of signal generation, recording, and analysis, and diversity of biological processes and analytes that can be

studied. Indeed, one of the attractive aspects of many of the colorimetric vesicle systems discussed as biosensing platforms is the “one step” characteristic: generation of the colorimetric signals does not require complex procedures or initiation of a cascade of chemical reactions, but is rather a “mix and observe” process.

PDA vesicles that further contain embedded lipids point to promising avenues for research applications and practical utilization. Such vesicle systems facilitate detection of varied biological events, including enzyme hydrolysis, peptide–membrane interactions, and drug permeation through lipid barriers. Lipid/PDA vesicles were also shown to constitute useful scaffolding for implanting receptor modules, thus facilitating detection and analysis of varied ligand–receptor interactions. Overall, the use of visible colour changes as the thrust of biosensing platforms most likely would continue to generate significant interest in further development and practical applications.

Acknowledgements Raz Jelinek is grateful to the Human Frontiers Science Program for generous financial support.

References

1. Linthicum DS, Patel J, Cairns N (2001) Antibody-based fluorescence polarization assay to screen combinatorial libraries for sweet taste compounds. *Comb Chem High Throughput Screen* 4:431–438
2. Ito Y et al. (2002) *Escherichia coli* and its application in a mediated amperometric glucose sensor. *Biosens Bioelectron* 17:993–998
3. Sargent A, Sadik OA (1999) Monitoring antibody–antigen reactions at conducting polymer-based immunosensors using impedance spectroscopy. *Electrochim Acta* 44:4667–4675
4. Eteshola E, Leckband D (2001) Development and characterization of an ELISA assay in PDMS microfluidic channels. *Sens Actuators B Chem* 72:129–133
5. Goddard NJ et al. (2002) Internally referenced resonant mirror devices for dispersion compensation in chemical sensing and biosensing applications. *Sens Actuators A Phys* 100:1–9
6. Ward CJ, Patel P, James T (2002) Molecular color sensors for monosaccharides. *Org Lett* 4:477–479
7. Poenar DP, Frencha PJ, Wolffenbuttel RF (1997) Colour sensors based on active interference filters using silicon-compatible materials. *Sens Actuators A Phys* 62:513–523
8. Bariaian C et al. (2001) Behavioral experimental studies of a novel vapochromic material towards development of optical fiber organic compounds sensor. *Sens Actuators B Chem* 76:25–31
9. Kyunghoa K et al. (1997) Active optical thin-film waveguide sensor for ion sensing. *Anal Chim Acta* 343:199–208
10. Gambari R (2001) Biospecific interaction analysis: a tool for drug discovery and development. *Am J Pharmacogenomics* 1:119–135
11. Anglina R (1996) Colorimetric toxicity test. *Biotechnol Adv* 14:331
12. Poenar DP, Siu TM, Kiang TO (2002) Colour sensor for (bio)chemical/biological discrimination and detection. *Mater Sci Semicond Process* 5:17–22

13. Lenarczuk T, Glab S, Koncki R (2001) Application of Prussian blue-based optical sensor in pharmaceutical analysis. *J Pharm Biomed Anal* 26:163–169
14. Hisamoto H et al. (1998) Two-color fluorescent lithium ion sensor. *Anal Chim Acta* 373:271–289
15. Ignatov SG, Ferguson JA, Walt DR (2001) Highlight: recent trends in the application of evanescent wave biosensors. *Biosens Bioelectron* 16:109–113
16. Costa-Fernandez JM, Pereiro R, Sanz-Medel A (2006) The use of luminescent quantum dots for optical sensing. *Trends Anal Chem* 25(3):207–218
17. Sankaranarayanan S et al. (2000) The use of pHluorins for optical measurements of presynaptic activity. *Biophys J* 79:2199–2208
18. Olson KD, Deval P, Spudich JL (1992) Absorption and photochemistry of sensory rhodopsin. I: pH effects. *Photochem Photobiol* 56:1181–1187
19. Cheng Z, Aspinwall CA (2006) Nanometre-sized molecular oxygen sensors prepared from polymer-stabilized phospholipid vesicles. *Analyst* 131(2):236–243
20. Lee KS et al. (1999) Disposable liposome immunosensor for theophylline combining an immunochromatographic membrane and a thick-film electrode. *Anal Chim Acta* 380:17–26
21. Carbonell RG et al. (1997) Immunodiagnostic assay using liposomes carrying labels thereof on outer liposome surface. *Biotechnol Adv* 15:181
22. Hianik T et al. (1999) Immunosensors based on supported lipid membranes, protein films and liposomes modified by antibodies. *Sens Actuators B Chem* 57:201–212
23. Cooper MA et al. (2000) A vesicle capture sensor chip for kinetic analysis of interactions with membrane-bound receptors. *Anal Biochem* 277:196–205
24. Yang Y et al. (2000) A glucose sensor with improved haemocompatibility. *Biosens Bioelectron* 15:221–227
25. Woodbury CPJ, Venton DL (1999) Methods of screening combinatorial libraries using immobilized or restrained receptors. *J Chromatogr B Biomed Sci Appl* 725:113–137
26. Toko K (2000) Taste sensor. *Sens Actuators B Chem* 64:205–215
27. Leatherbarrow RJ, Edwards PR (1999) Analysis of molecular recognition using optical biosensors. *Curr Opin Chem Biol* 3:544–547
28. Li SK, D'Emanuele A (2001) On-off transport through a thermoresponsive hydrogel composite membrane. *J Control Release* 75:55–67
29. Gonzalez-Manas JM, Kaschny P, Goni FM (1994) Use of merocyanine 540 as an optical probe in the study of membrane-surfactant interactions. *J Phys Chem* 98(41):10650–10654
30. Roberts MA, Durst RA (1995) Investigation of liposome-based immunomigration sensors for the detection of polychlorinated biphenyls. *Anal Chem* 67(3):482–491
31. Reeves SG, Durst RA (1995) Novel optical measurements approach for the quantitation of liposome immunomigration assays. *Anal Lett* 28(13):2347–2362
32. Okada S et al. (1998) Color and chromism of polydiacetylene vesicles. *Acc Chem Res* 31:229–239
33. Tanaka H et al. (1989) Thermochromic phase transitions of a polydiacetylene, poly(ETCD), studied by high-resolution solid-state C13 NMR. *Macromolecules* 22:1208–1215
34. Okada S, Charych DH (1997) Thermochromic transitions of synthetic lipid-polymer membranes. *Berkeley Sci J* 1:48–50
35. Lio A et al. (1997) Molecular imaging of thermochromic carbohydrate-modified polydiacetylene thin films. *Langmuir* 13:6524–6532
36. Lio A et al. (1996) Atomic force microscope study of chromatic transitions in polydiacetylene films. *J Vac Sci Technol* 14:1481–1484

37. Wenzel M, Atkinson GH (1989) Chromatic properties of polydiacetylene films. *J Am Chem Soc* 111:4123–4127
38. Berman A, Charych DH (1999) Oriented nucleation of inorganic salts on polymeric long chain acid monolayers. *J Cryst Growth* 198/199:796–801
39. Ringsdorf H, Schlarb B, Venzmer J (1988) Molecular architecture and function of polymeric oriented systems: models for the study of organization, surface recognition, and dynamics of biomembranes. *Angew Chem Int Ed Engl* 27:113–158
40. Jonas U et al. (1999) Reversible color switching and unusual solution polymerization of hydrazide-modified diacetylene lipids. *J Am Chem Soc* 121:4580–4588
41. Ahn DJ et al. (2003) Colorimetric reversibility of polydiacetylene supramolecules having enhanced hydrogen-bonding under thermal and pH stimuli. *J Am Chem Soc* 125(30):8976–8977
42. Kulusheva S, Shahal T, Jelinek R (2000) Peptide–membrane interactions studied by a new phospholipid/polydiacetylene colorimetric vesicle assay. *Biochemistry* 39:15851–15859
43. Jelinek R, Kulusheva S (2001) Polymerized lipid vesicles as colorimetric biosensors for biotechnological applications. *Biotechnol Adv* 19:109–118
44. Jelinek R et al. (1998) Interfacial catalysis by phospholipases at conjugated lipid vesicles: colorimetric detection and NMR spectroscopy. *Chem Biol* 5:619–629
45. Okada SY, Jelinek R, Charych DH (1999) Induced color change of conjugated polymeric vesicles by interfacial catalysis of phospholipase A2. *Angew Chem Int Ed* 38:655–659
46. Wilson TE et al. (1994) Enzymic modification and X-ray photoelectron spectroscopy analysis of a functionalized polydiacetylene thin film. *Langmuir* 10:1512–1516
47. Charych D, Nagy JO (1996) Artificial cell membranes for diagnostics and therapeutics. *Chemtech* 26:24–28
48. Kulusheva S, Wachtel E, Jelinek R (2003) Biomimetic lipid/polymer colorimetric membranes: molecular and cooperative properties. *J Lipid Res* 44:65–71
49. Song J, Cisar JS, Bertozzi CR (2004) Functional self-assembling bolaamphiphilic polydiacetylenes as colorimetric sensor scaffolds. *J Am Chem Soc* 126(27):8459–8465
50. Sarkar A et al. (2005) Colorimetric biosensors based on polydiacetylene (PDA) and polyamidoamine (PAMAM) dendrimers. *Polymer News* 30(12):370–377
51. Peng H et al. (2005) Polydiacetylene/silica nanocomposites with tunable mesostructure and thermochromatism from diacetylenic assembling molecules. *J Am Chem Soc* 127(37):12782–12783
52. Charych DH et al. (1993) Specific interactions of influenza virus with organized assemblies of polydiacetylenes. *Biomol Mater* 292:153–161
53. Spevak W, Nagy JO, Charych D (1995) Molecular assemblies of functionalized polydiacetylenes. *Adv Mater* 7(1):85–89
54. Reichert A et al. (1995) Polydiacetylene liposomes functionalized with sialic acid bind and colorimetrically detect influenza virus. *J Am Chem Soc* 117:829–830
55. Pan JJ, Charych DH (1997) Molecular recognition and colorimetric detection of cholera toxin by polymerized liposomes. *Langmuir* 13:1365–1367
56. Litvin AL et al. (1995) Langmuir films of amino acid-modified diacetylenes as organic templates for biomimetic mineralization. *Proc Soc Photo Opt Instrum Eng* 2441:54–60
57. Litvin AL et al. (1995) Liquid crystalline texture in glycine-modified diacetylene Langmuir monolayers at room temperature. *J Phys Chem* 99:492–495
58. Jung YK, Park HG, Kim JM (2006) Polydiacetylene (PDA)-based colorimetric detection of biotin–streptavidin interactions. *Biosens Bioelectron* 21(8):1536–1544

59. Cheng Q, Stevens RC (1997) Coupling of an induced fit enzyme to polydiacetylene thin films: colorimetric detection of glucose. *Adv Mater* 9:481
60. Yamanaka SA et al. (1997) Solid-phase immobilization of optically responsive liposomes in sol-gel materials for chemical and biological sensing. *Langmuir* 13:5049–5053
61. Charych DH et al. (1994) Direct colorimetric detection of virus by a polymerized bilayer assembly. *Biomol Mater Design* 330:295–308
62. Wang C, Ma Z (2005) Colorimetric detection of oligonucleotides using a polydiacetylene vesicle sensor. *Anal Bioanal Chem* 382(7):1708–1710
63. Wang C, Ma Z, Su Z (2006) Facile method to detect oligonucleotides with functionalized polydiacetylene vesicles. *Sens Actuators B Chem* B113(1):510–515
64. Rangin M, Basu A (2004) Lipopolysaccharide identification with functionalized polydiacetylene liposome sensors. *J Am Chem Soc* 126(16):5038–5039
65. Kim JM et al. (2003) Immobilized polydiacetylene vesicles on solid substrates for use as chemosensors. *Adv Mater* 15(13):1118–1121
66. Su YI (2005) Assembly of polydiacetylene vesicles on solid substrates. *J Colloid Interface Sci* 292(1):271–276
67. Baek M-G, Stevens RC, Charych DH (2000) Design and synthesis of novel glycopolythiophene assemblies for colorimetric detection of influenza virus and *E. coli*. *Bioconjug Chem* 11:777–788
68. Spevak W et al. (1993) Polymerized liposomes containing C-glycosides of sialic acid: potent inhibitors of influenza virus in vitro infectivity. *J Am Chem Soc* 115:1146–1147
69. Pan JJ, Charych DH (1997) Molecular recognition and optical detection of biological pathogens at biomimetic membrane interfaces. *Proc Soc Photo Opt Instrum Eng* 3040:211–217
70. Song J et al. (2002) Smart materials for biosensing devices: cell-mimicking supramolecular assemblies and colorimetric detection of pathogenic agents. *Biomed Microdevices* 4(3):213–221
71. Ma G, Cheng Q (2005) Vesicular polydiacetylene sensor for colorimetric signaling of bacterial pore-forming toxin. *Langmuir* 21(14):6123–6126
72. Ma G, Cheng Q (2006) Manipulating FRET with polymeric vesicles: development of a mix-and-detect type fluorescence sensor for bacterial toxin. *Langmuir* 22(16):6743–6745
73. Kolusheva S, Boyer L, Jelinek R (2000) A colorimetric assay for rapid screening of antimicrobial peptides. *Nat Biotechnol* 18:225–227
74. Shai Y (1999) Mechanism of the binding, insertion and destabilization of phospholipid bilayer membranes by α -helical antimicrobial and cell non-selective membrane-lytic peptides. *Biochim Biophys Acta* 1462:55–70
75. Charych DH, Spevak W, Nagy JO, Bednarski MD (1993) *Mater Res Soc Symp Proc* 292:153–161
76. Rozner S, Kolusheva S, Cohen Z, Dowhan W, Eichler J, Jelinek R (2003) Detection and analysis of membrane interactions by a biomimetic colorimetric lipid/polydiacetylene assay. *Anal Biochem* 319(1):96–104
77. Katz M, Tsubery H, Kolusheva S, Shames A, Fridkin M, Jelinek R (2003) Lipid binding and membrane penetration of polymyxin B derivatives studied in a biomimetic vesicle system. *Biochem J* 375(2):405–413
78. Halevy R et al. (2003) Membrane binding and permeation by indolicidin analogs studied by a biomimetic lipid/polydiacetylene vesicle assay. *Peptides* 24:1753–1761
79. Satchell DP et al. (2003) Quantitative interactions between cryptdin-4 amino terminal variants and membranes. *Peptides* 24:1795–1805

80. Tanabe H et al. (2004) Structure-activity determinants in paneth cell \pm -defensins: loss-of-function in mouse cryptdin-4 by charge-reversal at arginine residue positions. *J Biol Chem* 279:11976–11983
81. Sheynis T et al. (2003) Bilayer localization of membrane-active peptides studied in bio-mimetic vesicles by visible and fluorescence spectroscopies. *Eur J Biochem* 270:4478–4487
82. Porat Y et al. (2003) The human islet amyloid polypeptide forms transient membrane-active protofilaments. *Biochemistry* 42:10971–10977
83. Su Y, Sinko PJ (2006) Drug delivery across the blood–brain barrier: why is it difficult? How to measure and improve it? *Expert Opin Drug Deliv* 3(3):419–435
84. Liu X, C Chen (2005) Strategies to optimize brain penetration in drug discovery. *Curr Opin Drug Discov Devel* 8(4):505–512
85. Cucullo L et al. (2005) Drug delivery and in vitro models of the blood–brain barrier. *Curr Opin Drug Discov Devel* 8(1):89–99
86. Katz M et al. (2006) Rapid colorimetric screening of drug interaction and penetration through lipid barriers. *Pharm Res* 23(3):580–587
87. Silbert L et al. (2006) Rapid chromatic detection of bacteria using a new biomimetic polymer sensor. *Appl Environ Microbiol* 72(11):7339–7344
88. Rangin M, Basu A (2004) Lipopolysaccharide Identification with functionalized polydiacetylene liposome sensors. *J Am Chem Soc* 126:5038–5039
89. Ma Z, Li J, Jiang L (2000) Influence of the spacer length of glycolipid receptors in polydiacetylene vesicles on the colorimetric detection of *Escherichia coli*. *Langmuir* 16:7801–7804
90. Ma Z et al. (1998) Colorimetric detection of *Escherichia coli* by polydiacetylene vesicles functionalized with glycolipid. *J Am Chem Soc* 120:12678–12679
91. Gophna U et al. (2002) Role of fibronectin in curli-mediated internalization. *FEMS Microbiol Lett* 212:55–58
92. Gophna UB et al. (2001) Curli fibers mediate internalization of *Escherichia coli* by eukaryotic cells. *Infect Immun* 69:2659–2665
93. Gill I, Ballesteros A (2003) Immunoglobulin–polydiacetylene sol–gel nanocomposites as solid-state chromatic biosensors. *Angew Chem Int Ed* 42(28):3264–3267
94. Kulusheva S, Shahal T, Jelinek R (2000) Cation-selective color sensors composed of ionophore-phospholipid-polydiacetylene mixed vesicles. *J Am Chem Soc* 122(5):776–780
95. Pressman BC (1976) *Annu Rev Biochem* 45:501
96. Reed PW (1979) *Methods Enzymol* 55:435
97. Kulusheva S et al. (2001) Rapid colorimetric detection of antibody-epitope recognition at a bio-mimetic membrane interface. *J Am Chem Soc* 123:417–422
98. Killian JA et al. (1996) *Biochemistry* 35:1037–1045
99. Zhang YP et al. (1995) *Biochemistry* 34:2362–2371
100. Gerondakis S, Bishop JM (1986) *Mol Cell Biol* 6:3677–3684
101. Chiang CM, Roeder RG (1993) *Pept Res* 6:62–64
102. Wilson IA et al. (1984) *Cell* 37:767–778
103. Kulusheva S et al. (2005) Selective detection of catecholamines by synthetic receptors embedded in chromatic polydiacetylene vesicles. *J Am Chem Soc* 127:10000–10001
104. Molt O, Rübelling D, Schrader T (2003) *J Am Chem Soc* 125:12086–12087
105. Schrader T, Zadnavorac R (2004) *J Am Chem Soc* 126:7752–7753
106. Kulusheva S et al. (2006) Color fingerprinting of proteins by calixarenes embedded in lipid/polydiacetylene vesicles. *J Am Chem Soc* 128(41):13592–13598

Combining Molecular Recognition, Optical Detection, and Chemometric Analysis

Byron E. Collins · Aaron T. Wright · Eric V. Anslyn (✉)

The Department of Chemistry and Biochemistry, The University of Texas at Austin,
1 University Station A5300, Austin, TX 78712, USA
anslyn@ccwf.cc.utexas.edu

1	Introduction: Combining Molecular Recognition, Optical Detection, and Chemometric Analysis	182
1.1	Chemometric Analytical Methods	183
2	Micromachined Chip	184
2.1	Development of an “Electronic Tongue”	185
2.2	Electronic Tongue Enhancement	186
2.3	Differential Sensor Arrays with Synthetic Receptors	186
2.3.1	Differential Receptors for Recognition of ATP, AMP, and GTP	187
2.3.2	Proteins and Glycoproteins	188
2.3.3	Tripeptides and Mixtures	189
2.4	Chromatographic Receptors for Differential Sensor Arrays	191
3	Other Solid Supported Arrays	192
3.1	Molecularly Imprinted Polymers	192
3.1.1	Self-Assembled Monolayers: A Spreader-Bar Approach	193
3.1.2	Incorporation of IDAs into MIPs	193
3.2	Detection of Organics in Water	197
3.3	Small Molecule Microarrays for Protein Fingerprints	199
3.4	Fluorescent Self-Assembled Monolayers	201
4	Microtiter Plate Arrays	202
4.1	Multi-Ion Imaging with Fluorescent Sensors	202
4.2	Fluorescent Porphyrins for Discrimination of Proteins	204
4.3	Enantioselective Discrimination of Amino Acids	207
5	Biomolecules for Array Development	208
6	Multicomponent Sensing Ensembles	210
6.1	Dynamic Combinatorial Libraries as Sensors	211
6.1.1	Optimization of DCLs	212
7	Other Arrays Using IDAs	212
7.1	Prescreening Libraries for Improved Differentiation	212
7.2	Discrimination of 20 Natural Amino Acids	214
7.3	IDAs for Identification of Amino Sugars and Aminoglycosides	215
7.4	Detection of Carbohydrates Through pH Changes	216
8	Conclusion	217
	References	217

Abstract The mammalian olfactory and gustatory systems have inspired an emergent area of molecular recognition, which utilizes arrays of semiselective sensors to create patterns to distinguish analytes. Pattern-based recognition, combined with chemometric analysis, has provided chemists the tools necessary to create sensing ensembles that far exceed our ability to rationally design and synthesize sensors for complex molecules. These differential sensing arrays have been used for several biological, environmental, and industrial applications, and are becoming increasingly relevant to real world problems. Herein, we will examine the progress that has been made through differential molecular recognition. We will also discuss the different array platforms that have been employed and provide a brief introduction to the most commonly used chemometric analytical methods.

Keywords Chemometric analysis · Colorimetric sensing · Differential arrays · Pattern recognition

Abbreviations

LED	Light-emitting diode
pI	Isoelectric point
EDTA	Ethylenediamine tetraacetate
PEEK	Polyetheretherketone
PEG	Polyethylene glycol
PS	Polystyrene

1

Introduction: Combining Molecular Recognition, Optical Detection, and Chemometric Analysis

The design and synthesis of sensors that rival the selectivity of antibodies and enzymes found in biological systems is a daunting task. The traditional lock-and-key approach to sensor design, while effective for many applications, is limited by certain factors. First, the rational design of receptors for large biomolecules and analytes whose structures are not fully characterized is impractical. Further, designing specific receptors for every component in a complex mixture would be an impractical and time consuming venture.

Ever a source of inspiration, nature has provided supramolecular chemists with ideas for another approach to sensor design that is more applicable to complex mixtures and large biomolecules. The mammalian olfactory and gustatory systems both use series of semiselective receptors to differentiate tastes and smells [1, 2]. In the gustatory system, taste receptors are isolated in “taste buds” where they interact to variable degrees with a tastant. The composite receptor response provides discrimination and tastant identification. Pattern-based molecular recognition works in a similar manner by using arrays of differential sensing elements to generate fingerprint patterns for analytes [3].

These synthetic differential receptors excel beyond their individual potential by creating diagnostic patterns indicative of the entire array response.

These arrays do not rely on specific binding interactions, and in many cases it is not necessary to identify these interactions. Large and flexible biomolecules may have several different binding sites, but as long as a distinct pattern can be recognized, that analyte will be distinguished by the array. Also, our goal is often times not to identify every component in a complex mixture, but rather to simply identify the mixture itself. Again, in these cases, differential array analysis can be particularly advantageous.

There are already a considerable number of reviews dealing with the formation and application of both vapor and solution phase differential arrays involving electrochemical sensors, microelectrodes, fiber optic sensors, surface acoustic wave devices, conductive polymers, and metal oxide field effect transistors [5–9]. Therefore, this review will generally focus on arrays that employ synthetic receptors.

1.1

Chemometric Analytical Methods

It is common for the amount of data obtained from array analyses to be too great to permit naked-eye distinction or simple calibrations for the analytes. In these instances, chemometric analytical methods are employed to help reduce the dimensionality of the data set and provide graphical representation of the array data. The examples discussed herein have used primarily principal component analysis (PCA) and linear discriminant analysis (LDA). Hierarchical cluster analysis (HCA) and artificial neural networks (ANN) have also been employed. Therefore, a brief introduction to these analytical methods will be discussed in this section.

Principal component analysis is used to measure the classification ability of an array. To do this, the dimensionality of the data set is reduced to a level that can be represented graphically. This is done by decomposing the data into a series of eigenvectors and associated eigenvalues [10, 11]. The amount of variance in the array response is represented by the magnitude of the eigenvalues. The variance is displayed graphically through principal component (PC) axes. Usually, two or three PC axes can describe most of the variance. Therefore, the classification ability of the array can be visualized by creating a PCA score plot using the first two (or three) principal components as the axes. If all of the data points for an analyte are well separated and closely clustered on a PCA score plot, it can be concluded that the receptor array discriminated that analyte from the others. Further, loading values can be used to determine each receptors contribution to the formation of a PC axis. In this way, one can identify the receptors that are critical to the differential response to the analytes tested. Alternatively, loading values can identify those receptors providing little discriminatory effect.

Linear discriminant analysis can be used to classify data, but is most often used to assign new objects to an appropriate class [10]. With LDA, the

array response data as well as the analyte class is used as input data. Discriminant functions are then calculated with the goal of maximizing separation between classes while minimizing the separation of analytes in the same class. When only two or three discriminant functions are used, the data can be displayed graphically. The real power of LDA comes from its ability to take array response data from an unknown analyte and assign it to a particular class. This is a reliable way to quantitatively determine an array's ability to identify a particular analyte under the conditions used.

Hierarchical cluster analysis (HCA) is a qualitative method of separation that clusters data points based on the relative distances between all pairs of data points [10, 12]. When used in array analysis, HCA measures how different the response patterns are for each analyte and groups the analytes in a hierarchical fashion. The distance between the data points is measured using a distance metric, which is usually the Euclidean distance. The Euclidean distance metric calculates the distance between two data points using N -dimensions where N is typically the number of sensor responses. The data points are then clustered based on their relative similarities. HCA data is displayed using a dendrogram as shown in Fig. 10.

One final method of analysis discussed in this section is the artificial neural network (ANN) [13]. An ANN is a system of layers that can be adjusted or "trained" to give a desired response pattern. The layers are the input layer, one or more "hidden" layers, and the output layer. Each layer consists of a set number of units. The number of input units is usually equal to the number of data points in each data set. For example, if the input data were the change in absorbance of each well of an 8×12 array, there would be 96 units in the input layer. The number of units in a hidden layer as well as the number of hidden layers is determined by the creator of the ANN and can be adjusted to suit the application. The number of units in the output layer is the number of desired outputs from the system (e.g. ten if ten analytes were examined). The output from each unit in the input layer is used as input for each unit in the first hidden layer. This is perpetuated through the hidden layers and to the output layer. The system trains itself by adjusting the weight of the units in the hidden layers in order to maximize the number of times the desired output is obtained. Once the ANN is sufficiently trained, it can be used to predict the identity of an unknown data set. In this manner, ANNs can be used in the analysis of solutions whose exact composition is unknown. They can also be used as a way to determine the ability of an array to identify certain analytes.

2 Micromachined Chip

The mammalian sense of taste is regulated by a series of semi-selective receptors located in papillae on the tongue that send information to the brain.

These receptors each give differing responses to sweet, sour, salty, bitter, and umami (savory) tastes. The combined response patterns of each “taste bud” result in the identification of each tastant. Researchers at the University of Texas have developed an electronic tongue that mimics the mammalian gustatory system [14–17]. With this system, individual resin-bound receptors are isolated in small pits on a Si/SiN wafer. The micromachined wells on the chip are designed to isolate each receptor and allow solvent to flow around the beads and out the bottom of the array. The chip is contained within a transparent housing and PEEK tubing is used for solvent delivery and removal. The housing is attached to a stereoscope stand, which allows for top and bottom illumination of the array. A charge-coupled device (CCD) records changes in the absorption properties of each bead upon analyte delivery. With the CCD, the composite response of the entire array can be recorded simultaneously and used for analyte classification.

2.1

Development of an “Electronic Tongue”

In the initial proof of concept studies, a 3×3 array with functionalized poly(ethylene glycol)-polystyrene beads was used for the detection of multiple analytes [14]. The four sensors incorporated into the array were each expected to show preference for a particular analyte, but also provide some response to all the analytes examined. These sensors were: alizarin complexone for Ce^{3+} and Ca^{2+} , *o*-cresolphthalein complexone for $\text{Ca}(\text{II})$ and pH, fluorescein for pH, and a boronate ester of resorufin-derivatized galactose for

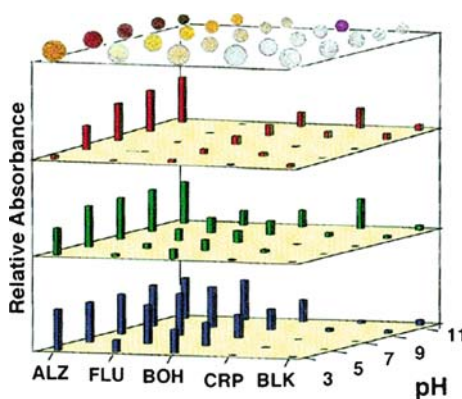


Fig. 1 The illustration shows the derivatized beads on top of the colorimetric bar graph charts. The extent of color attenuation (*linear scale*) obtained from the CCD in response to Ca^{2+} ($0.1 \text{ M Ca}(\text{NO}_3)_2$) is shown for *red* ($\lambda = 700 \text{ nm}$), *green* ($\lambda = 550 \text{ nm}$), and *blue* ($\lambda = 435 \text{ nm}$). Reprinted with permission from Neikirk et al. [14]. Copyright (1998) American Chemical Society

simple sugars. Changes to the red, green, and blue (RGB) absorbance properties of each receptor were recorded relative to a blank bead (an acetylated PEG-PS bead) after addition of metal ions and mixtures of metal ions at various pH values. It was found that the array gave distinct colorimetric changes that created quantifiable patterns with quick (< 60 second) response times. Figure 1 illustrates the relative RGB responses of each sensor upon addition of Ca(II) at pH 3, 5, 7, 9, and 11.

2.2

Electronic Tongue Enhancement

The array was later refined to the point that each well in the array could be used as an individual microreactor and microanalyzer [15–17]. Addition of a video capture card which could record multiple images over time also allowed for binding kinetics to be monitored during these assays. With the new system, an area of interest is drawn for each bead so that multiple receptors can be imaged simultaneously. The changes in absorbance are referenced to a blank acetylated bead in the array. The beads can also be “recharged” so that the array can be reused multiple times with reproducible results.

The pyramidal shape of the wells designates each resin-bound receptor to a unique microchamber permitting individual interactions with the analyte-containing solution. Additionally, a large number of structurally diverse receptors can be incorporated into a single array without problems with cross-reactivity. This broadens the applicability of the array to the extent that receptors for several different classes of analytes could potentially be placed in one array, and any number of incredibly diverse molecules could be analyzed with a single microchip. Our group has utilized this platform as a “programmable taste chip” by developing several arrays capable of detecting different biological analyte classes.

2.3

Differential Sensor Arrays with Synthetic Receptors

Combinatorial chemistry has become a popular method for rapidly creating large libraries of molecules. Our group has used this method to generate libraries of differential receptors for use in the electronic tongue array just discussed. Our approach to designing these libraries begins with the generation of a core host structure that provides a preorganized binding site complementary to a class of analytes. Combinatorial chemistry is subsequently employed to attach variable peptide arms that provide the impetus for differential binding. Of the large library of receptors generated, a few are chosen at random for incorporation into the array. This approach has led to synthetic receptor arrays capable of differentiating nucleotide phosphates [18], proteins and glycoproteins [19], and tripeptides and tripeptide mixtures [20].

2.3.1

Differential Receptors for Recognition of ATP, AMP, and GTP

To demonstrate the hypothesis that an array of randomly selected receptors can differentiate structurally similar analytes, library 1 was synthesized using split-and-pool combinatorial chemistry [18]. The hexa-substituted benzene core pre-organizes the binding site while guanidinium groups give the receptors affinity for nucleotide triphosphates. The tripeptide arms provide the differential binding element. Thirty beads were chosen at random and placed into a 7×5 array with five acetylated blank beads.

Our group commonly uses indicator displacement assays (IDA) to incorporate a colorimetric readout for quantification of binding events [21]. In the case of library 1, fluorescein was introduced to the array to “color” the beads prior to analyte introduction. After addition of the chromophore, a 2 mL injection of a 20 mM sample of ATP, GTP, or AMP was passed through the array. A CCD was used to record changes in the red, green, and blue transmitted light intensity as the analyte solution passed through the array and displaced the indicator. As can be seen in Fig. 2A, the displacement profiles

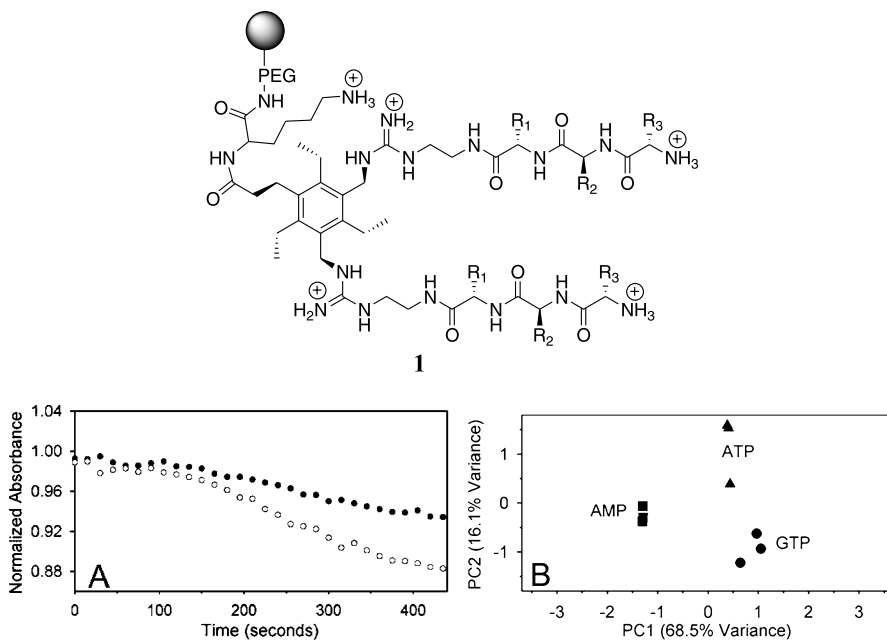


Fig. 2 **A** Indicator displacement profile showing the response of two receptors upon addition of AMP (20 mM in 25 mM HEPES buffered aqueous solution pH 7.5). Effective absorbance is equivalent to normalized absorbance. **B** A PCA score plot showing discrimination of ATP, AMP, and GTP by 30 receptors from library 1. Reprinted with permission from Anslyn et al. [18]. Copyright (2003) American Chemical Society

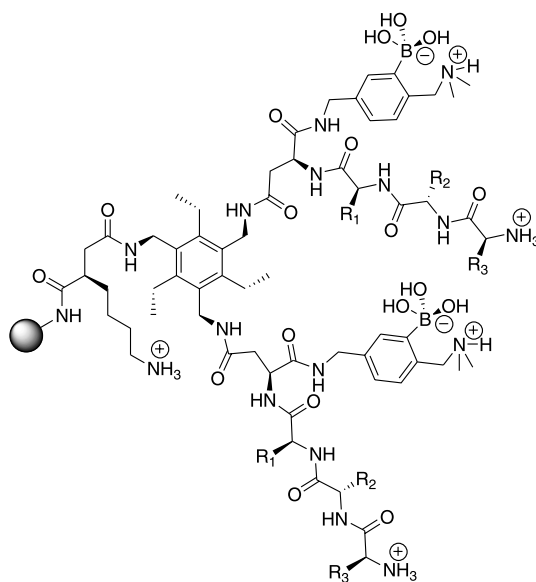
were clearly different for these two receptors upon introduction of AMP. To interpret this data, the slope of the displacement curve for each bead measured from 210 to 435 seconds was used as input for PCA. The PCA score plot shows clear differentiation of the analytes (Fig. 2B). Eight beads with nearly equal factor loading values were sequenced to look for structural similarities. It was found that aromatic amino acids along with serine and threonine were most prevalent in these receptors. This information was in agreement with previous screening studies using library 1 and ATP [22].

2.3.2

Proteins and Glycoproteins

There is a current need for accurate and robust methods of protein detection in various environments. Possible applications of this technology include medical diagnostics, proteomics, and bioterrorism. Hamilton [23, 24] and our group [19] have both developed sensor arrays for pattern-based recognition of proteins/glycoproteins in aqueous solutions.

For this application we again took advantage of a hexa-substituted benzene scaffold that created a binding site while boronic acid groups were appended to impart selectivity for diols and α -hydroxy carboxylic acids. Two combinatorially synthesized tripeptide arms provide a differential response (library 2). For this study, it was found that use of an indicator-uptake assay provided lower detection limits ($60 \mu\text{M}$) than the indicator displacement



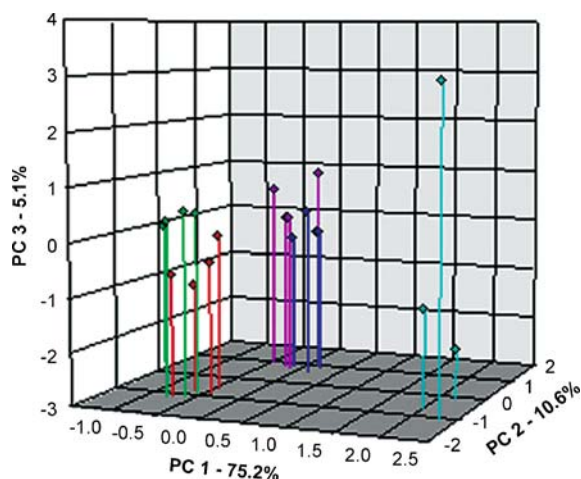


Fig. 3 A PCA score plot indicating the recognition and separation of five different proteins and glycoproteins by 2 (*red* • Lysozyme, *green* • Elastin, *blue* • Ovalbumin, *pink* • Fetuin, *light blue* • BSA). Percentages on the axes detail the amount of variance defined within the PC axes. Reprinted with permission from Anslyn et al. [19]. Copyright (2005) Wiley

assay used previously. This was necessary to make the assay more relevant to biological applications. In an indicator uptake assay, the analytes are introduced to the array first, followed by an indicator. The rate of indicator uptake was monitored over time and was inversely proportional to the analytes affinity for a particular receptor. During this assay, the CCD captured 215 images at each of the 29 receptors. PCA was used for protein identification (Fig. 3). This plot shows clear separation between proteins (lysozyme, elastin, and bovine serum albumin (BSA)) and glycoproteins (ovalbumin and fetuin). Also, the proteins lysozyme and elastin were clearly separated from BSA and were somewhat separated from each other. It was shown that differentiation was dependent upon specific contacts between the proteins and the peptide arms and not solely reliant on pI or molecular weight.

Again, some of the receptors with the largest loading values on the PC1 axis, as well as the one with the lowest value, were sequenced with Edman degradation. In this case, there were no significant similarities. This demonstrated that an array of diverse receptors could be used to differentiate structurally complicated and biologically relevant analytes.

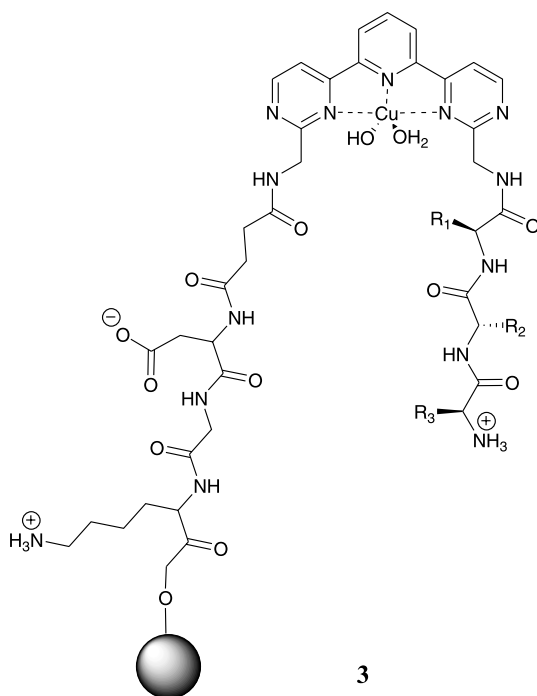
2.3.3

Tripeptides and Mixtures

Typically, the rational design of receptors for every analyte in a complex mixture of analytes is considered time consuming and overall very prohibitive. We have recently adapted the differential array-based approach for analysis

of tripeptides and mixtures in aqueous solutions. The design of library 3 involved the use of a tridentate copper ligand with variable peptide arms [20]. A solution phase version of this complex has been shown to selectively bind the tripeptide His-Lys-Lys [25]. The solid phase version maintained this Cu(II) core to impart selectivity for peptides with histidine and other Cu(II) coordinating amino acids at the N-terminus while the polyaza tricyclic ligand gave preorganization of the binding site. The receptor arm attached to the solid phase bead consisted of tripeptide Asp-Gly-Lys and was connected through a succinic acid linker. The other arm was created through combinatorial chemistry using 19 natural amino acids (Cys excluded).

As with our previous array systems, 30 receptors were selected at random and an indicator-uptake assay with Orange G was used to quantitate binding events. The four tripeptides chosen for analysis (His-Lys-Thr, His-Glu-Thr, His-Gly-Thr, Gly-His-Thr) were similar in sequence, and three differed only at the middle residue. Three mixtures of these tripeptides were also analyzed. As can be seen in Fig. 4, all of the tripeptides and mixtures were clearly separated. The mixtures were all in between their respective components, indicating that both tripeptides influenced the overall response of the array. Also, separation of the three analytes with N-terminal His residues confirms the hypothesis that the tripeptides and the receptor arms influenced binding events. If the only important binding event had been His coordination



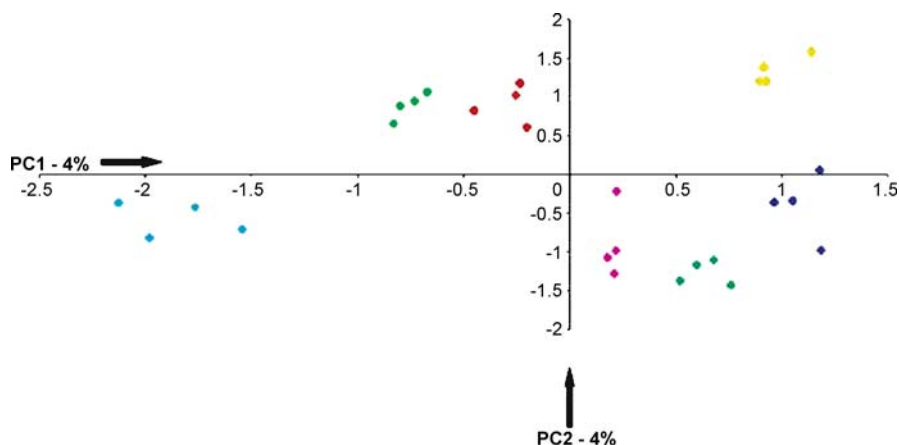


Fig. 4 Two-dimensional PCA plot describing 95% of the variance. Clustering of the analytes illustrates the ability of the differential array of resin-bound receptors to discriminate various tripeptides and mixtures of tripeptides (His-Glu-Thr *blue* ♦, His-Lys-Thr *pink* ♦, Gly-His-Thr *yellow* ♦, His-Gly-Thr *light blue* ♦, His-Lys-Thr & His-Glu-Thr *green* ♦, His-Gly-Thr & Gly-His-Thr *red* ♦, His-Lys-Thr & His-Gly-Thr *light green* ♦). Reprinted with permission from Anslyn et al. [20]. Copyright (2005) American Chemical Society

with the Cu(II) center, all of these would have given identical array response patterns.

2.4

Chromatographic Receptors for Differential Sensor Arrays

In another example of the utility of our electronic tongue, McDevitt combined chromatographic techniques with array sensing for the detection of several metal cations [26]. Instead of functionalizing the periphery of the beads with receptors, this approach involved placing an indicator at the core of a bead and differentially functionalizing the outer layers of the beads with metal ligands and “inert” functional groups. Alizarin complexone was chosen for the indicator due to its known response to a wide range of metals, and the beads were functionalized with either EDTA or acetic anhydride. Beads with both functionalities were placed in the array and metal ion solutions were introduced. To develop fingerprints for the metals, four variables were monitored during the analysis: (1) the color change of the bead taken as the difference in initial absorbance and final effective absorbance, (2) t_D is taken as the time from the beginning of the color change to the half-way point, (3) t_L was measured as the time elapsed before any color change was observed, and (4) the RGB transmission data collected via the CCD (Fig. 5).

Notably, the RGB data alone is not sufficient to distinguish two different concentrations of Pb(II), but the temporal data provides discrimination. Also,

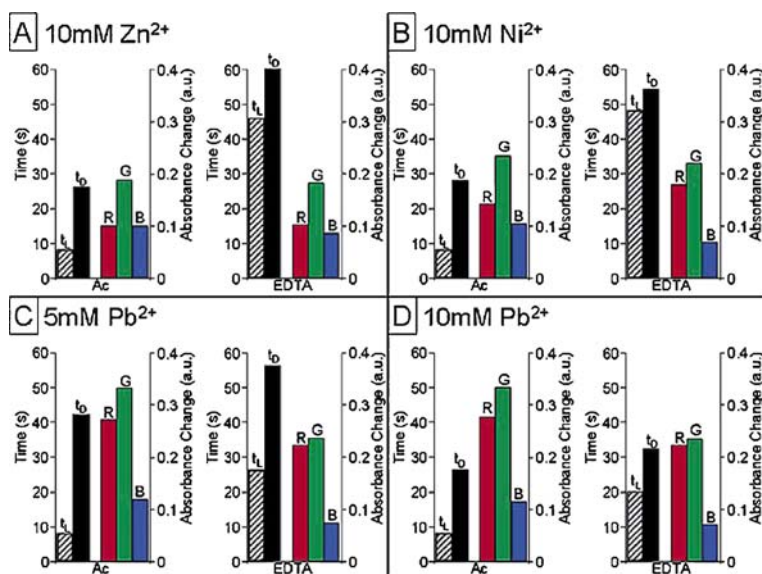


Fig. 5 Pattern responses to various metal cations by an array of microchromatographical receptors. **A** Zn^{2+} (10 mM), **B** Ni^{2+} (10 mM), **C** Pb^{2+} (5 mM), and **D** Pb^{2+} (10 mM). The bars on the left side indicate the t_L and t_D values (hatched and black bars, respectively). The red, green, and blue channels are shown on the right indicating bead color changes. In each quadrant two beads are shown for each metal cation (Ac = acetylated, and EDTA). Reprinted with permission from McDevitt et al. [26]. Copyright (2003) American Chemical Society

the observation that the t_L values for the acetylated beads vary minimally in all four cases indicated the importance of using EDTA for chromatographic purposes.

3 Other Solid Supported Arrays

There have been several other solid supported array formats used to date for pattern-based recognition. One attraction associated with solid phase sensors is that they are often times reusable, as is the case with our micromachined array and several others.

3.1 Molecularly Imprinted Polymers

Molecularly imprinted polymers are highly crosslinked polymer matrices created in the presence of a template analyte molecule [27, 28]. After polymer

formation, the template is removed, ideally leaving behind a polymer matrix containing binding sites specifically tailored to the template. Because of the diversity of these systems, they can be specially tuned to a number of applications. They can also be rapidly and inexpensively generated.

Problems typically associated with MIPs such as low affinities and high levels of cross-reactivity can actually make them an ideal platform for array sensing. The cross-reactivity of MIPs allows them to act as semiselective receptors in an array setting. As long as multiple MIPs react with each analyte, a distinct fingerprint can be generated, and pattern recognition algorithms can then be used for data manipulation.

3.1.1

Self-Assembled Monolayers: A Spreader-Bar Approach

Mirsky and co-workers provided the first example of MIPs used in an array format, utilizing a spreader-bar approach to the formation of self-assembled monolayers [29]. Thiol functionalized purines and pyrimidines were used as spreader-bars in a polymer matrix of dodecanethiol, and the polymer solution was allowed to form self-assembled monolayers on a gold surface. It was expected that purines and pyrimidines would make good spreader-bar molecules because their planar, rigid structures would help form well-defined binding sites on the SAM surface (Fig. 6).

The SAMs were formed on a gold electrode, and capacitive current was used as the method of detection. Five spreader-bar molecules were used to develop the array: 6-mercaptapurine, 2-amino-6-purinethiol, 4-amino-2-mercaptopyrimidine, 4-hydroxy-5-methyl-2-mercaptopyrimidine, and 4-hydroxy-2-mercaptopyrimidine. The coated electrodes were immersed in an analyte solution and the change in capacitive current was recorded upon analyte binding. With this data, unique signal patterns were created for six analytes (adenine, cytosine, thymine, uracil, caffeine, and uric acid). The order of reactivity with the six SAMs was different for all of the analytes except cytosine and uric acid (Table 1). However, the magnitude of the capacitance change for uric acid was 5 to 17 times greater than for cytosine. The arrays were analyzed using five different concentrations (20–470 μM) in all cases of each analyte, and it was found that the orders of reactivity remain valid throughout the entire concentration range. The PCA score plot shown in Fig. 7 clearly demonstrates that, in spite of the limited selectivity of the receptors in the array, good separation of the analytes was achieved.

3.1.2

Incorporation of IDAs into MIPs

Shimizu et al. have more recently developed a colorimetric sensor array based on MIP technology [30]. In this study, eight MIPs were prepared by co-

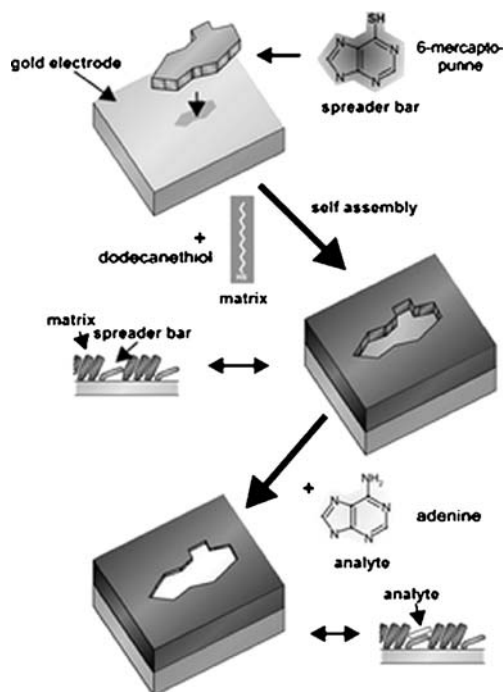


Fig. 6 Sensor arrays formed with a spreader-bar approach. The thiol modified spreader-bars self-assemble in a polymer matrix of dodecanethiol. After assembly, the spreader-bar is selectively removed from the polymer leaving an empty binding cavity. Reprinted with permission from Mirsky et al. [29]. Copyright (2003) The Royal Society of Chemistry

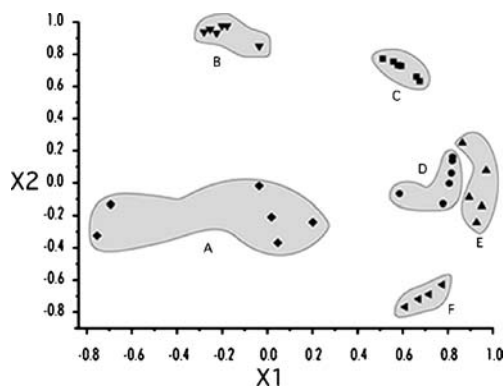


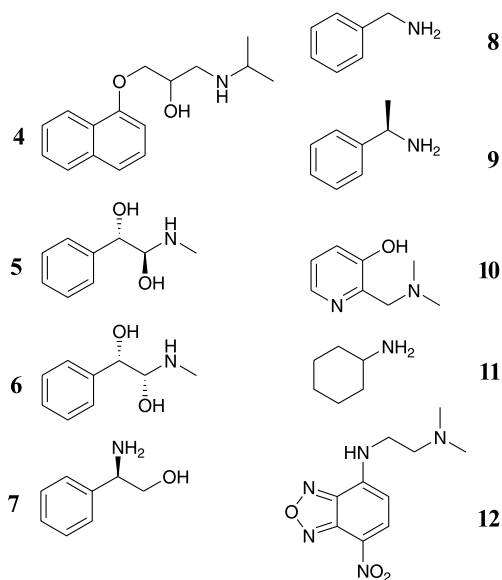
Fig. 7 PCA shows patterns for the five different analytes [cafeine (A), uracil (B), adenine (C), cytosine (D), thymine (E), and uric acid (F)] generated using an electrode array of artificial receptors developed with spreader-bar technology. X1 and X2 are the first and second principal components. These two principal components define 75% of the variance. Reprinted with permission from Mirsky et al. [29]. Copyright (2003) The Royal Society of Chemistry

Table 1 Response pattern of each analyte examined by SAMs created with spreader-bars. SAMs are named based on the spreader-bar used as follows A: 6-mecaptopurine, U: 4-hydroxy-2-mercaptopyrimidine, T: 4-hydroxy-5-methyl-2-mercaptopyrimidine, G: 2-amino-6-purinethiol, C: 4-amino-2-mercaptopyrimidine. A lower-case letter denotes signal change lower then 0.3%

Analyte	Signal pattern
Adenine	T > U > A > G > C
Cytosine	U > G > A > t > c
Thymine	g > a > t > u > C
Uracil	T > U > C > A > G
Caffeine	A > C ≈ T > U > g
Uric Acid	U > G > A > T > C

polymerizing methacrylic acid and ethylene glycol in the presence or absence of seven different aryl amines (4–10). Some of the amines chosen were biologically active and two were diastereomers.

The MIPs were ground to a fine powder, and a constant mass of each was mixed with 3 mM solutions of each analyte. UV-Vis absorption measurements were taken before and after shaking each solution. This produced eight different absorbance values for each analyte. LDA was used for graphical deconvolution of the data set (Fig. 8). This showed clear discrimination of the amines, and a “jack-knife” analysis provided correct analyte classification 94% of the time.



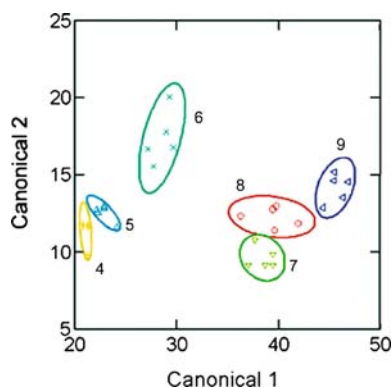
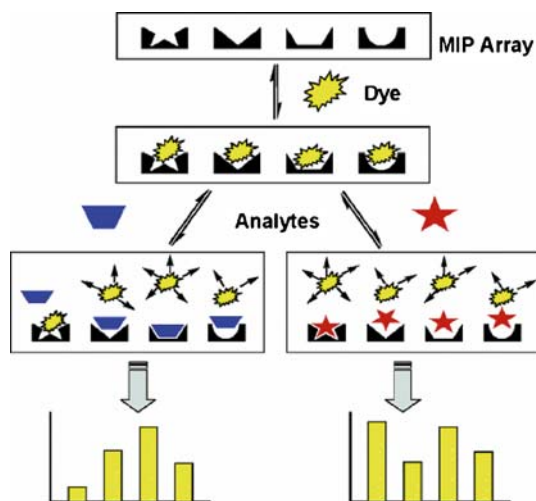


Fig. 8 LDA shows the patterns and clustering of the six analytes measured with the MIP array. Reprinted with permission from Shimizu et al. [30]. Copyright (2004) The Royal Society of Chemistry

Shimizu has also incorporated a dye displacement element into MIP arrays [31]. This approach is illustrated in Scheme 1 where a dye is introduced to the MIP array followed by displacement with the analyte. The changes in absorbance patterns create a diagnostic fingerprint for each analyte. The indicator, 12, was chosen for its structural similarity to the analytes and lack of spectral overlap with any analytes. Analytes 4–9 were used as templates using the same methacrylic acid/ethylene glycol polymer matrix to create a seven



Scheme 1 General scheme for a MIP sensor array using a colorimetric IDA. A unique colorimetric response from each sensor in the array results in diagnostic patterns for each of the analytes tested. Reprinted with permission from Shimizu et al. [31]. Copyright (2005) American Chemical Society

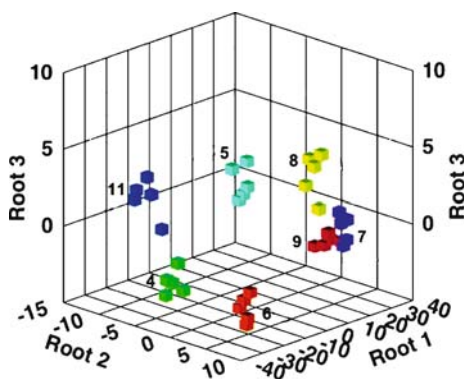


Fig. 9 A three-dimensional LDA plot that describes 99.7% of the variance in the original data. Response patterns to the seven analytes from the MIP array are demonstrated. Reprinted with permission from Shimizu et al. [31]. Copyright (2005) American Chemical Society

MIP sensor array (one MIP was not templated). The amines were analyzed as before by shaking a constant weight of each polymer with the analyte solution and measuring the absorbance before and after. Cyclohexylamine, 11, was also added to the analyte pool to test the arrays ability to detect a non-templated analyte.

After complete analysis, LDA was used for graphical display of the data (Fig. 9). All of the analytes were clearly separated including 11, and it was found that the classification ability of this array (94% accurate) was as accurate as the previous example that did not use an IDA. It was also found that each templated analyte had the highest affinity for its respective polymer, indicating that the selectivity of the array was a result of the templating process. The use of an array of imprinted polymers to access analytes not originally templated is definitely a great advance. Also, given the successful incorporation of indicator-displacement assays, it is now theoretically possible to create MIP sensor arrays capable of virtually any molecule of interest.

3.2

Detection of Organics in Water

Suslick and co-workers presented one of the first examples of vapor-phase colorimetric array sensing when they developed a porphyrin array to discriminate various metal-coordinating analytes [32]. More recently, this approach has been modified for analysis of organic compounds in aqueous solutions [33]. This array was made up of three different types of chromophores: (1) metalloporphyrins for detection of Lewis basicity, (2) derivatives and precursors of pH indicators for detection of Brønsted acidity/basicity, and (3) solvatochromic dyes for measurement of analyte polarity. A total of

36 sensors were printed on a hydrophobic surface and used to create fingerprints for multiple organic compounds and several common soft drinks.

The array was initially dipped into an aqueous solution with no analyte and imaged on a flatbed scanner. Next, the array was introduced to an analyte solution and imaged again. Color changes were remarkably fast and were complete within seconds. The output signal was taken as the difference in the RGB absorption values between these two measurements. Notably, the pH of all solutions was held constant to ensure that all observed color changes were caused by interactions with analytes and not subtle pH fluctuations.

Hierarchical cluster analysis (HCA) was used to display familial classifications obtained from the array (Fig. 10). Interestingly, rather subtle structural differences were distinguished such as degree of substitution, branching, and cyclic structures. There were also no misclassifications out of 144 cases. The analysis of soft drinks, while not part of the HCA analysis, provided easily distinguishable patterns for each of the 12 beverages tested (Fig. 11).

In a more recent example, which combines the vapor-phase array mentioned previously with the solution-phase array discussed here, 18 commercially available beers were discriminated using HCA [34]. Each of the beers was analyzed with both arrays, and fingerprints were developed for each method of analysis. At this point the data was analyzed with PCA both separately and combined. As mentioned earlier, the typical PCA analysis requires two or three PCs to most (95% or more) of the variance of the system. In this case, 22 PCs were required to capture 95% of the solution phase data, 32 PCs were needed for the gas phase analysis, and an unprecedented 38 dimensions were needed to capture 95% of the variance in the combined system. The abnormally high level of discrimination of this system was likely the result of the

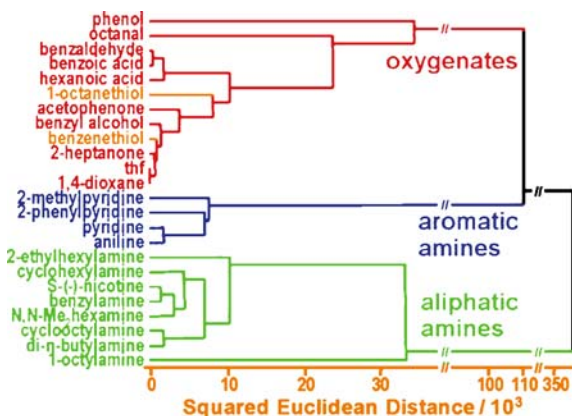


Fig. 10 A dendrogram showing the HCA results after analyzing organics in water. The analytes are grouped based on the similarities of their array responses. Reprinted with permission from Suslick et al. [33]. Copyright (2005) American Chemical Society

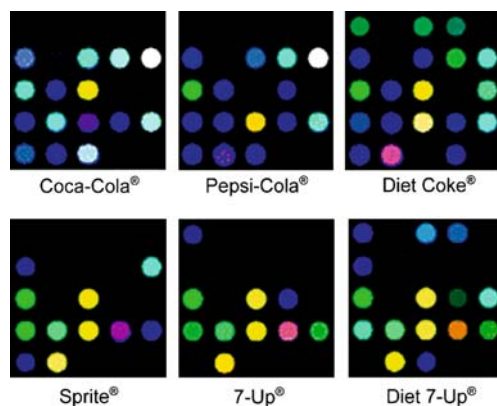


Fig. 11 Color change profiles for a series of soft drinks showing distinct patterns for commonly available mixtures. Reprinted with permission from Suslick et al. [33]. Copyright (2005) American Chemical Society

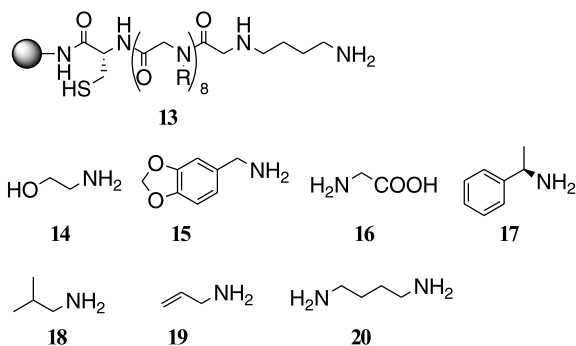
use of several different types of sensors (see above) as well as vapor and solution phase data. Again, HCA was used to display the discriminating ability of the array. The error rate was found to be 2.7%. This shows the potential for an inexpensive, disposable array sensor to be applied to real world applications such as industrial quality control.

3.3

Small Molecule Microarrays for Protein Fingerprints

Small molecule microarrays have become a standard platform for screening combinatorial libraries of small molecules in drug discovery experiments. With individual feature diameters well within the 100 μM range, SMMs with tens of thousands of receptors can be printed and analyzed simultaneously. The compact size, as well as the low volumes required for preparation, make SMMs a very desirable screening platform. Typically, SMMs are prepared by first synthesizing a library of receptors on solid phase resin beads through either combinatorial chemistry or diversity oriented synthesis. Each bead is placed individually into a 96-well plate, and the receptors are cleaved from the beads. The library members are then spotted robotically onto a functionalized glass slide.

Kodadek has demonstrated that SMMs can be used to create fingerprint patterns for proteins in biological solutions [35]. Library 13, consisting of 7680 octameric peptoids with terminal cysteine residues, was synthesized on solid phase beads. After cleavage, the entire library was covalently attached to a maleimide functionalized microscope slide. The array was then incubated in a solution containing one of three fluorescently labeled proteins [Ubiquitin (Ub), maltose binding protein (MBP), and anti-glutathione S-transferase



(GST)]. The solution also contained a 100-fold excess of a crude *E. coli* extract to mimic a biological milieu. The fluorescence intensity of each spot was measured before and after exposure. GENESPRING software was used to graphically compare the change in fluorescence intensity of each spot as shown in Fig. 12. It was clear from these bar graphs that each protein provided a unique pattern; focusing on small sections of the graph more clearly illustrated the differences in the graphs. Diagonal plots were used to display the reproducibility and individuality of the patterns. As an alternative method of analysis, native GST protein was introduced to the array followed by hybridization with fluorescently labeled anti-GST antibody. This demon-

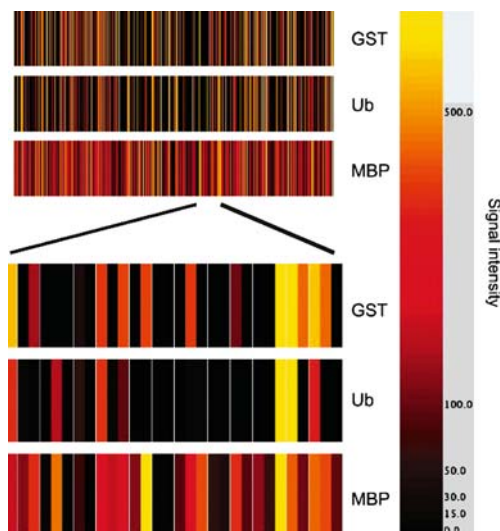


Fig. 12 Relative fluorescence intensity changes for each member of a peptoid library upon exposure to three proteins. The expanded portions more clearly display the differences in the response patterns. Reprinted with permission from Kodadek et al. [35]. Copyright (2005) National Academy of Sciences

strated that the array could be used to create fingerprints for proteins that had not been fluorescently labeled. While it was not proven explicitly, the data from this experiment suggested that the array could distinguish between labeled and native GST proteins. It was also determined that the concentration threshold for this array was in the range of 10–100 nM, making it applicable to many biological applications. This work clearly demonstrates that SMMs are an effective platform for solid phase sensing arrays.

3.4 Fluorescent Self-Assembled Monolayers

Crego-Calama and co-workers have shown that fluorescent self-assembled monolayers synthesized on a functionalized glass surface can be used to create patterns for metal cations in water [36]. One of the problems associated with SAMs in aqueous solutions is that the Si-O bonds hydrolyze over short periods of time. However, it was demonstrated that SAMs synthesized from 11-aminoundecyltrichlorosilane were water-stable. The SAMs were derivatized with three fluorophores and two binding molecules to form a 9-member library. The functionalized glass slides were placed in a fluorescence cuvette at a 45-degree angle and analyzed in the presence of metal ions Hg(II), Cu(II), Ca(II), and Co(II). Patterns were created using the fluorescence intensity changes as shown in Fig. 13. Both the fluorophore and the binding group influenced the binding patterns for each of the metal ions. This was a first example of metal-ion sensing in water with fluorescent self-assembled monolayers.

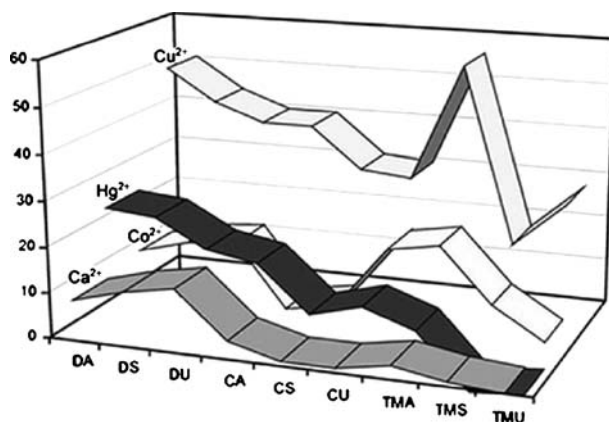


Fig. 13 Graphical representation of the fluorescence quenching patterns for each metal exposed to a self-assembled monolayer array made up of fluorophores: dansyl (D), coumarin (C), TAMRA (TM) and cation binders: amino (A), aryl-urea (U), aryl-sulfonamide (S). Reprinted with permission from Crego-Calama et al. [36]. Copyright (2005) The Royal Society of Chemistry

4 Microtiter Plate Arrays

Microtiter plate (MTP) technology is an adaptable and relatively inexpensive platform for array analysis that has become popular for applications incorporating large numbers of receptors and sensing conditions. The flexibility of MTP arrays has made them an often employed, widely accepted sensor platform. There have been several sensing arrays that use MTPs as a platform for analysis, and a few representative examples are presented here.

4.1 Multi-Ion Imaging with Fluorescent Sensors

Wolfbeis used MTP arrays to develop a sensor for metal ions and mixtures that was made out of commercially available materials [37]. They chose six fluorescent indicators (Oregon Green BAPTA-5N, Magnesium Green, Sodium Green, Lucigenin, Phen Green FL, and Oregon Green BAPTA-5N with $\text{Ba}(\text{NO}_3)_2$) that all had similar excitation wavelengths (470 nm), emission wavelengths (> 505 nm), and decay times (2–6 ns) so that a single blue LED light source could be used for each well of a 96-well MTP. Each indicator was dispersed in a thin film of poly(ethylene glycol), which dissolved upon addition of an aqueous analyte solution. A phosphorescent bead was also added to each well, which was illuminated by the light source but did not respond to the presence of an analyte. Dual lifetime referencing (DLR) was used to image the analytes. With DLR, each well is illuminated for a very short time (2 μs) by the LEDs, and a CCD camera is used to image the array during and after illumination. The difference between these two readings was recorded as the fluorescent response to the analyte. The use of DLR for a colorimetric readout made it imperative that all indicators have similar decay times. The second image was taken at a time when the fluorescent indicator had stopped emitting, but the phosphorescent indicator was still phosphorescing.

The data processing was simplified using threshold limits to display either red or green “on/off” signals. If a fluorophore emitted over a certain threshold limit, its signal was changed from red to green. Likewise, if analyte introduction caused a decrease in fluorescence, a low threshold limit would also change the signal from red to green. Some of these signals for several metal ions and mixtures are shown in Fig. 14.

This setup was later modified with fiber optics to reduce the image size from the array so that all 96 wells in a plate could be imaged simultaneously with a single CCD image [38]. This was also fitted with an LED array that allowed for each well in a 96-well plate to be illuminated by a single LED (Fig. 15). Again, DLR was used, and high and low threshold limits were employed to simplify the output signals. This setup could detect analytes at concentrations as low as 10 μM without signal amplification and could image

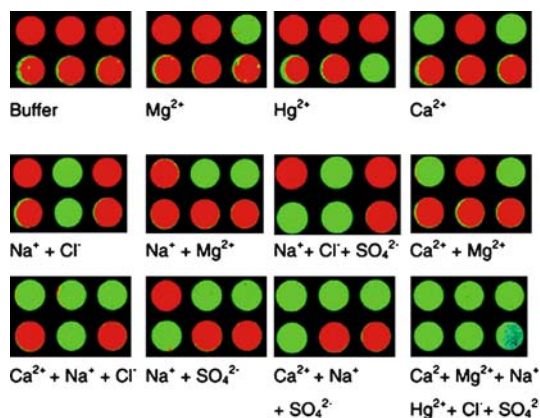


Fig. 14 Traffic light patterns for various ions and ion mixtures. Green indicates the presence of an ion, and red indicates the lack of an ion. Reprinted with permission from Wolfbeis et al. [37]. Copyright (2002) The Royal Society of Chemistry

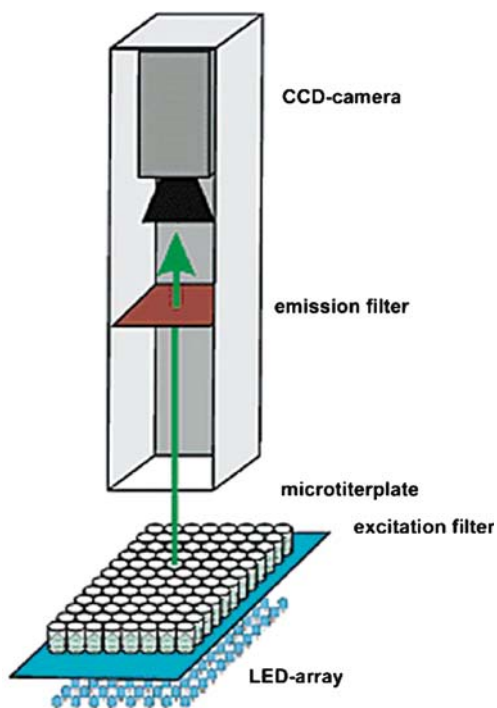


Fig. 15 Imaging setup used by Wolfbeis et al. for simultaneous illumination and imaging of a 96-well MTP array. An array of LEDs lights each well of the array, and, after passing through an emission filter, fiber optics are used to reduce the size of the image so that the CCD can view the entire array in one image. Reprinted with permission from Wolfbeis et al. [38]. Copyright (2003) American Chemical Society

an entire array in a few microseconds. Eight indicators were used to analyze five metal cations {Ca(II), Cu(II), Cd(II), Ni(II), Zn(II)}. A leave-one-out classification method was used to classify the analytes, and the technique was between 82.3% and 93.1% accurate at concentrations above 10 μ M. It was found that analytes that responded to greater numbers of indicators were more likely to be misclassified. The enhanced imaging capabilities and rapid data acquisition of this receptor system form a powerful imaging tool for array analysis.

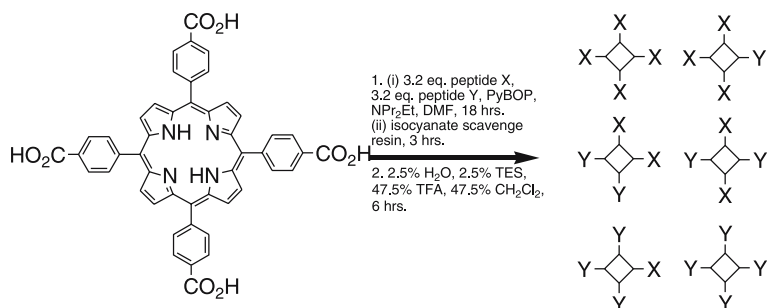
4.2

Fluorescent Porphyrins for Discrimination of Proteins

There is a current desire for robust sensing ensembles that can detect proteins in different environments without modification of the protein of interest. In many cases, fluorescently tagging a protein may cause unforeseen changes in its binding properties. Hamilton and co-workers have addressed this issue by developing an array of tetraphenylporphyrins (TPP) capable of detecting proteins in aqueous solutions [23]. TPPs have large hydrophobic surface areas and can be easily derivatized around the periphery. They also are highly fluorescent and can display fluorescence intensity changes upon protein binding [39].

Hamilton used a one-pot method to synthesize a 35-member library with varying charges (Scheme 2). Eight library members (A–H) were chosen with overall charges ranging from -8 to $+8$. A 96-well plate was used to observe the fluorescence change of each of the porphyrins upon incubation with one of four proteins (cytochrome *c*, cytochrome *c*551, and ferredoxin, and myoglobin). In the initial proof-of-concept article, the proteins were structurally different enough that characteristic fingerprints could be distinguished for each one (Fig. 16). In this case, the variable array response is a result of different charge characteristics of the four proteins. Cytochrome *c* ($pI = 10.6$), for example, bound mostly to the negatively charged porphyrins while ferredoxin ($pI = 2.75$) interacted strongest with the positively charged array members.

This approach was later expanded for analysis of non-metal containing proteins as well as protein mixtures through chemometric analysis with PCA [24]. Here, four proteins (cytochrome *c*, ferredoxin, lysozyme, and α -lactalbumin) as well as mixtures thereof were distinguished using the same eight porphyrin array (A–H) and separated graphically with a 3D Euclidian plot (Fig. 17). Note that a mixture of a strong interacting protein (cytochrome *c*) and a weak interacting protein (lysozyme) was clearly distinguished from both of the individual proteins. This suggests that both analytes were distinguished by the array, and that cytochrome *c* did not “mask” lysozyme. Also, analysis was done both with the original 8-member TPP array and with a 16-member array (A–P) and the results were compared. In this



21

	R ₁	R ₂	R ₃	R ₄
A	TyrAsp	TyrAsp	TyrAsp	TyrAsp
B	TyrAsp	TyrAsp	TyrAsp	LysPent
C	TyrAsp	Lys	Lys	TyrAsp
	Lys	TyrAsp		
D	Lys	Lys	Lys	LysPent
E	TyrLys	LysPent	LysPent	TyrLys
	LysPent	TyrLys		
F	Asp	Asp	Asp	Asp
G	TyrAsp	TyrLys	TyrLys	TyrAsp
	TyrLys	TyrAsp		
H	Lys	LysPent	LysPent	Lys
	LysPent	Lys		
I	TyrLys	TyrLys	TyrLys	TyrLys
J	Lys	Lys	Lys	Lys
K	Asp	Asp	Asp	TyrLys
L	Asp	Asp	Asp	Lys
M	Asp	Asp	Asp	LysPent
N	Asp	Asp	Asp	TyrAsp
O	Lys	Asp	Asp	Lys
	Asp	Lys		
P	Lys	TyrLys	TyrLys	Lys
	TyrLys	Lys		

Scheme 2 Mixed condensation strategy used for synthesis of porphyrin library 21 and porphyrins used for 8-member (A–H) and 16-member (A–P) array analysis

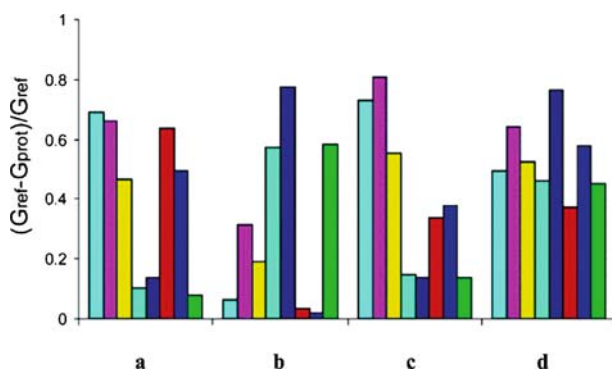


Fig. 16 Patterns for cytochrome c (14), ferredoxin (15), cytochrome c551 (16), and myoglobin (17) based on the eight-membered array of TPP derivatives. The bars quantify the extent of color attenuation measured as the quantity $(G_{\text{ref}} - G_{\text{prot}})/G_{\text{ref}}$ where G_{ref} is the average gray value for the blank wells and G_{prot} is the average gray value for the wells with proteins. Reprinted with permission from Hamilton et al. [23]. Copyright (2004) American Chemical Society

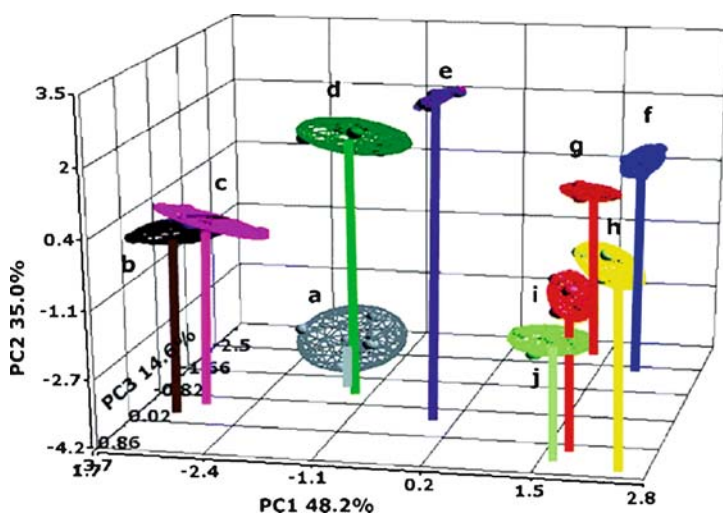


Fig. 17 3D PCA image of proteins identified by an 8-member array. Porphyrin concentrations are 7.5 mM (1.5e) or 15 mM (3e). Abbreviations: ferredoxin (FD), α -lactalbumin (Lact), lysozyme (Lys), cytochrome c (Cyt). Samples: **a** Lact1.5e, **b** FD1.5e, **c** FDLact1.5e, **d** CytFD1.5e, **e** CytFD3e, **f** Cyt3e, **g** Cyt1.5e, **h** CytLys3e, **i** CytLys1.5e, **j** Lys1.5e. Reprinted with permission from Hamilton et al. [24]. Copyright (2006) American Chemical Society

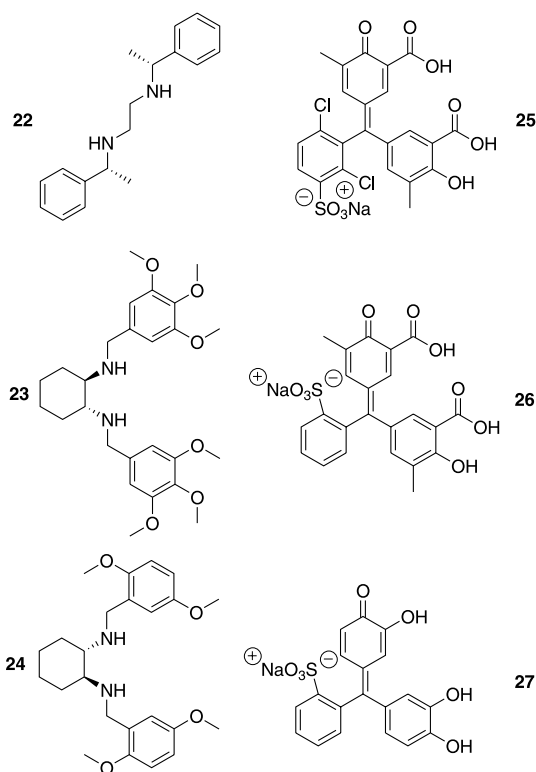
case, better separation was obtained by increasing the size of the array; the average overall separation increased from 1.27 to 1.62.

4.3

Enantioselective Discrimination of Amino Acids

Assays capable of closely mimicking the mammalian gustatory system will require the enantioselective discrimination of bioanalytes. To do this, we created an array of chiral inorganic coordination complexes capable of discriminating D- and L-amino acids [40]. The use of a 96-well MTP array alleviated the synthetic requirement of attaching the receptors to a solid support. Ligand **24** has been used previously to quantify enantiomeric excess of amino acids, and it was found that receptors **22** and **23** bound preferentially to L-amino acids while **24** showed preference for D-amino acids. Varying the ligand/indicator combinations as well as the concentrations of ligand, indicator, and Cu(II), created an array of 21 IDAs for analysis of each amino acid.

Notably, in this case, the PCA analysis indicated that binding affinity and chirality were identified as the two most important components of variance (Fig. 18). As can be seen in Fig. 18A, all of the L-amino acids have positive PC2 values while all of the D-amino acids have negative PC2 values. Also, the bind-



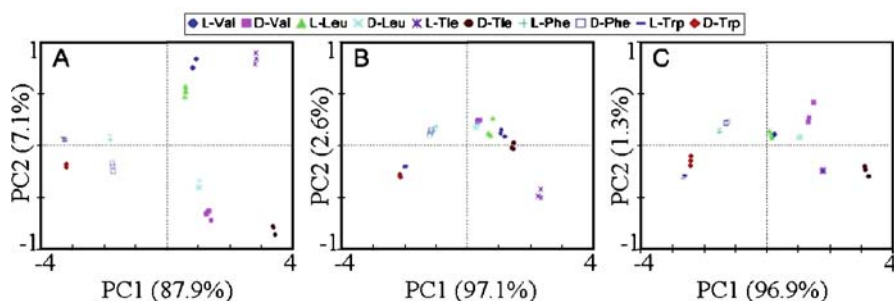


Fig. 18 2D PCA score plots display separation of amino acids using **A** receptors with both enantiomeric preferences, **B** only receptors selective for D amino acids, and **C** only receptors selective for L amino Acids. Reprinted with permission from Anslyn et al. [40]. Copyright (2006) American Chemical Society

ing constants increase as you move left to right along the PC1 axis so that the weakest binding amino acid (D,L-tryptophan) had the smallest PC1 value and the strongest binding amino acid (D,L-*tert*-leucine) had the largest PC1 value. Omission of the array data for ligands of either enantiomeric preference resulted in incomplete separation of the analytes (Fig. 18B,C). This is similar to the human taste response to amino acids in which D-amino acids are sweet and L-amino acids are bitter. It was concluded that this was likely the result of using oppositely biased receptors in the array.

5 Biomolecules for Array Development

The secondary structures of biomolecules can often be easily modified and tailored through small changes in primary structure. Landry has recently exploited this phenomenon by creating a library of receptors with nucleic acid based three-way junctions that form lipophilic cavities [41]. These were then used in an array format to fingerprint hydrophobic analytes.

Three-way junctions are created at the intersection of three double helices. At the site of intersection, a lipophilic cavity composed of three aromatic surfaces of unstacked base pairs is formed. It was shown that the introduction of unmatched base pairs in the stems could alter the shape of the cavities, leading to the formation of several different receptors. Systematically introducing a phosphorothioate group to the aptamer and then reacting with a thiol-reactive fluorophore incorporated a fluorescent tag (Fig. 19). In this way the fluorophore is positioned so that it sits in the binding cavity and is displaced by the analyte, causing a change in fluorescence. Varying the position of the phosphothioate group further increased the number of receptors created.

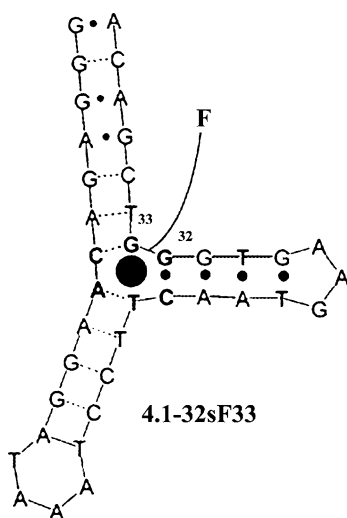


Fig. 19 Structure of the modified cocaine variant (4.1-32sF33). Reprinted with permission from Landry et al. [41]. Copyright (2003) American Chemical Society

A nine-member array was used to fingerprint four analytes as shown in Fig. 20. At the concentrations used for this analysis, receptor 4.1-32sF33 (Fig. 19) displayed nearly the same response for each analyte. This exemplifies how a single receptor would not have been able to discriminate these analytes, but an array of receptors could. This array was also used to quantitatively identify each analyte. As a final example of the utility of this system, array responses from standard and doped urine samples were compared. The fingerprint for a standard urine sample was compared to samples doped with either dehydroisoandrosterone 3-sulfate or deoxycorticosterone 21-glucoside.

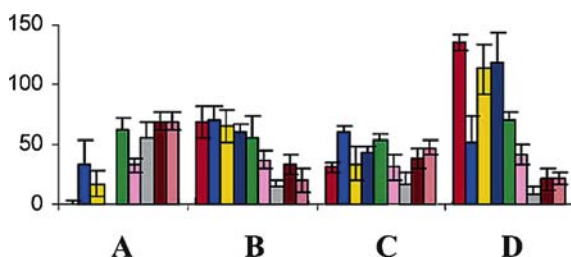
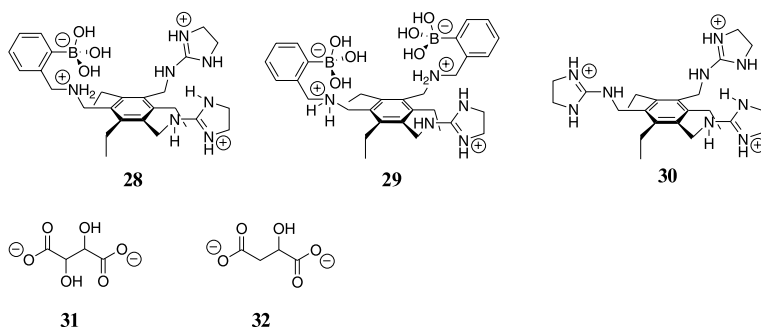


Fig. 20 Patterns based upon the responses of eight three-way junction receptors toward the following hydrophobic guests: **A** cocaine hydrochloride (500 μM) **B** deoxycorticosterone 21-glucoside (32 μM) **C** dehydroisoandrosterone 3-sulfate sodium (125 μM) and **D** sodium deoxycholate (2 mM). Triplicate measurements were taken and standard deviations are shown. Concentrations were used for each guest that would result in a 50–70% fluorescence intensity response. Reprinted with permission from Landry et al. [41]. Copyright (2003) American Chemical Society

Several of the receptors were unresponsive in this test, but the ones that were responsive created distinguishable response patterns. The nonresponsive receptors were presumably swamped by the naturally occurring steroids in the standard sample.

6 Multicomponent Sensing Ensembles

Many molecular recognition applications require the distinction of structurally similar analytes. It is often difficult to design synthetic receptors that are selective for analytes that differ by only a few atoms. To surmount this problem, we designed a multicomponent sensor consisting of two receptors, **28** and **29**, and two indicators, bromopyrogallol red and pyrocatechol violet (**27**) [42]. When all four of these components are mixed in one solution, the indicators and receptors interact reversibly and a single characteristic UV-Vis absorption spectrum is observed. Tartrate (**31**) and malate (**32**), which differ by only a single hydroxyl group, were used for analysis. In previous studies, **28** was found to bind tartrate and malate with similar affinity while **29** had greater affinity for tartrate than malate.



An array was created in which the concentration of tartrate and malate were varied from 0–1.2 mM independently (receptor and indicator concentrations held constant). The absorption changes at 27 wavelengths were recorded and analyzed with an ANN. Of the 49 different conditions examined, 45 were used as the training set for the ANN, and four were input as unknowns. The trained ANN was able to correctly predict the concentrations of both tartrate and malate with a maximum error of 6%, which was subsequently reduced to 2% with further training. Therefore, a single reading was sufficient to determine the concentration of two analytes in solution that would have been difficult to distinguish with a single sensor.

Encouraged by these results, we decided to apply this technique to a real world application [43]. A two component sensing system was developed

using a *tris*-guanidinium receptor **30** and the commercial dye xylenol orange. With this sensing ensemble, several flavored vodkas were analyzed, and their citrate and calcium contents were estimated using an ANN. The *tris*-guanidinium host interacts with the indicator and citrate, and the indicator interacts with the host as well as with Ca(II). Varying the relative concentration of citrate and calcium generated a unique balance between the complexed analytes in solution. Keeping the concentration of host and indicator constant, UV-Vis data was obtained from 80 different citrate/Ca(II) mixtures and 75 were used as the training set for an ANN. During training, a 25% (v/v) generic vodka in water solution was used so that the other components in the vodka were held constant. The trained ANN was then used to predict the citrate and calcium concentrations in the five control samples not used for training as well as five artificially flavored vodkas. The ANN gave predictions within 30% of the actual values for the control samples. NMR analysis was used to verify the citrate concentrations predicted by the ANN. It was determined that the error in these samples was between 1.5 and 33%. This work nicely demonstrates the application of newly developed sensing techniques to a real world application.

6.1

Dynamic Combinatorial Libraries as Sensors

A dynamic combinatorial library (DCL) is the result of the combination of several interacting components under thermodynamic control [44]. These reversible interactions create a virtual library consisting of every possible combination of the DCL components. The tartrate/malate sensing ensemble mentioned above is actually a DCL composed of all possible receptor/

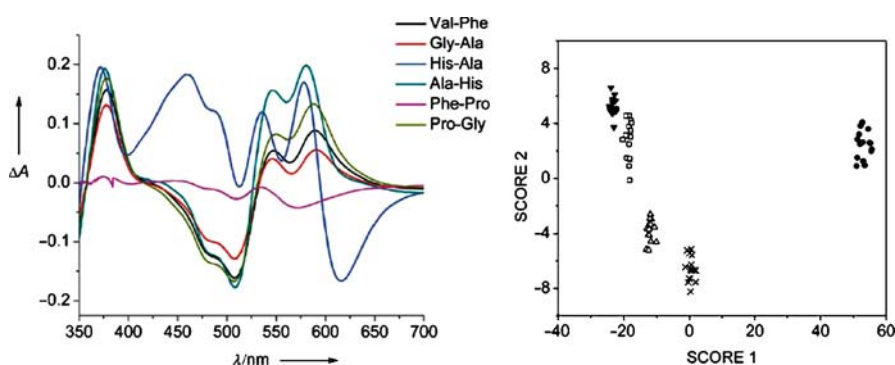


Fig. 21 **A** Variations in the UV-Vis spectrum of a DCL upon addition of various dipeptides. **B** LDA plot displaying the differentiation of five dipeptides: Gly-Ala (dark circles), Val-Phe (white squares), Ala-Phe (dark triangles), Phe-Ala (white triangles), and D-Phe-Ala (crosses). Reprinted with permission from Severin et al. [45]. Copyright (2005) Wiley

indicator combinations all interchanging reversibly. Introduction of an analyte to a DCL that interacts with one or more of the library members will shift the equilibrium of the system and thus the concentration of the actual library members.

Severin has presented a method for differentiating dipeptides with a DCL [45]. Elegantly demonstrating the potential simplicity of pattern-based systems, he used three metal coordinating indicators (arsenazo, methylcalcein blue, and glycine cresol red) and two metal salts to form a DCL with its own characteristic absorption spectrum. Introduction of a dipeptide to the DCL resulted in a characteristic shift in the spectrum (Fig. 21A). This absorption data was used as input for LDA analysis, and the graphical separation of the analytes can be seen in Fig. 21B. When a “jack-knife” classification matrix was used to identify the analytes the system correctly assigned the dipeptides 100% of the time. These impressive results clearly demonstrate the potential of DCLs for myriad sensing applications.

6.1.1

Optimization of DCLs

It has been further demonstrated that DCL sensors can be easily optimized for a particular application [46]. Three sequence isomeric tripeptide sequences HGG, GHG, and GGH were used as analytes with the goal of optimizing two DCLs for differentiation of either GHG and GGH, or HGG and GGH. The same dyes and metal ions used in Sect. 6.1 were employed here, and the concentrations of the metal cations were varied systematically. It was found that a high overall metal concentration was advantageous for both systems, but the relative metal concentrations were quite different. The optimized DCL for GHG and GGH consisted of a mixture of 25% Cu and 75% Ni while the optimized system for HGG and GGH consisted solely of copper ion. It was further demonstrated that, using the optimized DCL, it was possible to differentiate mixtures of GHG and GGH from pure samples and to quantitate the relative concentrations of these two analytes in the mixtures.

7

Other Arrays Using IDAs

7.1

Prescreening Libraries for Improved Differentiation

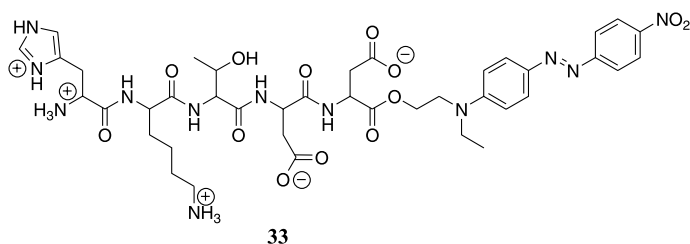
One particularly challenging set of substrates for sensing applications is the tachykinins. Tachykinins, α -neurokinin and substance P, are involved in pain transmission in the mammalian brain [47, 48]. It was hypothesized that a solution phase version of library 3 would be useful for differentiation of these

analytes (Wright et al., 2007, personal communication). This library utilized the same Cu(II) core with two tripeptide arms. One arm was consistently Lys-Gly-Asp while the other arm was synthesized via combinatorial chemistry. The results obtained from our previous work suggested that most of the receptors used for detection of tripeptides and tripeptide mixtures responded in a very similar manner to all of the analytes examined. The majority of the variance in the data (91%) was defined by a single PC axis and nearly all of the receptors had high loading values on this PC axis. This implies that none of the receptors were very selective for any of the tripeptides.

To transcend this problem, we prescreened this library with a UV-active tachykinin analogue **33** in order to identify receptors with selectivity for the analytes in question. After screening, it was found that only 0.5% of the receptors significantly bound the chromophore. Six of these receptors were sequenced, and it is evident from the results (Table 2) that hydrophobic groups were essential for binding **33**. These six receptors were combined with Cu(II)Cl₂, Cu(II)OTf, or Cd(II)OAc in a 96-well plate to form an 18-member array. Four α -neurokinin analogues (His-Lys-Thr, His-Glu-Thr, His-Lys-Thr-Asp, and His-Lys-Thr-Asp-Ser-Phe-Val-Gly-Leu-Met-C(O)-NH₂) as well as substance P (Arg-Pro-Lys-Pro-Gln-Gln-Phe-Phe-Gly-Leu-Met-C(O)-NH₂) were analyzed with this array. The PCA plot shows good separation and tight clustering for all the analytes (Fig. 22). There was also a signifi-

Table 2 Receptors A–F were chosen after a pre-screening process for inclusion in an array used to differentiate tachykinines. The tripeptide arms created through combinatorial chemistry were sequenced to look for similarities in the structure of the chosen receptors

Library member	R1	R2	R3
A	Ala	Asp	Ile
B	Thr	Phe	Thr
C	Thr	Met	Phe
D	Asp	Asp	Ser
E	Pro	Lys	Met
F	Arg	Met	Met



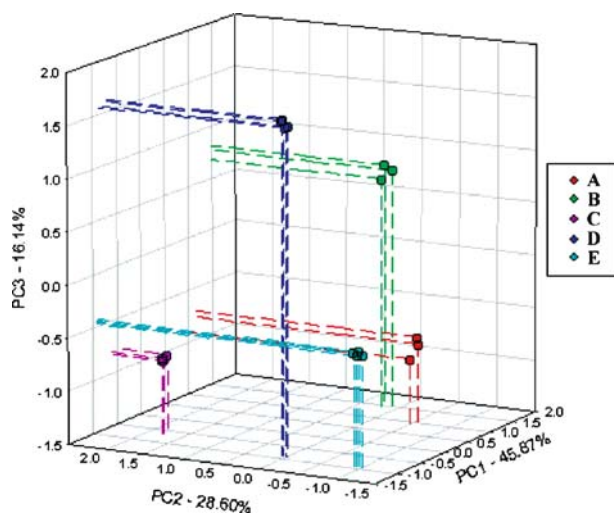


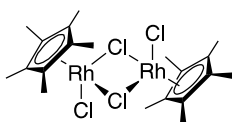
Fig. 22 A 3D-PCA plot shows tight clustering and good separation of analytes: **A** His-Lys-Thr **B** His-Glu-Thr **C** His-Lys-Thr-Asp **D** His-Lys-Thr-Asp-Ser-Phe-Val-Gly-Leu-Met-C(O)-NH₂ and **E** Arg-Pro-Lys-Pro-Gln-Gln-Phe-Phe-Gly-Leu-Met-C(O)-NH₂. The large percentage of variance on all three PC axes is indicative of increased differential ability of a prescreened library in comparison to previous libraries

cant amount of variance along all three of the PC axes used, which indicates good differentiation ability of the receptors in the array. Thus, the discriminatory ability of this smaller array (18 array members total compared to 35) is significantly increased due to the prescreening process.

7.2

Discrimination of 20 Natural Amino Acids

Several elegant studies exemplifying the simplicity with which array-based systems can be implemented have come from Severin's lab [49]. In one such example, it was shown that all 20 natural amino acids could be discriminated using just one organometallic receptor, **34**, and three commercially available indicators (gallocyanine, xylenol orange, and calcein blue). The amino acids were first analyzed with **34** and gallocyanine and divided into high-affinity (group I: His, Cys, Met, Asp, Asn) and low-affinity (group II) groups. The



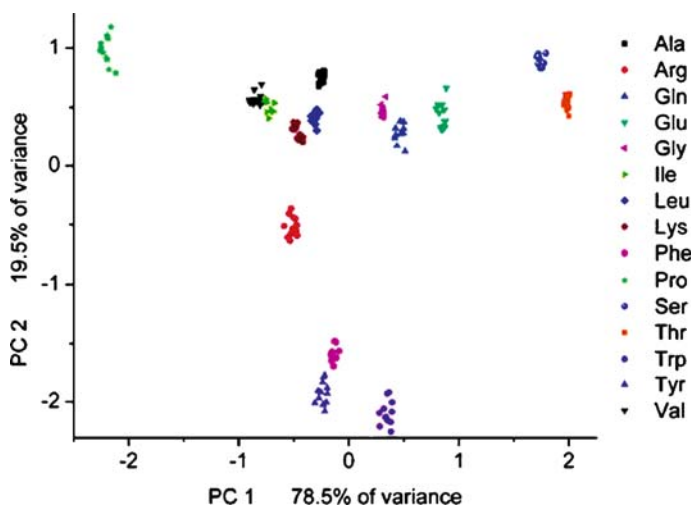


Fig. 23 PCA score plot for Group II amino acids. The two principal component axes contain 98% of the variance in the original data set. Reprinted with permission from Severin et al. [49]. Copyright (2005) American Chemical Society

high-affinity group was then analyzed with **34** and xylenol orange and calcein blue at different pH values while the low affinity group was analyzed further with **34** at several pHs. This data was used for LDA analysis and the predictive ability of the array was tested using a cross-validation routine. For group I, all data was correctly categorized 100% of the time. Group II gave accurate assignments 99.4% of the time. The group II amino acids were also graphically separated using PCA as shown in Fig. 23. All of the amino acids are loosely grouped based on the nature of the side chain (e.g. aromatic, aliphatic, etc.). Valine and isoleucine are the only two that somewhat overlap and were also misclassified most during LDA analysis. Systems such as this, in which useful analytical data can be obtained with little or no synthesis, are certainly a tribute to the power of chemometric analysis.

7.3

IDAs for Identification of Amino Sugars and Aminoglycosides

It has recently been demonstrated that IDA arrays can be made using only one receptor/indicator combination at various pH values [50]. Using the same rhodium complex, **34**, as above, several amino sugars and aminoglycosides were discriminated. To form an array, each analyte was used in an IDA with gallocyanine at pH 7, 8, and 9. After repeating each measurement eight times the data was analyzed by LDA. All of the analytes were clearly separated and well clustered, including stereoisomers glucosamine, galactosamine, and mannosamine (Fig. 24). To investigate the influence of concentration on this

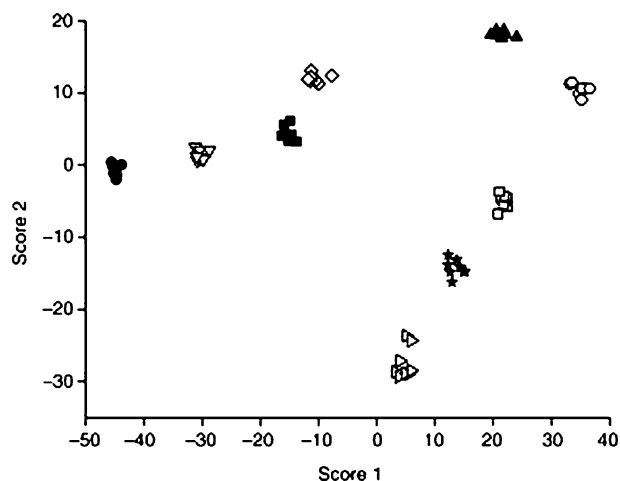


Fig. 24 Two-dimensional LDA plot from analysis of glucosamine (*light squares*), galactosamine (*light circles*), mannosamine (*light diamonds*), kanamycin A (*dark circles*), kanamycin B (*light downward triangles*), amikacin (*dark triangles*), apramycin (*dark squares*), paromomycin (*dark stars*), and streptomycin (*light triangles*). Reprinted with permission from Severin et al. [50]. Copyright (2006) Wiley

array, kanamycin A and kanamycin B were analyzed in an identical manner at concentrations of 50, 80, 100, and 120 μM . In this case, both analyte identity and concentration were distinguishable. This is a powerful observation in that only three measurements are required to distinguish these two analytes. Mixtures of aminoglycosides were also examined and compared to the responses of the individual analytes. As expected, the mixtures fall in between the individual analytes on the LDA plot.

7.4

Detection of Carbohydrates Through pH Changes

Chang et al. have created an array that can discriminate several carbohydrates without the amine handle required in the system discussed above [51]. This array uses two commercially available boronic acids with 12 pH sensitive dyes. The two boronic acids have different pK_a 's, which affect the pH of the solutions in the array. The main variables in this system are the pK_a 's of the carbohydrates analyzed as well as the analytes affinity for the boronic acids. Both of these work synergistically to affect the response, which is visualized by the indicator. The array data was analyzed with LDA and PCA. A PCA plot could not sufficiently discriminate all 23 carbohydrates tested, but the LDA analysis gave 100% accurate discrimination of the all analytes. To simplify the system, six indicator/boronic acid combinations were used in a minimal array analysis. It was found that this minimal array was 98% ac-

curate. This illustrates the first colorimetric array for the detection of a large number of unfunctionalized carbohydrates in aqueous solution. However, the pH change required for the success of this system excludes it from application to biological systems that are often buffered.

8 Conclusion

The implementation of differential sensing arrays and assays has allowed scientists to analyze a variety of analytes and mixtures. Through a combination of differential sensing and chemometric analysis, single sensing arrays can be tailored for the detection of structurally similar analytes as well as large and complex biomolecules. Several of these arrays have been applied to real-world situations. Further development of these types of sensors will certainly provide new opportunities in environmental, biological, and medical diagnostic applications.

Acknowledgements We would like to thank the National Institutes of Health for their generous funding in support of our own work presented in this chapter.

References

1. Doty RL (2003) Handbook of Olfaction and Gustation, 2nd edn. Marcel Dekker, New York
2. Axel R (2005) *Angew Chem Int Ed* 44:6111
3. Lavigne JJ, Anslyn EV (2001) *Angew Chem Int Ed* 40:3118
4. Albert KJ, Lewis NS, Schauer CL, Sotzing GA, Stitzel SE, Vaid TP, Walt DR (2000) *Chem Rev* 100:2595
5. Epstein JP, Walt DR (2003) *Chem Soc Rev* 32:203
6. Toko K (1998) *Biosens Bioelectron* 13:701
7. Toko K (1998) *Meas Sci Technol* 9:1919
8. Walt DR (1998) *Acc Chem Res* 31:267
9. Laukis LR (1998) *Acc Chem Res* 31:317
10. Jurs PC, Bakken GA, McClelland HE (2000) *Chem Rev* 100:2649 and references therein
11. Jolliffe IT (2002) *Principal Component Analysis*, 2nd edn. Springer, Berlin Heidelberg New York
12. Brereton RG (2003) *Chemometrics Data Analysis for the Laboratory and Chemical Plant*. Wiley, Chichester, West Sussex, UK
13. Burns JA, Whitesides GM (1993) *Chem Rev* 93:2583
14. Lavigne JJ, Savoy S, Clevenger MB, Ritchie JE, McDonie B, Yoo S-J, Anslyn EV, McDevitt JT, Shear JB, Neikirk D (1998) *J Am Chem Soc* 120:6429
15. Goodey A, Lavigne JJ, Savoy SM, Rodriguez MD, Curey T, Tsao A, Simmons G, Wright J, Yoo S-J, Sohn Y, Anslyn EV, Shear J, Neikirk DP, McDevitt JT (2001) *J Am Chem Soc* 123:2559

16. Christodoulides N, Tran M, Floriano PN, Rodriguez M, Goodey A, Ali M, Neikirk D, McDevitt JT (2002) *Anal Chem* 74:3030
17. Curey TE, Goodey A, Tsao A, Lvigne J, Sohn Y, McDevitt JT, Anslyn EV, Neikirk D, Shear JB (2001) *Anal Biochem* 293:178
18. McCleskey SM, Griffin MJ, Schneider SE, McDevitt JT, Anslyn EV (2003) *J Am Chem Soc* 125:1114
19. Wright AT, Griffin MJ, Zhong Z, McCleskey SM, Anslyn EV, McDevitt JT (2005) *Angew Chem Int Ed* 44:6375
20. Wright AT, Anslyn EV, McDevitt JT (2005) *J Am Chem Soc* 127:17405
21. Wiskur S, Ait-Haddou H, Lavigne JJ, Anslyn EV (2001) *Acc Chem Res* 34:963
22. Schneider SE, O'Neil SN, Anslyn EV (2000) *J Am Chem Soc* 122:542
23. Baldini L, Wilson AJ, Hong J, Hamilton AD (2004) *J Am Chem Soc* 126:5658
24. Zhou H, Baldini L, Hong J, Wilson AJ, Hamilton AD (2006) *J Am Chem Soc* 128:2421
25. Wright AT, Anslyn EV (2004) *Org Lett* 6:1341
26. Goodey AP, McDevitt JT (2003) *J Am Chem Soc* 125:2870
27. Wei S, Jakusch M, Mizaikoff B (2006) *Anal Chim Acta* 578:50
28. Haupt K (2001) *Analyst* 126:747
29. Hirsch T, Kettenberger H, Wolfbeis OS, Mirsky VM (2003) *Chem Commun*, p 432
30. Greene NT, Morgan SL, Shimizu KD (2004) *Chem Commun*, p 1172
31. Greene NT, Shimizu KD (2005) *J Am Chem Soc* 127:5695
32. Rakow NA, Suslick KS (2000) *Nature* 406:710
33. Zhang C, Suslick KS (2005) *J Am Chem Soc* 127:11548
34. Zhang C, Bailey DP, Suslick KS (2006) *J Agric Food Chem* 54:4925
35. Reddy MM, Kodadek T (2005) *Proc Natl Acad Sci* 102:12672
36. Zimmerman R, Basabe-Desmots L, van der Baan F, Reinhoudt DN, Crego-Calama M (2005) *J Mater Chem* 15:2772
37. Mayr T, Liebsch G, Klimant I, Wolfbeis OS (2002) *Analyst* 127:201
38. Mayr T, Igel C, Liebsch G, Klimant I, Wolfbeis OS (2003) *Anal Chem* 75:4389
39. Jain RK, Hamilton AD (2000) *Org Lett* 2:1721
40. Folmer-Andersen JF, Kitamura M, Anslyn EV (2006) *J Am Chem Soc* 128:5652
41. Stojanovic MN, Green EG, Semova S, Nikic DB, Landry DW (2003) *J Am Chem Soc* 125:6085
42. Wiskur SL, Floriano PN, Anslyn EV, McDevitt JT (2003) *Angew Chem Int Ed* 42:2070
43. McCleskey SC, Floriano PN, Wiskur SL, Anslyn EV, McDevitt JT (2003) *Tetrahedron* 59:10089
44. Rowan SJ, Cantrill SJ, Cousins GRL, Sanders JKM, Stoddart JF (2002) *Angew Chem Int Ed* 41:898
45. Buryak A, Severin K (2005) *Angew Chem Int Ed* 44:7935
46. Buryak A, Severin K (2006) *J Comb Chem* 8:540
47. Page NM (2005) *Peptides* 26:1356
48. Severini C, Improta G, Falconieri-Erspamer G, Salvadori S, Erspamer V (2002) *Pharm Rev* 54:285
49. Buryak A, Severin K (2005) *J Am Chem Soc* 127:3700
50. Zaubitzer F, Buryak A, Severin K (2006) *Chem Eur J* 12:3928
51. Lee JW, Lee J-S, Chang Y-T (2006) *Angew Chem Int Edn* 45:6485

Analyte Sensing Across Membranes with Artificial Pores

Stefan Matile (✉) · Hiroyuki Tanaka · Svetlana Litvinchuk

Department of Organic Chemistry, University of Geneva, Quai Ernest-Ansermet 30,
CH-1211 Geneva 4, Switzerland
stefan.matile@chiorg.unige.ch

1	Introduction	220
2	Sensing with Synthetic Pores	224
2.1	Concepts	224
2.2	Synthetic Multifunctional Pores	226
2.3	Optical Transduction of Chemical Reactions	232
2.4	Enzymes as Specific Signal Generators	235
2.5	Multicomponent Sensing in Complex Matrixes	236
3	Sensing with Bioengineered Pores	237
3.1	Immunosensing	237
3.2	Stochastic Sensing of Single Analytes	240
3.3	Covalent Amplifiers	242
3.4	Cell-Penetrating Peptides as Optical Transducers	244
4	Porous Sensors in Membranes Beyond Lipid Bilayers	245
5	Related Topics	246
6	Summary	247
	References	248

Abstract This review covers synthetic pores as sensors, an interdisciplinary topic that may appeal not only to bioorganic and supramolecular but also to analytical, organic, or physical chemists. In the introduction, fundamental concepts and methods are briefly reiterated. The next section introduces synthetic pores as multifunctional supramolecules that are created from abiotic scaffolds and act in lipid bilayer membranes. Then follows the introduction of the concept of synthetic multifunctional pores as general optical transducers of chemical reactions. For this purpose, synthetic pores that recognize small changes in bulk and/or charge of as many substrates and products as possible are best, and internal π -clamps are added to catch elusive analytes. For multicomponent sensing in complex matrixes, synthetic pores as general transducers are combined with enzymes as specific signal generators. Realized examples of practical applications to samples from the supermarket describe synthetic pores as sensors of sugar in soft drinks. Section 3 focuses on sensing with biological and bioengineered pores. Selected topics, such as general electrical transduction in planar and supported lipid bilayer membranes, the concept of stochastic sensing of single analytes, immunosensing, covalent polynucleotide amplifiers, and single gene sequencing, are briefly spotlighted to also outline future perspectives with synthetic pore sensors. Section 4 briefly covers initial breakthroughs on sensing with synthetic pores in membranes other than lipid bilayers, such as functionalized conical gold and cylindrical carbon nanotubes.

Keywords Biosensors · Enzymes · Enzyme assays · Immunosensing · Ion channels · Molecular recognition · Pores

1 Introduction

The reason why pores are of interest as sensors is a practical one: their activity can be detected in many different ways [1]. A conventional setup to characterize synthetic pores by fluorescence spectroscopy uses large unilamellar vesicles (LUVs) that are loaded with fluorescent probes such as carboxyfluorescein (CF) at concentrations high enough for self-quenching (Figs. 1 and 2). Efflux through large enough pores results in fluorophore dilution and therefore disappearance of self-quenching. To determine activity, fluorogenic ef-

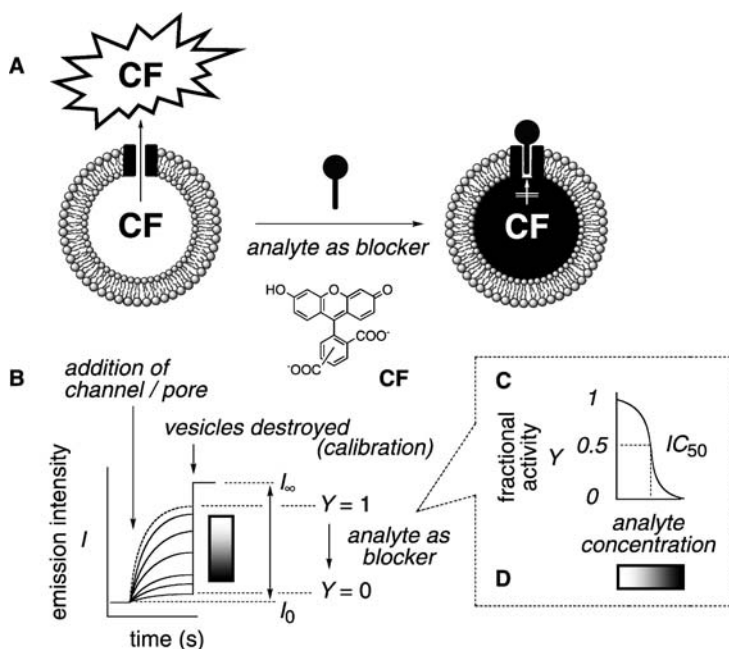


Fig. 1 Analyte detection with pores that close in response to chemical stimulation by fluorogenic CF efflux from vesicles (A). Pore activity as such is detected as increasing CF emission with time after pore addition (B, dotted lines). For analyte detection, the same experiment is repeated in the presence of increasing analyte concentrations. Decreasing CF emission with increasing analyte concentration is observed for analytes that act as blockers (B, solid lines). Hill analysis of dose–response curves reveals with the inhibitory concentrations (IC_{50}) the concentrations of maximal responsiveness for analyte sensing (C); naked-eye detection is possible as decreasing fluorescence with increasing analyte concentration (D)

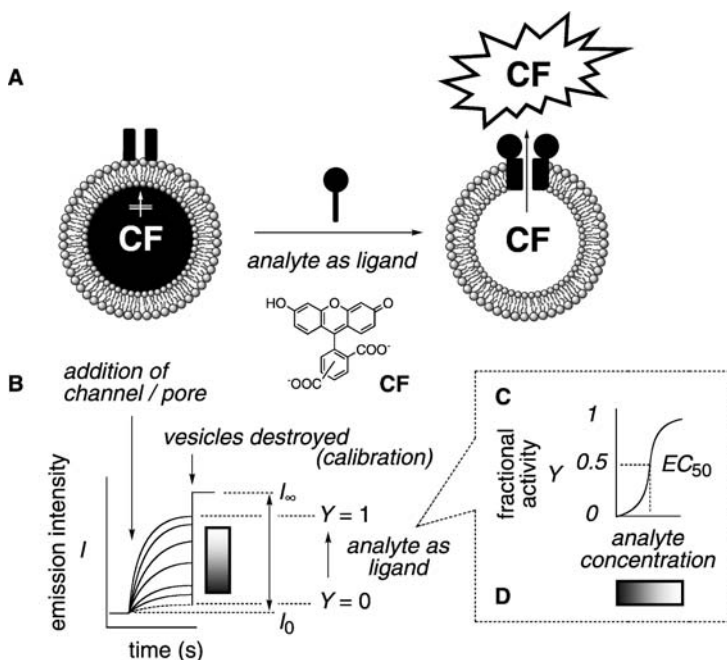


Fig. 2 Analyte detection with pores that open in response to chemical stimulation as increasing fluorogenic CF efflux from vesicles with increasing analyte concentration. Calibration curves (B) reveal with the effective analyte concentrations (EC_{50}) the concentrations of maximal responsiveness for sensing (C), also compatible with “naked-eye” detection (D, see Fig. 1 for details)

flux in response to the addition of synthetic ion channels or pores to the LUVs is usually measured as a function of time. All this is very easy to do, and compatible not only with multiwell-plate formats but also with just a hand-lamp or simply the “naked eye”.

A conventional setup to characterize synthetic ion channels and pores in planar or “black” lipid membranes (BLMs) uses two chambers named *cis* and *trans* that are filled with buffer (Fig. 3). Here, the *trans* chamber is arbitrarily connected to a reference electrode and the *cis* chamber to the input electrode. The BLM is formed in a tiny aperture (micrometers) between the two chambers. Without ion channel or pore, the BLM is an insulator because the electrolytes in the buffer cannot phase transfer across the hydrophobic core of the membrane. The current flowing through the ion channel or pore in the BLM is then recorded as a function of time. In multichannel experiments in BLMs and the related supported lipid bilayers on conducting surfaces, “macroscopic” currents flowing through many ion channels and pores are studied. In BLMs, the fast ion flux also allows resolution of the currents flowing through single ion channels and pores. These single-channel currents

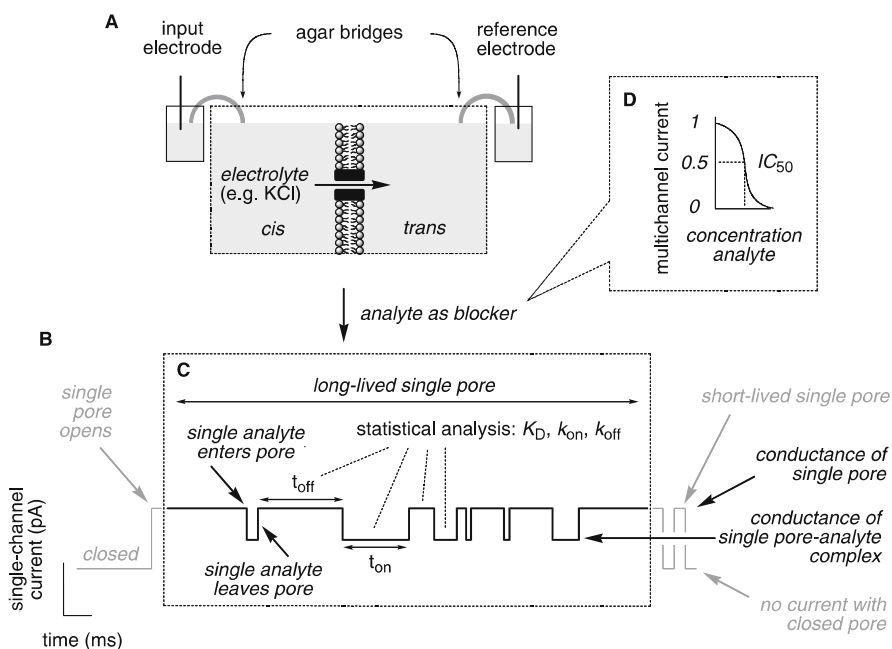


Fig. 3 Analyte detection with ion channels and pores as changes in (C) single and (D) multichannel conductance in planar bilayer lipid membranes. Pore activity as such can be detected as stochastic appearance and disappearance of one (or more) conductance levels after pore addition (A, B). Analytes that act as blockers can, at intermediate affinity, cause stochastic appearance and disappearance of one (or more) conductance levels for the analyte–pore complex on the single-molecule level (C) and, in any case, a global decrease in conductance on the multichannel level (D)

appear and disappear in a stochastic manner (Fig. 3b). The on–off transitions between open and closed channels are typical single-molecule phenomena that are invisible on the macroscopic or “multichannel” level and should not be confused with blockage or ligand gating (see below). The conductance of single ion channels or pores often relates to the inner channel diameter (from pico- to nano-Siemens). The lifetime is the “average” time single channels remain open and corresponds to their kinetic stability (often milliseconds, sometimes beyond minutes).

It is this variability to detect their activity, reaching from the single molecule to the naked eye, that makes ion channels and pores attractive for sensing. Detectability as fluorogenic efflux in vesicles is compatible with optical signal transduction. Pore closing (blockage, Fig. 1) or opening (ligand gating, Fig. 2) in response to analyte recognition is reflected as disappearance or appearance of color; dose–response curves readily reveal sensitivity and selectivity of the pore sensor. This method of detection has been used to introduce key topics of this review, such as the concept of synthetic pores as

general optical transducers of chemical reactions [2] and, in concert with enzymes as specific signal generators, as multicomponent sensors for complex matrixes [3, 4] (see Sects. 2.3–2.5).

The possibility of stochastic detection of single analytes in single-channel measurements in BLMs has been recognized early on. With inert single pores that do not frequently open and close by themselves (Fig. 3b), the entering and leaving of single analytes of intermediate affinity can possibly be observed in a stochastic appearance and disappearance of a new conductance of single pore–analyte complexes (Fig. 3c). Statistical analysis of these “on–off” transitions for analyte recognition gives both thermodynamic and kinetic data for the pore–analyte complex. Different conductances and lifetimes for different pore–analyte complexes allow, in principle, for “fingerprint-type” analyte identification (see Sect. 3.2).

The idea to use pores as sensors grew out of structural and functional studies on biological ion channels and pores. Kramer’s “patch cramming”, introduced in 1990, uses biological ion channels as sensors of their own natural ligands, such as cGMP in intact nerve cells [5]. Modifications of biological ion channels and pores to introduce multifunctionality with respect to molecular recognition and transformation were initially motivated by the method development for this purpose. The substituted cysteine accessibility method (SCAM), for example, measures the effects of the reaction of small, charged methanethiosulfonates with engineered cysteines on ion-channel currents to determine the amino acid residues that form the ion-conducting pathway [6]. It was in 1994 that Finkelstein and Collier realized that reactions can not only be used to characterize ion channels, but also that ion channels can be used to characterize reactions, also on the single-molecule level [7]. One year later, Woolley and coworkers used the classical gramicidin ion channel to study thermal *cis–trans* isomerization [8]. The next year, the bold and far from realized vision to sequence single genes with pores was formulated by Deamer and Branton [9]. Again one year later, in 1997, Cornell and coworkers modified the same gramicidin channel with a biotin–streptavidin–biotin–antigene conjugate to serve as electrical transducer for immunosensing in supported lipid bilayers [10]. The next milestone was the introduction of stochastic sensing of single adamantane analytes by the group of Bayley and Braha in 1999, using the biological α -hemolysin pore with a cyclodextrin adapter [11].

The concept of synthetic ion channels and pores that can be opened and closed reversibly in response to chemical stimulation can arguably be traced back to inspired creations by Fuhrhop and coworkers in the late 1980s [12]. The first systematic approach to synthetic multifunctional pores was introduced in 1999 [13]. A synthetic pore that closes in response to molecular recognition—exemplified by DNA double helices—was reported in the following year [14], whereas synthetic ion channels and pores that open in response to molecular recognition appeared only very recently [15, 16]. Synthetic catalytic pores [17] were introduced a year before the concept of syn-

thetic pores as general optical transducers of chemical reactions in 2002 [2]. Three years later, in 2005, this concept was applied to demonstrate the ability of pores to sense analytes in samples from the supermarket (such as sugar in Coca-Cola) [3].

2 Sensing with Synthetic Pores

2.1 Concepts

Because of the variable and straightforward detectability of their activity, synthetic, bioengineered, or biological pores that are sensitive to chemical stimulation can be considered as primitive sensors, where signal generation by molecular recognition of the analyte, either a blocker or a ligand, can be combined with optical or electrical signal transduction for detection by variable readouts ranging from single molecules to the naked eye (Fig. 4a). In an ideal sensor, signal transduction is not limited to a single analyte but is as nonspecific as possible to assure broadest applicability [4]. As pointed out by Anslyn during the development of strategies to sense the age of Scotch, sloppy recognition is one of the underestimated key characteristics accessible with synthetic hosts [18, 19]. Synthetic pores are attractive as sensors because they offer the sloppy molecular recognition and translocation that is needed to assure signal generation and transduction that is as broad as possible.

Enormously appealing as such, the vision of synthetic pores as sensors operating as signal generators and signal transducers that are both as general as possible is conceptually insufficient for practical applications, such as multicomponent sensing in complex matrixes (e.g., see Sect. 2.5). General signal generation coupled with general signal transduction is obviously compatible with the detection of many different analytes. However, the highest possible interference will obstruct sensing in simple two-, three-, or four-component mixtures, not to speak of samples from the supermarket or the hospital.

The creation of pores with active sites for highly selective analyte recognition to couple general transduction with specific signal generation will obviously produce a sensor that works in complex matrixes, but only for the one analyte that is recognized (Fig. 4b). This approach is thus also incompatible with the vision of pores as multicomponent sensors in complex matrixes. No problem with interference, but new sensors would have to be produced for every analyte of interest.

Despite these conceptual limitations, most current approaches to sensing aim to couple specific generation and general transduction. The use of biological ion channels or pores in patch cramming to serve as sensors of their own ligand is an illustrative example of an approach that is naturally incompati-

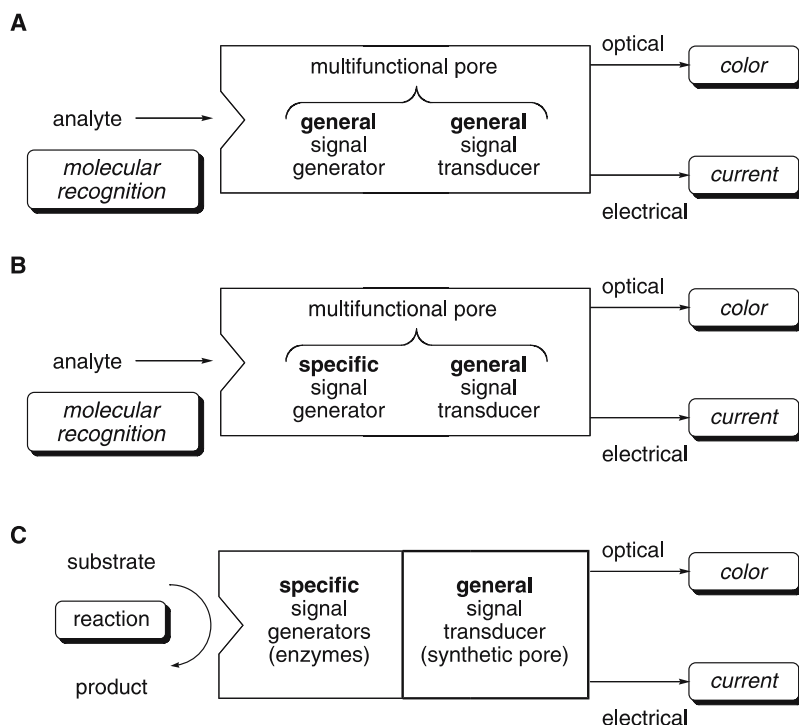


Fig. 4 Sensing with pores—concepts and possible misconceptions. **A** Multifunctional pores that generate and transduce signals with poor selectivity are incompatible with multicomponent sensing in complex matrixes because they can sense many different analytes but suffer from high interference. **B** Multifunctional pores that transduce signals with high selectivity are incompatible with multicomponent sensing in complex matrixes because they can sense one analyte only. **C** In combination with *decoupled* signal generators of high adaptability and high variability, multifunctional pores that transduce signals with poor selectivity are perfect for multicomponent sensing in complex matrixes. They can sense many different analytes and do not suffer from interference

ble with multicomponent sensing in complex matrixes [5]. Immunosensing with covalent attachment of antigen or antibody to the pore sensor suffers from the same lack of adaptability (although the creation of new sensors for new analytes is not very problematic in this case, see Sect. 3.1, [10]). The concept of stochastic sensing of single analytes with pores reverses rather than removes the source of incompatibility with multicomponent sensing in complex matrixes. It allows reduction of the specificity of analyte recognition, which naturally causes the reappearance of interference to obstruct sensing in simple mixtures of analytes (see Sect. 3.2, [11]).

In other words, the applicability of synthetic pores that recognize an analyte with high selectivity is limited to the sensing of that analyte, because the selectivity of signal generation is sufficient but not adaptable to different

analytes (Fig. 4b). Practical applicability of synthetic pores that recognize analytes with low selectivity is similarly limited, because multiple interference with general signal generation would hinder sensing in complex matrixes (Fig. 4a). It is the variable use of enzymes together with only one “universal” synthetic pore that produces the perfect combination of general signal transduction with decoupled, variable, and specific signal generation of an ideal biosensor (Fig. 4c). The fundamental nature of the resulting concept of synthetic pores as optical transducers of enzymatic reactions [2–4] is comparable with amperometric biosensing with electrical transduction of enzymatic reactions on the one hand [20, 21], and immunosensing with optical transduction of biomolecular recognition on the other [22].

2.2

Synthetic Multifunctional Pores

Synthetic multifunctional pores are synthetic pores that unify molecular translocation with molecular recognition and transformation, e.g., bind or convert analytes or substrates on their way across a lipid bilayer membrane [23]. Synthetic ion channels and pores are functional supramolecules that are constructed from scaffolds that do not occur in biological pores and can transport molecules across lipid bilayer membranes [24, 25]. Pore sensors with biological or chemically modified biological scaffolds are named bio-engineered pore sensors and are reviewed in Sect. 3; pore sensors that act in membranes other than lipid bilayer membranes are covered in Sect. 4.

The introduction of rigid-rod β -barrels provided synthetic access to multifunctional pores (Fig. 5) [13, 23]. In rigid-rod β -barrels, the nonplanar rigid *p*-octiphenyl rods serve as preorganizing “staves”. Self-assembly of these privileged scaffolds occurs by peptide interdigitation to produce antiparallel β -sheets and the rolling-up of the planar β -sheets by the nonplanar *p*-octiphenyl turns to give cylindrical supramolecular oligomers (rather than linear supramolecular polymers). Peptide rod conjugates **1** are synthesized from commercial biphenyls and amino acids in about 15–25 steps, depending on the nature of the peptide.

The multifunctionality of rigid-rod β -barrels **2–8** is introduced by internal and external pore design. The outer surface of synthetic multifunctional pores **2–6** is covered with leucine triads to maximize membrane affinity and barrel stability, whereas that of **7** features refined leucine–tryptophan–valine triads. In synthetic multifunctional pore **8**, external pore design is used for ligand gating [15, 26] (Figs. 2 and 6). Namely, amphiphilic argininophiles like pyrene, calixarene, or fullerene carboxylates recognize the external arginine arrays to increase the lipophilicity of the outer surface of pore **8**. The resulting improvement of barrel–membrane interactions yields open, ligand-gated pores in the bilayer that can still be blocked noncompetitively by internal α -helix recognition (Fig. 6).

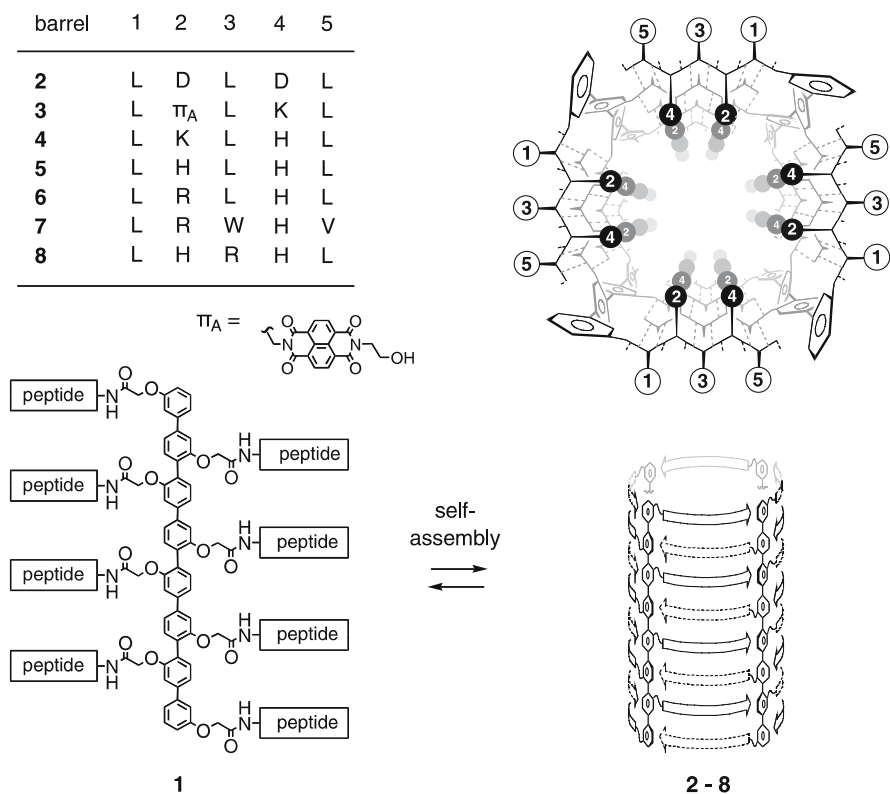


Fig. 5 Self-assembly of selected synthetic multifunctional pores 2–8 from *p*-octiphenyls 1. In axial view (*top*), peptide backbones in β -sheet conformation are given as *solid lines*, hydrogen bonds as *dotted lines*, external amino acid residues as *dark on white*, and internal ones as *white on dark* (single-letter abbreviations). In side view (*bottom*), β -sheets are given as *arrows* (N→C)

Internal pore design by varying amino acid residues 2 and 4 has been used to create pores that close in response to chemical stimulation (blockage). Histidine–histidine, histidine–lysine, histidine–arginine, and aspartate–aspartate dyads are positioned at the inner surface of synthetic rigid-rod β -barrels 2 and 4–8. These functional group arrays were envisioned for molecular recognition that is dominated by topologically matching ion pairing as well as acid/base catalysis with proximal histidines. Blockage of synthetic multifunctional pores 2–8 by internal molecular recognition has been realized in many variations (Figs. 1 and 6–9). Examples cover not only polymers like polysaccharides, polypeptides, DNA, RNA, or polyacetylenes, but also small molecules like nucleotides, carbohydrates, inositols, thiamines, *p*-oligophenyls, calixarenes, pyrenes, or naphthalenes and even ions like magnesium cations or pyrophosphate. Atomic force microscopy (AFM) images

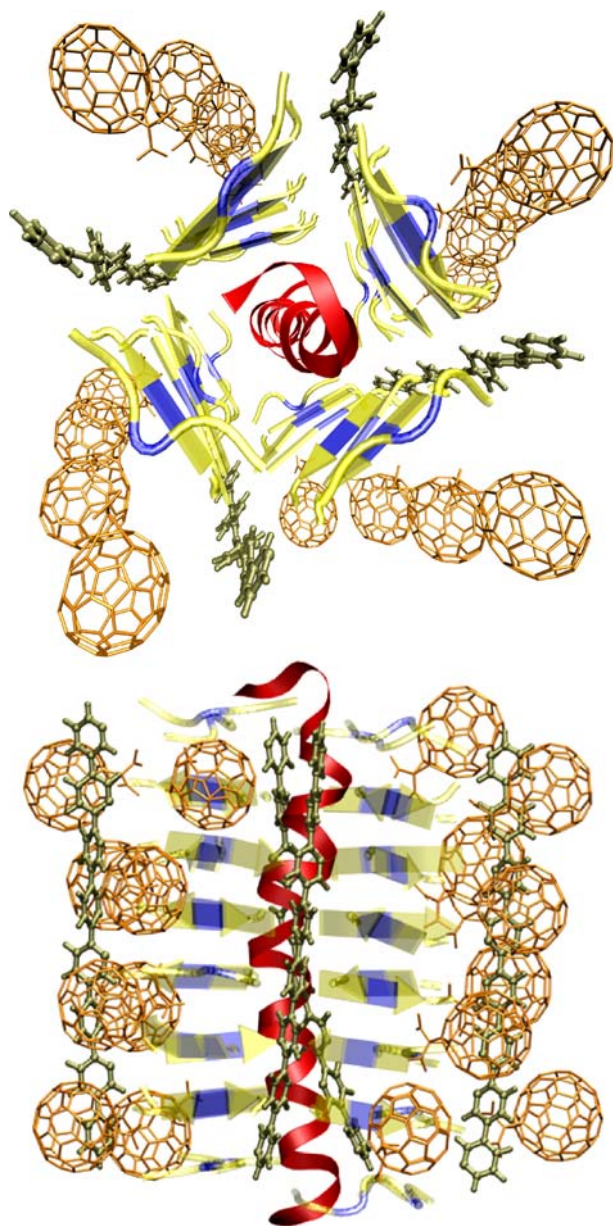


Fig. 6 Molecular model of pores **8** with external fullerene ligands (Bingel malonates, *spheres*) and internal α -helix blockers (polyglutamic acid, *red ribbon*). *p*-Octiphenyl staves are shown in ball-and-stick form, β -sheets as *arrows* (N \rightarrow C, compare Fig. 5). Adapted from [26], © Elsevier 2005

of pore-polymer complexes confirmed the existence of pseudo-rotaxanes as well as their formation by threading of the polymer blocker through pre-assembled barrel pores on the single-molecule level [27].

Recognition motifs of interest with synthetic pores include preorganized ion pairing and π -clamping, as well as topological matching and the depth of recognition. Excellent recognition was found for pyrene-1,3,6-trisulfonates **9** including Cascade Blue derivatives (CBs) [23, 28–30] (Fig. 7). The weak dependence on the nature of the substituent has already been applied to catalysis and seems particularly promising for the amplification of optical transduction with pore sensors. Perfect spatial preorganization of ion pairing with cationic residues on one face of a β -sheet was proposed as the origin of CB recognition within rigid-rod β -barrel pores such as **4**.

The artificial amino acid π_A in pore **3** was introduced for ion-pair assisted adhesive π -clamping between the sticky, positively charged surfaces of two naphthalenediimides [31]. Compared to pore **4** without π -clamps, molecular recognition of anionic aromatics such as π -basic dialkoxynaphthalenes **10** by pore **3** was up to 40 times better, depending on the electronic nature of the clamped arene (Fig. 7). About five to ten times weaker recognition of compa-

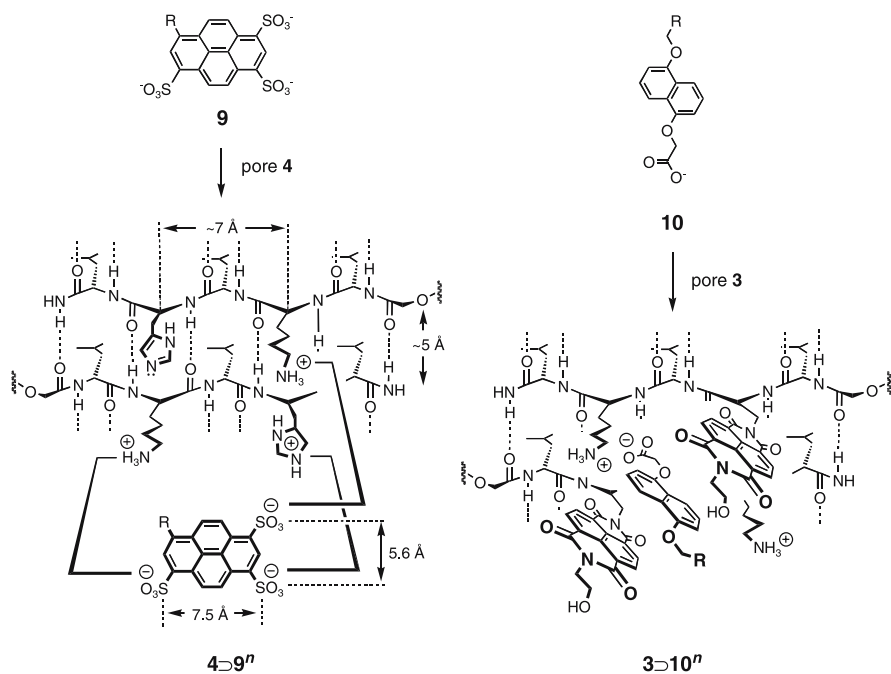


Fig. 7 Recognition motifs of interest with synthetic multifunctional pores include topological matching of ion pairing between pyrenetrisulfonate **9** and the internal cationic residues of pore **4**, or ion-pair assisted π -clamping of dialkoxynaphthalenes **10** by internal naphthalenediimide (NDI) residues of pore **3**. R is variable

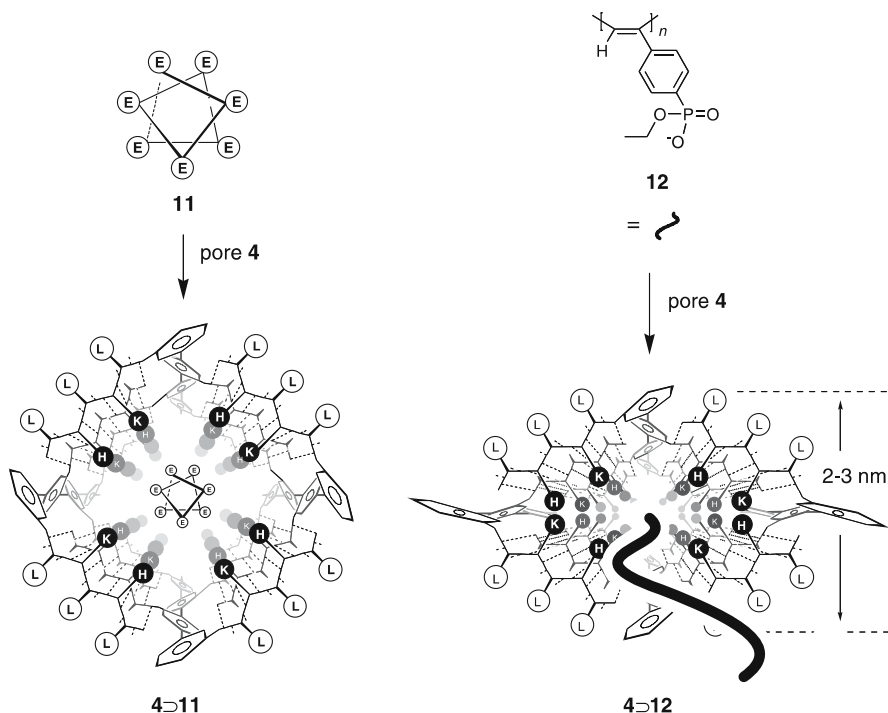


Fig. 8 α -Helix recognition as an example of molecular recognition by topological matching (*left*) and barrel contraction around poly(phenylacetylene) **12** as an example of guest \rightarrow host template effects to compensate for topological mismatch (*right*)

rable π -acidic aromatics indicated that π -clamping of π -basic aromatics like **10** within π -acidic pore **3** involves charge-transfer complex formation. Molecular recognition of comparable anionic alkyls by π -clamp **3** naturally was more than three orders of magnitude weaker.

The best explored example of the role of topological matching for molecular recognition by synthetic multifunctional pores is α -helix recognition (Figs. 6 and 8). The helix-coil transition of polyglutamate in comparison to shape-persistent rigid-rod α -helix mimics was used to dissect contributions from topological matching and ion pairing for α -helix recognition [32]. α -Helix recognition by synthetic multifunctional pores was not stereoselective.

AFM images revealed topological mismatch as the possible origin of template effects [27]. Polymer **12** is clearly thinner than an α -helix. According to single-molecule AFM images, pore **4** adapts a flattened diamond-like conformation to firmly bite into the reasonably shape-persistent macromolecule **12** (Fig. 8). The result of this template effect from the threaded guest on the holey host is a stable and giant pseudo-rotaxane.

Moving from polymer blockers to monomer blockers, the involved suprastructures change from pseudo-rotaxanes to inclusion complexes. Topo-

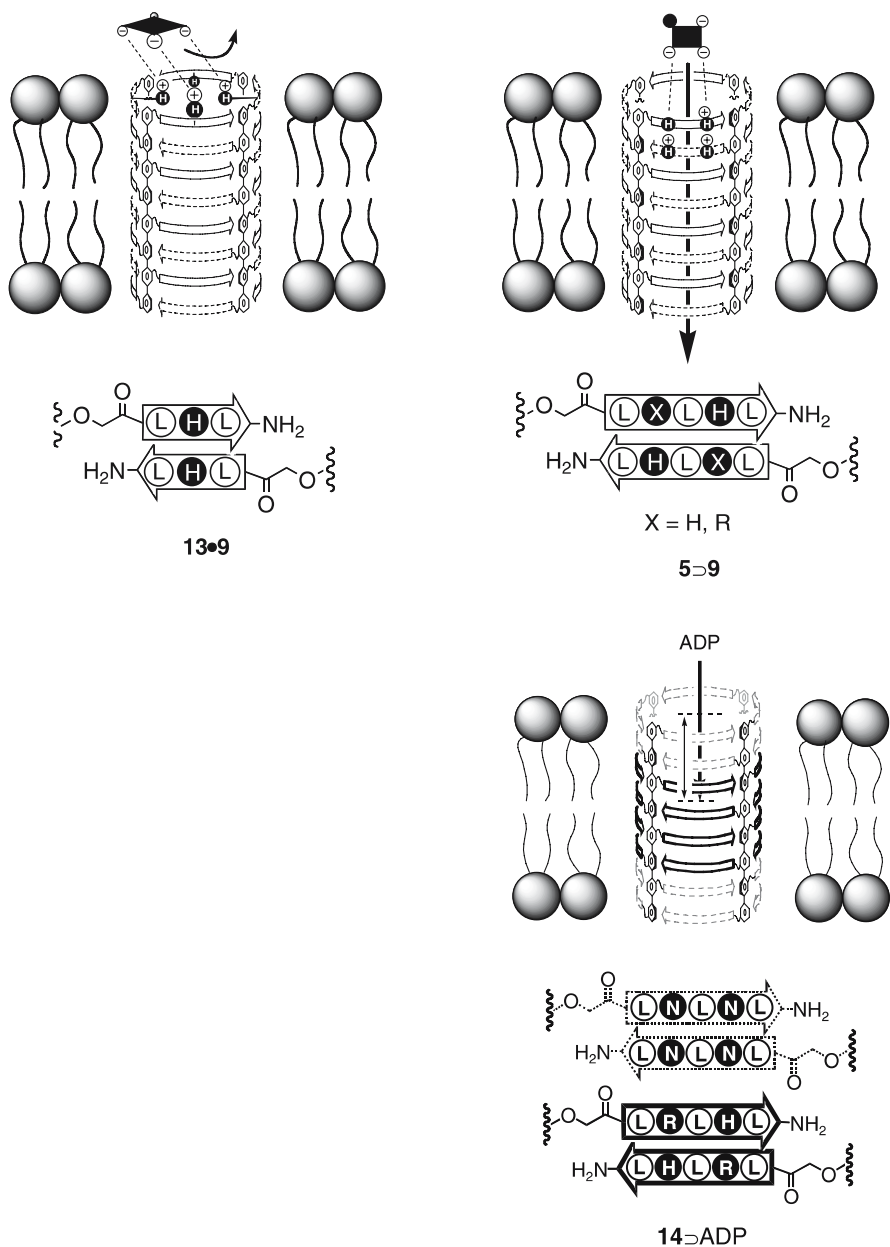


Fig. 9 The depth of molecular inclusion: poor recognition of peripheral guest association on top of contracted barrel 13 (*top left*), good recognition within expanded barrel 5 (or 6, *top right*), and excellent, voltage-sensitive, “in-depth” recognition by contracted active sites within expanded {242}-barrel 14 (*right*)

logical matching as well as the depth of inclusion were found to determine molecular recognition within inclusion complexes. With pores, the depth of inclusion is readily detectable from the voltage dependence of molecular recognition and can be reported as the Woodhull distance l_H , the distance from pore entrance to the active site. Contracted rigid-rod β -barrel pore 13 with shortened LHL-tripeptide β -sheets produced the negligible $l_H = 0.9 \text{ \AA}$ and poor molecular recognition of pyrene-1,3,6-trisulfonates 9, as expected in the absence of guest inclusion (Fig. 9) [29]. Covalent pore expansion to classical rigid-rod β -barrels like 5 with pentapeptide β -sheets improved CB recognition by more than three orders of magnitude and gave $l_H = 2.7 \text{ \AA}$, a value expected for rate-limiting binding of CB 9 to the two peripheral β -strands (Figs. 7 and 9) [28]. Refined rigid-rod β -barrel pores 14 beyond uniform peptide sequences have been created for active-site contraction and voltage-sensitive in-depth molecular recognition [33]. The expected $l_H = 10 \text{ \AA}$ was found together with, remarkably, a further increase of molecular recognition despite reduction of the size and charge of the active site by half (Fig. 9). Noncovalent expansion into hexameric rigid-rod β -barrel pores was of interest to accommodate analytes as large as DNA duplexes [14].

2.3

Optical Transduction of Chemical Reactions

The concept of synthetic multifunctional pores as general optical transducers of chemical reactions builds on the straightforward optical detectability of pore activity discussed in the Introduction (Figs. 1 and 2) [2–4]. To detect a reaction, the ability of substrate(s) and product(s) to either enable (ligand gating) or obstruct (blockage) CF efflux through the pore detector has to differ (Fig. 10). To detect many different reactions, the pore needs to recognize many different substrates or products. Synthetic pores are perfect for this purpose because of their sloppiness [2–4]. Highly selective biological pores would not be interesting because their applicability would be limited to the detection of one reaction (Fig. 4b). Biological pores that lack the “sloppy recognition motifs” of synthetic pores would not be interesting either because of insufficient sensitivity and selectivity. For example, more than 1000 times (!) higher concentrations of α -helical polyglutamic acid were needed to close the pores formed by melittin as representative biological pore compared to synthetic pore 7. This finding underscored the power of α -helix recognition within rigid-rod β -barrels [34].

Current synthetic pores are responsive to a combination of charge and bulk, with efficiencies increasing with increasing blocker charge at constant blocker size. Synthetic pore 3 was created to expand responsiveness to contributions from aromatic electron donor–acceptor interactions [31]. Small differences in substrate or product structure are usually sufficient to detect

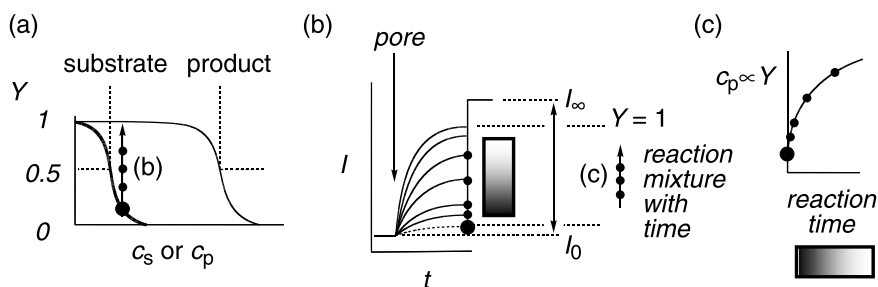
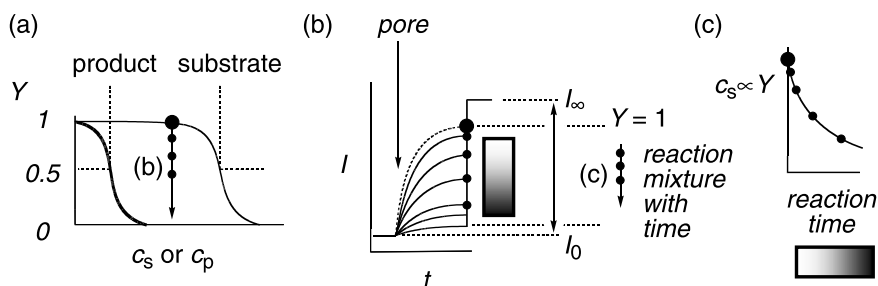
A substrate as blocker**B** product as blocker

Fig. 10 Fluorometric detection of chemical reactions with substrates (**A**) or products (**B**) acting as blockers (**a**). The ability of the reaction mixture to block the pore is measured as a function of time (**b**). Substrate conversion is reported as increasing fluorescence with reaction time for substrate blockers (**Ac**) and decreasing fluorescence with reaction time with product blockers (**Bc**). See Fig. 1 for experimental details

the corresponding reaction. Binary on/off discrimination of ATP and ADP with the naked eye, for example, is no problem [3].

The method developed to detect chemical reactions with pores is similar to chromatographic techniques like TLC or HPLC that chemists are familiar with. First, the IC_{50} or EC_{50} values of the involved substrates and products are determined. With reactions that operate on substrate blockage, the IC_{50} of the substrate is lower than the IC_{50} of the product (Fig. 10A). This is, for example, the case for the detection of the retroaldol reaction of fructose 1,6-diphosphate with pore 7 (Fig. 11). With substrate blockage, the assay system is calibrated to concentrations near the end of the quasilinear region below the IC_{50} of the reaction mixture at time zero (Fig. 10Aa). During the reaction, small aliquots are taken (like we are used to when following reactions by TLC or HPLC) and tested for their ability to block the pore (Fig. 10Ab).

Increasing emission with increasing reaction time reveals the progress of the reaction and can be calibrated to the change in substrate concentration as a function of reaction time (Fig. 10Ac). For reactions that operate on product blockage, emission decreases analogously with reaction time (Fig. 10B). A realized example of this situation is DNA synthesis, where the product blocker is detected with picomolar IC_{50} by pore 7 (Table 1, entry 6) [35]. The same occurs with ligand gating by substrates, whereas ligand gating by products is recorded as increasing emission with increasing reaction time (not shown). A realized example of the latter situation is the esterolysis to pyrenebutyrate,

Table 1 Enzymes as signal generators for synthetic pore sensors

Entry	Enzyme	EC ^a	Blocker ^b (analyte)	Pore	Refs.
1	Apyrase	3	ATP, ADP, or thiamine pyrophosphate	2 ^c , 7	[2]
2	Aldolase (RAMA) ^d	4	Fructose 1,6-diphosphate	2 ^c , 7	[2]
3	Triosephosphate isomerase TIM ^d	5	Fructose 1,6-diphosphate	2 ^c , 7	[2]
4	Glycosyltransferase	2	UDP	2 ^c , 7	[2]
5	Alkaline phosphatase	3	UDP	2 ^c , 7	[2]
6	DNA polymerase	2	DNA	7	[35]
7	Exonuclease III	3	DNA	7	[35]
8	RNase A	3	RNA	7	[35]
9	Esterase (PLE)	3	Pyrenebutyrate ^e	8	[15]
10	Hyaluronidase	3	Hyaluronan	7	[35]
11	Heparinase I	4	Heparin	7	[35]
12	Proteases ^f	3	Polypeptides (E, K, R, Q)	7	[35]
13	Phosphofructokinase	2	ATP	7	[35]
14	Acetate kinase	2	ATP (acetate)	7	
15	Hexokinase	2	ATP (glucose, fructose, galactose)	7, 4	[3]
16	Invertase ^g	3	ATP (sucrose)	4	[3]
17	Galactosidase ^g	3	ATP (lactose)	4	
18	Lactate oxidase	1	Pyruvate (lactate)	4	
19	Citrate lyase	2	Pyruvate (citrate)	4	

^a Enzyme class (1, oxidoreductases; 2, transferases; 3, hydrolases; 4, lyases; 5, isomerases; 6, ligases)

^b Only the substrate or product that acts as blocker (or ligand)^e is listed; all other components of the reaction are indirectly sensed as well (e.g., GlcNAc, UDPGal, and Gal β 1 \rightarrow 4GlcNAc besides UDP with galactosyltransferase, entry 4)

^c Activated with Mg²⁺

^d Coupled assay with RAMA and TIM

^e Detected as ligand

^f Pronase, subtilisin, papain, ficin, chymotrypsin

^g Coupled assay with hexokinase

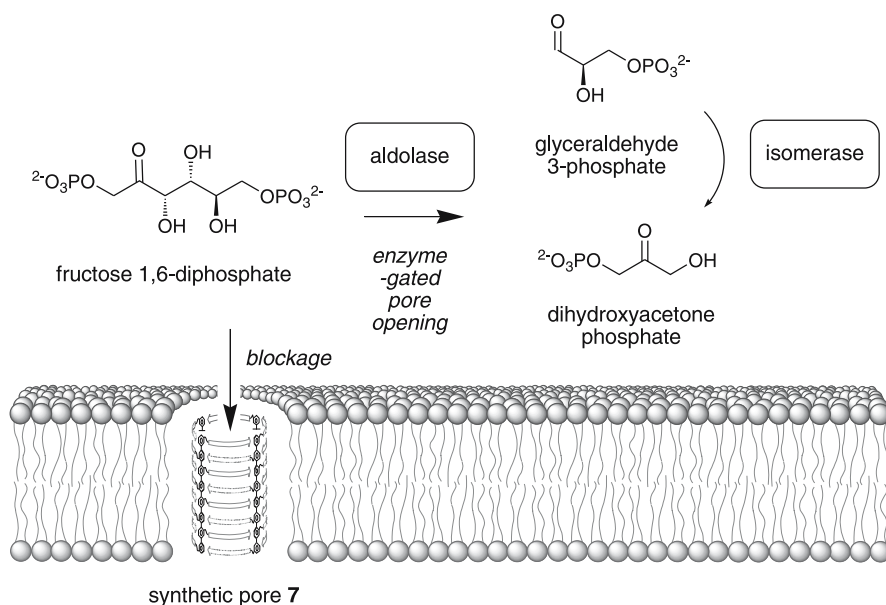


Fig. 11 Retroaldol reaction of fructose 1,6-diphosphate by rabbit muscle aldolase and triosephosphate isomerase as an example of the transduction of a reaction as appearance of color due to activation of pore 7 in response to blocker consumption

a ligand of pore 8 (Table 1, entry 9) [15]. In multiwell-plate screening assays, vesicles and pores are usually added once for end-point detection [2].

2.4

Enzymes as Specific Signal Generators

As mentioned before, synthetic multifunctional pores are perfect as optical transducers of reactions because molecular recognition occurs with relatively poor discrimination at relatively low concentrations. This modest selectivity at high sensitivity makes optical transduction by synthetic multifunctional pores general, that is, compatible with the detection of many different reactions. Sloppy analyte recognition, however, makes synthetic pores as such useless as sensors because of highest possible interference (Fig. 4a). Sensing with synthetic pores as optical transducers of reactions is, however, ideal in combination with enzymes as specific signal generators (Fig. 4c). Noninvasive, label-free, naked-eye detectability of enzyme activity with synthetic pores has been confirmed extensively (Table 1). For example, aldolase activity was detectable as consumption of the FDP blocker (Fig. 11; Table 1, entry 2), and the binary on/off discrimination of ATP and ADP provided rapid access to the optical transduction of kinase activity (Fig. 12; Table 1, entry 15). Their sensitivity to changes in substrate bulk as well as charge makes optical trans-

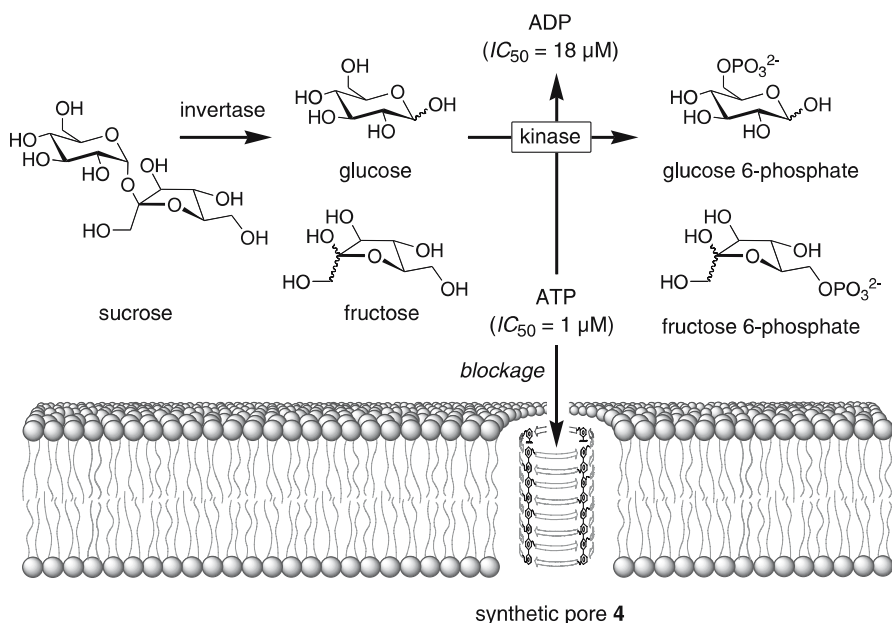


Fig. 12 Sugar sensing in soft drinks with synthetic pore 4 as general optical transducer and invertase and hexokinase as specific signal generators. The presence of sucrose is reported as fluorescence upon pore activation in response to the conversion of the good blocker ATP into the poor blocker ADP

duction of enzyme activity by synthetic pores orthogonal to conventional electrochemical transduction of enzymatic redox chemistry [4]. Naturally, electrochemical biosensors are compatible only with the enzymes of class 1, the oxidoreductases, as direct specific signal generators. The electroorthogonality of synthetic pores as general optical transducers dramatically expands the applicability of enzymes in biosensing to presumably soon cover all classes (Table 1).

The sensing of analytes that are intrinsically underrecognized by synthetic pores provides attractive chemical challenges. One solution is to refine the recognition motifs within synthetic multifunctional pores. An example of this approach is the introduction of artificial amino acids within synthetic pore 3 for ion-pair assisted adhesive π -clamping (Fig. 7) [31].

2.5

Multicomponent Sensing in Complex Matrixes

Sensing with synthetic pores was demonstrated first for sugar in soft drinks (Fig. 12; Table 1, entries 15 and 16, [3]). For this purpose, soft drinks were treated first with invertase to convert sucrose into glucose and fructose. Both

hexoses were then phosphorylated with hexokinase. During this reaction, ATP is converted into ADP. Optical transduction of this conversion of the excellent blocker ATP into the poorer blocker ADP by pore 4 reported the presence of sugar in soft drinks as appearance of color. With this, the expected sugar concentrations were confirmed quantitatively for Coca-Cola, Coca-Cola Light, Red Bull, Fanta Orange, and Nestea Lemon.

Synthetic pores are attractive sensors because their compatibility with enzymes for signal generation exceeds that of canonical biosensors by far (Table 1). Access to as many enzymatic signal generators as possible is essential for multicomponent sensing in complex matrixes. Ideally, one would like to use one and the same “universal” sensor to identify all analytes of interest in any real-life sample. Ongoing research in this direction focuses on the invention of reactive in situ amplifiers to catch otherwise underrecognized analytes (Litvinchuk et al., in preparation).

3 Sensing with Bioengineered Pores

3.1 Immunosensing

The concept of immunosensing is to use molecular recognition between antigen and antibody for specific signal generation (Fig. 13, [22]). This is attractive for sensing because the production of primary antibodies is compatible with many analytes. A secondary antibody that recognizes a constant re-

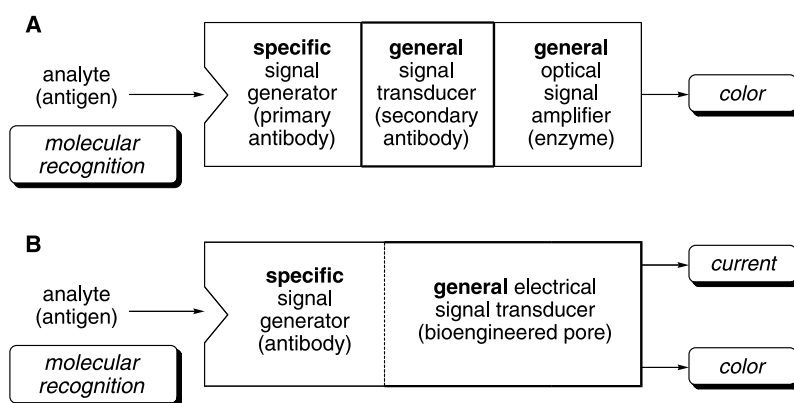


Fig. 13 Immunosensing with bioengineered multifunctional pores as electrical (or optical) transducers of molecular recognition (**b**, rather than reactions as Fig. 4C), compared to ELISA with enzymes as general optical signal amplifiers (**a**, rather than specific signal generators as in Figs. 11 or 12)

gion of the primary antibody and is labeled with an optical readout serves as general optical signal transducer. In enzyme-linked immunosorbent assay (ELISA), the most popular version of immunosensing, the secondary antibody is labeled with an enzyme for signal amplification by infinite conversion of chromogenic substrates (rather than for specific signal generation, as in Sect. 2).

Never considered with synthetic pores so far, immunosensing with bioengineered pores was explored early on (Fig. 14) [10]. Gramicidin channels in supported lipid bilayers on conducting gold surfaces were selected for electric signal generation (Fig. 14a). A tail with a terminal thiol was attached to the gramicidin half-channel in the lower leaflet for immobilization on the gold surface. A tail with a terminal biotin was attached to the gramicidin half-channel in the upper leaflet to reversibly bind antibody F_{ab} fragments with a biotin tag via a multivalent streptavidin linker. A second complementary F_{ab} fragment was immobilized directly on gold via a reversible biotin-streptavidin exchanger. Without antigen, the gramicidin dimers freely dimerize to form conducting channels. Addition of antigens with two complemen-

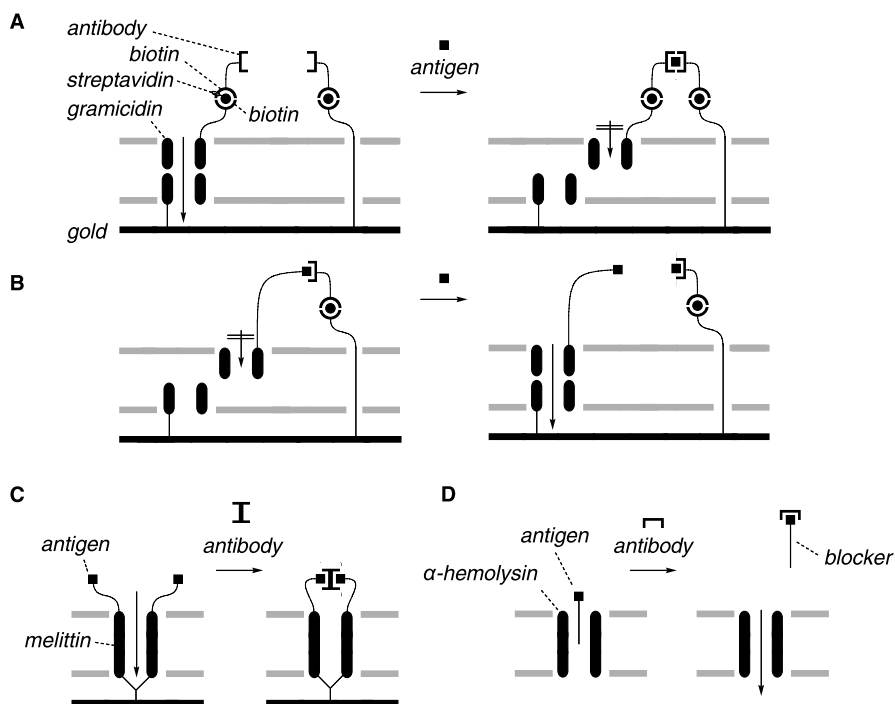


Fig. 14 Immun sensing with bioengineered gramicidin (a,b), melittin (c), and α -hemolysin pores (d) as electrical transducers in supported (a-c) and planar bilayer membranes (d)

tary binding domains links the upper gramicidin half-channel to the immobilized antibody. As a result, the active gramicidin dimer is disrupted. Antigens are thus reported as a decrease in conductivity of the supported bilayer. The thyroid-stimulating hormone (TSH), composed of α - and β -subunits that are recognized by different antibodies, was used initially to test the concept. Later on the same generic design was applied to other recognition motifs.

One advantage of this design is the reversible immobilization of antibody, allowing in principle for adaptable use of the sensor for many analytes. Limitations are the restriction to divalent analytes as well as the complexity of the system. For example, the effect of streptavidin binding to biotin-tagged gramicidins has been studied extensively in single-channel measurements in planar lipid bilayers. Double-channel conductance due to streptavidin-mediated gramicidin dimerization has been found for some systems [36], gramicidin removal from the bilayer for others [37]. Streptavidin binding to biotin tags has been studied for other bioengineered ion channels and pores (compare also Sect. 3.2).

A simpler alternative approach uses direct attachment of antigens to the gramicidin channel (Fig. 14b) [10]. Binding to the immobilized antibody will close the gramicidin channel by disruption of the active head-to-head dimer. Addition of antigen analytes then liberates the bound antigen–gramicidin conjugate from the immobilized antibody. As a result, the active dimer forms and the presence of the antigen is reflected as conductance of the supported bilayer. This sensor has been validated with digoxin as representative analyte.

Melittin, a toxic, α -helical peptide from bee venom that self-assembles into tetrameric pores, has recently been coupled to (NANP)₃ peptides, the major B-cell epitope of the circumsporozoite protein of *Plasmodium falciparum* (the cause of human malaria, **m-a**), and cross-linked using ornithine diamines X (Fig. 14c) [38]. This template was terminated with cysteine C for immobilization on gold surfaces (CGGGGGX(GGX(**m-a**)G**m-a**)GGGX(**m-a**)G**m-a**). Binding to the naturally divalent antibody was found to reduce conductivity of the supported bilayer. The (not reported) detection of free antigens as pore opening should then be possible by displacement experiments as in Fig. 14b.

In an elegant general amplifier approach to immunosensing with the α -hemolysin pore, antigens were attached to polyribonucleotides that were known to act as weak blockers (Fig. 14d) [39]. Antibody addition literally uncorks the pore and is detected as an increase in conductance. Displacement experiments as in Fig. 14b should then allow detection of free antigens as pore closing. Poly(dT) was used as blocker, and the antigen bromodeoxyuridine was attached to the 5'-terminus of the polynucleotide. Different to the previous examples, immunosensing with antigen–blocker conjugates was realized in single-channel conductance experiments in planar rather than supported bilayers (see Sect. 3.2).

3.2 Stochastic Sensing of Single Analytes

The electrical transduction of the translocation of molecules is routinely used to characterize biological pores in BLMs, also on the single-molecule level. Detectability by electrical transduction of molecular recognition has been confirmed, often for biochemical purposes, for protein translocation through autotransporter [40] and anthrax toxin pores [41, 42], for maltodextrins in maltoporin, or for single β -lactam antibiotics in outer membrane protein F (OmpF) [43], and so on. The study of biomolecular recognition is naturally a central part of the biochemical characterization of ion channels and pores that open or close in response to specific ligands. Kramer's patch cramming concept pointed out early on that such channels and pores can naturally be used as sensors of their own ligand in nerve cells [5].

The concept of stochastic sensing of single molecules considers the lifetime and conductance of single complexes formed within pores as unique fingerprints of individual analytes (Fig. 15) [11]. In single-pore conductance experiments, the presence of a given analyte 1 will cause the stochastic appearance and disappearance of the conductance of a single pore-analyte complex (Fig. 15a; compare Fig. 3 for background on method). The presence of a different analyte 2 will be visible as a signature of the conductance and

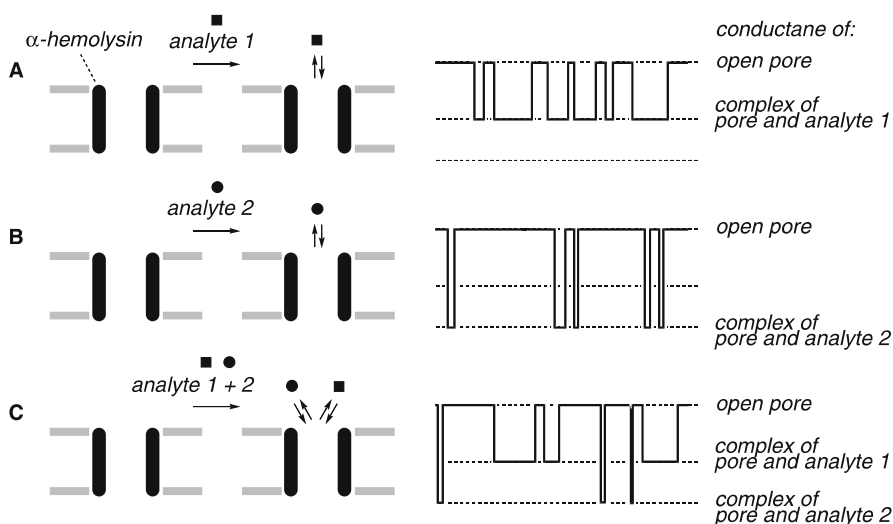


Fig. 15 The concept of stochastic sensing of single analytes with bioengineered biological pores in single-molecule measurements in BLMs. Binding of analytes 1 and 2 is detected as distinct formation and dissociation of pore-analyte complexes of characteristic lifetime and conductance (compare Fig. 3). The fingerprint of an individual analyte then reveals the presence and quantity in a mixture of two to four analytes

lifetime of this specific single pore–analyte complex (Fig. 15b). In a not overly complex mixture, the signatures will be distinguishable and reveal the presence and amount of both analytes (Fig. 15c).

Many host–guest complexes have been detected on the single-molecule level with bioengineered α -hemolysin pores. Examples include the interaction of streptavidin or kinases with biotin or peptide inhibitors that were attached to the pore in a bioconjugate approach similar to the one discussed in the preceding section on immunosensing (Fig. 16b) [44]. Examples are available for the detection of direct binding of single analytes to bioengineered α -hemolysin, covering of ssDNA (many variations), nucleotides, inositol phosphates, cyclodextrins, cucurbiturils, cyclopeptides, drugs (promethazine, imipramine), solvents (THF), or explosives (TNT, Fig. 16a) [11, 44].

Only a few examples of detection of single analytes in mixtures exist. Experimental support for the concept of stochastic sensing was secured with the simultaneous detection of two different cations in a mixture of two cations. An early mutant α -hemolysin with histidine ligands engineered into the pore was used to demonstrate simultaneous sensing of single divalent cations Zn^{2+} , Co^{2+} , and Cd^{2+} [45]. Successful detection of single polynucleotides in mixtures of polyA, polyC, and polyT with wild-type α -hemolysin was reported around the same time [9]. Direct recognition of IP_3 (inositol 1,4,5-triphosphate), a Ca^{2+} -mobilizing second messenger, was achieved within a mutant α -hemolysin pore equipped with two proximal rings of arginines

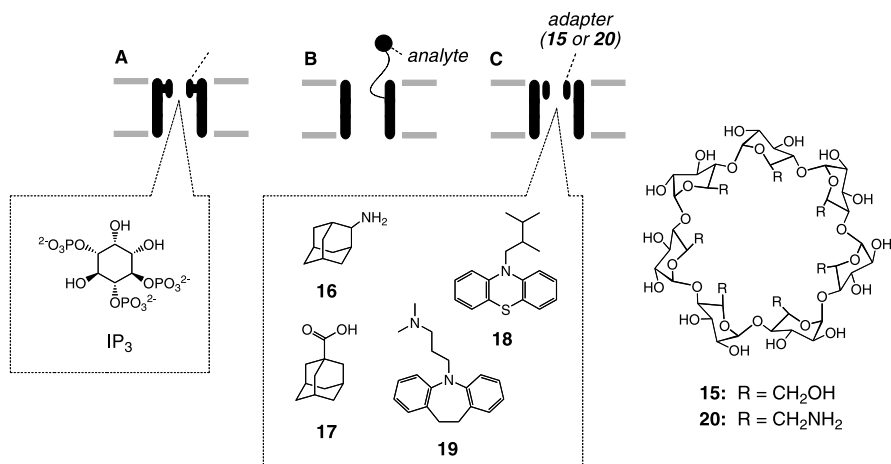


Fig. 16 Realized approaches toward stochastic multicomponent sensing in more complex matrixes include: **a** a bioengineered α -hemolysin pore for the detection of IP_3 in the presence of ATP and Mg^{2+} ; **b** covalent attachment of highly specific analytes to the pore (biotin, kinase inhibitors); and **c** cyclodextrin adapters for the simultaneous detection of two adamantanes, two drugs (promethazine **18** and imipramine **19**) or four nucleotides (dAMP, dGMP, dCMP, and dTMP). Compare Fig. 17

(M113R, T145R; IP₃: $K_D = 2.1$ nM, IP₁: $K_D = 23$ mM, IP₆: $K_D = 1.2$ pM, ATP: $K_D = 200$ μ M) [46]. With this pore, IP₃ concentrations down to 100 nM could be quantified by stochastic sensing in the presence of ATP (2 mM) and Mg²⁺ (500 μ M) at concentrations that are common in cells.

The introduction of the adapter concept provided three more elegant examples of the detection of single analytes in mixtures of two analytes. In the first example, β -cyclodextrin **15** was inserted as adapter into a modified α -hemolysin pore (M113N, L135N) [11]. The current levels of single inclusion complexes formed by 2-adamantanamine **16** and 1-adamantanecarboxylic acid **17** within β -cyclodextrin **15** within α -hemolysin pores were indeed different enough to detect their presence simultaneously. The same was true for the two-component mixture of antihistaminic promethazine (**18**) and antidepressant imipramine (**19**) [11] and racemic mixtures of either ibuprofen or thalidomide [47]. The mixture of highest complexity mastered so far with stochastic sensing concerns the simultaneous discrimination of the four deoxyribonucleoside 5'-monophosphates (dGMP, dAMP, dCMP, and dTMP) within the cationic β -cyclodextrin adapter **20** in a mutant α -hemolysin pore (M113R) [44]. This example is of interest because exonucleases are the likely solution [35] of the intrinsic resolution problem faced when considering the vision of sequencing intact single genes while moving through a pore [48].

The lack of examples of stochastic sensing of single analytes in more complex matrixes may reflect the conceptual paradox to expect specific signal generation and general (electrical) signal transduction from the same process (compare Sect. 2.1). The introduction of the concept of general covalent amplifiers for single analyte sensing is an important milestone because it decouples specific signal generation and general signal transduction (see Sect. 3.3). Another reason for relatively little progress with “real-life” stochastic sensing may be that, according to the experts, “practical application is cumbersome, time-consuming, and requires the hands of a skilled experimentalist” [49]. Rather than elaborating on stochastic sensing, current breakthroughs highlight the use of single pores in purely academic topics, such as the detection and study of chemical processes on the single-molecule level, with emphasis on host-guest chemistry and molecular transformations, particularly single reactive intermediates [50].

3.3

Covalent Amplifiers

General covalent amplifiers were conceived to decouple specific signal generation from general signal transduction, and thus to address the conceptual paradox of stochastic sensing (compare Sect. 3.2) [39]. With this concept, the sensing of many different analytes with the same pore and the same amplifier should become possible on the single-molecule level and, in principle, also in more complex matrixes. Although conceived for (but not limited to)

electrical single-molecule transduction, covalent amplification is conceptually unrelated to stochastic sensing (Fig. 17).

Exploiting the finding that single polynucleotides can be detected by wild-type α -hemolysin pores [48], a short poly(dC) as representative general amplifier was covalently attached to the otherwise undetectable biotin as representative analyte. In single-channel measurements, this analyte–amplifier conjugate produced the signature of amplifier–pore complexes without interference from the analyte. Addition of streptavidin reduced the affinity of the analyte–amplifier conjugate for the pore. This reduced recognition was reported as reduced probability of observing the conductance level of single pore–amplifier complexes. Statistical analysis of dose–response curves revealed the concentration of streptavidin. The presence of free biotin as representative analyte should then cause the release of the analyte–amplifier conjugate from streptavidin as representative host by simple guest displacement. Increasing analyte concentrations should thus be reported as increasing probability of observing the conductance level of single pore–amplifier complexes. Although this attractive sensing concept by guest replacement and amplifier release remains to be verified experimentally, it represents an imaginative strategy to decouple specific signal generation and general signal transduction in single-pore conductance experiments. The covalent amplifier concept is thus in principle compatible with multicomponent sensing with one and the same pore transducer (see Sect. 2.5) as long as specific hosts for all analytes are available. This limitation is, however, naturally unproblematic with immunosensing (compare Sect. 3.1).

Compatibility of the amplifier concept with stochastic sensing was explored by exploiting the observation that polynucleotides can be detected simultaneously by wild-type α -hemolysin in a length-dependent manner [9, 39]. The short poly(dC) with a biotin tag was complemented with a long

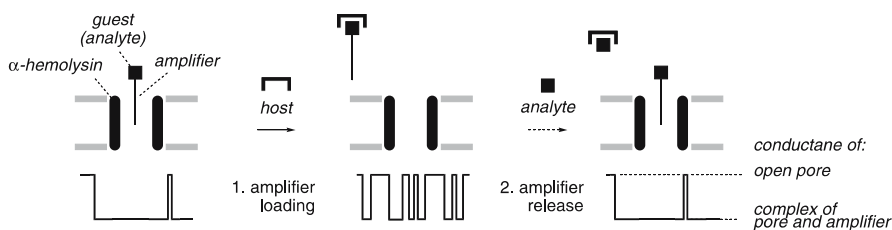


Fig. 17 The concept of general covalent amplifiers for multicomponent sensing in more complex matrixes with biological pores in single-molecule BLM measurements. The analyte is attached to a pore-blocking polymer as general amplifier; addition of a host recognizing the analyte will remove the analyte–amplifier complex from the pore, and analyte displacement will liberate the tagged amplifier and be detected as decreasing pore activity with increasing concentration. See Fig. 15 for comparison with stochastic sensing, and Fig. 14 for application to immunosensing

poly(dT) carrying a bromodeoxyuridine antigen. Addition of streptavidin cleanly removed the signature of single complexes with short poly(dC) amplifier from the subconductance levels reported by the pore detector for two-component mixtures, whereas addition of anti-bromodeoxyuridine antibody increased the lifetime of single complexes with long poly(dT) amplifier.

3.4 Cell-Penetrating Peptides as Optical Transducers

Efforts to replace synthetic multifunctional pores (Sect. 2.2) by commercially available biological pores as cost-effective optical transducers of chemical reaction (Sect. 2.3) failed in the case of melittin because of insufficient sensitivity [34]. Recently, however, certain complexes formed by arginine-rich cell-penetrating peptides (CPPs) and amphiphilic counteranions were shown to act as synergistic anion carriers in lipid bilayer membranes as well as live cells [51]. Although evidence in vesicles supports an anion carrier mechanism, pertinent observations, such as the rapid cytosolic delivery of molecules as large as green fluorescent proteins with CPP-counterion complexes, suggest that transient, so far elusive pores may be involved as well [52]. In any case, highly effective anion transport activity in vesicles suggested that polyion-counterion complexes, such as polyarginine (pR)-counteranion complexes, may serve well as affordable general optical transducers of chemical reactions (Fig. 18) [53]. Counterion screening revealed dodecyl phosphate (DP) as a convenient pR activator in CF-loaded DPPC vesicles (shelf-life of 3.5 years; compare Fig. 1). Optical transduction by pR-DP complexes was exemplified by hyaluronan (HA) hydrolysis with hyaluronidase (HAase) (Table 1, entry 10). Inactivation of pR-DP transducers by counterion exchange with the substrate HA caused the expected inactivation. Hydrolysis of the HA inactivators into less interfering tetrasaccharide products with

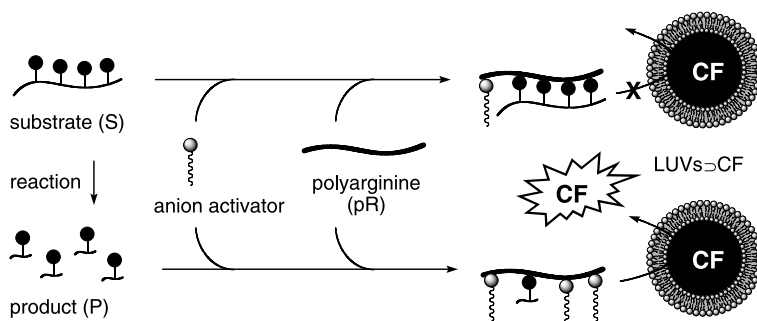


Fig. 18 The concept of polyarginine-counteranion complexes as general optical transducers of chemical reactions, exemplified for fluorogenesis during the consumption of inactivating substrates like the hydrophilic polyanion hyaluronan

testicular HAase was then detectable as increasing CF emission due to the reactivation of the pR–DP transducers. pR–DP complexes were further compatible with the optical detection of HA immobilization on solid supports and inhibitor screening for HAase (cromolyn, heparin), a central process in medicinal chemistry, particularly drug discovery.

4

Porous Sensors in Membranes Beyond Lipid Bilayers

Synthetic pores sculpted in membranes other than lipid bilayers are rapidly emerging as an attractive alternative for sensing applications. The key advantage of this approach is that stable membranes can be used. The key challenge is to reproducibly create uniform nanopores in these materials that can be functionalized in an adaptable manner.

Recently, several innovative fabrication methods to manipulate matter on the nanoscale became available. Conical gold nanopores are prepared by electrolytic plating of pores etched into polycarbonate membranes [54, 55]. This approach is attractive because it provides rapid access to small diameters. Because of their asymmetry, conical gold pores exhibit non-ohmic behavior. Their internal gold surface is ideal to attach functional groups via covalent Au–S bonds (Fig. 19a). Realized examples include DNA (several sequences), biotin, protein G, and an antiricin antibody. The functionalized pores can be specifically blocked with the corresponding guests, i.e., streptavidin, immunoglobulin G, and the antigen ricin. The last example identified conical gold nanopores as valid electrical transducers for immunosensing (compare Sect. 3.1). Electrical transduction of biotin–streptavidin pairing was also found for similarly prepared gold nanotubes in polycarbonate membranes [56]. An alternative approach to biotin–streptavidin pairing uses soft lithography to cast nanopores into poly(dimethylsiloxane) membranes and colloidal latex particle sizing rather than covalent pore functionalization for sensing [57, 58]. The same size exclusion approach has been applied to multi-analyte immunosensing.

The transmembrane alignment of multi- [59], double-, and single-walled [60] carbon nanotubes in thin, impermeable polymer and silicon nitride membranes was achieved recently. These breakthroughs provided access to the electrical detection of the frictionless water flux through these smooth and repellent pores. The found velocities were much faster than expected from fluid-flow theory and comparable with that through aquaporin water channels. These insights are thought to lead to new gas and liquid separation devices. More important for the topic of this review, it has become possible to functionalize transmembrane carbon nanotube pores by reacting the terminal carboxylates with amines of various size, hydrophilicity, and charge (Fig. 19b) [61]. The sensitivity of cation flux to increasing terminal

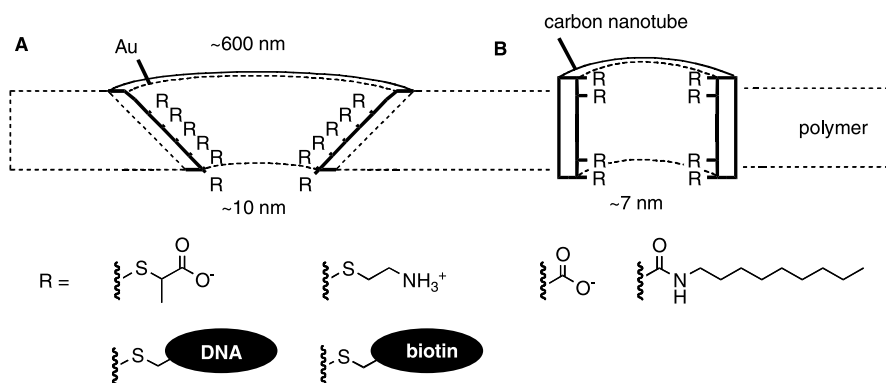


Fig. 19 Synthetic pores sculpted in polymer membranes include **a** conical gold pores and **b** carbon nanotubes, and their functionalization for sensing applications including immunosensing covers anions, cations, alkyl amides, DNA, biotin, and more

nanotube charge suggested that sensing applications of cylindrical carbon nanotube pores are only a matter of time.

The stochastic detection of single analytes, such as DNA or porphyrins, has been reported for several examples including conical gold nanopores [62, 63] and pores cast into poly(dimethylsiloxane) [64] or silicon nitride membranes [65]. Uniform sizing of the latter pores was achieved by feedback-controlled ion-sputtering erosion, measuring the ion flow through the pores during their creation.

5 Related Topics

Several topics that are related to sensing with synthetic pores could not be covered in this review. It cannot be overemphasized that without continuing efforts to improve our ability to create synthetic ion channels and pores (that is, without advanced synthetic organic chemistry as the hidden and too often underappreciated heart of the matter), any discussion on sensing would be redundant. Comprehensive reviews on the synthesis of ion channels and pores are available [24, 25].

Screening, the parallel detection of many separated, single, and pure compounds, is a topic closely related to sensing, the detection of single analytes in a mixture of compounds. Substrate as well as inhibitor screening is of central importance in drug discovery. The applicability of optical transduction of enzymatic reactions with synthetic pores to screening assays has been exemplified early on with substrate screening for apyrase in multiwell plates [2].

Another related topic is the detection of covalent modifications of pores by changes in their conductance. This research topic emerged from methods

to study biological ion channels such as SCAM, where the reaction of methanethiosulfonates with cysteines is used to reveal amino acid residues in the ion-conducting pathway [6]. If reactions can be used to characterize pores, pores will naturally be of use to characterize reactions [7]. Detection of reactions on the single-molecule level is particularly attractive for studying otherwise elusive single reactive intermediates [50]. Established for the low-energy transformation of covalent tags within the α -hemolysin pore, recent reports expand the approach to covalent transformation of externally tagged gramicidin channels in two high-energy steps [66]. Moving on from covalent to noncovalent transformation within pores naturally leads to catalytic pores, i.e., pores that can convert substrates on their way across the membranes. The only reported example so far is a synthetic (rather than a bioengineered) pore with esterolytic activity ($\Delta G_{ES} = -29.6$ kJ/mol, $\Delta G_{TS} = -52.2$ kJ/mol) [17, 67].

6 Summary

Current synthetic multifunctional pores can act like supramolecular tongues, differentiating analytes such as sucrose that determine the sweet taste of soft drinks like Coca-Cola. For sensing in reasonably complex matrixes, synthetic pores are used as general optical signal transducers of chemical reactions. For broad applicability, synthetic pores that recognize small changes in bulk and/or charge of many substrates and products are best. For specificity, pores as general optical transducers are combined with enzymes as specific signal generators. The compatibility of synthetic pores with many different enzyme families from different classes well beyond the limitation of amperometric biosensors to oxidoreductases has been confirmed. Current research focuses on the concept of general reactive amplifiers to catch otherwise elusive analytes in situ.

Approaches complementary to sensing with synthetic pores have been developed with biological and bioengineered pores. Often, they are used as general electrical transducers in planar or supported bilayers rather than as optical transducers in vesicles. For specific signal generation, the combination with molecular recognition, particularly immunosensing, is usually preferred (rather than enzymes as with synthetic pores). The stochastic detectability of single molecules by single-pore conductance measurements has provided novel insights into host-guest chemistry and covalent transformations, particularly reactive intermediates, and marvelous, probably not realizable, visions such as single gene sequencing. The complexity and fragility of the method is more of a problem when considering “real-life” applications to multicomponent sensing in more complex matrixes. The problem of stochastic sensing to expect specific signal generation and general sig-

nal transduction from the same process could be elegantly bypassed with the introduction of general covalent amplifiers, particularly when applied to single-molecule immunosensing.

Synthetic pores sculpted in solid-state membranes rapidly emerge as an alternative approach to sensing with pores in lipid bilayer membranes. Preliminary breakthroughs, particularly in the context of immunosensing, look very promising.

Acknowledgements We warmly thank all past and present coworkers and collaborators for their contributions, and the Swiss NSF for financial support.

References

1. Matile S, Sakai N (2007) The characterization of synthetic ion channels and pores. In: Schalley CA (ed) *Analytical methods in supramolecular chemistry*. Wiley, Weinheim, pp 391–418
2. Das G, Talukdar P, Matile S (2002) *Science* 298:1600–1602
3. Litvinchuk S, Sordé N, Matile S (2005) *J Am Chem Soc* 127:9316–9317
4. Das G, Matile S (2006) *Chem Eur J* 12:2936–2944
5. Kramer RH (1990) *Neuron* 4:335–341
6. Karlin A, Akabas MH (1998) *Methods Enzymol* 293:123–145
7. Mindell JA, Zhan H, Huynh PD, Collier RJ, Finkelstein A (1994) *Proc Natl Acad Sci USA* 91:5272–5276
8. Woolley GA, Jaikaran ASI, Zhang Z, Peng S (1995) *J Am Chem Soc* 117:4448–4454
9. Kasianowicz JJ, Brandin E, Branton D, Deamer DW (1996) *Proc Natl Acad Sci USA* 93:13770–13773
10. Cornell BA, Braach-Maksyvytis VLB, King LG, Osman PDJ, Raguse B, Wieczorek L, Pace RJ (1997) *Nature* 387:580–583
11. Gu LQ, Braha O, Conlan S, Cheley S, Bayley H (1999) *Nature* 398:686–690
12. Fuhrhop JH, Liman U, Koesling V (1988) *J Am Chem Soc* 110:6840–6845
13. Sakai N, Majumdar N, Matile S (1999) *J Am Chem Soc* 121:4294–4295
14. Sakai N, Baumeister B, Matile S (2000) *ChemBioChem* 1:123–125
15. Gorteau V, Perret F, Bollot G, Mareda J, Lazar AN, Coleman AW, Tran DH, Sakai N, Matile S (2004) *J Am Chem Soc* 126:13592–13593
16. Bhosale S, Sisson AL, Talukdar P, Fürstenberg A, Banerji N, Vauthey E, Bollot G, Mareda J, Röger C, Würthner F, Sakai N, Matile S (2006) *Science* 313:84–86
17. Baumeister B, Sakai N, Matile S (2001) *Org Lett* 3:4229–4232
18. Wiskur SL, Anslyn EV (2001) *J Am Chem Soc* 123:10109–10110
19. Collins BE, Wright AT, Anslyn EV (2007) *Combining Molecular Recognition, Optical Detection, and Chemometric Analysis, in this volume*
20. Clark LC, Lyons C (1962) *Ann NY Acad Sci* 102:29
21. Sanz Alaejos M, Garcia Montelongo FJ (2004) *Chem Rev* 104:3239–3265
22. Engvall E (1980) *Methods Enzymol* 70:419–439
23. Sakai N, Mareda J, Matile S (2005) *Acc Chem Res* 38:79–87
24. Sisson AL, Shah MR, Bhosale S, Matile S (2006) *Chem Soc Rev* 35:1269–1286
25. Matile S, Som A, Sordé N (2004) *Tetrahedron* 60:6405–6435
26. Gorteau V, Bollot G, Mareda J, Pasini D, Tran DH, Lazar AN, Coleman AW, Sakai N, Matile S (2005) *Bioorg Med Chem* 13:5171–5180

27. Kumaki J, Yashima E, Bollot G, Mareda J, Litvinchuk S, Matile S (2005) *Angew Chem Int Ed* 44:6154–6157
28. Baumeister B, Sakai N, Matile S (2001) *Org Lett* 3:4229–4232
29. Som A, Sakai N, Matile S (2003) *Bioorg Med Chem* 11:1363–1369
30. Som A, Matile S (2002) *Eur J Org Chem* 3874–3883
31. Tanaka H, Litvinchuk S, Tran DH, Bollot G, Mareda J, Sakai N, Matile S (2006) *J Am Chem Soc* 128:16000–16001
32. Litvinchuk S, Matile S (2005) *Supramol Chem* 17:135–139
33. Baudry Y, Pasini D, Nishihara M, Sakai N, Matile S (2005) *Chem Commun* 40:4798–4800
34. Sordé N, Matile S (2004) *Biopolymers* 76:55–65
35. Sordé N, Das G, Matile S (2003) *Proc Natl Acad Sci USA* 100:11964–11969
36. Antonenko YN, Rokitskaya TI, Kotova EA, Reznik GO, Sano T, Cantor CR (2004) *Biochemistry* 43:4575–4582
37. Futaki S, Zhang Y, Kiwada T, Nakase I, Yagami T, Oiki S, Sugiura Y (2004) *Bioorg Med Chem* 12:1343–1350
38. Terrettaz S, Ulrich WP, Guerrini R, Verdini A, Vogel H (2001) *Angew Chem Int Ed* 41:1740–1743
39. Kasianowicz JJ, Henrickson SE, Weetall HH, Robertson B (2001) *Anal Chem* 73:2268–2272
40. Oomen CJ, van Ulsen P, van Gelder P, Feijen M, Tommassen J, Gros P (2004) *EMBO J* 23:1257–1266
41. Zhang S, Udho E, Wu Z, Collier RJ, Finkelstein A (2004) *Biophys J* 87:3842–3849
42. Krantz BA, Melnyk RA, Zhang S, Juris SJ, Lacy DB, Wu Z, Finkelstein A, Collier RJ (2005) *Science* 309:777–781
43. Nestorovich E, Danelon C, Wintherhalter M, Bezrukov SM (2002) *Proc Natl Acad Sci USA* 99:9789–9794
44. Astier Y, Braha O, Bayley H (2006) *J Am Chem Soc* 128:1705–1710
45. Braha O, Gu LQ, Zhou L, Lu X, Cheley S, Bayley H (2000) *Nat Biotechnol* 18:1005–1007
46. Cheley S, Gu LQ, Bayley H (2002) *Chem Biol* 9:829–838
47. Kang XF, Cheley S, Guan X, Bayley H (2006) *J Am Chem Soc* 128:10684–10685
48. Deamer DW, Branton D (2002) *Acc Chem Res* 35:817–825
49. Holden MA, Bayley H (2005) *J Am Chem Soc* 127:6502–6503
50. Shin SH, Luchian T, Cheley S, Braha O, Bayley H (2002) *Angew Chem Int Ed* 41:3707–3709
51. Perret F, Nishihara M, Takeuchi T, Futaki S, Lazar AN, Coleman AW, Sakai N, Matile S (2005) *J Am Chem Soc* 127:1114–1115
52. Takeuchi T, Kosuge M, Tadokoro A, Sugiura Y, Nishi M, Kawata M, Sakai N, Matile S, Futaki S (2006) *ACS Chem Biol* 1:299–303
53. Miyatake T, Nishihara M, Matile S (2006) *J Am Chem Soc* 128:12420–12421
54. Siwy Z, Trofin L, Kohli P, Baker LA, Trautmann C, Martin CR (2005) *J Am Chem Soc* 127:5000–5001
55. Harrell CC, Kohli P, Siwy Z, Martin CR (2004) *J Am Chem Soc* 126:15646–15647
56. Gyurcsanyi RE, Vigassy T, Pretsch E (2003) *Chem Commun* 38:2560–2561
57. Saleh OA, Sohn LL (2003) *Proc Natl Acad Sci USA* 100:820–824
58. Carbonaro A, Sohn LL (2005) *Lab Chip* 5:1155–1156
59. Majumder M, Chopra N, Andrews R, Hinds BJ (2005) *Nature* 438:44
60. Holt J, Park HG, Wang Y, Stadermann M, Artyukin AB, Grigoropoulos CP, Noy A, Bakajin O (2006) *Science* 312:1034–1040
61. Majumder M, Chopra N, Hinds BJ (2005) *J Am Chem Soc* 127:9062–9070

62. Heins EA, Siwy ZS, Baker LA, Martin CR (2005) *Nano Lett* 5:1824–1829
63. Karhanek M, Kemp JT, Pourmand N, Davis RW, Webb CD (2005) *Nano Lett* 5:403–407
64. Saleh OA, Sohn LL (2003) *Nano Lett* 3:37–38
65. Li J, Stein D, McMullan C, Branton D, Aziz MJ, Golovchenko JA (2001) *Nature* 412:166–169
66. Blake S, Mayer T, Mayer M, Yang J (2006) *ChemBioChem* 7:433–435
67. Sakai N, Sordé N, Matile S (2003) *J Am Chem Soc* 125:7776–7777

Identification of Catalysts in Combinatorial Libraries

Jefferson D. Revell · Helma Wennemers (✉)

Department of Chemistry, University of Basel, St. Johannis Ring 19, 4056 Basel, Switzerland

Helma.Wennemers@unibas.ch

1	Introduction	252
2	Screening of Spatially Addressable Libraries	253
2.1	IR Thermographic Analysis	253
2.2	Colorimetric and Fluorimetric Analysis	254
2.2.1	Heck Reactions	254
2.2.2	Hydrosilations	255
2.2.3	Allylic Alkylations	256
2.3	Analysis by Enzyme Immunoassays	257
3	Screening of One-Bead-One-Compound Libraries for Catalytic Activity	258
3.1	IR Thermographic Analysis	258
3.2	Formation of Colored or Fluorescent Reaction Products	259
3.2.1	Insoluble Reaction Products	259
3.2.2	Soluble Reaction Products	260
3.3	Fluorescent pH Indicators	261
3.4	Gels as Reaction Media	262
3.5	Catalyst-Substrate Co-immobilization	263
4	Conclusions	264
	References	265

Abstract Combinatorial methods allow for the generation of a large number of structurally similar yet unique compounds. For catalyst discovery using combinatorial libraries, the challenge lies in the development of screening methods that allow for the fast, reliable, and general identification of catalytically active library members. This article reviews methods that allow not only simultaneous testing of but also read-out of catalytic activity with parallel libraries and one-bead-one-compound libraries.

Keywords Catalysis · Combinatorial chemistry · Sensing · High-throughput screening · One-bead-one-compound libraries

Abbreviations

Ac ₂ O	acetic anhydride
Asp	Aspartic acid
Cy3 and Cy5	Cyanine 3 and 5
DMAP	4-Dimethylaminopyridine
ee	Enantiomeric excess

GC	Gas chromatography
His	Histidine
HPLC	High performance liquid chromatography
MS	Mass spectrometry
PEGA	Polyethylene glycol acrylamide
Pmh	$\pi(\text{CH}_3)\text{His}$
Pro	Proline
PvdF	Polyvinylidene fluoride
TLC	Thin-layer chromatography
TMSCN	Trimethylsilylcyanide

1

Introduction

Catalytic efficiency is often determined by a subtle balance between steric, electronic, and stereoelectronic effects, and can often be modified significantly by seemingly slight structural changes that are difficult to predict. As a result, during the development of a new catalyst, a lot of time is often consumed by the sequential serial synthesis and testing of ligands with different yet similar substituents, and by trials for the best reaction conditions.

Nature optimizes enzymes through evolution, taking a “survival-of-the-fittest approach” to remove underachieving systems and further refine the best catalysts. In recent years, scientists have adopted the natural evolutionary principles of random mutation and selection of the fittest using combinatorial chemistry for catalyst discovery and optimization. Combinatorial chemistry allows for the simultaneous creation and evaluation of a large number of unique, yet structurally related molecules. Chemical approaches to the generation of molecular diversity use either parallel synthesis to create spatially addressable parallel libraries, split-and-mix synthesis for the generation of one-bead-one-compound libraries, or exploit equilibrating systems in dynamic combinatorial libraries. For the identification of catalytically active library members, the challenge lies in the development of screening methods that are general, fast, and reliable, a task which has been met with several smart screening methods [1–6].

This article reviews methods that allow not only for the simultaneous testing of but also readout of catalytic activity within the members of parallel libraries and one-bead-one-compound libraries. Approaches relying on the sequential analysis of products by high-throughput HPLC, GC, TLC etc., have been summarized in excellent reviews and will only be briefly highlighted here [7–9]. Furthermore, for the use of dynamic combinatorial libraries for catalyst discovery, the reader is referred to [6] and [10].

2 Screening of Spatially Addressable Libraries

The generation of parallel libraries encompasses the stepwise synthesis of each library member in a predetermined separate reaction container, often the wells of a 96-well microtitre plate. Screening for catalytic activity is typically performed with each compound individually, allowing for analysis of the reaction products by conventional means like HPLC, GC, TLC, MS or capillary array electrophoresis [7–9]. Given the relative ease of product identification, it is not surprising that the first approaches for the discovery of novel catalysts took advantage of this concept. In one of the earliest examples, Hoveyda and Snapper tested a parallel library of different Schiff bases as ligands for the $\text{Ti}(\text{OiPr})_4$ catalysed addition of TMSCN to meso-epoxides [11, 12]. Product yields and enantiomeric excesses were determined using HPLC. The screening resulted in the identification of a ligand that would have been difficult to design rationally, and has ever since been used successfully for a range of different reactions [13].

Parallel library screening using sequential analysis techniques is straightforward when the molecular diversity is limited in size, or when modern automation and miniaturization allows for a fast high-throughput monitoring of many thousands of reactions. Yet more efficient screening relies on monitoring a signal in parallel that is indicative of catalytic activity. Such methods visualize changes in the reaction heat ΔH_r° (Sect. 2.1), the emergence or disappearance of color or fluorescence (Sect. 2.2), or use enzyme based immunoassays (Sect. 2.3).

2.1 IR Thermographic Analysis

Perhaps the most general method for the identification of catalysts among the members of parallel libraries relies on monitoring changes in the reaction heat ΔH_r° . Infrared cameras enable recording of local spatial temperature changes with time and have been successfully used to visualize both the generation and the consumption of heat over the course of a catalytic reaction. IR thermography has been used by Reetz to develop catalysts for enantioselective acylations of secondary alcohols, enantioselective ring opening of epoxides, and metathesis reactions [14–16]. The first two examples are exothermic reactions, whereas the metathesis is an endothermic process. In the exothermic reactions, catalytic activity is indicated by “hot spots”, in the endothermic reaction “cold spots” are observed in the IR image. In all cases, the catalytic performance found by use of time-resolved IR thermography correlated well with the actual relative catalytic activities of the catalysts under examination [14, 15].

These examples and others [17–20] demonstrate the wide applicability of IR thermography to monitoring catalytic activity. A possible limitation of the method is the lack of structural information about reaction products formed, requiring analysis by other means. IR thermography has also been employed for the screening of one-bead-one-compound libraries (see Sect. 3.1).

2.2

Colorimetric and Fluorimetric Analysis

2.2.1

Heck Reactions

The Hartwig group used the formation of fluorescent products on a solid support to identify new catalysts for Heck reactions [21]. 45 different phosphine and diphosphine ligands were tested for their capacity to form active catalysts with Pd(dba)₂. As a test reaction, the coupling of a fluorescent alkene to an immobilized aryl halide was performed. Unreacted alkene was washed away, which allowed for the visualization of a successful coupling by the formation of fluorescent beads (Fig. 1).

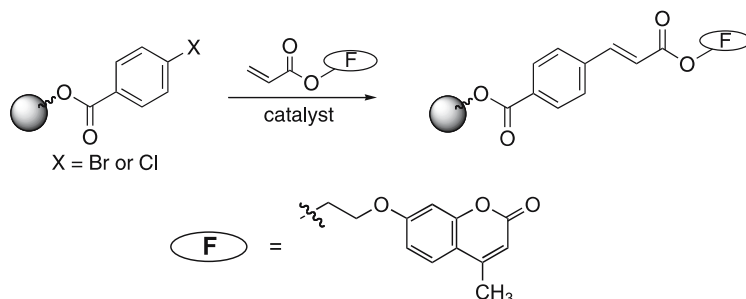


Fig. 1 Heck reaction on solid phase with a fluorescent reaction partner

The screening resulted in the identification of di(*tert*-butylphosphino)-ferrocene and tri(*tert*-butyl)phosphine as highly effective ligands for Heck reactions of not only aryl bromides but also less reactive aryl chlorides with alkenes.

A method to screen for Heck reaction catalysts in homogeneous solution was developed by Lavastre [22]. The screening relies on the formation of *N,N*-((dialkylamino)styryl)-pyridines followed by a subsequent alkylation to form the deeply red salts thereof (Fig. 2).

The intensity of the color of these charge-transfer complexes is so strong that even colored metal-ligand complexes can be tested if diluted sufficiently. Thus, the method should allow for the testing of a wide range of potential catalysts.

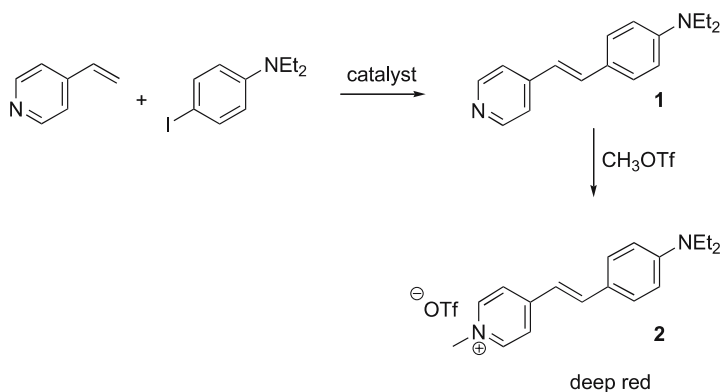


Fig. 2 Salts of *N,N*-((diethylamino)styryl)-*N*-methylpyridine as colored reaction products of Heck reactions followed by alkylation

2.2.2

Hydrosilations

The disappearance of color was used by Crabtree for the identification of catalysts for hydrosilations of imines and alkenes [23]. The group employed alkenes **3a** and imines **3b** with an electron donor (ferrocenyl substituent) on one side and an electron acceptor (pyrimidyl substituent) on the other side of the double bond. The color of these dark blue and purple compounds is bleached upon hydrosilation catalysed by an appropriate ligand-metal complex (Fig. 3). The group tested 12 potential catalysts, among them the known Wilkinson catalyst as a positive control. Besides the Wilkinson catalyst, $[\text{Pd}\{(\text{o-tolyl})_2\text{PC}_6\text{H}_4\}\text{OAc}]_2$ was found as a yet unknown catalyst for hydrosilations. The relative activities of the catalysts were quantified by recording the decrease in color by a digital camera and correlated well with those found in solution phase studies.

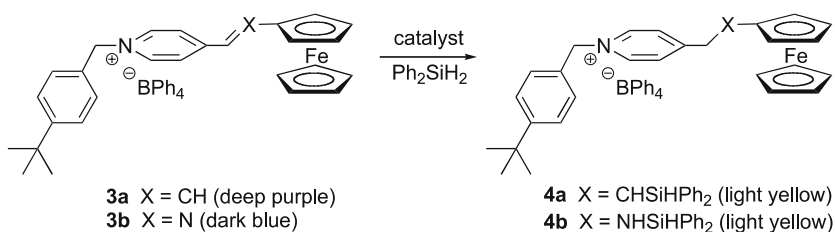


Fig. 3 Bleaching of reactive dyes to monitor hydrosilations

Catalysts identified in the screening proved their efficiency also for the hydrosilation of other imines and alkenes.

2.2.3 Allylic Alkylations

The formation of a colored side product was used by Morken and Lavastre for identifying catalytically active library members for allylic alkylations of β -dicarbonyl compounds [24]. The assay relies on the use of 1-naphthyl allyl carbonate **5** as an allyl source and the diazonium salt of Fast Red **6** as an indicator. Upon formation of an active π -allyl complex, CO_2 and 1-naphthyloxyde are liberated. The basicity of 1-naphthyloxyde is sufficient to deprotonate the β -dicarbonyl compounds which subsequently react with the π -allyl complex. The formed 1-naphthol is in turn the only compound in the reaction mixture that can react with the diazonium salt to form the red azo-dye Fast Red. The red color is therefore indicative of the formation of the π -allyl complex and naphthol (Fig. 4).

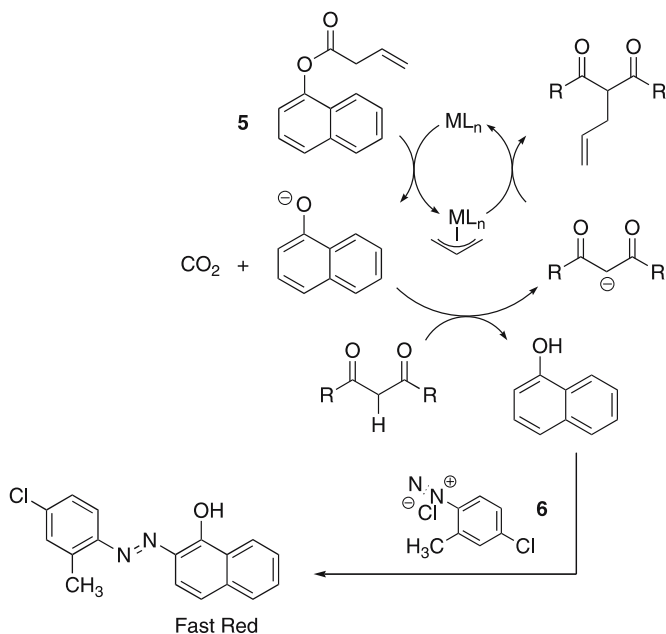


Fig. 4 Monitoring of a colored side product in allylic alkylations

The assay was employed to monitor the catalytic efficiency of combinations of 8 different ligands with 12 different metal salts for the allylation of β -dicarbonyl compounds. Aside from a well-known catalytically active $\text{Pd}(\text{OAc})_2$ /phosphine ligand complex that was used as a positive control, the group identified also Ir-based complexes like $[\{\text{IrCl}(\text{cod})\}_2]/i\text{Pr-pybox}$ as efficient catalysts. These are the first Ir-catalysts without a phosphine ligand capable of catalyzing allylic alkylations.

2.3

Analysis by Enzyme Immunoassays

Mioskowski and coworkers made use of competitive enzyme immunoassays (EIA) for the determination of both product yields and enantioselectivity [25]. The concept was introduced for the reduction of benzoyl formic acid to mandelic acid by screening combinations of 4 different metal species and 22 chiral diamine-based ligands using either $\text{HCO}_2\text{H}/\text{NET}_3$ or $i\text{PrOH}/\text{KOH}$ as hydrogen source. Yields were determined using an antibody that binds indiscriminately to both enantiomers of mandelic acid, while enantioselectivities were determined with a second enantiospecific antibody (Fig. 5). Competition for antibody-binding sites between an enzyme-product conjugate and reaction product resulted in a decrease in spectroscopic absorbance, relating directly to product concentration.

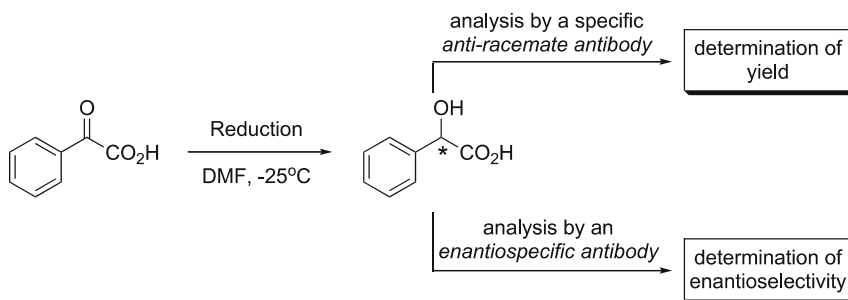


Fig. 5 Enzyme immunoassays to monitor catalytic activity and selectivity

Comparison between high-throughput screening and HPLC data indicated a very good correlation both in terms of catalytic conversion and specificity ($\pm 9\%$ ee). The screening demonstrated that $\text{HCO}_2\text{H}/\text{NET}_3$ is superior to $i\text{PrOH}/\text{KOH}$ as a hydrogen source, resulting in the identification of a $[\text{RuCl}_2(p\text{-cym})]_2$ - triflate ligand pair as a highly active and selective catalyst for the conversion of benzoyl formic acid to mandelic acid (98% yield, 80% ee). Provided that product-specific antibodies are available, the method is widely applicable. Noteworthy, the concept allows for the determination of both yields and enantioselectivities in parallel library screenings.

Another approach to the parallel monitoring of enantioselectivities that has so far not been linked with monitoring of activity, is based on kinetic resolution. This method, developed by Shair, exploits the difference in reactivity between enantiomeric reactive probes labelled with different fluorophores towards chiral analytes [26]. Other interesting approaches for monitoring the enantioselectivity of a given catalyst towards different substrates rely on the use of, for example, chiral liquid crystals or MS-based methods [27–31].

3

Screening of One-Bead-One-Compound Libraries for Catalytic Activity

One-bead-one-compound libraries allow for the facile generation of a significantly larger molecular diversity in comparison to parallel libraries without the need for automated synthesis [32, 33]. Successive cycles of 1. splitting the beads into equal portions, 2. subjecting each portion to a different reaction and 3. mixing of the beads, result in an exponential increase of the molecular diversity relative to the number of reactions performed. In split-and-mix libraries, each compound is located on a different bead, thus, the total amount of each compound on a single bead is much smaller compared to the amount of compounds prepared in a parallel library. The analysis of the compound on a single bead (1 bead carries typically only 100 pmol of compound) can be accomplished using, e.g., MS or NMR techniques [34], or by chemical encoding [35]. In comparison to parallel libraries, the screening of one-bead-one-compound libraries is a much greater challenge if the ensemble of beads is to be tested simultaneously. In parallel libraries, the catalyst is located together with reactants and products in a defined reaction container. In contrast, reactants and products are free to diffuse within the solvent surrounding all beads and leave the bead-bound catalyst—naturally—unchanged. This challenge has been met by the use of IR-thermography (Sect. 3.1), the formation of colored or fluorescent products (Sect. 3.2), fluorescent pH indicators (Sect. 3.3), the use of gels as reaction media (Sect. 3.4), and catalyst-substrate co-immobilization (Sect. 3.5).

3.1

IR Thermographic Analysis

Visualization of a change in the heat of reaction using IR-cameras, as described in Sect. 2.1 for screening of parallel libraries, has also been applied to the screening of one-bead-one-compound libraries. Morcken and Taylor tested a 3150-membered library for peptidic acylation catalysts by monitoring the change in reaction heat upon mixing the library with a solution of CHCl_3 : EtOH : NEt_3 : Ac_2O (8 : 1 : 1 : 1) [36]. IR thermographic analysis showed several “hot spots” around beads bearing active catalysts. Analysis of the compounds on the “hot beads” revealed a consensus for library members containing *N*-4-pyridylproline (Fig. 6).

Berkessel and Davis extended the IR thermographic on-bead screening to the use of gels as reaction media (see also Sect. 3.4) [37]. In a proof-of-concept experiment, polymer-bound DMAP was spread on the surface of a PvdF/ CH_3CN gel containing benzylalcohol, Et_3N and Ac_2O . IR thermographic imaging showed changes in the heat around these positive control beads. The use of gels as reaction media for IR thermographic analysis fa-

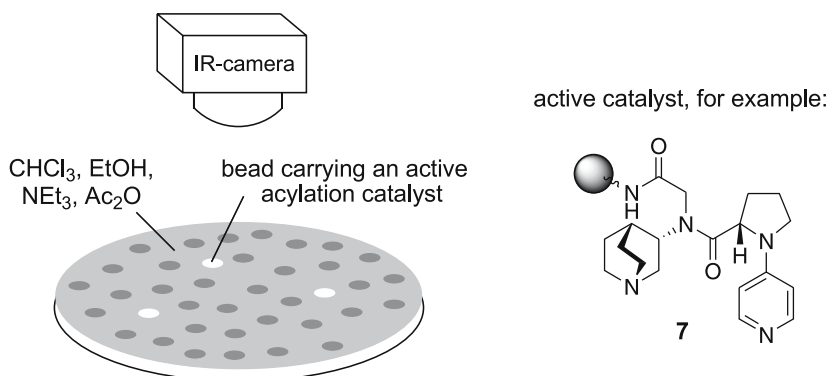


Fig. 6 On-bead IR thermographic screening for acylation catalysts

facilitates the isolation of active beads since they cannot float away during the isolation process.

3.2

Formation of Colored or Fluorescent Reaction Products

3.2.1

Insoluble Reaction Products

To monitor phosphatase activity among the members of a one-bead-one-compound library, Berkessel and Héroult developed phosphate ester **8** [38]. Upon hydrolysis of **8**, the water-insoluble turquoise indigo dye **9** forms and precipitates on beads carrying hydrolytically active compounds. Substrate **8** was used to test the Zr(IV) complexes of a 625-membered undecapeptide library for hydrolytic activity. Beads with active metal-complexes were easily identified using a low-power microscope. The screening resulted in several hits with serine at the N-terminus and His-Phe at the C-terminus. The corresponding Zr(IV) complexes showed slight phosphatase activity (Fig. 7). The same assay was used by Goldberg for the discovery of hydrolytically active Zn-peptide complexes [39].

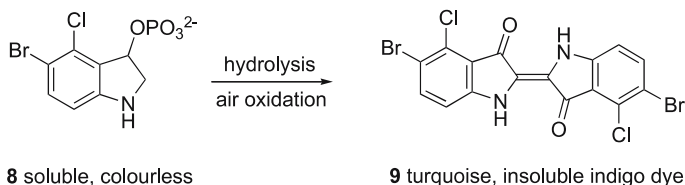


Fig. 7 Insoluble indigo as a colored product of phosphate ester hydrolysis

The group also introduced the “Prussian blue assay” and the “cresyl violet assay” to develop compounds with phosphodiesterase activity [40]. Both assays monitor the ability of the members of one-bead-one-compound libraries to transesterify phosphodiester substrates [41].

A further assay for monitoring phosphatase activity among the members of split-and-mix libraries was developed by Morken [42]. Hydrolysis of the water soluble naphthyl phosphate **10** leads to precipitation of the insoluble naphthol derivative **11** on beads carrying hydrolytically active compounds. The hydrolysis product **11** was visualized by reaction with the diazonium salt **12** generating the red diazo dye **13** (Fig. 8). Using this detection system, Gd(III)-salicylaldimine complexes with phosphatase activities that are 4–10 times above background level were identified.

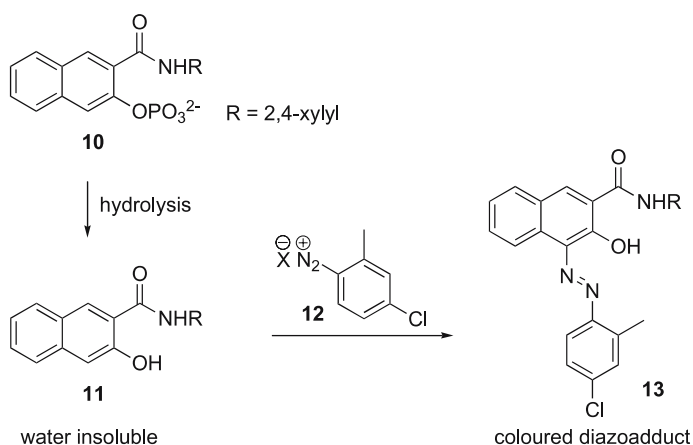


Fig. 8 Colored probes to test for phosphatase activity

3.2.2

Soluble Reaction Products

Reymond demonstrated that soluble colored reaction products can also be used to identify catalysts among the members of one-bead-one-compound libraries [43, 44]. The assay relies on soaking the library beads with a solution of a colorless substrate that is upon reaction converted to a colored product. Since no solvent surrounds the library beads, the rate of product diffusion away from the beads is limited to an extent that allows for product identification on the beads where it was generated. The group showed the value of the screening technique by identifying peptide dendrimers as catalysts for hydrolysis [43, 44] and aldol reactions [45, 46]. Pyrene ester **14** and coumarin derivative **15** were used to screen for hydrolytic and retro-aldol activity, respectively, since their products are highly fluorescent (Fig. 9).

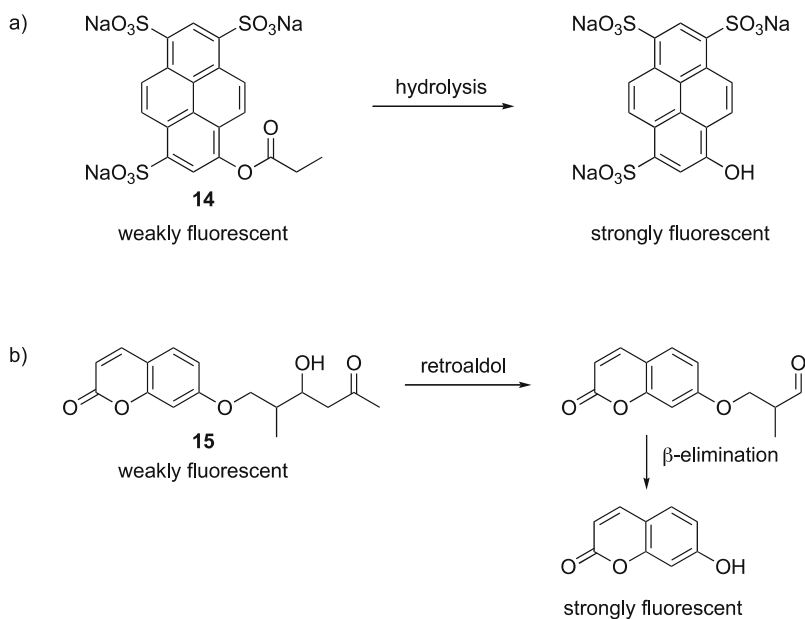


Fig. 9 Fluorescent probes to monitor (a) hydrolytic and (b) retroaldol activity

The screening for dendrimers with hydrolytic activity resulted in the identification of catalysts with enhanced activity over background level [43, 44]. Catalytic dendrimers selected for aldol reactions showed modest to good activities and enantioselectivities in aldol reactions between aldehydes and acetone [45, 46]. The work demonstrated that the efficiency of catalytic peptide dendrimers examined increases with higher dendrimer generations [47].

3.3

Fluorescent pH Indicators

Miller pioneered the use of pH-sensitive molecular sensors for the discovery of catalysts for reactions during which a change in pH occurs [48]. The group used aminomethylantracene as a pH-sensor that responds proportionally to decreasing pH with an increase in its fluorescence. The sensor was employed both for the screening of parallel arrays and for single-bead analysis [49]. For the latter, beads were co-functionalized with the sensor and the potential catalyst. The method was employed for the identification of peptides capable of catalyzing the acylation of alcohols with Ac_2O . Catalytic activity was monitored based on the acetic acid generated in the acyl transfer reaction, triggering the fluorescence response (Fig. 10).

Within a 7.5×10^6 membered octapeptide library with π -(CH_3)-histidine (Pmh) at the N-terminus and alanine at the C-terminus, catalysts were iden-

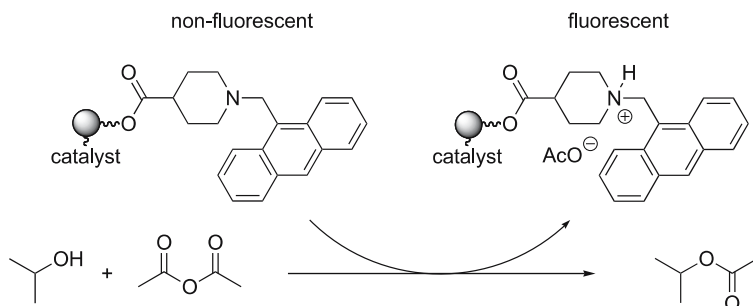


Fig. 10 pH-sensitive fluorescence indicators

tified with acylating activities that are significantly higher compared to that of DMAP [50, 51]. In a second generation library built around the initial lead Boc-Pmh-L-Asn(Trt)-D-Val-L-His(Trt)-D-Phe-D-Val-D-Val-L-Ala-resin, catalysts with yet greater activities and specificities were identified [50, 51]. Catalysts were in general more active and selective when removed from the solid support and tested in homogeneous solution. Furthermore, the catalysts with the highest activities also proved to be the most selective in acylating, for example, one enantiomer of *sec*-phenylethanol over the other. Thus, although the assay was designed to screen for catalysts with high activity, these catalysts also proved highly selective. The identified peptidic acylation catalysts have found manifold use, for example in the kinetic resolution of secondary and tertiary alcohols, and regioselective acylations [48, 50–53].

3.4

Gels as Reaction Media

Gels reduce the diffusion of reactants and products and fix beads to defined positions. As a result, the area around an embedded bead is a miniature reaction compartment where reaction products remain long enough to allow for detection. Miller pioneered this idea using a cross-linked PEGA polymer functionalized with a pH sensor (see above) as reaction media to test a one-bead-one-compound library for acylation catalysts [54]. Screening of a peptide library resulted in fluorescent halos only around beads with active catalysts. The PEGA-based polymer swells in a range of different solvents, thereby allowing screening in a wide variety of solvents.

Davis subsequently showed that low-melting agarose can be used as a reaction medium for screening in aqueous environments [55]. In proof-of-concept experiments the group used immobilized β -D-galactosidase in agarose gel to assay the formation of yellow *o*-nitrophenolate during hydrolysis of *o*-nitrophenyl- β -D-galactopyranoside **16** (Fig. 11).

From a mixture of both enzyme-bearing and enzyme-free beads added to the surface of the pyranoside-containing gel, only those beads functionalized

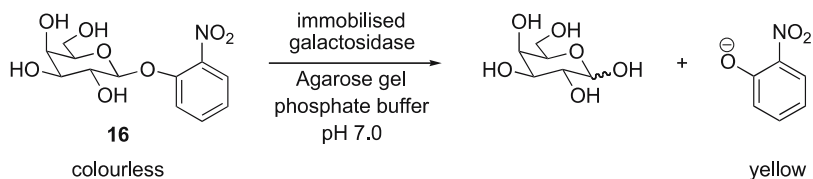


Fig. 11 Gel-based screening for hydrolytic activity

with galactosidase developed colored regions around themselves, indicative of hydrolytic activity. The scope of agarose-based screens was further expanded by Davis to encompass reactions during which a pH change occurs, simply by adding a non-covalently bonded pH indicator (methyl red) to the agarose [55]. Esterase activity was monitored based on the concomitant generation of acid leading to the formation of red halos around active beads.

Furthermore, Davis and Berkessel demonstrated the use of poly(vinylidene fluoride) (PvdF)-based gels for monitoring reactions in organic solvents [37]. In proof-of-concept-experiments bead-bound piperazine was spread on a PvdF gel containing pyrenecarboxaldehyde and either malonitrile or ethyl cyanoacetate. The Knoevenagel condensation resulted in red and yellow fluorescent products, respectively, that were readily visualized in the surroundings of the beads functionalized with piperazine (Fig. 12).

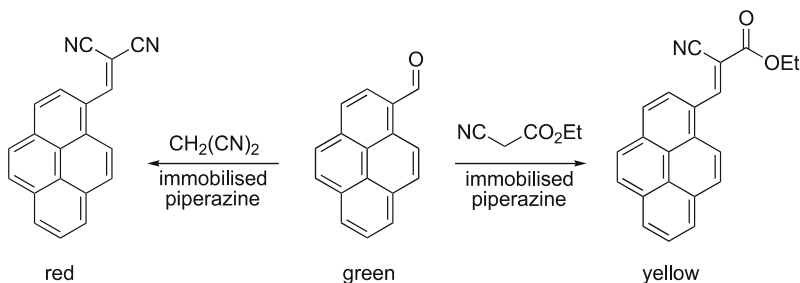


Fig. 12 Fluorescent probes to monitor Knoevenagel condensation

Thus, the use of gels is a versatile technique when either colored or fluorescent reaction products are formed or when product specific sensors can be employed.

3.5

Catalyst-Substrate Co-immobilization

Wennemers developed a screening method based on the immobilization of one reaction partner (**A**) together with each library member, the potential catalysts, on the same bead [56, 57]. A second reaction partner (**B**) is labelled

with a marker, for example a dye, fluorophor or radiolabel. Incubation of the catalyst-substrate co-immobilized library with the marked reaction partner **B** results in covalent attachment of the marker on beads carrying compounds that are able to mediate the reaction between **A** and **B** (Fig. 13). These beads are readily identified with a low-power microscope. A similar method was developed by Bradley employing a Diels–Alder cycloaddition as a model reaction [58].

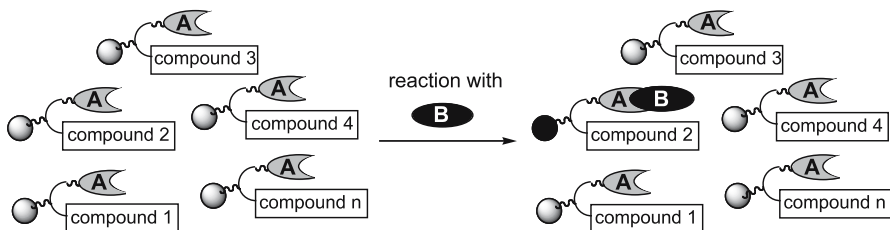


Fig. 13 Catalyst–substrate co-immobilization

The method was used for the discovery of peptidic catalysts for aldol reactions [59]. Screening of a library with maximally 3375 different tripeptides using levulinic acid and benzaldehyde derivatives as reaction partners **A** and **B** resulted in the identification of the peptides H-L-Pro-D-Ala-D-Asp-NH₂ and H-L-Pro-L-Pro-L-Asp-NH₂. Evaluation of the catalytic properties in solution phase showed that both peptides are highly active and selective catalysts for aldol reactions [59].

4 Conclusions

Over the last decade, smart combinatorial screening methods have emerged as valuable tools to accelerate the catalyst discovery and development process. Catalytic motives have been discovered that would otherwise not have been disclosed through rational design alone. Once a catalytically active moiety is identified, combinatorial chemistry allows for further improvement by the preparation and testing of a 2nd-generation library based on the initial lead structure. It is then the integration of smart combinatorial screening methods and insightful rational design that allows for the highly expedient catalyst discovery and development. To date, most smart-screening methods are based on disclosure of activity rather than selectivity, and noteworthily, the most active catalyst often proves to be the most selective. Nevertheless, there remains a need to establish more versatile methods that not only allow visualization of catalytic activity, but also sensing of enantioselectivity.

Acknowledgements We are grateful for support from the Swiss National Science Foundation and Bachem. H.W. thanks Bachem for an endowed professorship.

References

1. Fonseca MH, List B (2004) *Curr Opin Chem Biol* 8:319
2. Goddard J-P, Reymond J-L (2004) *Curr Opin Biotech* 15:314
3. Wennemers H (2004) In: Schmuck C, Wennemers H (eds) *Highlights in Bioorganic Chemistry*. Wiley, Weinheim, p 436
4. Berkessel A (2003) *Curr Opin Chem Biol* 7:409
5. Archibald B, Brummer O, Devenney M, Gorer S, Jandeleit B, Uno T, Weinberg HW, Weskamp T (2002) In: Nicolaou KC, Hanko R, Hartwig W (eds) *Handbook of Combinatorial Chemistry*. Wiley, Weinheim, p 885
6. Breit B (2005) *Angew Chem Int Ed* 44:6816
7. Bonnette F, Gallard L, Lavastre O (2004) *Curr Opin Chem Biol* 8:311
8. Kenseth JR, He Y, Tallman D, Pang H, Coldiron SJ (2004) *Curr Opin Chem Biol* 8:327
9. Ding K, Du H, Yuan Y, Long J (2004) *Chem Eur J* 10:2872
10. Otto S, Severin K (2007) *Dynamic Combinatorial Libraries for the Development of Synthetic Receptors and Sensors*. *Top Curr Chem*, in this volume
11. Cole BM, Shimizu KD, Krueger CA, Harrity JPA, Snapper ML, Hoveyda AH (1996) *Angew Chem Int Ed* 35:1668
12. Shimizu KD, Cole BM, Krueger CA, Snapper ML, Hoveyda AH (1997) *Angew Chem Int Ed* 36:1704
13. Hird AW, Kacprzyński MA, Hoveyda AH (2004) *Chem Commun* p 1779
14. Reetz MT, Becker MH, Kühling KH, Holzwarth A (1998) *Angew Chem* 110:2792
15. Reetz MT, Becker MH, Kühling KH, Holzwarth A (1998) *Angew Chem Int Ed* 37:2647
16. Reetz MT, Becker MH, Liebl M, Fürstner A (2000) *Angew Chem Int Ed* 39:1236
17. Ashkenazi E, Andreae MRM, Berkessel A (2003) *Appl Cat A: Gen* 254:27
18. Moates FC, Somani M, Annamalai J, Richardson JT, Luss D, Willson RC (1996) *Ind Eng Chem Res* 35:4801
19. Holzwarth A, Schmidt HW, Maier WF (1998) *Angew Chem* 110:2788
20. Holzwarth A, Schmidt HW, Maier WF (1998) *Angew Chem Int Ed* 37:2644
21. Shaughnessy KH, Kim P, Hartwig JF (1999) *J Am Chem Soc* 121:2123
22. Regnier T, Garbacia S, Laurent P, des Abbayes H, Lavastre O (2005) *QSAR Comb Sci* 10:1164
23. Cooper AC, McAlexander LH, Lee DH, Torres MT, Crabtree RH (1998) *J Am Chem Soc* 120:9971
24. Lavastre O, Morken JP (1999) *Angew Chem Int Ed* 38:3163
25. Taran F, Gauchet C, Mohar B, Meunier S, Valleix A, Renard PY, Créminon C, Grassi J, Wagner A, Mioskowski C (2002) *Angew Chem Int Ed* 41:124
26. Korbelt GA, Lalic G, Shair MD (2001) *J Am Chem Soc* 123:361
27. Van Delden RA, Feringa BL (2001) *Angew Chem Int Ed* 40:3198
28. Markert C, Pfaltz A (2004) *Angew Chem Int Ed* 43:2498
29. Becker MH, Klein H-W, Stöckigt D, Reetz MT (1999) *Angew Chem Int Ed* 38:1758
30. Guo J, Wu J, Siuzdak G, Finn MG (1999) *Angew Chem Int Ed* 38:1755
31. Finn MG (2002) *Chirality* 14:534
32. Furka Á, Sebestyén F, Asgedom M, Dibó G (1991) *Int J Pept Protein Res* 37:487
33. Lam KS, Salmon SE, Hersh EM, Hruby VJ, Kazmierski WM, Knapp RJ (1991) *Nature* 354:82

34. Yan B (2002) *Curr Opin Chem Biol* 6:328
35. Krämer T, Antonenko VV, Mortezaei R, Kulikov NV (2002) In: Nicolaou KC, Hanko R, Hartwig W (eds) *Handbook of Combinatorial Chemistry*. Wiley, Weinheim, p 170
36. Taylor SJ, Morken JP (1998) *Science* 280:267
37. Johansson K-J, Andrae MRM, Berkessel A, Davis AP (2005) *Tetrahedron Lett* 46:3923
38. Berkessel A, Héroult DA (1999) *Angew Chem Int Ed* 38:102
39. Namuswe F, Goldberg DP (2006) *Chem Commun* p 2326
40. Berkessel A, Riedl R (2000) *J Comb Chem* 2:215
41. DeMuyndck H, Maddar A, Farcy N, De Clercq PJ, Pérez-Payán MN, Öhberg LM, Davis AP (2000) *Angew Chem Int Ed* 39:145
42. Danek SC, Queffelec J, Morken JP (2002) *Chem Commun* p 528
43. Clouet A, Darbre T, Reymond J-L (2004) *Angew Chem Int Ed* 43:4612
44. Clouet A, Darbre T, Reymond J-L (2006) *Biopolymers (Pept Sci)* 84:114
45. Kofoed J, Darbre T, Reymond J-L (2006) *Org Biomol Chem* 4:3268
46. Kofoed J, Nielsen J, Reymond J-L (2003) *Bioorg Med Lett* 13:2445
47. Kofoed J, Reymond J-L (2005) *Curr Opin Chem Biol* 9:656
48. Miller SJ (2004) *Acc Chem Res* 37:601
49. Copeland GT, Miller SJ (1999) *J Am Chem Soc* 121:4306
50. Copeland GT, Miller SJ (2001) *J Am Chem Soc* 123:6496
51. Fierman MB, O'Leary DJ, Steinmetz WE, Miller SJ (2004) *J Am Chem Soc* 126:6967
52. Lewis CA, Miller SJ (2006) *Angew Chem Int Ed* 45:5616
53. Sculimbrene BR, Miller SJ (2001) *J Am Chem Soc* 123:10125
54. Harris RF, Nation AJ, Copeland GT, Miller SJ (2000) *J Am Chem Soc* 122:11270
55. Müller M, Mathers TW, Davis AP (2001) *Angew Chem Int Ed* 40:3813
56. Krattiger P, McCarthy C, Pfaltz A, Wennemers H (2003) *Angew Chem Int Ed* 42:1722
57. Krattiger P, Kovásy R, Revell JD, Wennemers H (2005) *QSAR Comb Sci* 24:1158
58. Lingard I, Bhalay G, Bradley M (2003) *Chem Commun* 18:2310
59. Krattiger P, Kovásy R, Revell JD, Ivan S, Wennemers H (2005) *Org Lett* 7:1101

Dynamic Combinatorial Libraries for the Development of Synthetic Receptors and Sensors

Sijbren Otto¹ (✉) · Kay Severin² (✉)

¹Department of Chemistry, University of Cambridge, Lensfield Road,
Cambridge CB2 1EW, UK
so230@cam.ac.uk

²Institut des Sciences et Ingénierie Chimiques, École Polytechnique Fédérale
de Lausanne, 1015 Lausanne, Switzerland
kay.severin@epfl.ch

1	Introduction	268
2	Dynamic Combinatorial Libraries as Tools for Developing New Synthetic Receptors	269
2.1	Synthetic Receptors Developed Using Imine Exchange	269
2.2	Synthetic Receptors Developed Using Hydrazone Exchange	272
2.3	Synthetic Receptors Developed Using Disulfide Exchange	275
2.4	Synthetic Receptors Developed Using Acetal Exchange	278
3	Sensing with Dynamic Combinatorial Libraries	279
4	Conclusions	286
	References	287

Abstract Dynamic combinatorial libraries are mixtures of compounds that continuously interchange their subunits, resulting in a thermodynamically controlled product distribution. Such mixtures are responsive to their environment. Thus, introducing a guest or analyte into a mixture of potential receptors will result in a change in the product distribution in response to molecular recognition events. One way of utilizing this response is for the discovery of new synthetic receptors. We show several examples where new receptors have been identified from the increase in their concentration in the dynamic mixture after introducing a guest. Alternatively, rather than focusing on one particular species in the complex mixture, the response of the entire library can be used as a reporter on the nature of the guest. We show how libraries made from building blocks that are UV-Vis or fluorescently active can act as sensors. When analyzed with chemometrics methods, sensor DCLs can give remarkable results.

Keywords Combinatorial chemistry · Molecular recognition · Sensors · Systems chemistry · Synthetic receptors · Thermodynamic control

Abbreviations

DCC Dynamic combinatorial chemistry
DCL Dynamic combinatorial library
CHES *N*-Cyclohexyl-2-aminoethane sulfonic acid
LDA Linear discriminant analysis

1 Introduction

Traditionally, the development of chemosensors has involved preparing selective synthetic receptors and equipping these with a mechanism that converts a binding event into a signal of some sort. Recently, the development of more complex sensors has received increasing attention. In these systems the sensing is performed by a collection of separate sensors acting simultaneously. While the desired information (e.g., concentration) is more difficult to derive from these complex sensors, they may display an enhanced analytical power.

Dynamic combinatorial chemistry (DCC) is a potent tool for further development of both these approaches. DCC was pioneered by the groups of Sanders and Lehn in the mid-1990s. In the last decade, DCC has emerged as a powerful method for discovering molecules that are good at molecular recognition [1–9]. It has been used to develop small molecule ligands for biomolecules [1, 3, 9, 10], to identify molecules that fold into specific structures driven by intramolecular noncovalent interactions [9], and for the discovery and synthesis of synthetic receptors [6, 8, 9, 11, 12]. In DCC a mixture of compounds is generated by connecting simple building blocks using a reversible reaction. Reversibility ensures that the compounds in the resulting dynamic combinatorial library (DCL) continuously interchange their building blocks, producing an equilibrium mixture. When a DCL of potential synthetic receptors is exposed to a guest (or template) those receptors with a high affinity will be stabilized, resulting in a shift in the equilibrium towards, ideally (*vide infra*), the best binders at the expense of their inferior counterparts (Fig. 1).

Some leading examples of the use of DCLs as tools to identify new synthetic receptors are discussed in Sect. 2. However, rather than isolating the individual new receptors, DCLs can also be used in their entirety as complex sensors, where a signal is derived from the collective response of all potential binders to the introduction of the analyte. This application is discussed in Sect. 3.

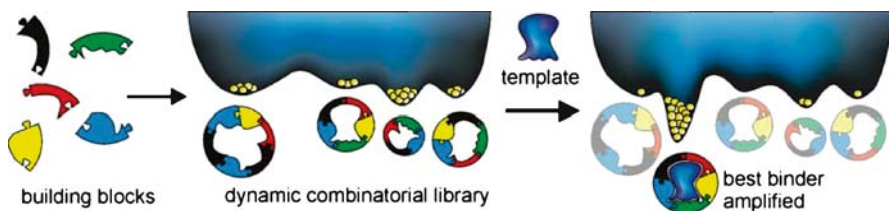


Fig. 1 Schematic representation of a DCL and its free energy landscape, showing how introduction of a template can lead to the amplification of the receptor with the highest affinity for the guest

2

Dynamic Combinatorial Libraries as Tools for Developing New Synthetic Receptors

Developing synthetic receptors by design remains a formidable challenge, largely as a result of the fact that the current understanding of noncovalent interactions and conformational preferences of large molecules is still limited. Developing synthetic receptors using a combinatorial strategy is an attractive alternative as it reduces the level of detail required in the design of the receptors. Rather than having to construct the complete receptor, it is sufficient to design and synthesize a series of potential subunits that contain certain recognition elements and functional groups that can engage in reversible bond formation. During the dynamic combinatorial experiment the molecules will construct themselves, in the presence of the guest, automatically adopting the optimum arrangement of subunits to give the best receptor in an increased (amplified) amount. Thus, these synthetic receptors can be identified by comparing the library distribution in the absence of the guest with that in the presence of the guest. For small libraries such comparison can be made using NMR. Larger libraries will require the use of chromatographic techniques to analyze product distributions, with multidimensional techniques such as LC-MS being particularly powerful.

Care should be taken to choose the experimental conditions carefully to avoid potential pitfalls where amplification is not necessarily selective for the best binders. An extensive discussion of this subject can be found in [13–17]. In practice, performing the screening of DCLs with modest amounts of template dramatically reduces the chance of encountering potentially misleading results. Use of substoichiometric amounts of template eliminates such problems altogether, but also gives smaller amplifications.

We will now discuss some selected examples of synthetic receptors developed using a dynamic combinatorial approach. These examples are organized on the basis of the type of reversible chemistry used and are restricted to robust covalent bonds. A very recent and comprehensive review of dynamic combinatorial receptors can be found in [9]. Surprisingly, thus far none of the receptors developed using DCC has found application as a sensor.

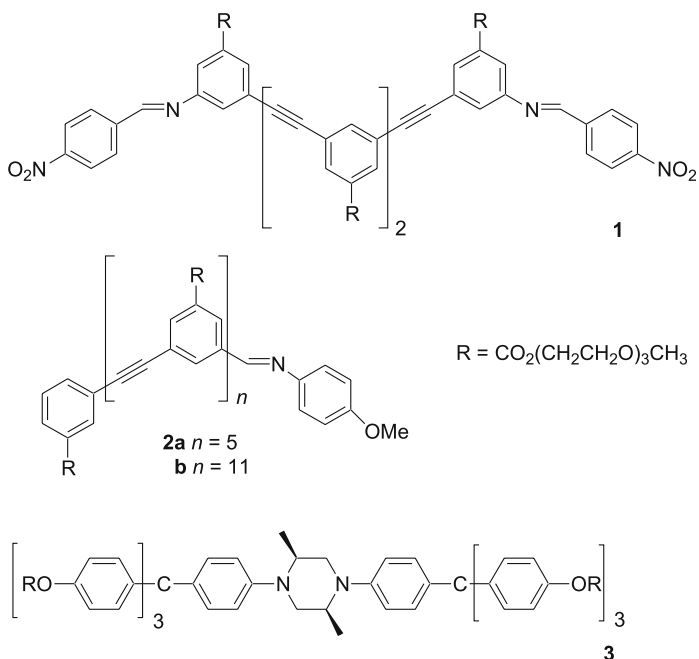
2.1

Synthetic Receptors Developed Using Imine Exchange

Imine ($C=N$) linkages are amongst the most labile covalent bonds that have been used in DCC. While exchange can take place under relatively mild conditions, a disadvantage of imine bonds is their susceptibility to hydrolysis, hampering the analysis of DCLs of imines by chromatographic methods. Also, isolation of individual library members can be troublesome. These problems

can often be solved by the in-situ reduction of the labile imines to give stable amines. However, the geometric and electronic properties of the resulting amines are somewhat different from the original imines.

The Moore group has developed imine building blocks **1** and **2** which, upon mixing, can equilibrate to form a small DCL of linear oligomers of different lengths (Scheme 1) [18].

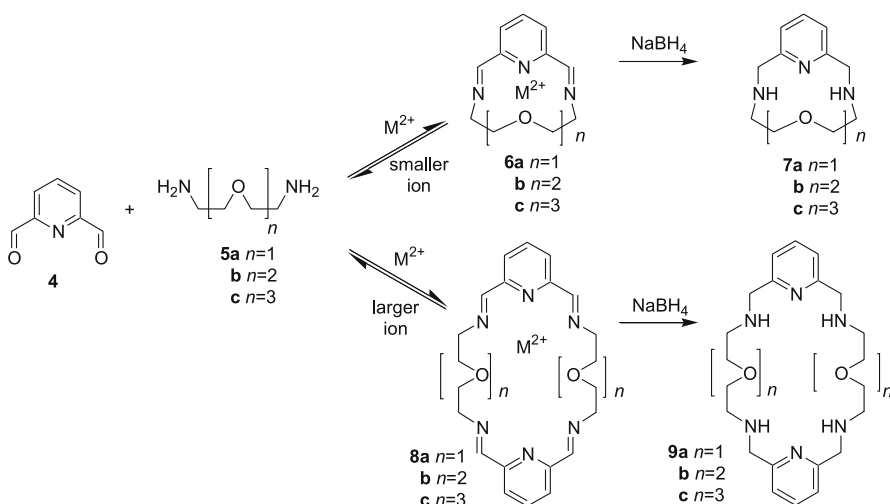


Scheme 1 Imine oligomers **1** and **2** used as building blocks and rod-shaped guest **3** used to amplify its receptor from a DCL made from **1** and **2** [18]

When using chloroform as a solvent a statistical distribution of oligomers is obtained. However, in the more polar acetonitrile, the longer oligomers fold into helical structures as a result of solvophobic interactions. The favorable interactions that occur upon folding shift the equilibrium in the direction of the **1(2)₂** oligomers. In their folded conformation these molecules define a tubular cavity in their interior that has the potential to act as a binding site for a guest. Indeed, exposure of the small DCL to rod-shaped guest **3** resulted in the amplification of receptor **1(2a)(2b)**, which has a cavity length that matches the length of guest **3**. These results suggest that tailored size-selective recognition of guests using such systems should be possible.

The Lünig group has developed macrocyclic receptors for metal ions using imine chemistry [19, 20]. The size of the metal ion that was used as the

template dictated the size of the resulting macrocycle. The building blocks that were used were pyridinedicarboxaldehyde **4** and a series of ethyleneoxide oligomers with two terminal amine functionalities **5a–c** (Scheme 2).

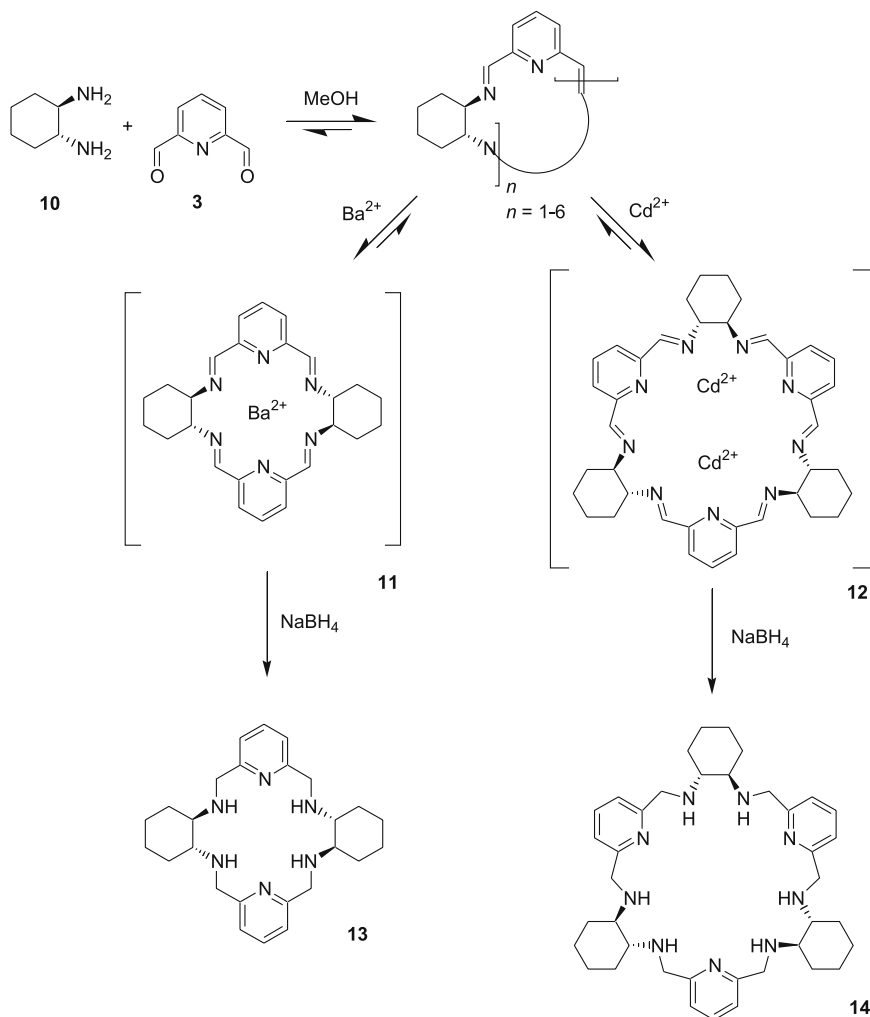


Scheme 2 The Luning approach to macrocyclic imine receptors for metal ions and their reduction to stable amines [19, 20]

When using the small Mg^{2+} ion and building blocks **4** and **5a**, the smallest [1 + 1] macrocycle **6a** was amplified. In the presence of larger cations such as Sr^{2+} the [2 + 2] macrocycle **8a** was also formed. When mixing all four building blocks and three different metal ions (Mg^{2+} , Ca^{2+} and Ba^{2+}) all three macrocycles **6a–c** were formed simultaneously in good yields. The analysis of the library composition required the unstable imines to be converted to the amine macrocycles **7** and **9** through the addition of sodium borohydride.

Gotor and coworkers have used the same dialdehyde **4** in combination with a different diamine **10** (Scheme 3) [21, 22].

When using a homochiral version of the diamine [2 + 2] and [3 + 3] macrocycles were amplified, again depending on the size of the cation: Ba^{2+} induced the amplification of the smaller macrocycle **11**, while Cd^{2+} gave the larger macrocycle **12** in almost quantitative yield [21]. Interestingly, when *trans*-diamine **10** was used as a racemic mixture, addition of Cd^{2+} resulted in the diastereoselective amplification of the heterochiral [3+3] macrocycle, producing a racemic mixture of the (*R,R*)(*S,S*)₂ and (*R,R*)₂(*S,S*) receptors [22]. Also here, the initial imine macrocycles were reduced in situ to the amines **13** and **14**, which resulted in a reduction of binding affinity.



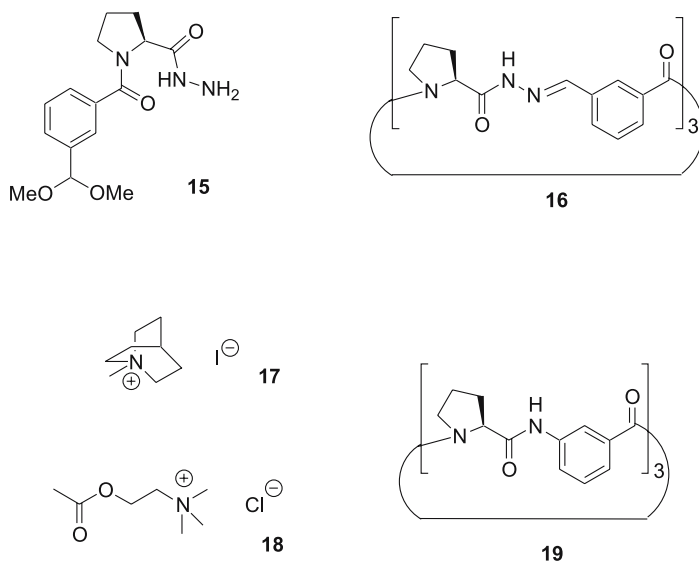
Scheme 3 The Gotor approach to macrocyclic imine receptors for metal ions and their reduction to stable amines [21, 22]

2.2

Synthetic Receptors Developed Using Hydrazone Exchange

Like imines, hydrazones feature an exchangeable $\text{C}=\text{N}$ bond, but when compared to imines, hydrazones are hydrolytically much more stable. Hydrazone exchange typically requires acidic conditions, although for some substrates containing strongly electron withdrawing groups, exchange is feasible even under neutral conditions [23]. The hydrazone exchange reaction was first

used for DCC by the Sanders group, who developed a family of bifunctional building blocks featuring an aldehyde unit on one end (protected as a dimethoxyacetal) and a hydrazide unit on the opposite end [24]. The building block design was based on amino acids and dipeptides. The first synthetic receptor to come out of these studies was based on the L-proline-containing building block **15**, which is similar to the repeating unit in a macrocyclic receptor for cations (**19**) developed by Kubik [25] (Scheme 4). The latter receptor is known to bind cations like *N*-methylquinuclidium iodide (**17**) and acetylcholine chloride (**18**).

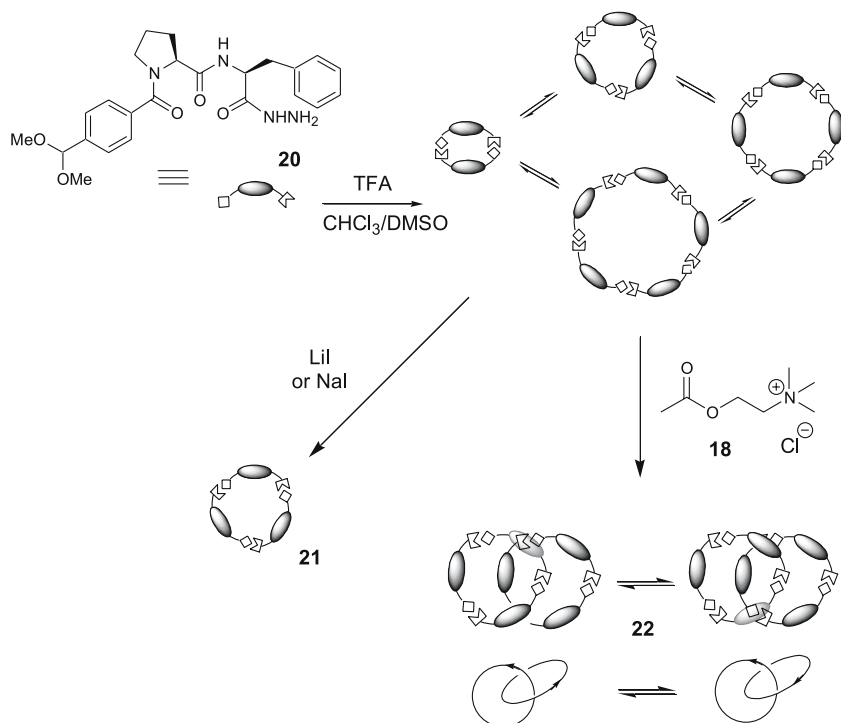


Scheme 4 In the presence of templates **17** or **18**, hydrazide building block **15** can be converted into receptor **16** [26, 27], which has some similarity to a previously described designed receptor **19** [25]

Exposing a small DCL made from building block **15** to these cations indeed induced the amplification of the analogous trimeric receptor **16** [26, 27]. The affinity of this new receptor for the cationic guests in chloroform was modest (150 and 230 M⁻¹ for **17** and **18**, respectively) and two orders of magnitude smaller than that of the original Kubik receptor.

More impressive results were obtained using dipeptide-derived building block **20**, which contains a L-phenylalanine unit in addition to a L-proline unit (Scheme 5).

Exposure of a small DCL made from this compound to Li⁺ or Na⁺ salts induced the amplification of trimeric macrocycle **21**, which was found to bind Li⁺ with a binding constant of 4 × 10⁴ M⁻¹ (in 98 : 2 chloroform/methanol) [28, 29]. NMR studies revealed that the receptor undergoes



Scheme 5 Exposing a DCL made from hydrazone building block **20** to different templates results in the amplification of a trimeric receptor for alkali metal ions [28, 29] and a catenane that binds acetylcholine [30]

a substantial conformational change upon binding the cation and that the binding most likely occurs through coordination of several of the carbonyl oxygens.

Undoubtedly the most impressive result to come out of these studies was the discovery of a [2]-catenane (**22**) that emerged after exposing the DCL made from building block **20** to acetylcholine chloride (**18**) [30]. In the course of 44 days the amount of [2]-catenane increased to ultimately account for 70% of the material in the library. While in principle two stereoisomeric catenanes can be formed, a clear preference for the formation of one of these was observed. The catenane binds acetylcholine chloride with an exceptionally high affinity ($1.4 \times 10^7 \text{ M}^{-1}$ in 95 : 5 chloroform/DMSO). While the exact mode of binding is still under investigation, it appears that the binding site for acetylcholine is located where the two rings of the catenane **22** meet.

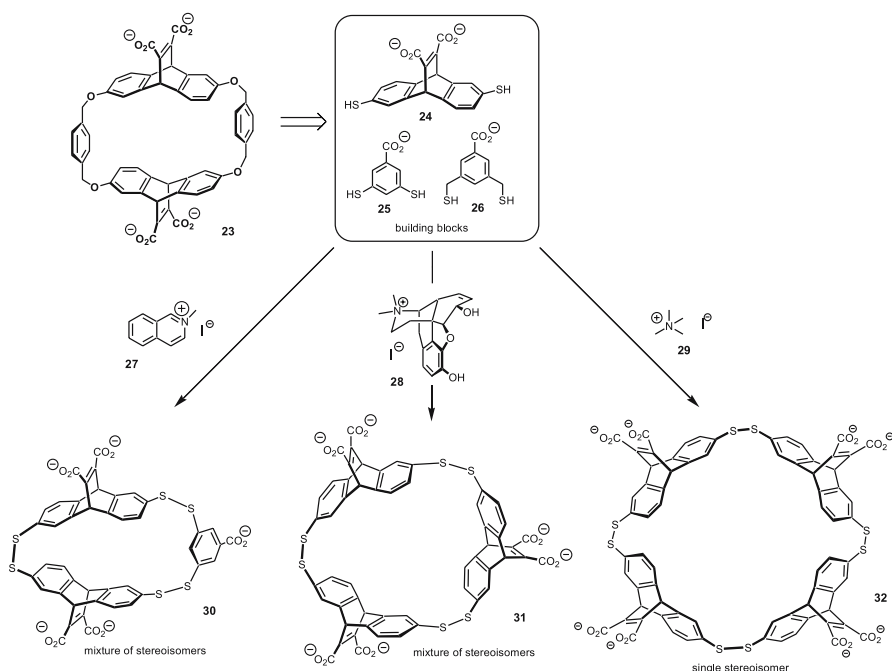
Discovery of this unpredictable and highly complex host is a clear demonstration of the power of DCC as a tool for the development of new synthetic receptors.

2.3

Synthetic Receptors Developed Using Disulfide Exchange

Disulfide exchange is one of the few reversible reactions currently used for DCC that operates under physiological conditions [31, 32]. Disulfide DCLs are often generated starting from thiol building blocks, which are allowed to irreversibly oxidize to form the desired disulfides. While oxidation is taking place the reaction passes through a phase where thiol and disulfide coexist, allowing the actual exchange process to occur through the nucleophilic attack of thiolate anion on the disulfide bond, liberating another thiolate anion in the process. Thus, exchange requires a catalytic amount of thiolate anion, which provides a handle to switch the exchange process off through protonation of the thiolate nucleophile or through allowing the oxidation process to go to completion.

We have developed a series of macrocyclic receptors that bind ammonium ions in water from DCLs made from building blocks **24–26** (Scheme 6) [33, 34].

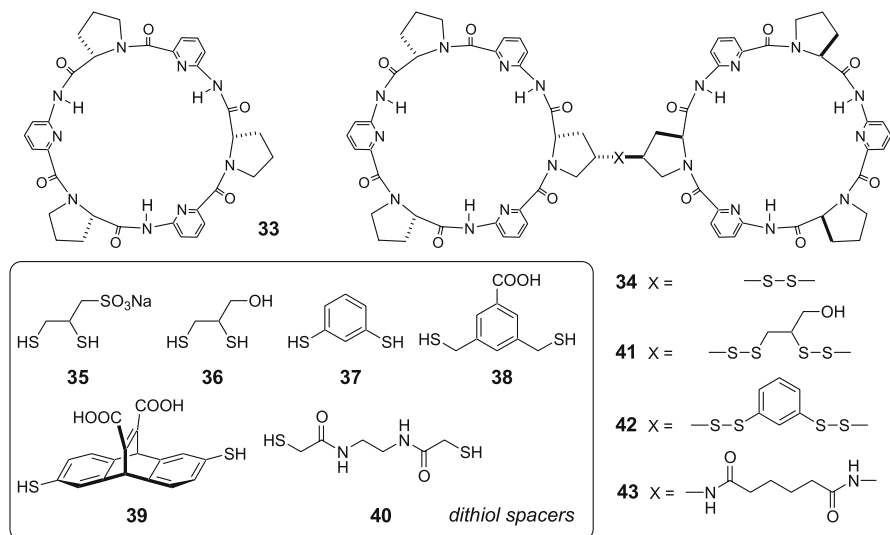


Scheme 6 Exposing a DCL made from three different dithiol building blocks to three different templates results in the amplification of three different receptors [33, 34]

These DCLs contain a considerably larger number of compounds than the previous examples. The design of the dithiol building blocks was inspired by the successful cyclophane receptor **23**, developed by the Dougherty laboratory [35]. For our initial studies we selected guest **27**, which is one of the best

binders to the original Dougherty host. We expected this guest to amplify a [2 + 2] disulfide macrocycle with a structure analogous to the cyclophane **23**. However, much to our surprise we found that [2 + 1] macrocycle **30** was amplified instead. Exposing the same library to morphine derivative **28**, which is considerably larger than guest **27**, did not result in the amplification of the expected [2 + 2] macrocycle either. This time a cyclic trimer of building block **24** was amplified [33]. The biggest surprise in this library came when we used tetramethylammonium iodide **29** as template and discovered that it amplified the cyclic tetramer of dithiol **24** [34]. Given that **24** was used as a racemic mixture, four diastereomeric disulfides can in principle be formed. It turned out that only the diastereomer in which the four subunits have alternating chirality (**32**) was significantly amplified. Only this isomer can fold up in a way that effectively surrounds the small cationic guest. These results provide another demonstration that DCC is an effective method for identifying unpredictable receptors. At the same time, the reversible chemistry also provides an efficient synthetic route to the selected receptors, which can be formed in up to 96% yield in the biased DCLs containing only the required building blocks in the proper ratio.

In collaboration with the Kubik group we have used DCC for the optimization of a synthetic anion receptor. Kubik had earlier designed cyclic peptide **33** and found that it bound efficiently to anions even in highly competitive aqueous solvents by forming a 2 : 1 sandwich complex [36] (Scheme 7).



Scheme 7 Kubik's original designed cyclopeptide **33** [36] and dimers thereof that are linked covalently through a designed spacer (**43**) [37] and spacers identified from a DCL containing a variety of dithiol building blocks (**41** and **42**) [38, 39]

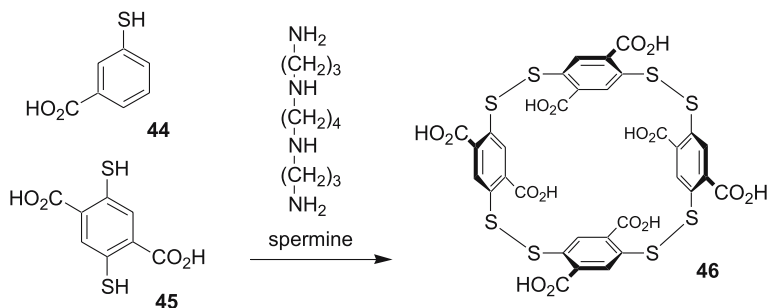
These observations prompted the development of a new receptor in which the two peptide rings would be linked covalently. This was achieved by designing an appropriate linker based on the crystal structure of the 2 : 1 iodide complex [37] as well by using a dynamic combinatorial approach in which cyclopeptide disulfide **34** was allowed to choose its best spacer from a selection of dithiols **35–40** [38]. Introducing sulfate or iodide anions into the resulting DCL resulted in the amplification of two new synthetic anion receptors **41** and **42** that contained spacers **36** and **37**, respectively. These receptors were an order of magnitude more efficient in binding sulfate and iodide anions than the designed receptor **43**.

A detailed study of the structure and complexation behavior of these receptors has allowed us to identify an important binding mechanism that was not previously recognized but that may well become an important strategy for generating synthetic receptors with much improved binding affinities. We found that a significant part of the binding affinity derived from hydrophobic interactions between the two peptide rings that did not directly involve the anion [39]. Thus noncovalent interactions within the structure of the receptor were found to enhance guest binding. Given the extensive network of noncovalent interactions in proteins, it is likely that similar effects operate in these biomolecules [40, 41]. Such intrareceptor interactions may well be the key to the development of a new generation of synthetic receptors that can rival the binding efficiencies of their biological counterparts. Our work on cyclic peptides suggests that DCC is the method of choice for developing these structurally complex molecules that are otherwise very difficult to access.

To date, most of the receptors developed using DCC have been discovered by chance or have been inspired by known designed receptors. While these results have established proof of principle, the next phase in the development of the dynamic combinatorial approach involves identifying rules to guide the design of libraries to target *specific* guests.

We have addressed this issue while developing a synthetic receptor for spermine [42]. Spermine is a polyamine that plays an important but poorly understood role in numerous cellular processes including apoptosis and cancer. Developing a synthetic receptor with sufficient affinity to bind spermine in a biological system is the first step to developing a spermine sensor that could assist in elucidating the exact biological role of the polycation.

The design of the building blocks for the recognition of spermine started with identifying carboxylate–amine interactions as a suitable noncovalent interaction. Next we needed to have some idea about the overall receptor architecture. At the outset of the study it was not clear whether the receptors should have a linear or cyclic structure. Thus the building blocks were designed so as to generate both types of structures, which could be achieved by mixing monothiol and dithiols together. Carboxylate-functionalized monothiol building block **44** and dithiol **45** were identified as suitable candidates (Scheme 8).



Scheme 8 Exposing a DCL made from monothiol **44** and dithiol **45** leads to the amplification of a receptor for spermine (**46**) with nanomolar affinity [42]

Indeed, upon introducing spermine into a DCL generated from these two building blocks, a cyclic tetramer of dithiol **45** was amplified. This compound turned out to have a remarkably high affinity for spermine ($K = 4.5 \times 10^7 \text{ M}^{-1}$ in 3 mM TRIS buffer pH 7.4) and binds it by forming a pseudorotaxane-type complex. Binding is strong enough to enable the receptor to sequester spermine from one of its natural hosts, DNA. Binding of spermine to DNA is known to induce a change in the helicity of some DNA sequences from the normal right-handed form to a left-handed helix. Receptor **46** was able to reverse this process, regenerating the original right-handed DNA [42].

2.4

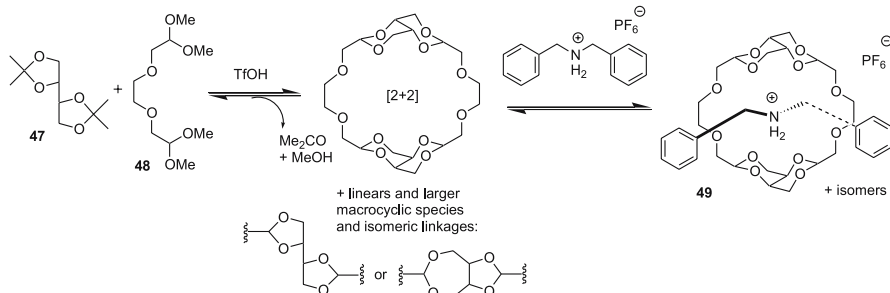
Synthetic Receptors Developed Using Acetal Exchange

The groups of Fuchs and Mandolini have used acetal exchange as the reversible reaction for the construction of synthetic receptors [43, 44]. Acetal exchange proceeds smoothly in organic solvents in the presence of a strong acid catalyst (typically triflic acid) but is generally not compatible with the presence of water.

The Fuchs laboratory, in collaboration with Stoddart, have produced a DCL of crown ether-like acetals starting from building blocks **47** and **48** (Scheme 9) [43].

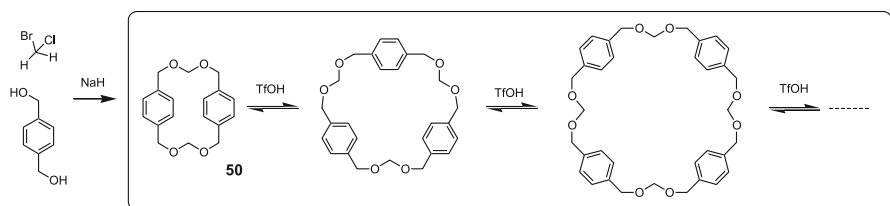
There are three different ways of linking these building blocks together giving rise to five, six, or seven-membered cyclic acetals. In the absence of a template a complex mixture is obtained. However, upon addition of dibenzylammonium salt the [2 + 2] macrocycle connected by fused six-membered cyclic acetals (**49**) is amplified to become 64% of the material in the library. Using CsPF_6 as a template gave even more efficient amplification, producing macrocycle **49** in > 95% yield.

The Mandolini group used acetal chemistry to develop a cyclophane receptor for Ag^+ ions [44]. A mixture of macrocycles was preformed under kinetic control by reacting 1,4-benzenedimethanol with bromochloromethane under



Scheme 9 Identification of a crown-ether like receptor for dibenzylammonium cation through acetal-based DCC [43]

basic conditions. A DCL was then generated from isolated macrocycles under acidic conditions. The addition of $\text{Ag}(\text{CF}_3\text{SO}_2)_2\text{N}$ induced the amplification of macrocycle **50** in 60% yield, whereas this compound constituted only 11% of the library material in the absence of the guest (Scheme 10).



Scheme 10 Identification of a cyclophane receptor for Ag^+ through acetal-based DCC [44]

3 Sensing with Dynamic Combinatorial Libraries

In the previous section we summarized how selection experiments with DCLs can be used to identify new receptors with high affinity. These receptors can potentially be converted into sensors by attachment of signaling units. Below, we describe a conceptually different approach: the utilization of the entire DCL as a sensor.

The concentrations of the DCL members depend on the chemical and physical environment of the systems (solvent, pH, concentration of target molecules, etc.). A certain library composition is therefore a characteristic feature of the respective environment. If the DCL composition can be transduced into a signal output, it is possible to use the DCL as a sensor. For sensing purposes, a fast and cheap analysis method such as fluorescence or UV-Vis spectroscopy is advantageous. These techniques can be employed

if the DCL is composed of compounds with different color or fluorescence properties (Fig. 2). For such a sensor, the information about the sample is distributed over the entire spectrum, which represents a “fingerprint” for the analyte. In this regard, a DCL sensor is related to sensor arrays [45, 46]. But, contrary to sensor arrays with independent sensor units, a DCL sensor is comprised of compounds that are connected by exchange reactions. Furthermore, the various sensors of an array have to be addressed separately, whereas for a DCL sensor, a single UV-Vis or fluorescence measurement is sufficient as the read-out.

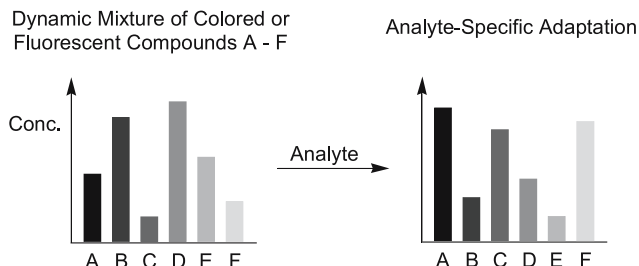
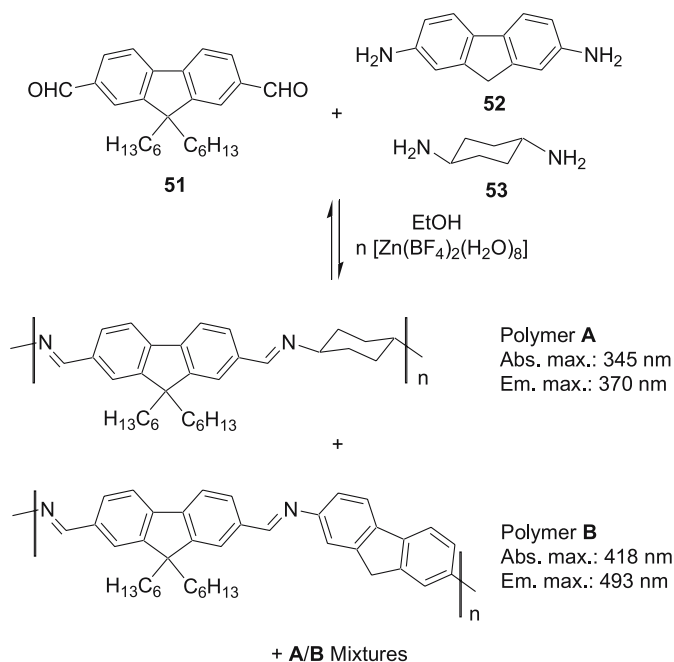


Fig. 2 The adaptive behavior of a DCL upon addition of an analyte can be used to identify this analyte, given that the library members possess a characteristic feature such as color or fluorescence

The group of Lehn has investigated the condensation reaction of 2,7-fluorenebis-carboxaldehyde (**51**) with 2,7-diaminofluorene (**52**) and *trans*-1,4-diaminocyclohexane (**53**) in the presence of variable amounts of $[\text{Zn}(\text{BF}_4)_2(\text{H}_2\text{O})_8]$ (Scheme 11) [47, 48].

In the absence of zinc, the dominant product was found to be polymer A, containing the aliphatic monomer **53**. The addition of increasing amounts of zinc shifted the equilibrium in favor of polymers containing the aromatic monomer **52**. Polymer B was found to be the dominant species when the system was equilibrated in the presence of two equivalents of Zn^{2+} . This shift was explained by the preferential complexation of Zn^{2+} to the more nucleophilic diamine **53**. Since polymers A and B show different absorption spectra, the zinc-modulated change in polymer composition resulted in a change in color. Similarly, the fluorescence emission maximum was shifted from 370 to 493 nm with a concomitant increase in intensity. Interestingly, the addition of more than two equivalents of Zn^{2+} resulted in a further enhancement of the fluorescence. The dynamic polymer (“dynamer”) [49] can therefore be regarded as a system that is able to detect zinc due to an analyte-induced constitutional rearrangement.

A different way to construct a DCL, in which the library members have a characteristic color, was described by Buryak and Severin [50]. The metal salts CuCl_2 and NiCl_2 were mixed with the commercially available dyes



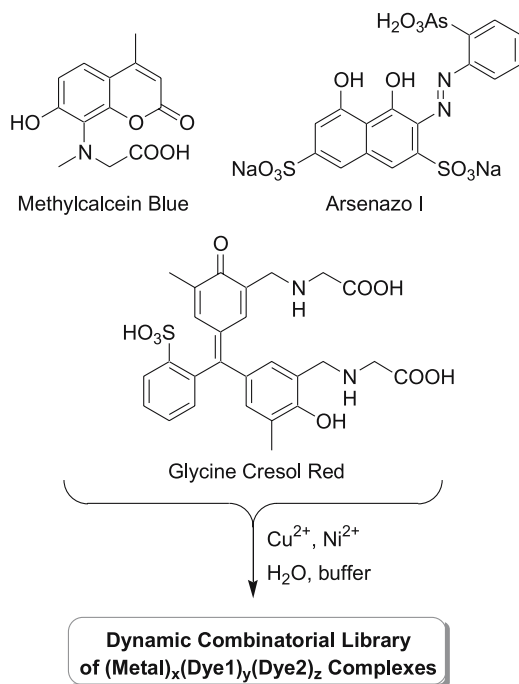
Scheme 11 Condensation of the dialdehyde **51** with the diamines **52** and **53** results in the formation of a dynamic mixture of polymers. The addition of Zn^{2+} leads to a constitutional rearrangement in favor of polymer B, accompanied by a change of color and fluorescence [47, 48]

Methylcalcein Blue, Arsenazo I, and Glycine Cresol Red in aqueous buffer (Scheme 12).

The resulting solution contained a diverse mixture of $(\text{metal})_x(\text{dye1})_y(\text{dye2})_z$ complexes of variable composition. Since coordination to a metal changes the UV-Vis absorption of the dye, each library member displays a distinct color. A re-equilibration of the DCL in response to addition of an analyte was therefore expected to result in a characteristic UV-Vis spectrum.

Dipeptides were used as analytes. They are known to form stable complexes with Cu^{2+} and Ni^{2+} ions. The addition of a dipeptide to the DCL sensor therefore resulted in a partial liberation of dyes accompanied by a re-equilibration of the remaining metal-dye complexes. The results obtained for the sequence isomers His-Ala and Ala-His are shown in Fig. 3.

The data depicted are the UV-Vis difference spectra obtained from equilibrated solutions before and after addition of the respective dipeptide. Clearly, the two analytes are easily distinguishable. Importantly, the UV-Vis spectra not only differ in terms of amplitude at a certain wavelength but also in terms of the position of inflection points and maxima.



Scheme 12 Generation of a DCL of metal–dye complexes by a mixture of Arsenazo I, Methylcalcein Blue, and Glycine Cresol Red with CuCl_2 and NiCl_2 in buffered aqueous solution [50]

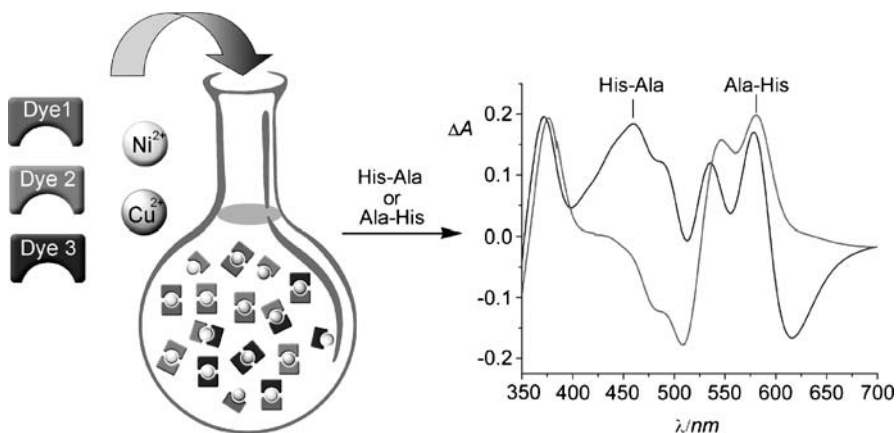


Fig. 3 Changes in the UV-Vis spectrum upon addition of the dipeptides His-Ala or Ala-His to an aqueous solution containing a DCL sensor composed of the metal salts CuCl_2 and NiCl_2 and the dyes (cf. Scheme 12) Methylcalcein Blue, Arsenazo I, and Glycine Cresol Red ([dipeptide] = 1.0 mM, $[\text{CuCl}_2] = [\text{NiCl}_2] = [\text{dye}1/2/3] = 75 \mu\text{M}$, 35 mM CHES buffer, pH 8.4) [50]

Peptides with His residues result in a rather pronounced re-equilibration of the DCL because the side-chain of His has good metal-coordinating abilities. In order to test the scope of this sensing approach with more challenging analytes, the structurally closely related dipeptides Gly-Ala, Val-Phe, Ala-Phe, Phe-Ala, and D-Phe-Ala were investigated. As expected, the UV-Vis difference spectra were more similar to each other, and chemometrics methods [51] were used to classify the analytes. For each dipeptide, 15 UV-Vis measurements were performed. To verify that the discrimination between the analytes was not due to small differences of the peptide stock solutions, the concentration for each analyte was varied on purpose by $\pm 5\%$. Therefore, 5×3 measurements were performed with peptide concentrations of 1.00 mM, 0.95 mM, and 1.05 mM (the sensor composition was the same as described in the legend of Fig. 3). Data analysis was carried out with the help of a commercial statistics program. In order to determine the most relevant wavelengths in the region between 350 and 700 nm, a preselection was performed using an automatic variable selection algorithm. The data of the eight selected wavelengths were then classified by a linear discriminant analysis (LDA) [51]. A graphic representation of this analysis in the form of a score plot is given in Fig. 4.

A 100% discrimination was achieved for a “jack-knifed” classification matrix, in which one measurement at a time was treated as an unknown and the rest of the data was used as the training set. This is quite remarkable, given that closely related analytes such as the regioisomers Ala-Phe and Phe-Ala and the stereoisomers Phe-Ala and D-Phe-Ala were used and that none of the dipeptides contained coordinating side-chains.

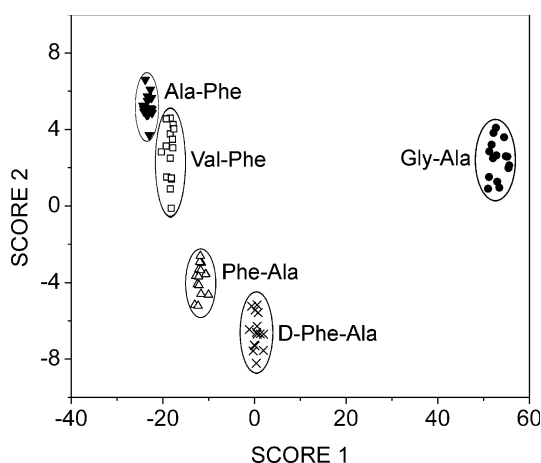


Fig. 4 Two-dimensional LDA score plot for the dipeptide analytes Gly-Ala (●), Val-Phe (□), Ala-Phe (▼), Phe-Ala (△), and D-Phe-Ala (×). The five different analytes can be clearly distinguished [50]

A key advantage of this DCL sensor is that the method is experimentally very simple. All that is required is to dissolve commercially available dyes together with transition metal salts in a buffer and to record a UV-Vis spectrum. But the approach has another advantage: its inherent flexibility. A DCL sensor is generated by self-assembly of multiple subunits. Consequently, it is possible to rapidly optimize the system for a particular sensing problem by variation of the total amounts and the relative ratios of the constituent building blocks in a combinatorial fashion. This was demonstrated for the analysis of sequence-isomeric tripeptides composed of two glycine and one histidine residue [52]. The building blocks for the DCL sensor were the same as described above. To screen the sensor performance, 20 different DCLs were generated for two analyte pairs (His-Gly-Gly vs. Gly-Gly-His and Gly-His-Gly vs. Gly-Gly-His) by variation of the total and the relative metal concentration using constant dye concentrations. To approximate the ability of the respective DCL sensor to discriminate between the two peptides, the area between the UV-Vis curves obtained for the two analytes was calculated. A graphic representation of the results of this screening is depicted in Fig. 5.

In both cases, a high total metal concentration of $320\ \mu\text{M}$ was found to give the best discrimination between the analytes. Interesting differences,

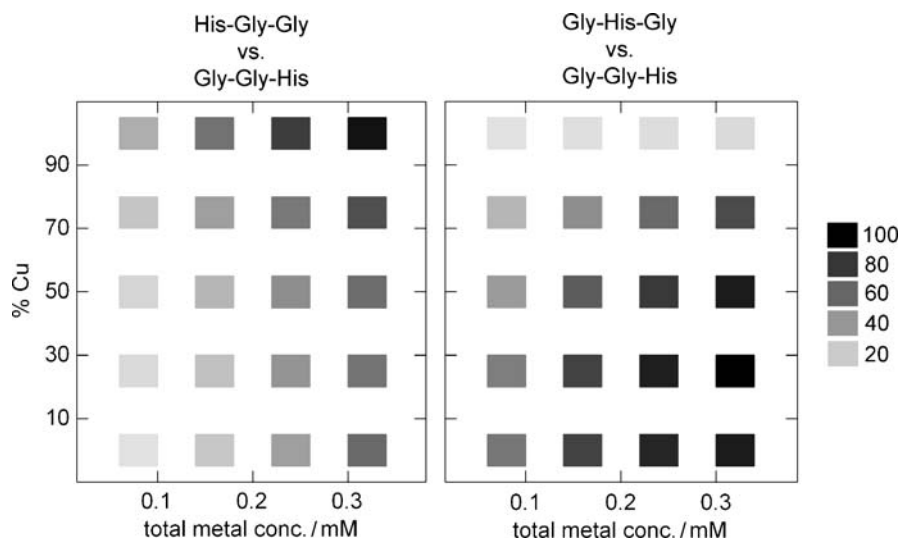


Fig. 5 Ability of a DCL sensor to discriminate between the sequence isomers His-Gly-Gly and Gly-Gly-His (*left*) and Gly-His-Gly and Gly-Gly-His (*right*) as a function of the total metal concentration and the $\text{Cu}^{2+}/\text{Ni}^{2+}$ ratio ($[\text{peptide}] = 1.00\ \text{mM}$, $[\text{M}]_{\text{total}} = 80, 160, 240,$ and $320\ \mu\text{M}$, $[\text{dye}1/2/3] = 75\ \mu\text{M}$, $100\ \text{mM}$ CHES buffer, pH 8.4). The *gray scale* indicates the differentiation that was achieved for the respective sensor composition. The data (arbitrary units) are based on five independent measurements; the errors are less than five units [52]

however, were observed for the best $\text{Cu}^{2+}/\text{Ni}^{2+}$ ratio. For the analyte pair His-Gly-Gly and Gly-Gly-His, a sensor containing exclusively copper gave the best results (Fig. 5, left). For the analyte pair Gly-His-Gly and Gly-Gly-His, on the other hand, a mixture of 25% Cu^{2+} and 75% Ni^{2+} resulted in the largest difference in the UV-Vis spectra (Fig. 5, right). The results show that the optimal sensor composition can vary substantially, even for closely related analytes.

In the small screening of 20 different sensors, only the metal concentrations were varied. Other important parameters such as the total or relative dye concentration were not changed. It is therefore unlikely that the best sensor composition, which was identified, also represents the optimum sensor composition. Nevertheless, these semi-optimized sensors already possess a remarkable analytical power. For the tripeptides Gly-His-Gly and Gly-Gly-His, for example, it has been shown that it is possible to simultaneously obtain qualitative and quantitative information [52]. For each peptide, four samples with concentrations between 0.25 and 1.00 mM were analyzed by five independent UV-Vis measurements. The data was treated as described above and the resulting LDA score plot is shown in Fig. 6. From the plot it is evident that the DCL sensor is indeed able to identify the respective tripeptide and to determine its concentration. The accuracy of a quantitative analysis was estimated to be ± 100 mM.

One should note that the sensing approach with libraries of metal-dye complexes described above is conceptually related to the work of Anslin, in which he uses multicomponent indicator displacement assays

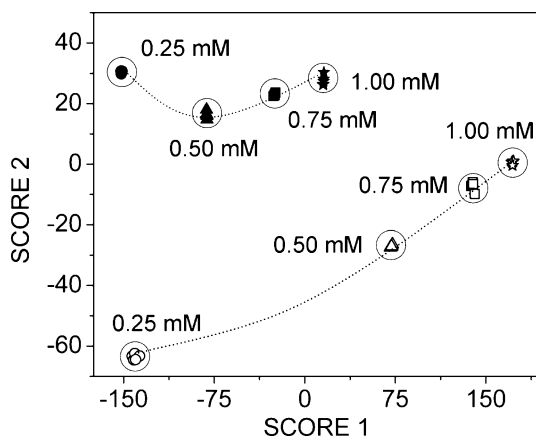


Fig. 6 Two-dimensional LDA score plot for the analysis of the tripeptides Gly-His-Gly (*filled symbols*) and Gly-Gly-His (*open symbols*) at various concentrations (0.25–1.00 mM). It is possible to simultaneously identify the respective tripeptide and to determine its concentration [52]. The data are based on five independent measurements

based on synthetic receptors in combination with artificial neural network analyses [53, 54]. These systems can likewise be regarded as DCLs, although of low complexity. This work is described in more detail in another chapter of this volume [55].

4

Conclusions

In the last 10 years, DCC has emerged as a powerful technique for the development of molecules that are good at molecular recognition. In Sect. 2 we have presented selected examples of synthetic receptors that have been discovered using this technique, which include some receptors with exceptionally high affinities for biologically relevant guests such as acetylcholine and spermine. The thermodynamically controlled reactions that mediate the exchange of building blocks in a DCL can also be used as a method to synthesize the selected compounds. Thus DCC can speed up two slow steps in the development of synthetic receptors: identification of structures with receptor properties, and the synthesis of these often complex molecules. Moreover, the technique allows access to unpredictable new receptor architectures. We anticipate that DCLs will become a rich source of synthetic receptors for the development of specific sensors in the near future.

In Sect. 3 we have described some pioneering work showing that the adaptive behavior of entire DCLs can be used for sensing purposes. This approach requires that the library composition can be transduced into a signal output and that the addition of the analyte results in a detectable re-equilibration. It is sufficient that the analytes of interest display an unspecific but differential interaction with several library members. This is in contrast to DCL selection experiments aimed at identifying a high-affinity receptor. Here, a specific and strong interaction with a certain library member facilitates its detection.

For colorimetric or fluorescence DCL sensors, the information about the analyte is distributed over the entire spectrum. This distinguishes them from classical chemosensors, for which the analysis is generally performed at either a single wavelength or by comparison of two wavelengths (ratiometric sensor). The multidimensional nature of the DCL sensor data can best be analyzed by pattern recognition protocols. In this regard, DCL sensors are related to sensor arrays such as “electronic noses” or “electronic tongues” [45, 46, 56, 57].

DCL sensors are by definition complex chemical systems. Consequently, it is difficult to predict the response for a particular analyte. However, the lack of control is compensated by two key advantages. First of all, the experimental setup for a DCL sensor is very simple: all that is required is to equilibrate the respective building blocks. Furthermore, DCL sensors can easily be modified, and thus optimized, by variation of the nature, the amounts, and the relative

ratios of the constituent building blocks. Given these advantages it is likely that sensors based on DCLs will find increasing interest in the future.

Acknowledgements We are grateful for support from the Royal Society, the EPSRC (SO), the EU (COST D-31 WG 0013-04), the Swiss National Science Foundation (KS), and the EPFL (KS).

References

1. Karan C, Miller BL (2000) *Drug Discov Today* 5:67
2. Lehn J-M, Eliseev AV (2001) *Science* 291:2331
3. Ramström O, Lehn J-M (2002) *Nat Rev Drug Discov* 1:26
4. Rowan SJ, Cantrill SJ, Cousins GRL, Sanders JKM, Stoddart JF (2002) *Angew Chem Int Ed* 41:898
5. Ramström O, Bunyapaiboonsri T, Lohmann S, Lehn J-M (2002) *Biochim Biophys Acta* 1572:178
6. Otto S (2003) *Curr Opin Drug Discov Dev* 6:509
7. Cheeseman JD, Corbett AD, Gleason JL, Kazlauskas RJ (2005) *Chem Eur J* 11:1708
8. de Bruin B, Hauwert P, Reek JNH (2006) *Angew Chem Int Ed* 45:2660
9. Corbett PT, Leclaire J, Vial L, West KR, Wietor J-L, Sanders JKM, Otto S (2006) *Chem Rev* 106:3652
10. Otto S, Furlan RLE, Sanders JKM (2002) *Curr Opin Chem Biol* 6:321
11. Sanders JKM (2004) *Philos Trans R Soc Lond Ser A Math Phys Eng Sci* 362:1239
12. Otto S (2005) *J Mater Chem* 15:3357
13. Grote Z, Scopelliti R, Severin K (2003) *Angew Chem Int Ed* 42:3821
14. Severin K (2004) *Chem Eur J* 10:2565
15. Saur I, Severin K (2005) *Chem Commun*, p 1471
16. Corbett PT, Otto S, Sanders JKM (2004) *Chem Eur J* 10:3139
17. Corbett PT, Sanders JKM, Otto S (2005) *J Am Chem Soc* 127:9390
18. Nishinaga T, Tanatani A, Oh KC, Moore JS (2002) *J Am Chem Soc* 124:5934
19. Lüning U (2004) *J Incl Phenom Macrocycl Chem* 49:81
20. Storm O, Lüning U (2002) *Chem-Eur J* 8:793
21. Gonzalez-Alvarez A, Alfonso I, Lopez-Ortiz F, Aguirre A, Garcia-Granda S, Gotor V (2004) *Eur J Org Chem*, p 1117
22. Gonzalez-Alvarez A, Alfonso I, Gotor V (2006) *Chem Commun*, p 2224
23. Nguyen R, Huc I (2003) *Chem Commun*, p 942
24. Cousins GRL, Poulsen SA, Sanders JKM (1999) *Chem Commun*, p 1575
25. Kubik S, Goddard R (1999) *J Org Chem* 64:9475
26. Cousins GRL, Furlan RLE, Ng Y-F, Redman JE, Sanders JKM (2001) *Angew Chem Int Ed* 40:423
27. Furlan RLE, Ng Y-F, Cousins GRL, Redman JE, Sanders JKM (2002) *Tetrahedron* 58:771
28. Roberts SL, Furlan RLE, Otto S, Sanders JKM (2003) *Org Biomol Chem* 1:1625
29. Furlan RLE, Cousins GRL, Sanders JKM (2000) *Chem Commun*, p 1761
30. Lam RTS, Belenguer A, Roberts SL, Naumann C, Jarrosson T, Otto S, Sanders JKM (2005) *Science* 308:667
31. Otto S, Furlan RLE, Sanders JKM (2000) *J Am Chem Soc* 122:12063
32. Ramström O, Lehn J-M (2000) *ChemBioChem* 1:41

33. Otto S, Furlan RLE, Sanders JKM (2002) *Science* 297:590
34. Corbett PT, Tong LH, Sanders JKM, Otto S (2005) *J Am Chem Soc* 127:8902
35. Ngola SM, Kearney PC, Mecozzi S, Russell K, Dougherty DA (1999) *J Am Chem Soc* 121:1192
36. Kubik S, Goddard R, Kirchner R, Nolting D, Seidel J (2001) *Angew Chem Int Ed* 40:2648
37. Kubik S, Kirchner R, Nolting D, Seidel J (2002) *J Am Chem Soc* 124:12752
38. Otto S, Kubik S (2003) *J Am Chem Soc* 125:7804
39. Rodriguez-Docampo Z, Pascu SI, Kubik S, Otto S (2006) *J Am Chem Soc* 128:11206
40. Williams DH, Stephens E, O'Brien DP, Zhou M (2004) *Angew Chem Int Ed* 43:6596
41. Otto S (2006) *Dalton Trans*, p 2861
42. Vial L, Ludlow RE, Leclaire J, Perez-Fernandez R, Otto S (2006) *J Am Chem Soc* 128:10253
43. Fuchs B, Nelson A, Star A, Stoddart JF, Vidal SB (2003) *Angew Chem Int Ed* 42:4220
44. Cacciapaglia R, Di Stefano S, Mandolini L (2005) *J Am Chem Soc* 127:13666
45. Albert KJ, Lewis NS, Schauer CL, Sotzing GA, Stitzel SE, Vaid TP, Walt DR (2000) *Chem Rev* 100:2595
46. Wright AT, Anslyn EV (2006) *Chem Soc Rev* 35:14
47. Giuseppone N, Lehn J-M (2004) *J Am Chem Soc* 126:11448
48. Giuseppone N, Fuks G, Lehn JM (2006) *Chem Eur J* 12:1723
49. Lehn JM (2005) *Prog Polym Sci* 30:814
50. Buryak A, Severin K (2005) *Angew Chem Int Ed* 44:7935
51. Jurs PC, Bakken GA, McClelland HE (2000) *Chem Rev* 100:2649
52. Buryak A, Severin K (2006) *J Comb Chem* 8:540
53. McCleskey SC, Floriano PN, Wiskur SL, Anslyn EV, McDevitt JT (2003) *Tetrahedron* 59:10089
54. Wiskur SL, Floriano PN, Anslyn EV, McDevitt JT (2003) *Angew Chem Int Ed* 42:2070
55. Anslyn EV, Collins BE, Wright AT (2007) *Combining Molecular Recognition, Optical Detection, and Chemometric Analysis*. *Top Curr Chem*, in this volume
56. James D, Scott SM, Ali Z, O'Hare WT (2005) *Microchim Acta* 149:1
57. Gouma P, Sberveglieri G, Dutta R, Gardner JW, Hines EL (2004) *MRS Bull* 29:697

Author Index Volumes 251–277

Author Index Vols. 26–50 see Vol. 50
Author Index Vols. 51–100 see Vol. 100
Author Index Vols. 101–150 see Vol. 150
Author Index Vols. 151–200 see Vol. 200
Author Index Vols. 201–250 see Vol. 250

The volume numbers are printed in italics

- Ajayaghosh A, George SJ, Schenning APHJ (2005) Hydrogen-Bonded Assemblies of Dyes and Extended π -Conjugated Systems. *258*: 83–118
- Akai S, Kita Y (2007) Recent Advances in Pummerer Reactions. *274*: 35–76
- Albert M, Fensterbank L, Lacôte E, Malacria M (2006) Tandem Radical Reactions. *264*: 1–62
- Alberto R (2005) New Organometallic Technetium Complexes for Radiopharmaceutical Imaging. *252*: 1–44
- Alegret S, see Pividori MI (2005) *260*: 1–36
- Alfaro JA, see Schuman B (2007) *272*: 217–258
- Amabilino DB, Veciana J (2006) Supramolecular Chiral Functional Materials. *265*: 253–302
- Anderson CJ, see Li WP (2005) *252*: 179–192
- Anslyn EV, see Collins BE (2007) *277*: 181–218
- Anslyn EV, see Houk RJT (2005) *255*: 199–229
- Appukkuttan P, Van der Eycken E (2006) Microwave-Assisted Natural Product Chemistry. *266*: 1–47
- Araki K, Yoshikawa I (2005) Nucleobase-Containing Gelators. *256*: 133–165
- Armitage BA (2005) Cyanine Dye–DNA Interactions: Intercalation, Groove Binding and Aggregation. *253*: 55–76
- Arya DP (2005) Aminoglycoside–Nucleic Acid Interactions: The Case for Neomycin. *253*: 149–178
- Bailly C, see Dias N (2005) *253*: 89–108
- Balaban TS, Tamiaki H, Holzwarth AR (2005) Chlorins Programmed for Self-Assembly. *258*: 1–38
- Baltzer L (2007) Polypeptide Conjugate Binders for Protein Recognition. *277*: 89–106
- Balzani V, Credi A, Ferrer B, Silvi S, Venturi M (2005) Artificial Molecular Motors and Machines: Design Principles and Prototype Systems. *262*: 1–27
- Barbieri CM, see Pilch DS (2005) *253*: 179–204
- Barchuk A, see Daasbjerg K (2006) *263*: 39–70
- Bargon J, see Kuhn LT (2007) *276*: 25–68
- Bargon J, see Kuhn LT (2007) *276*: 125–154
- Bayly SR, see Beer PD (2005) *255*: 125–162
- Beer PD, Bayly SR (2005) Anion Sensing by Metal-Based Receptors. *255*: 125–162
- Bertini L, Bruschi M, de Gioia L, Fantucci P, Greco C, Zampella G (2007) Quantum Chemical Investigations of Reaction Paths of Metalloenzymes and Biomimetic Models – The Hydrogenase Example. *268*: 1–46
- Bier FF, see Heise C (2005) *261*: 1–25
- Blum LJ, see Marquette CA (2005) *261*: 113–129

- Boiteau L, see Pascal R (2005) 259: 69–122
- Bolhuis PG, see Dellago C (2007) 268: 291–317
- Borovkov VV, Inoue Y (2006) Supramolecular Chirogenesis in Host–Guest Systems Containing Porphyrinoids. 265: 89–146
- Boschi A, Duatti A, Uccelli L (2005) Development of Technetium-99m and Rhenium-188 Radiopharmaceuticals Containing a Terminal Metal–Nitrido Multiple Bond for Diagnosis and Therapy. 252: 85–115
- Braga D, D’Addario D, Giaffreda SL, Maini L, Polito M, Grepioni F (2005) Intra-Solid and Inter-Solid Reactions of Molecular Crystals: a Green Route to Crystal Engineering. 254: 71–94
- Braverman S, Cherkinsky M (2007) [2,3]Sigmatropic Rearrangements of Propargylic and Allenic Systems. 275: 67–101
- Brebion F, see Crich D (2006) 263: 1–38
- Brizard A, Oda R, Huc I (2005) Chirality Effects in Self-assembled Fibrillar Networks. 256: 167–218
- Bruce IJ, see del Campo A (2005) 260: 77–111
- Bruschi M, see Bertini L (2007) 268: 1–46
- Bur SK (2007) 1,3-Sulfur Shifts: Mechanism and Synthetic Utility. 274: 125–171
- del Campo A, Bruce IJ (2005) Substrate Patterning and Activation Strategies for DNA Chip Fabrication. 260: 77–111
- Carney CK, Harry SR, Sewell SL, Wright DW (2007) Detoxification Biominerals. 270: 155–185
- Chaires JB (2005) Structural Selectivity of Drug–Nucleic Acid Interactions Probed by Competition Dialysis. 253: 33–53
- Cherkinsky M, see Braverman S (2007) 275: 67–101
- Chiorboli C, Indelli MT, Scandola F (2005) Photoinduced Electron/Energy Transfer Across Molecular Bridges in Binuclear Metal Complexes. 257: 63–102
- Coleman AW, Perret F, Moussa A, Dupin M, Guo Y, Perron H (2007) Calix[n]arenes as Protein Sensors. 277: 31–88
- Cölfen H (2007) Bio-inspired Mineralization Using Hydrophilic Polymers. 271: 1–77
- Collin J-P, Heitz V, Sauvage J-P (2005) Transition-Metal-Complexed Catenanes and Rotaxanes in Motion: Towards Molecular Machines. 262: 29–62
- Collins BE, Wright AT, Anslyn EV (2007) Combining Molecular Recognition, Optical Detection, and Chemometric Analysis. 277: 181–218
- Collyer SD, see Davis F (2005) 255: 97–124
- Commeyras A, see Pascal R (2005) 259: 69–122
- Coquerel G (2007) Preferential Crystallization. 269: 1–51
- Correia JDG, see Santos I (2005) 252: 45–84
- Costanzo G, see Saladino R (2005) 259: 29–68
- Cotarca L, see Zonta C (2007) 275: 131–161
- Credi A, see Balzani V (2005) 262: 1–27
- Crestini C, see Saladino R (2005) 259: 29–68
- Crich D, Brebion F, Suk D-H (2006) Generation of Alkene Radical Cations by Heterolysis of β -Substituted Radicals: Mechanism, Stereochemistry, and Applications in Synthesis. 263: 1–38
- Cuerva JM, Justicia J, Oller-López JL, Oltra JE (2006) Cp_2TiCl in Natural Product Synthesis. 264: 63–92

- Daasbjerg K, Svith H, Grimme S, Gerenkamp M, Mück-Lichtenfeld C, Gansäuer A, Barchuk A (2006) The Mechanism of Epoxide Opening through Electron Transfer: Experiment and Theory in Concert. *263*: 39–70
- D'Addario D, see Braga D (2005) *254*: 71–94
- Danishefsky SJ, see Warren JD (2007) *267*: 109–141
- Darmency V, Renaud P (2006) Tin-Free Radical Reactions Mediated by Organoboron Compounds. *263*: 71–106
- Davis F, Collyer SD, Higson SPJ (2005) The Construction and Operation of Anion Sensors: Current Status and Future Perspectives. *255*: 97–124
- Deamer DW, Dworkin JP (2005) Chemistry and Physics of Primitive Membranes. *259*: 1–27
- Dellago C, Bolhuis PG (2007) Transition Path Sampling Simulations of Biological Systems. *268*: 291–317
- Deng J-Y, see Zhang X-E (2005) *261*: 169–190
- Dervan PB, Poulin-Kerstien AT, Fechter EJ, Edelson BS (2005) Regulation of Gene Expression by Synthetic DNA-Binding Ligands. *253*: 1–31
- Dias N, Vezin H, Lansiaux A, Bailly C (2005) Topoisomerase Inhibitors of Marine Origin and Their Potential Use as Anticancer Agents. *253*: 89–108
- DiMauro E, see Saladino R (2005) *259*: 29–68
- Dittrich M, Yu J, Schulten K (2007) PcrA Helicase, a Molecular Motor Studied from the Electronic to the Functional Level. *268*: 319–347
- Dobrawa R, see You C-C (2005) *258*: 39–82
- Du Q, Larsson O, Swerdlow H, Liang Z (2005) DNA Immobilization: Silanized Nucleic Acids and Nanoprinting. *261*: 45–61
- Duatti A, see Boschi A (2005) *252*: 85–115
- Dupin M, see Coleman AW (2007) *277*: 31–88
- Dworkin JP, see Deamer DW (2005) *259*: 1–27
- Edelson BS, see Dervan PB (2005) *253*: 1–31
- Edwards DS, see Liu S (2005) *252*: 193–216
- Ernst K-H (2006) Supramolecular Surface Chirality. *265*: 209–252
- Ersmark K, see Wannberg J (2006) *266*: 167–197
- Escudé C, Sun J-S (2005) DNA Major Groove Binders: Triple Helix-Forming Oligonucleotides, Triple Helix-Specific DNA Ligands and Cleaving Agents. *253*: 109–148
- Evans SV, see Schuman B (2007) *272*: 217–258
- Van der Eycken E, see Appukkuttan P (2006) *266*: 1–47
- Fages F, Vögtle F, Žinić M (2005) Systematic Design of Amide- and Urea-Type Gelators with Tailored Properties. *256*: 77–131
- Fages F, see Žinić M (2005) *256*: 39–76
- Faigl F, Schindler J, Fogassy E (2007) Advantages of Structural Similarities of the Reactants in Optical Resolution Processes. *269*: 133–157
- Fantucci P, see Bertini L (2007) *268*: 1–46
- Fechter EJ, see Dervan PB (2005) *253*: 1–31
- Fensterbank L, see Albert M (2006) *264*: 1–62
- Fernández JM, see Moonen NNP (2005) *262*: 99–132
- Fernando C, see Szathmáry E (2005) *259*: 167–211
- Ferrer B, see Balzani V (2005) *262*: 1–27
- De Feyter S, De Schryver F (2005) Two-Dimensional Dye Assemblies on Surfaces Studied by Scanning Tunneling Microscopy. *258*: 205–255

- Fischer D, Geyer A (2007) NMR Analysis of Bioprotective Sugars: Sucrose and Oligomeric (1→2)- α -D-glucopyranosyl-(1→2)- β -D-fructofuranosides. *272*: 169–186
- Flood AH, see Moonen NNP (2005) *262*: 99–132
- Fogassy E, see Faigl F (2007) *269*: 133–157
- Fricke M, Volkmer D (2007) Crystallization of Calcium Carbonate Beneath Insoluble Monolayers: Suitable Models of Mineral–Matrix Interactions in Biomineralization? *270*: 1–41
- Fujimoto D, see Tamura R (2007) *269*: 53–82
- Fujiwara S-i, Kambe N (2005) Thio-, Seleno-, and Telluro-Carboxylic Acid Esters. *251*: 87–140
- Gansäuer A, see Daasbjerg K (2006) *263*: 39–70
- Garcia-Garibay MA, see Karlen SD (2005) *262*: 179–227
- Gelinck GH, see Grozema FC (2005) *257*: 135–164
- Geng X, see Warren JD (2007) *267*: 109–141
- George SJ, see Ajayaghosh A (2005) *258*: 83–118
- Gerenkamp M, see Daasbjerg K (2006) *263*: 39–70
- Gevorgyan V, see Sromek AW (2007) *274*: 77–124
- Geyer A, see Fischer D (2007) *272*: 169–186
- Giaffreda SL, see Braga D (2005) *254*: 71–94
- Giernoth R (2007) Homogeneous Catalysis in Ionic Liquids. *276*: 1–23
- de Gioia L, see Bertini L (2007) *268*: 1–46
- Di Giusto DA, King GC (2005) Special-Purpose Modifications and Immobilized Functional Nucleic Acids for Biomolecular Interactions. *261*: 131–168
- Greco C, see Bertini L (2007) *268*: 1–46
- Greiner L, Laue S, Wöltinger J, Liese A (2007) Continuous Asymmetric Hydrogenation. *276*: 111–124
- Grepioni F, see Braga D (2005) *254*: 71–94
- Grimme S, see Daasbjerg K (2006) *263*: 39–70
- Grozema FC, Siebbeles LDA, Gelinck GH, Warman JM (2005) The Opto-Electronic Properties of Isolated Phenylenevinylene Molecular Wires. *257*: 135–164
- Guiseppi-Elie A, Lingerfelt L (2005) Impedimetric Detection of DNA Hybridization: Towards Near-Patient DNA Diagnostics. *260*: 161–186
- Guo Y, see Coleman AW (2007) *277*: 31–88
- Haase C, Seitz O (2007) Chemical Synthesis of Glycopeptides. *267*: 1–36
- Hansen SG, Skrydstrup T (2006) Modification of Amino Acids, Peptides, and Carbohydrates through Radical Chemistry. *264*: 135–162
- Harmer NJ (2007) The Fibroblast Growth Factor (FGF) – FGF Receptor Complex: Progress Towards the Physiological State. *272*: 83–116
- Harry SR, see Carney CK (2007) *270*: 155–185
- Heise C, Bier FF (2005) Immobilization of DNA on Microarrays. *261*: 1–25
- Heitz V, see Collin J-P (2005) *262*: 29–62
- Herrmann C, Reiher M (2007) First-Principles Approach to Vibrational Spectroscopy of Biomolecules. *268*: 85–132
- Higson SPJ, see Davis F (2005) *255*: 97–124
- Hirayama N, see Sakai K (2007) *269*: 233–271
- Hirst AR, Smith DK (2005) Dendritic Gelators. *256*: 237–273
- Holzwarth AR, see Balaban TS (2005) *258*: 1–38
- Homans SW (2007) Dynamics and Thermodynamics of Ligand–Protein Interactions. *272*: 51–82

- Houk RJT, Tobey SL, Anslyn EV (2005) Abiotic Guanidinium Receptors for Anion Molecular Recognition and Sensing. *255*: 199–229
- Huc I, see Brizard A (2005) *256*: 167–218
- Ihmels H, Otto D (2005) Intercalation of Organic Dye Molecules into Double-Stranded DNA – General Principles and Recent Developments. *258*: 161–204
- Imai H (2007) Self-Organized Formation of Hierarchical Structures. *270*: 43–72
- Indelli MT, see Chiorboli C (2005) *257*: 63–102
- Inoue Y, see Borovkov VV (2006) *265*: 89–146
- Ishii A, Nakayama J (2005) Carbodithioic Acid Esters. *251*: 181–225
- Ishii A, Nakayama J (2005) Carboselenothioic and Carbodiselenoic Acid Derivatives and Related Compounds. *251*: 227–246
- Ishi-i T, Shinkai S (2005) Dye-Based Organogels: Stimuli-Responsive Soft Materials Based on One-Dimensional Self-Assembling Aromatic Dyes. *258*: 119–160
- James DK, Tour JM (2005) Molecular Wires. *257*: 33–62
- James TD (2007) Saccharide-Selective Boronic Acid Based Photoinduced Electron Transfer (PET) Fluorescent Sensors. *277*: 107–152
- Jelinek R, Kolusheva S (2007) Biomolecular Sensing with Colorimetric Vesicles. *277*: 155–180
- Jones W, see Trask AV (2005) *254*: 41–70
- Justicia J, see Cuerva JM (2006) *264*: 63–92
- Kambe N, see Fujiwara S-i (2005) *251*: 87–140
- Kano N, Kawashima T (2005) Dithiocarboxylic Acid Salts of Group 1–17 Elements (Except for Carbon). *251*: 141–180
- Kappe CO, see Kremsner JM (2006) *266*: 233–278
- Kaptein B, see Kellogg RM (2007) *269*: 159–197
- Karlen SD, Garcia-Garibay MA (2005) Amphidynamic Crystals: Structural Blueprints for Molecular Machines. *262*: 179–227
- Kato S, Niyomura O (2005) Group 1–17 Element (Except Carbon) Derivatives of Thio-, Seleno- and Telluro-Carboxylic Acids. *251*: 19–85
- Kato S, see Niyomura O (2005) *251*: 1–12
- Kato T, Mizoshita N, Moriyama M, Kitamura T (2005) Gelation of Liquid Crystals with Self-Assembled Fibers. *256*: 219–236
- Kaul M, see Pilch DS (2005) *253*: 179–204
- Kaupp G (2005) Organic Solid-State Reactions with 100% Yield. *254*: 95–183
- Kawasaki T, see Okahata Y (2005) *260*: 57–75
- Kawashima T, see Kano N (2005) *251*: 141–180
- Kay ER, Leigh DA (2005) Hydrogen Bond-Assembled Synthetic Molecular Motors and Machines. *262*: 133–177
- Kellogg RM, Kaptein B, Vries TR (2007) Dutch Resolution of Racemates and the Roles of Solid Solution Formation and Nucleation Inhibition. *269*: 159–197
- Kessler H, see Weide T (2007) *272*: 1–50
- King GC, see Di Giusto DA (2005) *261*: 131–168
- Kirchner B, see Thar J (2007) *268*: 133–171
- Kita Y, see Akai S (2007) *274*: 35–76
- Kitamura T, see Kato T (2005) *256*: 219–236
- Kniep R, Simon P (2007) Fluorapatite-Gelatine-Nanocomposites: Self-Organized Morphogenesis, Real Structure and Relations to Natural Hard Materials. *270*: 73–125

- Koenig BW (2007) Residual Dipolar Couplings Report on the Active Conformation of Rhodopsin-Bound Protein Fragments. *272*: 187–216
- Kolusheva S, see Jelinek R (2007) *277*: 155–180
- Komatsu K (2005) The Mechanochemical Solid-State Reaction of Fullerenes. *254*: 185–206
- Kremsner JM, Stadler A, Kappe CO (2006) The Scale-Up of Microwave-Assisted Organic Synthesis. *266*: 233–278
- Kriegisch V, Lambert C (2005) Self-Assembled Monolayers of Chromophores on Gold Surfaces. *258*: 257–313
- Kuhn LT, Bargon J (2007) Transfer of Parahydrogen-Induced Hyperpolarization to Heteronuclei. *276*: 25–68
- Kuhn LT, Bargon J (2007) Exploiting Nuclear Spin Polarization to Investigate Free Radical Reactions via in situ NMR. *276*: 125–154
- Lacôte E, see Albert M (2006) *264*: 1–62
- Lahav M, see Weissbuch I (2005) *259*: 123–165
- Lambert C, see Kriegisch V (2005) *258*: 257–313
- Lansiaux A, see Dias N (2005) *253*: 89–108
- LaPlante SR (2007) Exploiting Ligand and Receptor Adaptability in Rational Drug Design Using Dynamics and Structure-Based Strategies. *272*: 259–296
- Larhed M, see Nilsson P (2006) *266*: 103–144
- Larhed M, see Wannberg J (2006) *266*: 167–197
- Larsson O, see Du Q (2005) *261*: 45–61
- Laue S, see Greiner L (2007) *276*: 111–124
- Leigh DA, Pérez EM (2006) Dynamic Chirality: Molecular Shuttles and Motors. *265*: 185–208
- Leigh DA, see Kay ER (2005) *262*: 133–177
- Leiserowitz L, see Weissbuch I (2005) *259*: 123–165
- Lhoták P (2005) Anion Receptors Based on Calixarenes. *255*: 65–95
- Li WP, Meyer LA, Anderson CJ (2005) Radiopharmaceuticals for Positron Emission Tomography Imaging of Somatostatin Receptor Positive Tumors. *252*: 179–192
- Liang Z, see Du Q (2005) *261*: 45–61
- Liese A, see Greiner L (2007) *276*: 111–124
- Lingerfelt L, see Guiseppi-Elie A (2005) *260*: 161–186
- Litvinchuk S, see Matile S (2007) *277*: 219–250
- Liu S (2005) 6-Hydrazinonicotinamide Derivatives as Bifunctional Coupling Agents for ^{99m}Tc -Labeling of Small Biomolecules. *252*: 117–153
- Liu S, Robinson SP, Edwards DS (2005) Radiolabeled Integrin $\alpha_v\beta_3$ Antagonists as Radiopharmaceuticals for Tumor Radiotherapy. *252*: 193–216
- Liu XY (2005) Gelation with Small Molecules: from Formation Mechanism to Nanostructure Architecture. *256*: 1–37
- De Lucchi O, see Zonta C (2007) *275*: 131–161
- Luderer F, Walschus U (2005) Immobilization of Oligonucleotides for Biochemical Sensing by Self-Assembled Monolayers: Thiol-Organic Bonding on Gold and Silanization on Silica Surfaces. *260*: 37–56
- Maeda K, Yashima E (2006) Dynamic Helical Structures: Detection and Amplification of Chirality. *265*: 47–88
- Magnera TF, Michl J (2005) Altitudinal Surface-Mounted Molecular Rotors. *262*: 63–97
- Maini L, see Braga D (2005) *254*: 71–94
- Malacria M, see Albert M (2006) *264*: 1–62
- Marquette CA, Blum LJ (2005) Beads Arraying and Beads Used in DNA Chips. *261*: 113–129

- Mascini M, see Palchetti I (2005) 261: 27–43
- Matile S, Tanaka H, Litvinchuk S (2007) Analyte Sensing Across Membranes with Artificial Pores. 277: 219–250
- Matsumoto A (2005) Reactions of 1,3-Diene Compounds in the Crystalline State. 254: 263–305
- McGhee AM, Procter DJ (2006) Radical Chemistry on Solid Support. 264: 93–134
- Meyer B, Möller H (2007) Conformation of Glycopeptides and Glycoproteins. 267: 187–251
- Meyer LA, see Li WP (2005) 252: 179–192
- Michl J, see Magnera TF (2005) 262: 63–97
- Milea JS, see Smith CL (2005) 261: 63–90
- Mizoshita N, see Kato T (2005) 256: 219–236
- Modlinger A, see Weide T (2007) 272: 1–50
- Möller H, see Meyer B (2007) 267: 187–251
- Moonen NNP, Flood AH, Fernández JM, Stoddart JF (2005) Towards a Rational Design of Molecular Switches and Sensors from their Basic Building Blocks. 262: 99–132
- Moriyama M, see Kato T (2005) 256: 219–236
- Moussa A, see Coleman AW (2007) 277: 31–88
- Murai T (2005) Thio-, Seleno-, Telluro-Amides. 251: 247–272
- Murakami H (2007) From Racemates to Single Enantiomers – Chiral Synthetic Drugs over the last 20 Years. 269: 273–299
- Mutule I, see Suna E (2006) 266: 49–101
- Naka K (2007) Delayed Action of Synthetic Polymers for Controlled Mineralization of Calcium Carbonate. 271: 119–154
- Nakayama J, see Ishii A (2005) 251: 181–225
- Nakayama J, see Ishii A (2005) 251: 227–246
- Narayanan S, see Reif B (2007) 272: 117–168
- Neese F, see Sinnecker S (2007) 268: 47–83
- Nguyen GH, see Smith CL (2005) 261: 63–90
- Nicolau DV, Sawant PD (2005) Scanning Probe Microscopy Studies of Surface-Immobilised DNA/Oligonucleotide Molecules. 260: 113–160
- Niessen HG, Woelk K (2007) Investigations in Supercritical Fluids. 276: 69–110
- Nilsson P, Olofsson K, Larhed M (2006) Microwave-Assisted and Metal-Catalyzed Coupling Reactions. 266: 103–144
- Niyomura O, Kato S (2005) Chalcogenocarboxylic Acids. 251: 1–12
- Niyomura O, see Kato S (2005) 251: 19–85
- Nohira H, see Sakai K (2007) 269: 199–231
- Oda R, see Brizard A (2005) 256: 167–218
- Okahata Y, Kawasaki T (2005) Preparation and Electron Conductivity of DNA-Aligned Cast and LB Films from DNA-Lipid Complexes. 260: 57–75
- Okamura T, see Ueyama N (2007) 271: 155–193
- Oller-López JL, see Cuerva JM (2006) 264: 63–92
- Olofsson K, see Nilsson P (2006) 266: 103–144
- Oltra JE, see Cuerva JM (2006) 264: 63–92
- Onoda A, see Ueyama N (2007) 271: 155–193
- Otto D, see Ihmels H (2005) 258: 161–204
- Otto S, Severin K (2007) Dynamic Combinatorial Libraries for the Development of Synthetic Receptors and Sensors. 277: 267–288

- Palchetti I, Mascini M (2005) Electrochemical Adsorption Technique for Immobilization of Single-Stranded Oligonucleotides onto Carbon Screen-Printed Electrodes. *261*: 27–43
- Pascal R, Boiteau L, Commeyras A (2005) From the Prebiotic Synthesis of α -Amino Acids Towards a Primitive Translation Apparatus for the Synthesis of Peptides. *259*: 69–122
- Paulo A, see Santos I (2005) *252*: 45–84
- Pérez EM, see Leigh DA (2006) *265*: 185–208
- Perret F, see Coleman AW (2007) *277*: 31–88
- Perron H, see Coleman AW (2007) *277*: 31–88
- Pilch DS, Kaul M, Barbieri CM (2005) Ribosomal RNA Recognition by Aminoglycoside Antibiotics. *253*: 179–204
- Pividori MI, Alegret S (2005) DNA Adsorption on Carbonaceous Materials. *260*: 1–36
- Piwnica-Worms D, see Sharma V (2005) *252*: 155–178
- Plesniak K, Zarecki A, Wicha J (2007) The Smiles Rearrangement and the Julia–Kocienski Olefination Reaction. *275*: 163–250
- Polito M, see Braga D (2005) *254*: 71–94
- Poulin-Kerstien AT, see Dervan PB (2005) *253*: 1–31
- de la Pradilla RF, Tortosa M, Viso A (2007) Sulfur Participation in [3,3]-Sigmatropic Rearrangements. *275*: 103–129
- Procter DJ, see McGhee AM (2006) *264*: 93–134
- Quiclet-Sire B, Zard SZ (2006) The Degenerative Radical Transfer of Xanthates and Related Derivatives: An Unusually Powerful Tool for the Creation of Carbon–Carbon Bonds. *264*: 201–236
- Ratner MA, see Weiss EA (2005) *257*: 103–133
- Raymond KN, see Seeber G (2006) *265*: 147–184
- Rebek Jr J, see Scarso A (2006) *265*: 1–46
- Reckien W, see Thar J (2007) *268*: 133–171
- Reggelin M (2007) [2,3]-Sigmatropic Rearrangements of Allylic Sulfur Compounds. *275*: 1–65
- Reif B, Narayanan S (2007) Characterization of Interactions Between Misfolding Proteins and Molecular Chaperones by NMR Spectroscopy. *272*: 117–168
- Reiher M, see Herrmann C (2007) *268*: 85–132
- Renaud P, see Darmency V (2006) *263*: 71–106
- Revell JD, Wennemers H (2007) Identification of Catalysts in Combinatorial Libraries. *277*: 251–266
- Robinson SP, see Liu S (2005) *252*: 193–216
- Saha-Möller CR, see You C-C (2005) *258*: 39–82
- Sakai K, Sakurai R, Hirayama N (2007) Molecular Mechanisms of Dielectrically Controlled Resolution (DCR). *269*: 233–271
- Sakai K, Sakurai R, Nohira H (2007) New Resolution Technologies Controlled by Chiral Discrimination Mechanisms. *269*: 199–231
- Sakamoto M (2005) Photochemical Aspects of Thiocarbonyl Compounds in the Solid-State. *254*: 207–232
- Sakurai R, see Sakai K (2007) *269*: 199–231
- Sakurai R, see Sakai K (2007) *269*: 233–271
- Saladino R, Crestini C, Costanzo G, DiMauro E (2005) On the Prebiotic Synthesis of Nucleobases, Nucleotides, Oligonucleotides, Pre-RNA and Pre-DNA Molecules. *259*: 29–68

- Santos I, Paulo A, Correia JDG (2005) Rhenium and Technetium Complexes Anchored by Phosphines and Scorpionates for Radiopharmaceutical Applications. *252*: 45–84
- Santos M, see Szathmáry E (2005) *259*: 167–211
- Sato K (2007) Inorganic–Organic Interfacial Interactions in Hydroxyapatite Mineralization Processes. *270*: 127–153
- Sauvage J-P, see Collin J-P (2005) *262*: 29–62
- Sawant PD, see Nicolau DV (2005) *260*: 113–160
- Scandola F, see Chiorboli C (2005) *257*: 63–102
- Scarso A, Rebek Jr J (2006) Chiral Spaces in Supramolecular Assemblies. *265*: 1–46
- Schaumann E (2007) Sulfur is More Than the Fat Brother of Oxygen. An Overview of Organosulfur Chemistry. *274*: 1–34
- Scheffer JR, Xia W (2005) Asymmetric Induction in Organic Photochemistry via the Solid-State Ionic Chiral Auxiliary Approach. *254*: 233–262
- Schenning APHJ, see Ajayaghosh A (2005) *258*: 83–118
- Schindler J, see Faigl F (2007) *269*: 133–157
- Schmidtchen FP (2005) Artificial Host Molecules for the Sensing of Anions. *255*: 1–29 Author Index Volumes 251–255
- Schmuck C, Wich P (2007) The Development of Artificial Receptors for Small Peptides Using Combinatorial Approaches. *277*: 3–30
- Schoof S, see Wolter F (2007) *267*: 143–185
- De Schryver F, see De Feyter S (2005) *258*: 205–255
- Schulten K, see Dittrich M (2007) *268*: 319–347
- Schuman B, Alfaro JA, Evans SV (2007) Glycosyltransferase Structure and Function. *272*: 217–258
- Seeber G, Tiedemann BEF, Raymond KN (2006) Supramolecular Chirality in Coordination Chemistry. *265*: 147–184
- Seitz O, see Haase C (2007) *267*: 1–36
- Senn HM, Thiel W (2007) QM/MM Methods for Biological Systems. *268*: 173–289
- Severin K, see Otto S (2007) *277*: 267–288
- Sewell SL, see Carney CK (2007) *270*: 155–185
- Sharma V, Piwnica-Worms D (2005) Monitoring Multidrug Resistance P-Glycoprotein Drug Transport Activity with Single-Photon-Emission Computed Tomography and Positron Emission Tomography Radiopharmaceuticals. *252*: 155–178
- Shinkai S, see Ishi-i T (2005) *258*: 119–160
- Sibi MP, see Zimmerman J (2006) *263*: 107–162
- Siebbeles LDA, see Grozema FC (2005) *257*: 135–164
- Silvi S, see Balzani V (2005) *262*: 1–27
- Simon P, see Kniep R (2007) *270*: 73–125
- Sinnecker S, Neese F (2007) Theoretical Bioinorganic Spectroscopy. *268*: 47–83
- Skrydstrup T, see Hansen SG (2006) *264*: 135–162
- Smith CL, Milea JS, Nguyen GH (2005) Immobilization of Nucleic Acids Using Biotin–Strept(avidin) Systems. *261*: 63–90
- Smith DK, see Hirst AR (2005) *256*: 237–273
- Specker D, Wittmann V (2007) Synthesis and Application of Glycopeptide and Glycoprotein Mimetics. *267*: 65–107
- Sromek AW, Gevorgyan V (2007) 1,2-Sulfur Migrations. *274*: 77–124
- Stadler A, see Kremsner JM (2006) *266*: 233–278
- Stibor I, Zlatušková P (2005) Chiral Recognition of Anions. *255*: 31–63
- Stoddart JF, see Moonen NNP (2005) *262*: 99–132
- Strauss CR, Varma RS (2006) Microwaves in Green and Sustainable Chemistry. *266*: 199–231

- Suk D-H, see Crich D (2006) 263: 1–38
Suksai C, Tuntulani T (2005) Chromogenetic Anion Sensors. 255: 163–198
Sun J-S, see Escudé C (2005) 253: 109–148
Suna E, Mutule I (2006) Microwave-assisted Heterocyclic Chemistry. 266: 49–101
Süssmuth RD, see Wolter F (2007) 267: 143–185
Svith H, see Daasbjerg K (2006) 263: 39–70
Swerdlow H, see Du Q (2005) 261: 45–61
Szathmáry E, Santos M, Fernando C (2005) Evolutionary Potential and Requirements for Minimal Protocells. 259: 167–211
- Taira S, see Yokoyama K (2005) 261: 91–112
Takahashi H, see Tamura R (2007) 269: 53–82
Takahashi K, see Ueyama N (2007) 271: 155–193
Tamiaki H, see Balaban TS (2005) 258: 1–38
Tamura R, Takahashi H, Fujimoto D, Ushio T (2007) Mechanism and Scope of Preferential Enrichment, a Symmetry-Breaking Enantiomeric Resolution Phenomenon. 269: 53–82
Tanaka H, see Matile S (2007) 277: 219–250
Thar J, Reckien W, Kirchner B (2007) Car-Parrinello Molecular Dynamics Simulations and Biological Systems. 268: 133–171
Thayer DA, Wong C-H (2007) Enzymatic Synthesis of Glycopeptides and Glycoproteins. 267: 37–63
Thiel W, see Senn HM (2007) 268: 173–289
Tiedemann BEF, see Seeber G (2006) 265: 147–184
Tobey SL, see Houk RJT (2005) 255: 199–229
Toda F (2005) Thermal and Photochemical Reactions in the Solid-State. 254: 1–40
Tortosa M, see de la Pradilla RF (2007) 275: 103–129
Tour JM, see James DK (2005) 257: 33–62
Trask AV, Jones W (2005) Crystal Engineering of Organic Cocrystals by the Solid-State Grinding Approach. 254: 41–70
Tuntulani T, see Suksai C (2005) 255: 163–198
- Uccelli L, see Boschi A (2005) 252: 85–115
Ueyama N, Takahashi K, Onoda A, Okamura T, Yamamoto H (2007) Inorganic–Organic Calcium Carbonate Composite of Synthetic Polymer Ligands with an Intramolecular $\text{NH} \cdots \text{O}$ Hydrogen Bond. 271: 155–193
Ushio T, see Tamura R (2007) 269: 53–82
- Varma RS, see Strauss CR (2006) 266: 199–231
Veciana J, see Amabilino DB (2006) 265: 253–302
Venturi M, see Balzani V (2005) 262: 1–27
Vezin H, see Dias N (2005) 253: 89–108
Viso A, see de la Pradilla RF (2007) 275: 103–129
Vögtle F, see Fages F (2005) 256: 77–131
Vögtle M, see Žinić M (2005) 256: 39–76
Volkmer D, see Fricke M (2007) 270: 1–41
Volpicelli R, see Zonta C (2007) 275: 131–161
Vries TR, see Kellogg RM (2007) 269: 159–197
- Walschus U, see Luderer F (2005) 260: 37–56
Walton JC (2006) Unusual Radical Cyclisations. 264: 163–200

- Wannberg J, Ersmark K, Larhed M (2006) Microwave-Accelerated Synthesis of Protease Inhibitors. *266*: 167–197
- Warman JM, see Grozema FC (2005) *257*: 135–164
- Warren JD, Geng X, Danishefsky SJ (2007) Synthetic Glycopeptide-Based Vaccines. *267*: 109–141
- Wasielewski MR, see Weiss EA (2005) *257*: 103–133
- Weide T, Modlinger A, Kessler H (2007) Spatial Screening for the Identification of the Bioactive Conformation of Integrin Ligands. *272*: 1–50
- Weiss EA, Wasielewski MR, Ratner MA (2005) Molecules as Wires: Molecule-Assisted Movement of Charge and Energy. *257*: 103–133
- Weissbuch I, Leiserowitz L, Lahav M (2005) Stochastic “Mirror Symmetry Breaking” via Self-Assembly, Reactivity and Amplification of Chirality: Relevance to Abiotic Conditions. *259*: 123–165
- Wennemers H, see Revell JD (2007) *277*: 251–266
- Wich P, see Schmuck C (2007) *277*: 3–30
- Wicha J, see Plesniak K (2007) *275*: 163–250
- Williams LD (2005) Between Objectivity and Whim: Nucleic Acid Structural Biology. *253*: 77–88
- Wittmann V, see Specker D (2007) *267*: 65–107
- Wright DW, see Carney CK (2007) *270*: 155–185
- Woelk K, see Niessen HG (2007) *276*: 69–110
- Wolter F, Schoof S, Süßmuth RD (2007) Synopsis of Structural, Biosynthetic, and Chemical Aspects of Glycopeptide Antibiotics. *267*: 143–185
- Wöltinger J, see Greiner L (2007) *276*: 111–124
- Wong C-H, see Thayer DA (2007) *267*: 37–63
- Wong KM-C, see Yam VW-W (2005) *257*: 1–32
- Wright AT, see Collins BE (2007) *277*: 181–218
- Würthner F, see You C-C (2005) *258*: 39–82
- Xia W, see Scheffer JR (2005) *254*: 233–262
- Yam VW-W, Wong KM-C (2005) Luminescent Molecular Rods – Transition-Metal Alkynyl Complexes. *257*: 1–32
- Yamamoto H, see Ueyama N (2007) *271*: 155–193
- Yashima E, see Maeda K (2006) *265*: 47–88
- Yokoyama K, Taira S (2005) Self-Assembly DNA-Conjugated Polymer for DNA Immobilization on Chip. *261*: 91–112
- Yoshikawa I, see Araki K (2005) *256*: 133–165
- Yoshioka R (2007) Racemization, Optical Resolution and Crystallization-Induced Asymmetric Transformation of Amino Acids and Pharmaceutical Intermediates. *269*: 83–132
- You C-C, Dobrawa R, Saha-Möller CR, Würthner F (2005) Metallo-supramolecular Dye Assemblies. *258*: 39–82
- Yu J, see Dittrich M (2007) *268*: 319–347
- Yu S-H (2007) Bio-inspired Crystal Growth by Synthetic Templates. *271*: 79–118
- Zampella G, see Bertini L (2007) *268*: 1–46
- Zard SZ, see Quiclet-Sire B (2006) *264*: 201–236
- Zarecki A, see Plesniak K (2007) *275*: 163–250
- Zhang W (2006) Microwave-Enhanced High-Speed Fluorous Synthesis. *266*: 145–166

- Zhang X-E, Deng J-Y (2005) Detection of Mutations in Rifampin-Resistant *Mycobacterium Tuberculosis* by Short Oligonucleotide Ligation Assay on DNA Chips (SOLAC). 261: 169–190
- Zimmerman J, Sibi MP (2006) Enantioselective Radical Reactions. 263: 107–162
- Žinić M, see Fages F (2005) 256: 77–131
- Žinić M, Vögtle F, Fages F (2005) Cholesterol-Based Gelators. 256: 39–76
- Zipse H (2006) Radical Stability—A Theoretical Perspective. 263: 163–190
- Zlatušková P, see Stibor I (2005) 255: 31–63
- Zonta C, De Lucchi O, Volpicelli R, Cotarca L (2007) Thione–Thiol Rearrangement: Miyazaki–Newman–Kwart Rearrangement and Others. 275: 131–161

Subject Index

- Adamantine 223
Adenine 194
Alizarin complexone 191
Allylic alkylations 256
Amine–boron (N–B) interactions 119
Amino acids, complexation 33
–, discrimination 212
–, enantioselective discrimination 206
Amino sugars, IDAs 215
Aminoglycosides, IDAs 215
Amplifiers, covalent 242
Anti-bacterial activities, calixarenes 57
Antibiotic resistance 168
Antibody detection, epitope/lipid/PDA vesicles 171
Anti-cancer activity, calixarenes 60
Anti-thrombotic activity, calixarenes 61
Anti-tuberculosis activity, calixarenes 56
Anti-viral properties, calixarenes 57
Artificial neural networks (ANN) 183
ATP/AMP 187
- Bacterial fingerprinting 160
Bacterial resistance, colorimetric screening 168
Bacterial sensing, lipid/PDA vesicles 167
Biomimetic sensors 156
Biomolecules, array development 208
Biosensing, KE2-PL 103
Biotin–streptavidin–biotin antigen 223
Bis(cyclopeptide) receptors 26
Black lipid membranes (BLMs) 221
Boronic acids 107
–, complexation with saccharides 110
Bovine serum albumin (BSA) 53, 189
- Caffeine 194
Calix[n]arenes 32, 174
- Carbohydrates 107
–, pH changes 216
Carboxyfluorescein (CF) 220
Catalysis 251
Catalyst–substrate co-immobilization 263
Catalytic activity, one-bead-one-compound libraries 258
CBS-KKF 25
Cell-penetrating peptides, optical transducers 244
Charge-coupled device (CCD) 185
Chemometric analysis 182
Chromatic polymers 156
Chromatic sensors, vesicle-based 157
Colorimetric analysis 254
Colour biosensors 156
Combinatorial chemistry 251
–, dynamic 26
Combinatorial receptors 8
Creutzfeldt–Jacobs disease 32
Cyclodextrins 33
Cyclopeptide dimers 27
Cyclotrimeratrylene (CTV) 15
Cytochrome C 50
Cytosine 194
- Diboronic acid modular systems 147
Differential sensor arrays, chromatographic receptors 191
Diketopiperazine receptors 15
Dipeptides, complexation 45
Diversity-oriented synthesis (DOS) 17
Donor–bridge–acceptor motif 116
Dynamic combinatorial libraries, sensors/sensing 211, 279
–, synthetic receptors 269
- EKAA 19
Elastin 189

- Electron transfer, photoinduced 107
Electronic tongue 185
Energy transfer systems 135
Entropy, molecular recognition 92
Enzymatic catalysis, colorimetric detection 163
Enzyme immunoassays 257
Enzyme inhibition, calixarenes 62
Enzymes, specific signal generators 235
- Fetuin 189
Fluorescent pH indicators 261
Fluorescent sensor 107
Fluorimetric analysis 254
Fluorophore 220
– dependence 138
Fluorophore–spacer–receptor 117
Forces between biomolecules 91
- Gels, reaction media 262
Glycoproteins 188
Gramicidin ion channel 223
GTP 187
Gustatory system 182
- Heck reactions 254
Helix-loop-helix motif/dimer 96, 98
Hemolysin 223
Her-2/Neu receptor tyrosine kinase 17
Hierarchical cluster analysis (HCA) 183
High-throughput screening 251
Human carbonic anhydrase II 95, 99
Hydrogen bonding receptor, D-glucose 110
Hydrolytic activity, gel-based screening 263
Hydrosilations 255
- Immunosensors/immunosensing 157, 237
Indicator displacement assays (IDA) 187
–, MIPs 193
Internal charge transfer (ICT) 116
Ion channels, calixarenes 62
Ion discrimination, ionophore/lipid/PDA vesicles 170
IR thermographic analysis 253, 258
- KE2-PL, HCAII 99
Kinase inhibitors 17
- Large unilamellar vesicles (LUVs) 220
Lectin complexation 48
Libraries 10, 211, 251
Linear discriminant analysis (LDA) 183
Lipid/PDA vesicles 161
–, recognition elements 168
Lipopolysaccharide 160
Lysozyme 189
- Mammalian olfactory system 182
Membranes, porous sensors 245
N-Methyl-*o*-(aminomethyl) phenyl-boronic acid recognition unit 117
Micromachined chip 184
Microtiter plate arrays 202
Molecular recognition 182
–, proteins 91
Monoboronic acids, D-fructose 125
Monolayers, self-assembled 193
Multicomponent sensing ensembles 210
–, complex matrixes 236
Multi-ion imaging, fluorescent sensors 202
- Nakjiquinones 17
Neurodegenerative diseases 66
o-Nitrophenyl- β -D-galactopyranoside 262
- p*-Octiphenyl rods 226
Olfactory system 182
One-bead-one-compound libraries 251
Optical detection 182
Optical signals 115
Optical transduction, chemical reactions 232
Organics, in water 197
Ovalbumin 189
Oxygen sensors, phospholipid vesicles 157
- Patch cramming 223
Peptide receptors, artificial 5
–, tweezer 10
Peptide–membrane interactions, colorimetric detection 164
pH indicators, fluorescent 261
Pharmaceutical screening, colorimetric vesicles 165

- Phenylboronic acid, saturated mannitol 111
- Phosphodiesterase activity 260
- Photoinduced electron transfer (PET) 116
- Polyamidoamine (PAMAM) dendrimers 159
- Polydiacetylene 156
- vesicles 158
- Polydiacetylene-based sensors, colorimetric 158
- Poly(ethylene glycol)-polystyrene beads 185
- Polymers, molecularly imprinted 192
- Polypeptide conjugates, protein recognition 104
- Pores, bioengineered, sensing 237
- , synthetic multifunctional 226
- Porphyrins, fluorescent, discrimination of proteins 204
- Principal component analysis (PCA) 183
- Prions 32
- , proteins 69
- , related diseases, diagnostic tool 72
- Protein complexation 48
- Protein fingerprints, small molecule microarrays 199
- Protein recognition 94
- , polypeptide conjugate binder 95
- Protein sensors 64, 172
- Proteins 188
- PrP, ELISA-based detection, *para*-sulfonato calix[n]arenes, capture antibodies 78
- , Western blot 75
- PrP^{sc}, prion, supramolecular sensing 72
- Pyranose, furanose interconversion 122
- Pyrene 142
- Quantitative structure–activity relationships (QSAR) 23
- Radio-frequency tagging 19
- Rational design/synthesis 5
- Receptor modules, PDA-based vesicles 169
- Receptor tyrosine kinases 17
- Receptors, artificial, lipid/PDA vesicles 172
- , small peptides 3
- Rigid-rod β -barrels 226
- Saccharides 107
- Self-assembled monolayers, fluorescent 201
- Semiselective sensors 182
- Sensors, fluorescent 115
- Spreader-bar 193
- Stochastic sensing, single analytes 240
- Streptomycin, reticulating supramolecular system, prion protein 73
- Substituted cysteine accessibility method (SCAM) 223
- Supramolecular chemistry 4
- Synthetic pores, sensing 224
- Synthetic receptors, acetal exchange 278
- , disulfide exchange 275
- , hydrazone exchange 272
- , imine exchange 269
- Target-oriented synthesis (TOS) 17
- Taste chip, programmable 186
- Thymine 194
- Triboronic acid sensors 147
- Tripeptides 189
- , complexation 45
- Tryptase recognition 48
- Tweezer peptide receptors 10
- Uracil 194
- Uric acid 194
- Vancomycin 6
- Vesicle biosensors 156